

Predicting hydrates plugging risk in subsea gas pipeline: CFD, analytical and linear regression modelling.

UMUTEME, O.M.

2024

The author of this thesis retains the right to be identified as such on any occasion in which content from this thesis is referenced or re-used. The licence under which this thesis is distributed applies to the text and any original images only – re-use of any third-party content must still be cleared with the original copyright holder.

**PREDICTING HYDRATES PLUGGING RISK IN SUBSEA GAS
PIPELINE: CFD, ANALYTICAL AND LINEAR REGRESSION
MODELLING**

OGHENETHOJA MONDAY UMUTEME

**Predicting Hydrates Plugging Risk in Subsea gas Pipelines: CFD,
Analytical and Regression Modelling**

Oghenethoja Monday Umuteme

A thesis submitted in partial fulfilment of the requirements of the
Robert Gordon University
(School of Engineering)
for the award of the degree of
Doctor of Philosophy

May 2024



**Predicting Hydrates Plugging Risk in Subsea gas Pipelines: CFD,
Analytical and Regression Modelling**

PhD Candidate

Oghenethoja Monday Umuteme

Supervisory Team

Dr Sheikh Z. Islam (Principal Supervisor)

Dr Mamdud Hossain

Dr Aditya Kanik

School of Engineering, Robert Gordon University, The Sir Ian Wood Building,
Riverside East, Garthdee Road, Aberdeen, AB10 7GJ, United Kingdom.

DEDICATION

Dedicated to my children – *Elomezino, Aghoghomena, Ewevino* and *Onavize*, for their resilience amid all the uncertainties that surrounded this PhD and to God for giving me the strength to complete this doctoral work.

ACKNOWLEDGEMENT

I cannot thank you enough, my beautiful wife – Pst. (Mrs.) Adokiye Obele Umuteme, for initiating this PhD, and all the sacrifice you put in to ensure it was completed. My special appreciation goes to my principal supervisor – Dr. Sheikh Zahidul Islam, for your experience, expertise, drive and all the guidance and supervision you provided throughout this journey. My appreciation also goes to my second supervisor - Professor Mamdud Hossain, for providing the first spike of knowledge that helped me realise the CFD scope of this study early. Another depth of appreciation goes to my third supervisor – Dr. Aditya Karnik, for all the constructive feedbacks and for your experience in CFD. I also express my acknowledgement of the supports provided by the school of graduate studies and the school of engineering at RGU for periodic assessment of progress and all the support I received during this research. My thanks also go to my assessor at the transfer to doctorate, Dr. Taimor Asim for your constructive assessment and feedbacks.

I am equally grateful to the IT unit of the Robert Gordon University for the timely availability of the needed software for this study. I also want to extend this appreciation to my parents Elder Umuteme Moses Eboh and Mrs Ulemi Florence Umuteme, for giving me the early opportunity to become educated. I also appreciate Dr. Ibiba Emmanuel Douglas, the former Director of the Shell Centre of Excellence in Marine and Offshore Engineering – Rivers State University, Port Harcourt Nigeria for his encouragement. My appreciation also goes to Engr. Onoriode Uriri and Engr. and Bar. (Mrs.) Pankyes Hirse for the prayers and encouragement. Finally, I also thank the Royal Diamonds International Church for the support, prayers, and encouragement.

ABSTRACT

This study addresses critical limitations in managing hydrate plugging risk for gas pipelines. The main challenges lie in accurately predicting hydrate deposition rates and associated pressure drops. To overcome these limitations, the study developed and validated a 3D computational model using computational fluid dynamics (CFD) and mathematical models. The model simulates a 10-meter long, 0.0204-meter diameter horizontal pipe section. The core of the model employs Eulerian-Eulerian multiphase modeling within ANSYS Fluent software. This approach successfully predicted hydrate deposition rates within a $\pm 10\%$ uncertainty range across various subcooling temperatures and gas velocities. At lower gas velocities (4.7 m/s), the model exhibited significant improvement over existing methods. Compared to a 925.7% deviation from experimental results, the model outperformed an analytical model which underpredicted by 27-33%. Similarly, at higher velocities (8.8 m/s) and varying subcooling temperatures, the CFD model demonstrated high accuracy, with deviations ranging from a slight underprediction (1%) to a moderate overprediction (14%).

The study revealed a significant finding related to pipewall shear stress. The model predicted a sequential increase in average shear stress along the pipe at different gas velocities (2 m/s, 4 m/s, 6 m/s, and 8 m/s). These values exceeded 100 Pa, aligning well with established experimental observations. Beyond deposition rates, the CFD model accurately predicted the location, phase changes, and pressure drop profiles during hydrate formation, agglomeration, and deposition. This aligns with findings from previous experimental studies. Furthermore, the model achieved a mean relative error of 4%, significantly outperforming models with higher errors. The model for predicting plugging flowtime also yielded valuable results. While it underpredicted plugging time by a mean relative error of 9%, this level of discrepancy is considered acceptable for proactive intervention strategies. The study acknowledges practical limitations and emphasizes the need for field validation of its propositions. Nonetheless, the findings provide valuable insights and pave the way for future research in this domain.

Keywords: Hydrate deposition rates, Gas pipeline, Pipeline diameter, Hydraulic diameter, Subcooling temperature, Wall shear stress, Hydrate plugging flowtime, Analytical modelling, Hydrates deposition rates CFD modelling, Locating hydrate plug

PUBLICATIONS

UMUTEME, O. M. et al., 2021. Computational fluid dynamics prediction of hydrates deposition rates in subsea gas pipelines. In: 34th Scottish Fluid Mechanics Meeting (SFMM) - *Poster Presentation*. School of Engineering, Robert Gordon University, Aberdeen, Scotland, UK.

UMUTEME, O.M. et al., 2022. An improved computational fluid dynamics (CFD) model for predicting hydrate deposition rate and wall shear stress in offshore gas-dominated pipeline. *Journal of Natural Gas Science and Engineering*, 107. [online]. Available from: doi.org/10.1016/j.jngse.2022.104800.

UMUTEME, O. M. et al., 2023a. Analytical Modelling of the Hydraulic Effect of Hydrate Deposition on Transportability and Plugging Location in Subsea Gas Pipelines. *Proceedings of the Institution of Mechanical Engineers, Part C: Journal of Mechanical Engineering Science*.

UMUTEME, O.M. et al., 2023b. Computational fluid dynamics simulation of natural gas hydrate sloughing and pipewall shedding temperature profile: Implications for CO₂ transportation in subsea pipeline. *Gas Science and Engineering*, 116, p. 205048. Available from: <https://www.sciencedirect.com/science/article/pii/S2949908923001760>.

UMUTEME, O.M. et al., 2023c. Modelling Hydrate Deposition in Gas-Dominant Subsea Pipelines in Operating and Shutdown Scenarios. *Sustainability (Switzerland)*, 15(13824).

TABLE OF CONTENTS

DEDICATION	iii
ACKNOWLEDGEMENT.....	iv
ABSTRACT	v
PUBLICATIONS	vii
TABLE OF CONTENTS.....	viii
LIST OF FIGURES	xiv
LIST OF TABLES.....	xxiii
NOMENCLATURE	xxvi
CHAPTER 1: INTRODUCTION	1
1.0 Preamble	1
1.1 Background Information.....	1
1.2 Rational for the Study.....	4
1.3 Motivation for the Work.....	7
1.4 Aims and Objectives	8
1.5 Thesis Presentation Outline.....	9
CHAPTER 2: LITERATURE REVIEW	10
2.0 Preamble	10
2.1 Theory of Gas Flow in Horizontal Pipelines	11
2.2 Pressure and Temperature Concerns.....	11
2.3 The Dynamics of Gas Flow in Pipeline.....	12
2.4 The Formation of Natural Gas Hydrates	14
2.5 Flow Regimes in Horizontal Gas Pipeline	16
2.6 Hydrates Prediction in Gas-Dominated Systems.....	18
2.6.1 Experimental Studies on Hydrate Prediction.....	19
2.6.2 Analytical Hydrates Prediction Models	23
2.6.3 Regression Modelling of Hydrates Deposition Rate	28
2.6.4 Prediction of Hydrates Plugging Event Location	29
2.7 Hydrates Plugging Risk	31
2.8 Computer Program for Predicting Hydrates Plugging Risk....	32
2.9 Theoretical Implications for Current Study	33
2.10 Gaps in Current Knowledge and Justification for Research Objectives.....	35
2.11 Summary of Literature Review	37

CHAPTER 3: STUDY DESIGN/METHODOLOGY	39
3.0 Preamble	39
3.1 CFD Modelling Methodology	40
3.1.1 CFD Model Development	42
3.1.2 Computational Domain	44
3.1.3 Governing Equations	45
3.1.4 Turbulence Models	49
3.1.5 Wall shear stress	52
3.1.6 Enhanced near wall effects	52
3.1.6.1 Pressure Gradient Effect	52
3.1.6.2 Thermal Effect	52
3.1.7 Mesh Grid Sensitivity and UDF Performance.....	53
3.1.8 Fluent solver configuration	57
3.1.9 Solution Method.....	57
3.1.10 Approach to CFD Results Analysis and Model Validation .	59
3.2 Regression Modelling Methodology.....	61
3.2.1 Defining Variables and Data Generation	63
3.2.2 Regression Model Development.....	64
3.2.3 Model Selection Criteria	66
3.3 Analytical Modelling Methodology	69
3.3.1 Model Development Stages	70
3.3.2 Equations and Derivations.....	71
3.3.3 Mass Conservation Equation	73
3.3.4 Volume of Hydrates Deposited	76
3.3.5 Pipeline Hydraulic Diameter	79
3.3.6 Final Models	80
3.4 Hydrate Plugging Risk Table.....	82
3.5 MATLAB® Programming.....	83
3.6 Chapter Summary	83
CHAPTER 4: CFD MODELLING OF HYDRATES DEPOSITION RATES AND PIPEWALL SHEAR STRESS IN SUBSEA GAS PIPELINES	84
4.0 Introduction	84
4.1 Model Validation and Discussion	90
4.1.1 CFD Model Validation.....	92
4.1.1.1 Hydrate Deposition Rates.....	92

4.1.1.2	Temperature contours showing the effect of changes in velocity and subcooling temperatures during hydrate deposition.....	100
4.1.1.3	Gas density contours showing cross-sectional increase in gas density towards the wall of the pipe	104
4.1.1.4	Pressure drop during hydrate formation, agglomeration and deposition with change in velocity and subcooling temperature.	104
4.1.1.5	Quantitative measurement of hydrate deposition rates	106
4.2	Parametric Analysis	112
4.2.1	Effect of Hydrates on Volume Fraction of Gas and Water	112
4.2.2	Effect of Turbulence and Tangential Velocity on Hydrate Deposition.....	114
4.2.3	Effect of Pipe Length on Hydrate Deposition Rate.....	117
4.2.4	Effect of Pipe Diameter on Hydrate Deposition Rate	117
4.2.5	The Relationship between Velocity and Shear Stress on Hydrate Deposition	120
4.2.6	Change in Pipeline Geometry: Effect of 90-degree riser on hydrates formation	125
4.3	Chapter Summary	128
CHAPTER 5: CFD PREDICTION OF HYDRATES SLOUGHING AND PIPEWALL SHEDDING BY HYDRATES IN SUBSEA GAS PIPELINES ..		131
5.0	Introduction	131
5.1	Results and Discussion	135
5.1.1	Mist-Annular Flow Pattern During Hydrates Formation and Deposition.....	135
5.1.2	Variation of Hydrates Thickness with Velocity and Subcooling Temperature.....	138
5.1.3	Effect of Gas Velocity on Molecular Viscosity of the Multiphase.....	141
5.1.4	Effect of Pipewall Skin Friction	142
5.1.5	Effect of Velocity on the Strain Rate of Hydrate Deposits	143

5.2 Hydrates Sloughing and Pipewall Shedding	144
5.2.1 Sloughing and Pipewall Shedding Shear Stress.....	146
5.2.2 Pressure Drop and Shedding Stress	148
5.3 Chapter Summary	154
CHAPTER 6: MULTIPLE REGRESSION MODELLING OF HYDRATES DEPOSITION RATE IN SUBSEA GAS PIPELINE IN OPERATING AND SHUTDOWN SCENARIOS	156
6.0 Introduction	156
6.1 Result, Validation and Model Selection	158
6.1.1 Results	158
6.1.2 Validation with Experimental Data	161
6.1.3 Model Selection	164
6.2 Dimensionally Homogenous Deposition Rate Model	167
6.3 Practical Application of Regression Model.....	169
6.3.1 Pipeline Shutdown Planning.....	169
6.3.2 Effect of change in Subcooling temperature on Hydrates Deposition	171
6.3.3 Effect of Change in Water Volume Fraction on Hydrates Deposition	171
6.3.4 Effect of Change in Pipeline Size on Hydrates Deposition in Design Phase	172
6.4 Chapter Summary	173
CHAPTER 7: ANALYTICAL MODELLING OF HYDRATE-INDUCED PRESSURE DROP AND LOCATION OF HYDRATE PLUGGING EVENT IN SUBSEA GAS PIPELINE.....	175
7.0 Introduction	175
7.1 Model Validation and Discussion of Results.....	183
7.1.1 Input Data	185
7.1.2 Hydrate Plugging Flowtime and Transient Pressure Drop	186
7.1.3 Validation of model predictions at gas velocity of 4.6m/s	187
7.1.4 Validation of model predictions at gas velocity of 8.7m/s	188
7.2 Hydrates Transportability	189

7.3	Location of Hydrates Plugging Event.....	193
7.3.1	Effect of Hydrates Deposition on Transient Pressure Drop and Plugging Flowtime	194
7.3.2	Effect of increase in pipeline diameter.....	196
7.3.3	Effect of hydrates deposition rates on pipe inner diameter	197
7.3.4	Hydraulic Effect of Hydrates Plug at Different Sections of the Pipeline	198
7.3.5	Effect of Pressure Drop on the Bulk Modulus of Gas and Hydrate.....	201
7.3.6	Hydraulic Effect of Hydrate Plug Location on Shear Rate and Shear Stress	203
7.3.7	Effect of Hydrate Plug Location on Hydraulic Thrust Upstream of the Hydrate Plug	208
7.4	Hydraulic Flow Parameters for Locating Hydrate Plug.....	210
7.5	Hydrates Plug Location Prediction Table	212
7.6	Hydrates Plug Location Prediction Steps.....	215
7.7	Chapter Summary	217
CHAPTER 8: PREDICTING HYDRATES PLUGGING RISK: CASE STUDY		
	220
8.0	Introduction	220
8.1	Stages of Proposed Hydrates Severity Investigation	223
8.1.1	Investigating Hydrates Formation.....	224
8.1.2	Locate Pipeline Hydrates Section	225
8.1.3	Estimating Hydrates Deposition Rates	225
8.1.4	Predicting Hydrates Plugging Flowtime	226
8.1.5	Predicting Transient Pressure Drop	226
8.1.6	Investigating Risk Level for Proactive Intervention Decision	227
8.2	Case Study.....	230
8.3	Results and Discussion	232
8.3.1	Likelihood of Hydrates in Pipeline	232
8.3.2	Hydrates Section Length	233
8.3.3	Deposition Rate	233
8.3.4	Plugging Flowtime and Transient Pressure Drop	233

8.3.5 Risk Level Estimation.....	234
8.4 Chapter Summary	235
CHAPTER 9: MATLAB CODE FOR HYDRATES PLUGGING RISK PREDICTIVE (HPRP) MODEL FOR SUBSEA GAS PIPELINES	237
9.0 Introduction	237
9.1 HPRP Model Algorithm.....	238
9.2 Equations.....	239
9.3 Hydrates Plugging Risk Definition	240
9.4 HPRP Model Validation	241
9.5 Parametric Analysis	242
9.5.1 Effect of Change in Subcooling Temperature on Hydrates Plugging Risk.....	242
9.5.2 Effect of Velocity Change on Hydrates Plugging Risk at Constant Subcooling Temperature	244
9.5.3 Effect of Change in Pipeline Diameter on Hydrates Plugging Risk.....	245
9.5.4 Effect of Change in Hydrates Plug Distance	248
9.5.5 Effect of Change in Water Volume Fraction on Hydrates Plugging Risk.....	249
9.6 Prioritisation of Hydrates Intervention Planning.....	250
9.7 Chapter Summary	253
CHAPTER 10: CONCLUSIONS AND RECOMMENDATIONS FOR FUTURE WORK.....	255
10.1 Major Conclusions from the Work	255
10.2 Contribution to Knowledge	257
10.3 Limitation of the Work	258
10.4 Future Work Recommendation	259
REFERENCES	260
APPENDIX A: MATLAB CODE FOR HYDRATES PLUGGING RISK PREDICTION	273
APPENDIX B: SAMPLE OUTPUT OF MATLAB CODE	277
APPENDIX C: UDF CODES.....	281

LIST OF FIGURES

Figure 1.1:	Industrial hydrates control (adapted from Kinnari et al. 2015)	2
Figure 1.2:	Conceptual framework	7
Figure 1.3:	Process flow for achieving the research objectives	9
Figure 2.1:	Schematic of literature review flowchart	10
Figure 2.2:	The three forms of hydrates crystals (Koh, Sloan and Sum 2011, p. 3). Structure II are formed in gas pipelines and it is the focus of this study.....	15
Figure 2.3:	Horizontal cross-sectional flow regimes for gas-water mixtures in a pipe (Adapted from Brennen (2013)). Annular flow describes the multiphase flow pattern during hydrates formation in gas dominant pipeline.	16
Figure 3.1:	Research work scope and methodology	39
Figure 3.2:	Adopted CFD framework (Adapted from Tu, Yeoh and Liu 2018, p.35)	41
Figure 3.3:	Computation Process	41
Figure 3.4:	CFD model development stages.....	43
Figure 3.5:	2D representation of the computational domain.....	44
Figure 3.6:	900,000 cells 3D mesh computational domain	44
Figure 3.7:	Mesh sensitivity	54
Figure 3.8:	Comparison of pressure drop (with and without hydrate deposition UDFs) at gas flow velocity of 8.8m/s.....	54
Figure 3.9:	Comparing average hydrate deposition curves at a velocity of 4.7 m/s (7.0K) for various timestep sizes. The identification of hydrates formation, agglomeration and deposition sections are provided later in Figure 4.7.	58
Figure 3.10:	CFD simulation result at 8.8m/s and 7.1K. (a) CFD replication of the experimental hydrates pressure and temperature curve by Liu et al. (2020). (b) Superimposition of the CFD pressure curve on the simulated hydrates profile.	60
Figure 3.11:	CFD simulation result for the gas density at a velocity of 8.8m/s and subcooling temperature of 7.1K.....	60

Figure 3.12:	Stages of the adopted methodology.....	62
Figure 3.13:	Interaction of regressor variables with the deposition rate of hydrates	64
Figure 3.14:	The development stages of plugging flowtime and transient pressure drop models	70
Figure 3.15:	Computational fluid domain	72
Figure 3.16:	Solution Algorithm.....	81
Figure 4.1:	Methane hydrate loci showing experimental region	91
Figure 4.2:	10% bound Q-Q plot comparison of CFD model prediction of hydrate deposition rates at a gas velocity of 4.7 m/s with experimental and analytical model results	94
Figure 4.3:	10% bound Q-Q plot comparison of CFD model prediction of hydrates deposition rates at a gas velocity of 8.8 m/s with experimental and analytical model results	94
Figure 4.4:	Comparing % deviation from experimental results at gas velocity of 4.7 m/s	95
Figure 4.5:	Comparing % deviation from experimental results at gas velocity of 8.8 m/s	96
Figure 4.6:	Relationship between pressure and temperature variation at 8.8 m/s and subcooling temperature of 7.0K.....	97
Figure 4.7:	Relationship between pressure drop and hydrate deposition rate at 8.8 m/s and subcooling temperature of 7.0K	98
Figure 4.8:	Comparing hydrate temperatures at subcooling temperature of 7.0K with gas flow velocities of 4.7 m/s and 8.8 m/s ..	99
Figure 4.9:	Comparing the stability of hydrate near the pipe wall and at the core at subcooling temperature of 7.0K with gas flow velocity of 8.8 m/s	100
Figure 4.10:	Temperature contour at varying velocities and constant subcooling temperature of 7.0K for the gas phase	101
Figure 4.11:	Temperature contour at varying subcooling temperatures and constant velocities of 4.7 m/s and 8.8 m/s for the gas phase	102
Figure 4.12:	Temperature contour tapering effect of hydrate deposition along the pipe at a velocity of 8.8 m/s and subcooling temperature of 7.1K	103

Figure 4.13:	Temperature contours of gas and water phase at gas velocity of 8.8 m/s and subcooling temperature of 7.1K indicating the formation of Hydrates as dispersed phase and deposition on the wall of the pipe.	103
Figure 4.14:	Gas density contour increasing towards the wall of the pipe at subcooling temperature of 7.0K.	104
Figure 4.15:	Effect of velocity change under constant subcooling temperature on pressure drop during hydrate formation, agglomeration, and deposition	105
Figure 4.16:	Effect of change in subcooling temperature at constant velocity on pressure drop during hydrate formation, agglomeration, and deposition.	106
Figure 4.17:	Gas mass flowrate during hydrate formation, agglomeration, and deposition	107
Figure 4.18:	Comparison of gas mass flowrate 'with' and 'without' hydrate deposition UDFs. Higher agglomeration of hydrates at 1.6 s to 2.6 s is observed when the UDFs were implemented.	107
Figure 4.19:	Comparing hydrate deposition curves at a velocity of 4.7 m/s for various subcooling temperatures.	108
Figure 4.20:	Comparing hydrate deposition curves at a velocity of 8.8 m/s for various subcooling temperatures.	109
Figure 4.21:	Comparing hydrate formation for various gas supply rate at a velocity of 8.8 m/s and constant subcooling temperature of 8.0K	110
Figure 4.22:	The relationship between hydrate deposition rate and gas supply rate at a velocity of 8.8 m/s and subcooling temperature of 8.0K	111
Figure 4.23:	Relationship between hydrate deposition rate and gas supply rate at a velocity of 4.7 m/s and subcooling temperature of 7.0K.	111
Figure 4.24:	Phase change during hydrate formation, agglomeration, and deposition at gas velocity of 8.8 m/s and subcooling temperature of 7.0K	112
Figure 4.25:	Effect of temperature on hydrate plugging risk at subcooling temperature of 7.0K.	114
Figure 4.26:	Effect of water volume fraction on hydrate deposition rates at subcooling temperature of 7.0K and gas velocity of 8.8 m/s.	114

Figure 4.27:	Effect of hydrate formation, agglomeration, and deposition on turbulent Reynolds number at subcooling temperature of 7.0K.....	115
Figure 4.28:	Tangential velocity of hydrates at subcooling temperature of 7.0K.....	116
Figure 4.29:	Impact of change in pipe diameter on hydrate deposition rate at 8.8m/s and 7.1K subcooling temperature.	118
Figure 4.30:	Relationship between hydrate deposition rate and pipe diameter at constant flow velocity. Higher diameter at constant velocity implies higher flowrate.	118
Figure 4.31.	Maximum y^+ plot at subcooling temperature of 7.0K indicating that the simulation is dominated by viscous forces.....	122
Figure 4.32:	Maximum shear stress on hydrate deposits at subcooling temperature of 7.0K and at velocity of 8.8 m/s.	123
Figure 4.33.	Maximum shear stress on hydrate deposits at subcooling temperature of 7.0K and at velocity of 4.7m/s	123
Figure 4.34:	A 90-degree riser base section with diameter of 0.0204m (654,624 mesh cells).....	126
Figure 4.35:	Change in gas density contour map during the growth, erosional and transportation of hydrates in the riser at 2.5 m/s and subcooling temperature of 7.0 K	126
Figure 4.36:	(a) Change in gas mass flowrate and (b) change in pressure and temperature, in the fluid domain during the growth, erosional and transportation of hydrates in the riser at 2.5 m/s and subcooling temperature of 7.0K	127
Figure 4.37:	The gas temperature at the pipewall dropped below the hydrate equilibrium temperature of 292K to 291.9K, indicating a relatively stable temperature, hence the hydrates were not stable.....	128
Figure 5.1:	Temperature profile of hydrates at constant subcooling temperature of 8K and varying gas velocity. Deposited hydrates are stable below 290K. Unstable hydrates are formed at 292K at the core of the pipe.....	136
Figure 5.2:	Temperature profile at constant gas velocity of 4.0 m/s and varying subcooling temperature. Deposited hydrates are stable below 290K. Unstable hydrates are formed at 292K at the core of the pipe.	136
Figure 5.3:	Hydrates profile obtained from the gas density. The higher gas density at the wall indicates hydrates deposition....	137

Figure 5.4:	Labelled profile of deposited hydrates.....	137
Figure 5.5:	Hydrates profile at a subcooling temperature of 8.0K and varying gas flow velocity of 2-8 m/s.....	139
Figure 5.6:	The effect of increasing gas velocity on volume of deposited hydrates at subcooling temperature of 8.0K.	140
Figure 5.7:	Increasing molecular viscosity of the multiphase flow during hydrates formation, agglomeration, and deposition.	141
Figure 5.8:	Increasing coefficient of pipe wall skin friction during hydrates formation, agglomeration, and deposition. The wall skin friction is obtained from the secondary water phase.	143
Figure 5.9:	The strain rate of hydrate deposits on the pipe wall by obtaining strain rate data of the secondary phase in the presence of the heavier gas.	144
Figure 5.10:	Locations of hydrates sloughing and wall shedding along the pipe.....	145
Figure 5.11:	Representation of shedding and sloughing along the shear stress plot at 4 m/s and subcooling temperature of 8.0K	146
Figure 5.12:	Variation of shear stress with gas velocity at constant subcooling temperature of 8.0K.....	147
Figure 5.13:	Variation of hydrates sweep length with gas velocity at constant subcooling temperature of 8.0K.....	149
Figure 5.14:	Effect of gas velocity on sweep ratio at a subcooling temperature of 8.0K.	150
Figure 5.15:	Effect of change in the density of the gas on the Euler number at a subcooling temperature of 8.0K.....	151
Figure 5.16:	Hydrates profile at a subcooling temperature of 8.0K and varying gas flow velocity. (a) 2 m/s – sloughing angle of 125o. (b) 4 m/s – sloughing angle of 151o. (c) 6 m/s – sloughing angle of 153o. (d) 8 m/s – sloughing angle of 155o.....	152
Figure 5.17:	Effect of sloughing on hydrates plugging distance at a subcooling temperature of 8.0K and varying gas flow velocity.....	152
Figure 5.18:	Effect of sloughing on pipeline hydraulic diameter at a subcooling temperature of 8.0K and varying gas flow velocity.....	153

Figure 5.19:	Velocity profile of gas and water phase during hydrates formation at a subcooling temperature of 7.0K.	153
Figure 6.1:	Comparing plots for each regression modelling approach	160
Figure 6.2:	Residuals plots for each regression modelling approach	161
Figure 6.3:	Prediction of experimental results by each regression modelling approach	163
Figure 6.4:	Comparing predictions by each regression modelling approach with experimental results	164
Figure 6.5:	Normal probability plots (Q-Q plots). (a) with 90% certainty band. (b) with 10% prediction band.....	164
Figure 6.6:	Normalized violin plots	166
Figure 6.7:	Change in the deposition rate of hydrates as the gas velocity increases at constant subcooling temperature of 7.0K, water volume fraction of 0.06 and pipeline size of 8 inches (0.204m)	170
Figure 6.8:	Change in the deposition rate of hydrates as the subcooling temperature increases at constant gas velocity of 4m/s, water volume fraction of 0.06 and pipeline size of 8 inches (0.204m)	171
Figure 6.9:	Change in the deposition rate of hydrates as the water volume fraction increases at constant gas velocity of 4 m/s, subcooling temperature and pipeline size of 8 inches (0.204m)	172
Figure 6.10:	Change in the deposition rate of hydrates as the pipe diameter increases at constant gas velocity of 4 m/s, subcooling temperature and water volume fraction.	173
Figure 7.1:	Comparing model predictions of first significant spike in transient pressure drop with experimental results: (a) Experiment 1 - hydrate deposition rate of 0.078 L/min at 4.6 m/s (Aman et al. 2016); (b) Experiment 1 - hydrate deposition rate of 0.129 L/min at 8.7 m/s (Di Lorenzo et al. 2014b).	185
Figure 7.2.	Comparing predictions of hydrates density estimation model with experimental results: (a) pressure and density of hydrates; (b) temperature and density of hydrates.	191
Figure 7.3:	Determining the temperature for hydrates transportability at gas pressure of 6.0 MPa	193
Figure 7.4:	Methane hydrates loci (Di Lorenzo et al. 2014a)	193

Figure 7.5:	Comparing pressure drop curves at different rates of hydrates deposition at a gas velocity of 8.7 m/s, and pipeline temperature of 287.5K and pressure of 10.9 MPa.195
Figure 7.6:	Comparing pressure drop curves at different pipeline diameter and corresponding hydrates deposition rates at gas velocity of 8.7 m/s, pipeline temperature of 287.5 K and pressure of 10.9 MPa.196
Figure 7.7:	Comparing pipeline hydraulic diameter reduction at different hydrates deposition rates at gas velocity of 8.7 m/s, pipeline temperature of 287.5K and pressure of 10.9 MPa197
Figure 7.8:	Pipeline hydraulic diameter reduction rate as hydrates deposition rates increases at gas velocity of 8.7 m/s, and pipeline temperature of 287.5K and pressure of 10.9 MPa.198
Figure 7.9:	Pressure drop curves at different hydrates plug location along the pipeline at gas velocity of 8.7 m/s, and pipeline temperature of 287.5 K and pressure of 10.9 MPa198
Figure 7.10:	The hydraulic effect of transient pressure drop on the ratio of pressure drop to change in density at constant temperature of 285 K when the hydrate plug is located 500 m downstream of the hydrate equilibrium point along the pipeline.....202
Figure 7.11:	The hydraulic effect of transient pressure drop on bulk modulus of hydrates as the gas pressure was increased from 4-7 MPa at constant temperature 285 K and various hydrate plug location downstream of the hydrate equilibrium condition along the pipeline.203
Figure 7.12:	The hydraulic effect of bulk modulus on shear rate at constant temperature 285 K at various hydrate plug locations.204
Figure 7.13:	Comparing the hydraulic effect of pressure drop on shear rate at constant temperature of 285K and varying hydrate plug location along the gas pipeline.205
Figure 7.14:	Comparing the hydraulic effect of transient pressure drop on the viscosity of hydrate at constant temperature of 285K and varying hydrate plug distance downstream of the hydrates generation point.....206
Figure 7.15.	Comparing the hydraulic effect of transient pressure drop on the hydrates shear stress at constant temperature of 285K and varying hydrate plug location beyond the hydrate's generation point.207

Figure 7.16:	Comparing the hydraulic effect of pressure drop on the hydrates plug velocity at constant temperature of 285K and varying hydrate plug location downstream of the hydrates equilibrium condition point along the pipeline.....	208
Figure 7.17:	Comparing the hydraulic effect of pressure drop on the hydraulic thrust upstream of the hydrate plugs located at temperature of 285K and varying hydrate plug location downstream of the hydrates generation point along the pipeline.....	209
Figure 7.18:	Locating hydrates plug at gas velocity of 8.7 m/s, and pipeline temperature of 287.5K and pressure of 10.9 MPa.	211
Figure 7.19:	Comparing transient pressure drop at gas velocities of 4 m/s and 8 m/s with respect to the plugging distance when the hydrates deposition rate is 10 L/min.	214
Figure 7.20:	Proposed hardware installation on gas pipeline for real-time data transfer for hydrates plug location detection	215
Figure 8.1:	Proactive hydrates plugging risk investigative framework	223
Figure 8.2:	Locating pipeline hydrates section	225
Figure 8.3:	Locating the hydrates section: (a) at 50MMSCFD; (b) at 20MMSCFD.....	231
Figure 8.4:	Transient Pressure Drop and Plugging Flowtime Predictions at 50 MMSCFD and 20 MMSCFD for the data in Table 8.4.	234
Figure 9.1:	Algorithm for HPRP MATLAB code	238
Figure 9.2:	Effect of increase in subcooling temperature on hydrates plugging risk at constant gas velocity of 8.0 m/s. (a) reduction in plugging flowtime. (b) increase in transient pressure drop. (c) slight increase in gas flowrate because of a reduction in gas temperature from equation (9.6). (d) increase in hydrates deposition rate. (e) increase in the density of hydrates. (f) increase in the density of the gas.	243
Figure 9.3:	Effect of change in gas velocity on hydrates deposition rate	244
Figure 9.4:	Effect of change in gas velocity on hydrates plugging risk. (a) pressure drop increases with increasing gas velocity. (b) plugging flowtime reduces with increasing gas velocity.	245

Figure 9.5:	Effect of change in pipe diameter on hydrates deposition rate at gas velocity of 5.0m/s and subcooling temperature of 12K.	247
Figure 9.6:	Effect of change in pipe diameter on hydrates plugging risk at constant velocity of 5 m/s and subcooling temperature of 12K. (a) pressure drop decreases with increasing gas velocity. (b) plugging flowtime increases with increasing pipe diameter.	247
Figure 9.7:	Effect of change in pipe diameter on hydrates deposition rate at gas constant gas flowrate 0.2 m ³ /s and subcooling temperature of 12K.	247
Figure 9.8:	Effect of change in pipe diameter on hydrates plugging risk at constant gas flowrate 0.2 m ³ /s and subcooling temperature of 12K. (a) pressure drop decreases with increasing pipe diameter. (b) plugging flowtime increases with increasing pipe diameter.....	248
Figure 9.9:	Effect of change in hydrates plug distance. (a) pressure drop increases. (b) extension of plugging time.....	249
Figure 9.10:	Effect of change in water volume fraction at constant velocity 8.0m/s, pipe diameter of 0.0408 m and subcooling temperature of 12K. (a) hydrates deposition rate reduces as water volume fraction increases. (b) plugging flowtime extends as water volume fraction increases.	250
Figure 9.11:	HPRP Code predicted results for hydrates intervention planning for the three pipelines. (a) hydrates deposition rate. (b) Hydrates density. (c) plugging flowtime. (d) transient pressure drop.	252
Figure 9.12:	HPRP Code predicted plugging flowtime versus pressure drop for hydrates intervention planning of the three pipelines	253

LIST OF TABLES

Table 3.1:	Natural gas properties (Ansys Fluent Version 2020 R1)....	55
Table 3.2:	Liquid water properties (Ansys Fluent Version 2020 R1) ..	56
Table 3.3:	Gas hydrate properties.....	56
Table 3.4:	Input parameters/boundary conditions (Di Lorenzo et al, 2018).....	56
Table 3.5:	Range of input data for the CFD simulations	64
Table 3.6:	Criteria for model selection	69
Table 4.1:	Hydrate deposition rate validation at 4.7m/s	93
Table 4.2:	Hydrate deposition rate validation at 8.8m/s	93
Table 4.3:	CFD model predicted hydrate deposition rates.....	109
Table 4.4:	Comparison of hydrate deposition rates for CFD model lengths	117
Table 5.1:	Volumes of deposited hydrates at a subcooling temperature of 8.0K and varying gas flow velocity of 2-8 m/s	140
Table 5.2:	Sweep length and sweep ratio at a subcooling temperature of 8.0K	150
Table 6.1:	Coefficients of predictor variables for each regression model	159
Table 6.2:	Validation of regression models with experimental data.	162
Table 6.3:	Comparing values of each model selection criteria for all regression models	165
Table 6.4:	Parameter ranking based on fitness of each regression model to experimental results.....	165
Table 6.5:	Relative impact of each predictor variable on hydrates deposition rate	166
Table 6.6:	Comparing the predicted hydrates deposition rate by the dimensionally homogenous model with experiential and CFD results.....	169
Table 7.1:	Input Parameters.....	186
Table 7.2:	Comparing model predictions with experimental results by Aman et al. (2016) at 4.6 m/s	188

Table 7.3:	Comparing model predictions with experimental results by (Di Lorenzo et al. 2014a) at 8.7 m/s.	189
Table 7.4:	Correlation between the location of hydrate plug and the parameters that defines the transportability of hydrates	199
Table 7.5:	Hydrates plug location prediction at hydrates deposition rate of 10L/min	213
Table 7.6:	Hydrates plug location prediction at hydrates deposition rate of 20L/min	213
Table 8.1:	Criteria for classifying hydrates plugging risk	229
Table 8.2:	Breakdown of hydrates plugging risk by categories of measurement.....	229
Table 8.3:	Gas Composition.....	230
Table 8.4:	Input variables for CFD and analytical model simulation	232
Table 8.5:	Overall hydrates plugging risk classification for the case study	235
Table 9.1:	Hydrate plugging risk matrix.....	241
Table 9.2:	Comparing model predictions with experimental results by Aman et al. (2016) at 4.6m/s	241
Table 9.3:	Comparing model predictions with experimental results by (Di Lorenzo et al. 2014a) at 8.7m/s.....	242
Table 9.4:	Effect of subcooling temperature at constant velocity of 8.0 m/s	243
Table 9.5:	Effect of velocity change at constant subcooling temperature of 7.0K	244
Table 9.6:	Effect of change in pipe diameter at constant velocity of 5.0m/s and subcooling temperature of 12K – pipe wall temperature of 280K	246
Table 9.7:	Effect of change in pipe diameter at constant flowrate of 0.2 m ³ /s and subcooling temperature of 12 K – pipe wall temperature of 280K	246
Table 9.8:	Effect of change in length of hydrates section at constant gas flowrate of 0.88 m ³ /s and subcooling temperature of 12K – pipe wall temperature of 280K)	248

Table 9.9:	Effect of change in water volume fraction at constant velocity 8.0m/s, pipe diameter of 0.0408 m and subcooling temperature of 12K – pipe wall temperature of 280K	249
Table 9.10:	Input data for the three pipelines	251
Table 9.11:	HPRP Code predicted results for hydrates intervention planning for the three pipelines	251
Table 9.12:	Hydrates intervention prioritisation ranking table	253

NOMENCLATURE

Notations Symbols	Descriptions	Units
$A:$	Pipe cross-sectional area	m^2
$A_i:$	Interfacial area	m^2
C_a	Cauchy number	Dimensionless
$C_\mu:$	Turbulent viscosity constant	Dimensionless
$C_{1\varepsilon}$ $C_{2\varepsilon}$ and $C_{3\varepsilon}:$	Constants	Dimensionless
$D:$	Diameter of the pipe section prone to hydrates formation	M
$D_h:$	Pipeline hydraulic diameter	M
$D_{h_{sw}}$	Pipeline hydraulic diameter at the end of the sweep length	M
$dp:$	Pressure drop	Pa
$dt:$	Timestep	S
$D_{t,pq}:$	Binary diffusivity ($D_{t,pq} = \frac{1}{3} K_{pq} \tau_{t,pq}$)	Pa
$E_u:$	Euler number	Dimensionless
$E_v:$	Bulk modulus	Pa
$G_{k,q}:$	Turbulent kinetic energy production term per phase	Dimensionless
$h_q:$	The q^{th} phase specific enthalpy	J/kg
$h_{pq}:$	Interphase enthalpy	J/kg
$K_{ft}:$	Empirical approximation constant	Dimensionless
$K_H:$	Empirical model fit constant	Dimensionless
$K_{pq}:$	Covariance of the phase velocities	Dimensionless
k_1 and $k_2:$	Constants	Dimensionless
$K_{ex_factor}:$	Extrapolation factor	Dimensionless
$k:$	Turbulent kinetic energy rate	m^2s^{-3}

$L:$	Length of hydrates section; distance from point of hydrates equilibrium condition – is also the location of the hydrates plug	m
$L_{sw}:$	The difference between the length of the pipe and the uniform section of hydrates layer	M
$\dot{m}_{CH_4}:$	Methane gas consumption rate ($\frac{dm_g}{dt}$)	kg/s
$\dot{m}_{pq}:$	Rate of mass transfer from the p^{th} to the q^{th} phase	kg/s
$\dot{m}_{qp}:$	Rate of mass transfer from the q^{th} to the p^{th} phase	kg/s
$P:$	Hydrate formation equilibrium pressure	KPa
$P_{eq}:$	Hydrate formation equilibrium pressure	KPa
$v:$	Velocity	m/s
$V_g:$	Volume of gas	m^3
$v_g:$	Velocity of the primary continuous gas phase	m/s
$\vec{v}_q:$	Velocity vector of the phase in the control volume	m/s
$\vec{v}_{dr}:$	Drift velocity vector between the gas and liquid phase	m/s
$\vec{v}_{pq}:$	Relative velocity vector between both phases	m/s
$Q_H:$	Hydrates formation, agglomeration, and deposition rate	L/min
$Q_{pq}:$	Intensity of the heat exchange between the phases	W
$\vec{q}_q:$	Heat flux vector	W/m ²
$\dot{s}:$	Strain rate	1/s
$S_q:$	Source/sink term: gas consumption rate or source energy rate	Kg/s-m ³ or J/s-m ³

S_{sw_r} :	Ratio of the sweep length to the length of the hydrates section along the gas pipeline	Dimensionless
T, T_w :	Pipeline/pipe wall temperature	K
T_{eq} :	Hydrate formation equilibrium temperature	K
t_n :	Instantaneous flowtime	S
t_{plug} :	Plugging flowtime	S
T_{sys} :	System temperature	K

<i>Greek Symbol</i>	Descriptions	Units
α_q :	Phase fraction	dimensionless
$\frac{\partial p_q}{\partial t}$:	Transient system pressure	Pa/s
ε :	Turbulent dissipation rate	m^2s^{-3}
f :	Friction factor	dimensionless
ρ_g :	Density of gas	kg/m^3
$\rho_{H_{hwc}}$:	Density of hydrate in the hydrate-water composite	kg/m^3
ρ_H :	Density of hydrates	kg/m^3
ρ_q :	Density of the phase	kg/m^3
ρ_k :	Density of the k th phase	kg/m^3
$\tilde{\rho}$:	Averaged density	kg/m^3
η_g :	Gas viscosity	$Nm^{-2}.s$
σ :	Shear strength/stress	Pa
η :	Viscosity	$Nm^{-2}.s$
$\mu_{t,k}$:	Turbulent viscosity	$Nm^{-2}.s$
ΔT_{sub} :	Sub-cooling temperature	K
θ_{sl} :	Sloughing angle	dimensionless
ΔH_{Hyd} :	Enthalpy of hydrate generation	J/kg
∇_{α_p} and ∇_{α_q} :	Variations in concentration of the gas and liquid phase respectively	dimensionless

Π :	The ratio of the circumference of the pipe annulus to the diameter of that pipe, given as 3.142	dimensionless
$\Pi_{\kappa q}$ and $\Pi_{\varepsilon q}$:	Source terms for the turbulence interactions of the entrained water phase on the primary gas phase ($\Pi_{\kappa q}$: turbulent and $\Pi_{\varepsilon q}$: dissipation)	dimensionless
$\sigma_{\kappa q}$ and $\sigma_{\varepsilon q}$:	Ratio of the temperature-dependent kinematic eddy viscosity of the continuous gas phase to the dispersed liquid phase. $\sigma_{\kappa q}$ is turbulent kinetic energy (TKE) and $\sigma_{\varepsilon q}$ turbulent dissipation rate (TDR) Prandtl numbers	dimensionless
$\tau_{t,pq}$ and τ_c^t	Turbulent shear stress	Pa

Acronyms/ Abbreviations

ANSYS FLUENT	Software used for the numerical simulation
CFD	Computational Fluid Dynamics
CSMHyK	Colorado School of Mines Hydrate Kinetics
DNVGL-ST-F101	DNV standard for Submarine pipeline systems
DP	Design Pressure
EOS	Equation of State
GA	Genetic Algorithm
LSSVM	Least Square Support Vector Machine
HFT	Hydrates Formation Temperature
HPHT	High Pressure High Temperature
HPRP	Hydrates Plugging Risk Prediction/Predictive
MAIP	Maximum Allowable Incidental Pressure
MAOP	Maximum Allowable Operating Pressure
MATLAB	A computer programming software
OLGA	Hydraulic simulation software
RANS	Reynolds Averaged Navier-Stokes Simulation
RBFN	Radial Basis Functions Neural Network

STAR-CCM	A commercial CFD package
SVM	Support Vector Machine Regression
UDF	User Defined Function

CHAPTER 1: INTRODUCTION

1.0 Preamble

This section introduces the problem and purpose statements for this PhD research. Sections: (1.1) provides the background information regarding the importance of hydrates management in the oil and gas industry; (1.2) discusses the rationale for the research with focus on current industry and academic need; (1.3) present the motivation for the work; (1.4) is the aim(s) and objectives of the study; and (1.5) presents the outline of this report.

1.1 Background Information

Hydrates in gas-dominated transport pipelines is still a safety issue in the oil and gas industry (Koh and Creek 2011). Previous studies indicates that natural gas is still the energy of choice due to its low carbon emission level, as hydrogen gas transportability in pipelines is still an issue for large-scale industrial application (Melaina, Antonia and Penev 2013; Meng et al. 2017; Umuteme 2020). For offshore gas pipelines, the sea floor creates varied subcooling temperatures providing the thermal gradient between the natural gas and the pipe wall to form hydrates at the right temperature and pressure conditions.

Consequently, the availability of gas to costumers through the affected offshore pipelines can be constrained because of the reduction in pipeline hydraulic annulus from hydrates plugging events. Since the nineteenth century, the formation of hydrates in oil and gas transport pipelines has become an intellectual curiosity (Carroll 2014). This can be inferred from the recent volume of research papers on the subject, that in 2024 there are still increasing studies on the initiation, formation, agglomeration, deposition, transportability and plugging mechanisms of hydrates in pipelines (He 2022; Yu and Tian 2022; Zhang et al. 2022a, 2022b, 2023; Marques et al. 2022; Nasir et al. 2022; Rao et al. 2022; Umuteme et al. 2022, 2023b, 2023c, 2023a; Lv et al. 2023; Ma et al. 2024).

Previous studies focused on how hydrates are formed, and the temperatures and pressures of formation (Carroll 2014). The three approaches currently

implemented in the oil and gas industry for managing hydrates are prediction, prevention and problem solving (Kinnari et al. 2015). First, hydrates prediction deals with understanding how hydrates are formed and all the related issues, such as pressure rise and pipeline rupture (Di Lorenzo et al. 2014a; Kinnari et al. 2015). Hydrates prediction is one of the components of a robust capacity utilization and optimization framework in the operation of gas pipelines (Umuteme and Umeh 2019). Second, the prevention of hydrates in natural gas pipelines is usually achieved through the modification of flow parameters and conditions (Lederhos et al. 1996; Li et al. 2013; Carroll 2014; Lim et al. 2020). Third, problem solving is usually cost intensive and not an approach recommended for effective control of hydrates.

Therefore, it is important to understand and monitor the conditions leading to hydrates formation, and the need for accurate hydrate deposition predictive model. The generally adopted methods for the control of hydrates in the oil and gas industry are provided in **Figure 1.1**.

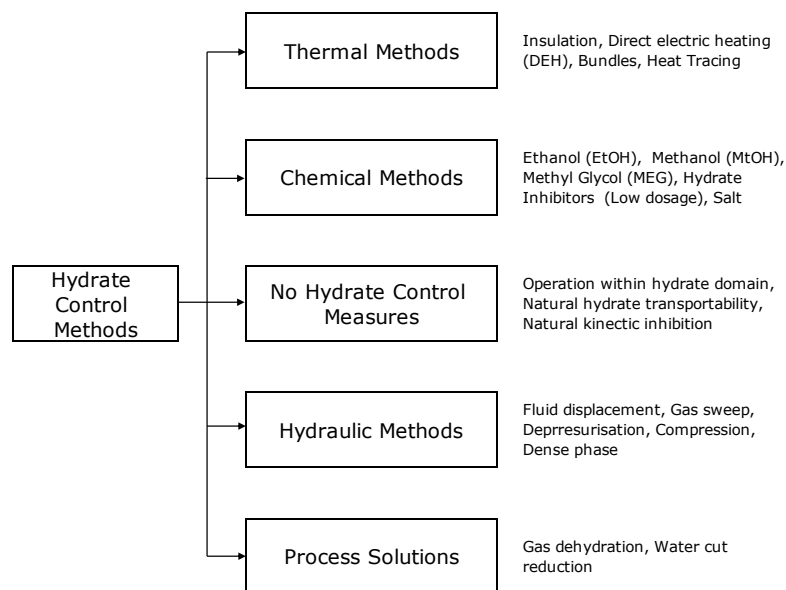


Figure 1.1: Industrial hydrates control (adapted from Kinnari et al. 2015)

The key problem in the management of hydrates is to mitigate plugging risk (Kinnari et al. 2015). In all the methods presented above and discussed extensively in the literature (Sloan and Koh 2007; Palermo and Sloan 2011; Sloan, Koh and Sum 2011a; Carroll 2014), research emphasis is currently

on adopting a “no hydrate control measure” approach. This will reduce both CAPEX and OPEX costs in transporting natural gas to costumers and improve the robustness in gas exploration investment. The uncertainties in the other control measures can include faulty thermal heating system, failure of thermal coating when damaged by offshore fishing trawler, and faulty hydrates inhibition chemical injection skid. Thus, there is increasing need to understand the deposition rate of hydrates to enhance operation within hydrate domain and transportability measures. This need is also balanced with the inevitability of kinetic inhibition when required.

While hydrates can be managed by chemical injections and the depressurisation of hydrate plugs (Koh and Creek 2011), with regasification techniques available today, hydrates can be transported to surface facilities and converted to sales gas saving millions of dollars that would have been spent on chemical injection and the maintenance of injection equipment. Again, glycol and methanol are poisonous in higher dose and can affect the purity of natural gas (Carroll 2014). Hence, current interest is on the understanding of the dynamics of hydrates formation and transportability (Di Lorenzo et al. 2014a).

The prevention of hydrates in natural gas pipelines is usually achieved through the modification of flow parameters and conditions (Li et al. 2013; Carroll 2014; Lim et al. 2020). Therefore, it is possible to predict hydrates formation, agglomeration and deposition using CFD transport and energy equations, and other physical models that define the intensive and extensive properties of the fluid medium. A model that can accurately predict hydrates deposition rates is invaluable in planning hydrates intervention and maintenance programmes, and in the design of hydrates prone pipelines.

An extensive and detailed review of the literature identified some gaps, especially the need to predict hydrates plugging risks at low gas flow velocity outside experimental arrangements because of the limitations of size, cost and difficulty in extrapolating experimental results for field application. Thus, the full scope of this doctoral research is to develop both CFD and analytical models for monitoring hydrates plugging risk in gas pipelines. The CFD model predicted hydrates deposition in gas pipelines by simulating the thermo-

mechanistic conditions of flow, while the semi-empirical analytical model directly incorporates hydrates deposition rate to predict hydrates-induced transient pressure drop and the time to plug the pipeline. The outcomes of the CFD and analytical models are validated with experimental results available in the literature (Di Lorenzo et al. 2014b, 2014a, 2018; Aman et al. 2016). Sensitivity analyses were carried out to better understand the influence of velocity and temperature on hydrates deposition rates, pressure drop and wall shear stress to ascertain the predictability of the models.

1.2 Rational for the Study

Current industry and research concerns is that thermodynamic predictions are not sufficient to estimate the risk associated with hydrates formation (Carroll 2014). Also, there is currently no validated model for hydrates prediction in gas-dominant systems which have been incorporated into software simulators (Charlton et al. 2018a). The existing hydrate kinetics model in OLGA[®] predicts hydrates growth for oil-dominant systems, hence the need for a gas-specific hydrate formation and growth model.

Again, there are reported limitations in the accurate prediction of hydrates growth in gas-dominant systems by existing analytical models and transient flow simulators (e.g., Zerpa et al. 2013; Odutola et al. 2017; Charlton et al. 2018a; Wang et al. 2018). Previous studies have already explained the formation kinetics and growth mechanisms for gas hydrates (e.g., Turner et al. 2005; Carroll 2014; Yin et al. 2018). While there are recent advances in experimental studies (e.g., Di Lorenzo et al. 2014a, 2014b; Aman et al. 2016; Ding et al. 2017; Odutola et al. 2017; Zhang, Wu and Mu 2017) and analytical modelling (Wang et al. 2017, 2018; Di Lorenzo et al. 2018; Liu et al. 2019) on hydrates formation, agglomeration, and deposition in gas-dominated pipelines, progress in CFD modelling has been relatively lacking.

Although experimental models are useful, yet they are expensive and are not easily extrapolated for various flow scenario except a new or modified experiment is set up. Hence, studying hydrates formation experimentally is a difficult task (Lim et al. 2020). The hydrates formation CFD approach by Neto et al. (2016) was modelled using a commercial CFD software (ANSYS

CFX), although the model was not validated with experimental results, and was identified as a research gap in the literature. Again, recent CFD models focused on hydrates slurry transportability (e.g., Berrouk et al., 2020; Jujuly et al., 2017) and not specially on hydrates deposition rate which is important for proactive prediction of plugging risk.

Analytical models for the prediction of hydrates and pressure drop in gas-dominated system have gained some attention in recent years, with the following significant findings: (i) pressure and shear stress fluctuations occur along the pipeline due to the effect of sloughing and shedding of hydrates at the wall (Di Lorenzo et al. 2018; Liu et al. 2019); (ii) hydrates deposition and growth occur in three-pattern stages of flow: gas-water-hydrates (stage 1); gas-hydrate (stage 2); and water-saturated gas (stage 3), and that hydrates plugging risk is more likely in stage 1 (Wang et al. 2018); (iii) there is non-uniform distribution of hydrates thickness along the pipeline, and 50% of hydrates deposited at the pipe wall are from the dispersed water in the continuous gas phase (Wang et al. 2017); and (iv) increasing the Reynolds number of the flow increases the distance of deposition from the inlet (Jassim, Abdi and Muzychka 2010).

To successfully model hydrates deposition rates in a gas pipeline, it is necessary to understand some theoretical basis. Carroll (2014), report three necessary conditions for natural gas hydrates to form: (i) the right combination of low temperature and high pressure based on gas composition; (ii) presence of gas hydrate formers such as methane, ethane, and carbon-dioxide; and (iii) sufficient amount of water. Also, hydrates formation is reported in the literature to be equally enhanced other flow and physical phenomena such as turbulence from high flow velocity and agitation; nucleation sites such as elbows, tees, and valves; and free water which creates a good gas-water interface for nucleation.

Furthermore, the increased solubility of methane gas in water at higher pressure and lower temperatures below the hydrate formation condition (Lekvam and Bishnoi 1997), can be used as basis for estimating gas consumption rate. From experimental observations, hydrate growth rate is dependent on the temperature driving force and the gas-water interfacial

area (Aman et al., 2016; Di Lorenzo et al., 2014b, 2014a; Ding et al., 2017; Turner et al., 2005; Zhang et al., 2017). Thus, the induction time before the formation of hydrates and subsequent growth is dependent on the thermal driving force resulting from the temperature gradient between the pipe centre and the wall (Lim et al. 2020). Also, experimental visual inspection indicates that the flow pattern present in gas systems with liquid film and a dispersed water-vapour phase is annular dispersed (Di Lorenzo et al. 2014a, 2014b; Aman et al. 2016; Ding et al. 2017). This flow pattern can also create corrosion risk at the site of hydrates nucleation (Obanijesu 2012).

Therefore, the proactive prevention of hydrate plugs in gas pipelines involves monitoring hydrate deposition rate, plugging flowtime, and transient pressure drop. This approach allows for the proactive estimation of the potential risk of hydrate-induced pipeline failure. The prediction of hydrate deposition rate for gas pipelines can be achieved by analytical and CFD modelling, considering the limitations of the experimental approach discussed earlier. However, the deposition rates predicted by the analytical model of Di Lorenzo et al. (2018) underpredicted the experimental results by a range of 27-33% at low gas velocity of 4.7m/s; and this is not admissible for a proactive predictive model. Again, the transient pressure drops of the same model overpredicted experimental results up to 50%, which can lead to over-estimation of pipeline wall thickness during design and non-optimisation of hydrates intervention and pipeline pigging programs.

Consequently, the two main knowledge gaps of interest that necessitated this PhD work include:

- i. The need to improve on the accurate prediction of hydrates deposition rates in gas-dominated pipelines, and
- ii. The need to improve on the hydrates plugging flowtime and the resulting transient pressure drop predictions.

This study closes these concerns and other gaps discussed in chapter 2. Based on the above gaps, this study adopts the conceptual framework below.

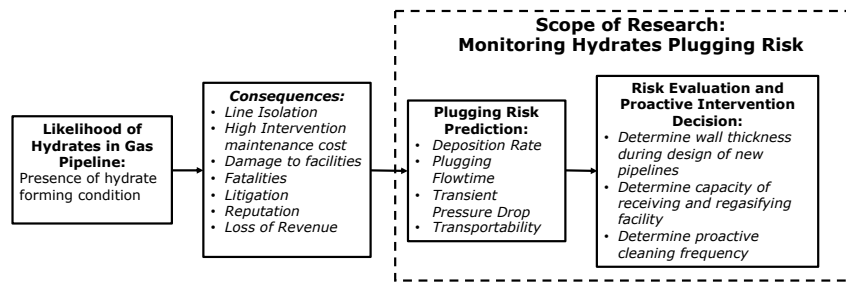


Figure 1.2: Conceptual framework

Two research questions are answered in this study: (i) How can analytical and CFD modelling be refined to more accurately predict hydrates deposition rates in gas pipelines, and (ii) How can these models be optimized to improve predictions of hydrate plugging flowtime and transient pressure drops, ensuring practical applicability for pipeline design and intervention strategies?

1.3 Motivation for the Work

The growing importance of natural gas in the green and digital economy demands efficient and reliable flow assurance enhancement through subsea pipelines. However, hydrate formation is a major hurdle causing blockages and flow disruptions. Existing hydrate risk assessment methods, heavily reliant on thermodynamics, often struggle to accurately predict hydrate formation and growth in gas-dominant pipelines. Current analytical models and simulators have limitations, while experimental studies, though valuable, are expensive and inflexible. Existing CFD models mainly focus on hydrate transport as a slurry, neglecting crucial deposition rate prediction for proactive risk assessment.

This PhD research is driven to address these limitations by developing a more robust approach. By significantly improving prediction accuracy of plugging location, a critical challenge despite high error rates in current models, this research has the potential for major impact in the field. The proposed combined CFD and mathematical modeling approach seeks to achieve improved prediction of deposition rates and transient pressure drop, leading to more efficient pipeline design and operation. Additionally, it aims for dimensionally homogeneous prediction for simplified calculations and user-

friendliness, and enhanced workflow and cost savings through accurate predictions, minimizing the need for expensive experiments.

This research aligns with the focus green and digital economies by enhancing the availability of a cleaner-burning low-carbon-emission fossil fuel. It also ensures reliable gas supplies for digital infrastructure, contributing to the stability and security of digital economies by ensuring reliable gas supplies for powering data centers and other critical facilities. Addressing the limitations of previous studies on managing hydrates plugging risk in gas pipelines and leveraging a robust theoretical framework, this PhD research has the potential to significantly improve hydrate plugging risk prediction in gas pipelines, contributing to a more efficient, reliable, and sustainable energy future. This research aims to significantly improve the design, maintenance, and overall hydrate management strategies for subsea gas pipelines by achieving the aims and objectives discussed in the next section.

1.4 Aims and Objectives

This research aims to enhance subsea gas pipeline design and maintenance by predicting hydrate plugging risks through deposition rates, flow time, and pressure drop. To achieve this, the following objectives were achieved:

- i. Optimize hydrate prediction through CFD modeling
- ii. Develop comprehensive hydrate Plugging Risk management models
- iii. Create a gas-specific hydrate plugging risk assessment tool
- iv. Improve overall hydrate management strategy

Informed by a comprehensive literature review in chapter 2, objective i focuses on using CFD to accurately predict and understand how various factors influence hydrate deposition rates. Objective ii encompasses both predicting deposition rates under different conditions (operational and shutdown) and understanding the consequences of hydrate plugging (flow time and pressure drop). Similarly, objective iii focuses on establishing a risk table and a mathematical model specifically designed for gas-dominated pipelines to assess hydrate plugging severity. Finally, objective iv highlights the ultimate goal: using the developed models and tools to create a more

effective strategy for managing hydrates in gas pipelines. The flow process adopted in achieving the above objectives is described in **Figure 1.3**, below.

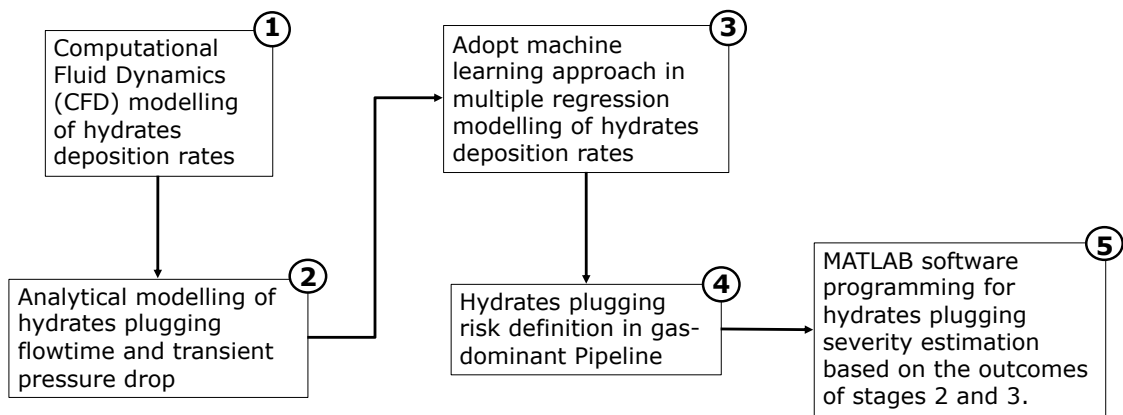


Figure 1.3: Process flow for achieving the research objectives

1.5 Thesis Presentation Outline

The rest of the thesis report is structured as follows:

Chapter 2 provided the outcome of the literature review, formed the theoretical framework, and identified the research gaps.

Chapter 3 discussed the multi-layer methodology adopted to achieve the objectives of this research.

Chapter 4 presented the results, sensitivity analysis and validation of the CFD model.

Chapter 5 provided further results of the CFD model for estimating the pipewall shedding shear stress and connected the results to the possibility of internal corrosion because of hydrates pipewall shedding.

Chapter 6 provided the results and validation of the multiple regression model developed from the outcome in chapter 4.

Chapter 7 followed with the results of the analytical model, sensitivity analysis and validation and used the model to propose an approach to locating possible location of hydrates plugging events.

Chapter 8 developed the matrix table for hydrates plugging risk classification for gas-dominant pipelines.

Chapter 9 provided the MATLAB program development stages, sensitivity analysis and validation.

Chapter 10 provided the conclusion, and recommendation for future studies.

CHAPTER 2: LITERATURE REVIEW

2.0 Preamble

This literature review establishes both the theoretical framework and identified the gaps for this doctoral research work. A schematic representation of the scope of the review is provided in **Figure 2.1**, below.

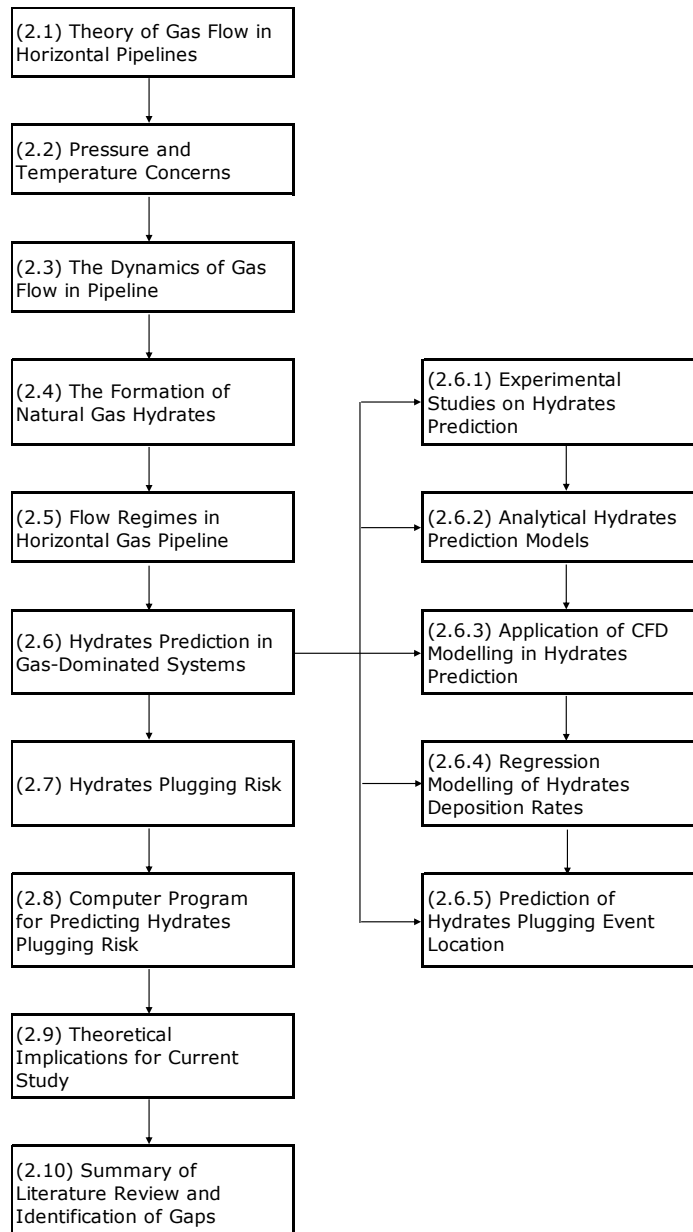


Figure 2.1: Schematic of literature review flowchart

Sections: (2.1) discusses the theory of gas flow in horizontal pipelines; (2.2) discusses pressure and temperature concerns in gas flow; (2.3) discusses

gas flow dynamics; (2.4) discusses natural gas hydrates formation; (2.5) discusses multiphase flow regimes in horizontal gas-liquid pipelines; (2.6) presents the literature review on the prediction of hydrates deposition rates and pressure drop using experimental, analytical, CFD, and regression approaches and the prediction of plugging event location; (2.7) reviews the literature on the definition and classification of hydrates plugging risks; (2.8) reviews the application of computer programming in predicting hydrates plugging risks; (2.9) discusses the theoretical implication of the literature review on current study; and (2.10 and 2.11) summarises the findings and the identification of gaps from the literature review.

2.1 Theory of Gas Flow in Horizontal Pipelines

The availability of a pipeline throughout the designed life depends on the properties of the transported fluid. For a specific gas pipeline, the operating pressure and temperature, gas specific volume, compressibility factor, specific heat, Joule-Thompson coefficient, isentropic temperature change exponent, enthalpy, entropy and viscosity are important factors that influences gas transportability (Mohitpour, Golshan and Murray 2007; Munson et al. 2013; Marfo et al. 2019).

Also, water drop-out from the gas stream due to variation in temperature and pressure under certain flow characteristics can lead to the formation of hydrates. The formation of hydrates can lead to multiphase slurry flow with high pressure drop because of increasing viscosity (Di Lorenzo et al. 2014a; Berrouk et al. 2020). Thus, it is not uncommon to expect unstable high-pressure spikes during hydrates deposition, sloughing and pipe plugging (Di Lorenzo et al. 2018; Hou et al. 2019; Liu et al. 2020). Hence, it is important to understand temperature and pressure concerns in enhancing flow assurance of gas pipelines.

2.2 Pressure and Temperature Concerns

For a given gas flow rate, a rise in temperature increases the pressure drop and the compressor power requirements by lowering gas transmissibility in gas pipelines (Mohitpour, Golshan and Murray 2007). Temperature drop along the pipeline is mostly caused by heat transfer across the fluid boundary

at the pipe wall to a colder environment through a phenomenon referred to as subcooling (Turner et al. 2005; Di Lorenzo et al. 2014a). Graph of temperature and pressure variations have been used to predict natural gas hydrates in pipeline transmission lines (Carroll 2014). Therefore, to overcome hydrates formation, the management of the pipeline temperature within safe flow zone is important. There are existing temperature correlations used to predict hydrate formation temperatures (Carroll 2014).

2.3 The Dynamics of Gas Flow in Pipeline

The interrelationship of pressure, temperature and other parameters for liquid and gas pipeline design can be summarized through a review of relevant flow equations. The following equations explain the relationships of pressure and temperature, pipe characteristics such as diameter and pipe roughness, flow rate, pipeline length and elevation profiles, and the properties of the fluid to be transported.

The Weymouth and Panhandle equations described in the literature (Mohitpour, Golshan and Murray 2007, pp. 80-82) are some of the empirical estimations for the design of gas pipelines. For short pipelines with high Reynolds number (Re), the Weymouth equation relates the friction factor to the pipe diameter (Equation 2.1). The assumption that the friction is dependent on the pipe size makes the Weymouth equation useful for shorter lines mainly within a gas processing plant, where higher gas velocities are expected.

$$Q = 433.5 * \frac{T_{stp}}{P_{stp}} * \left[\frac{P_1^2 - P_2^2}{G * T * L * Z} \right]^{0.5} * D^{2.667} \quad (2.1)$$

For longer pipelines, the Panhandle equation (Equation 2.2), estimates the pressure drop for gas transmission pipelines. This equation is ideal for estimating the expected lower velocity at the point of delivery.

$$Q = 435.7 * \left[\frac{T_{stp}}{P_{stp}} \right]^{1.0788} * \left[\frac{P_1^2 - P_2^2}{G^{0.8539} * T * L * Z} \right]^{0.5392} * D^{2.6182} \quad (2.2)$$

For both equations: Q is the gas flowrate (m^3/d); T_{stp} is the gas standard temperature (K); P_{stp} is the gas standard pressure (bara); P_1 is inlet pressure

of the gas (bara); P_2 is the gas outlet pressure (bara); G is the gas specific gravity (dimensionless quantity); T is the average gas temperature (K); L is the pipe length (km); Z is the average gas compressibility; and D is internal pipe diameter (m).

It is important to note the continuous pressure drop along the pipeline ($P_1^2 - P_2^2$) in both equations. Also, the flowrate is directly proportional to the pipeline diameter, and inversely proportional to the gas gravity, gas compressibility and the distance from the point of gas reception. Hence, higher gas flowrate is expected when the gas is less dense and optimum gas expansion possible in shorter pipelines with larger diameter. Implying further that for longer pipelines, the need to sustain the optimum capacity utilization to ensure flow assurance is obvious. Generally, the pressure drop in a gas pipeline is estimated from equation 2.3, below as provided in the literature (Mohitpour, Golshan and Murray 2007, p. 69).

$$\frac{P_{in}^2 - P_{out}^2}{L} = C * f * Z * T * \rho * \frac{Q^2}{d^5} \quad (2.3)$$

where the parameters are defined as follows: C is a constant ($5.7 \times 10^{-10} MPa/K$); d = pipe bore (m); f = Fanning friction factor; L is the pipeline length (m); P_{in} is the inlet pressure (MPa); P_{out} is the outlet pressure (MPa); Q is the flow rate at standard conditions (m^3/s); T is the gas temperature (K); Z is the gas compressibility factor; and ρ is the gas density at standard conditions (kg/m^3).

From equation 2.3, the gas pressure drop along the pipeline is a function of the pipe length, gas density, temperature, flowrate, pipe wall friction, and the pipeline diameter. Consequently, the relationship between the above parameters is important in assessing the expected flow behaviour downstream of the gas pipeline. Variations in pressure drop in the design of gas pipeline are mostly accounted for by the pipe roughness ratio and the friction factor (Coelho and Pinho 2007). This can explain why aged pipelines can experience higher pressure drops than newly installed pipelines, with implications on hydrates formation as the pressure drop is equally related to temperature drop, and especially for subsea gas pipelines.

Another important factor that can influence the pressure drop in a gas pipeline is the equation of state (EOS), because of the compressible nature of natural gas. However, empirical results indicate that pressure drop in gas pipelines are rarely altered by the equation of state (EOS) adopted in the design (Chaczykowski 2009). This is because gas pipelines are treated as non-isothermal systems to obtain a more accurate prediction of flow, because change in gas density in a non-isothermal scenario results in a higher temperature variation when compared with an isothermal scenario (Osiadacz and Chaczykowski 2001).

Implying that for gas pipelines operating in non-isothermal environment, there will be complexities in estimating the pressure drop. Thus, the effect of heat transfer on the flow mechanics in gas pipelines can influence the possibility of having hydrates blockage in the pipeline. Hence, there is the need for accurate measurement of the gas temperature, pressure and velocity (Thorley and Tiley 1987), based on the variations in topography along the pipeline route (Ibragimovna, Nikolaevna and Borisovich 2018). This can have implication on the flow regime present at every section of the gas pipeline. For instance, change in flow regime from stratified to slug flow during hydrates formation has been reported in the literature (e.g., Zerpa et al. 2013). For hydrates prediction, the flow is treated as incompressible as stated earlier, and equations 2.1, 2.2, and 2.3 can no longer hold.

This calls for an understanding of the actual multiphase flow regime(s) that can accurately define the formation of hydrates. Consequently, multiphase flow governing equations and physical models have been implemented in the prediction of pipeline hydrates in the literature (e.g., Balakin et al. 2010, 2016; Aman et al. 2018; Di Lorenzo et al. 2018; Liu et al. 2018; Berrouk et al. 2020).

2.4 The Formation of Natural Gas Hydrates

Hydrates are structurally ice-like and formed from a mixture of water and natural gas components (Carroll 2014). The hydrogen bond in water enables the molecules to form regular shapes and orientations. Water molecules serves as host for hydrates-forming gas molecules, which are also refer to

as guest molecules. Accordingly, hydrate crystals are three dimensional complex structures with guest formers trapped in the cage formed by the water molecules.

The stabilization of hydrates is possible because of the strong electrostatic van der Waals forces linking the molecules (Carroll 2014). Koh, Sloan and Sum (2011) explains that natural gas hydrates are “clathrates” formed in the cages of the network of water molecules that can trap small paraffins (e.g., methane, ethane, and propane) guest molecules. The dissociation of hydrates is also possible because there is no real chemical bond between the “host” and “guest” molecules in the hydrate crystal structure. Hydrates have been classified into “structures I, II and H” (Sloan 2011; Carroll 2014), as shown in **Figure 2.2**.

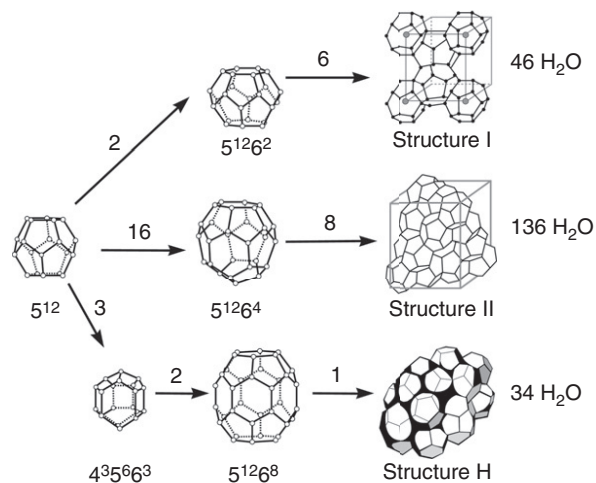


Figure 2.2:The three forms of hydrates crystals (Koh, Sloan and Sum 2011, p. 3). Structure II are formed in gas pipelines and it is the focus of this study.

Detail discussion of these structures is provided in the literature (e.g., Koh, Sloan and Sum 2011; Carroll 2014). Hydrates form in subsea pipelines because of instances of water entrainment in the gas stream, which can lead to the initiation and nucleation of hydrates in gas pipelines in colder environments. Hydrates deposition and blockage can damage natural gas pipelines from over-pressurisation of upstream facilities (Koh and Creek 2011; Carroll 2014) and internal corrosion at the point of nucleation (Obanijesu 2012). A typical cost implication from repairs and breach in gas sales’ contract because of hydrates is estimated at \$1,000,000 (Carroll

2014). Fatalities have also been associated with hydrates and their mishandling (Carroll 2014).

As indicated in the literature (Sloan and Koh 2007; Carroll 2014), hydrates are formed in natural gas-dominated pipelines at low temperature and high pressure in the presence of sufficient amount of free-water interface. Additionally, the right amount of turbulence from gas velocity and agitation, and the presence of nucleation sites such as elbows, tees, and valves can intensify the formation of hydrates in subsea pipelines and flowlines (Carroll 2014).

2.5 Flow Regimes in Horizontal Gas Pipeline

In gas-water multiphase flow, pipeline geometry affects mass, momentum and energy exchange among the phases because of the interfacial area created by the topology (Brennen 2013). The interfacial interaction can create shear stress and shear strain by modifying other flow characteristic such as velocity, enthalpy, and temperature. Hence, the starting point in multiphase modelling is the phenomenological description of the distribution geometry or flow pattern (Brennen 2013). The general multiphase flow regimes in a horizontal gas-water pipeline system are shown below:

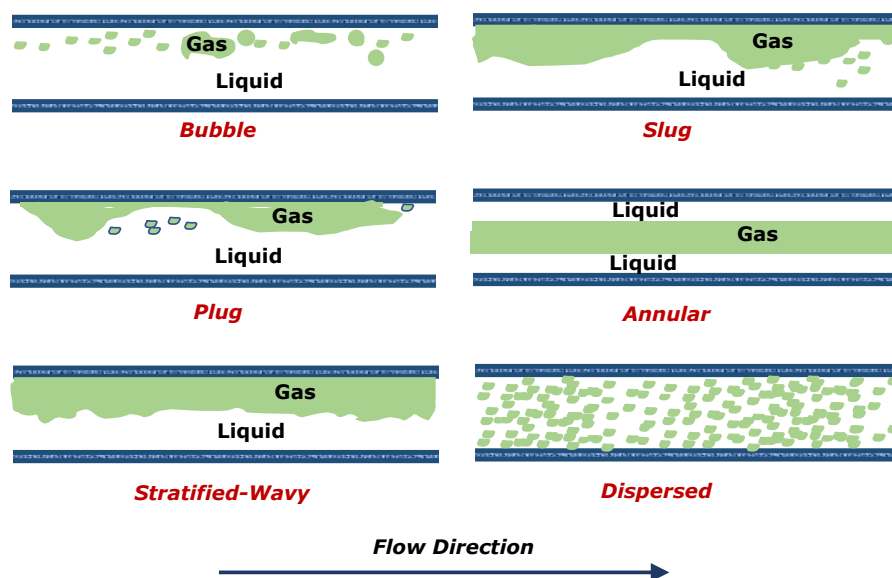


Figure 2.3: Horizontal cross-sectional flow regimes for gas-water mixtures in a pipe (Adapted from Brennen (2013)). Annular flow describes the multiphase flow pattern during hydrates formation in gas dominant pipeline.

The flow patterns in **Figure 2.3**, are discussed extensively in the literature (e.g., Baker 1954; Hubbard and Dukler 1966; Weisman 1983). Through experimental visual inspection, it is widely agreed that the flow pattern present in gas systems with liquid water dropout and a dispersed water-vapour phase is “annular-dispersed” (Sum, Koh and Sloan 2012; Di Lorenzo et al. 2014a; Aman et al. 2016).

In annular-dispersed flow, the gas flows at very high gas velocity along the centre of the pipe with water vapour droplets, while the liquid film flows at low liquid velocity in the form of annulus along the pipe wall. The stoichiometric chemistry reaction creates hydrates both at the core and at the wall (Wang et al. 2017, 2018). Thus, evidence in the literature indicates that hydrates annular dispersed flow pattern include light packing of hydrates at the core and a slowly moving bed of hydrates slugs at the wall (e.g., Hegde, Sum and Danielson 2015; Berrouk et al. 2020; Pickarts et al. 2020).

Finally, at the pipe wall, it is expected that wall friction will gradually lead to the hydrate bed becoming packed and immovable, where it will agglomerate to plug the pipe (Ding et al. 2017). The schematic provided by Charlton et al. (2018) is based on the suggestion of Lingelem, Majeed and Stange (1994) for gas-dominant pipelines did not represent the expected annular pattern of liquid on the pipewall as the settling of liquid due to gravity is typical of low velocity floe scenario. Hydrates deposition grows from the pipeline wall into the core, as corroborated in the literature (McMullen 2011). This understanding will guide the development of both the CFD and analytical models in this study.

The deposition of hydrates is higher in annular flow than in stratified flow (Ding et al. 2017), hence gas pipelines experience higher degree of hydrate blockage than oil pipelines. Although the subsea environment is undulating in nature, pipelines are installed in a horizontal profile to prevent flow assurance issues such as blockage by hydrates. Hydrate plugs are located near or at the base of the pipeline riser section because of the change in geometry and flow against gravity. This study focused on the horizontal

section of the pipeline because of the higher risk of hydrate deposition resulting from annular gas-water flow.

2.6 Hydrates Prediction in Gas-Dominated Systems

Earlier studies on the predictions and correlations of hydrates were based on thermodynamic calculations (Carroll 2014). The prediction of hydrates dates back to the 1930s when Hammerschmidt (1934) discovered the presence of hydrates in pipelines. A detailed historical overview of the methods and applications adopted to manage hydrates in flowlines are discussed in the literature (Sloan et al. 2011). The prediction of hydrates has been achieved through empirical thermodynamic correlations and mechanistic flow modelling equations to enhance risk management.

While the thermodynamic charts are useful for early estimation of formation temperatures and pressures based on variations in field compositions of hydrocarbon, there are wider error margins at higher pressures when compared with empirical results (Carroll 2014). The use of modern computers increased interest in computational fluid dynamics (CFD) through mathematical modelling of conservation equations, heat transfer phenomenon and flow kinetics. Gas hydrate growth kinetic models are discussed extensively in the literature (Yin et al. 2018).

Mathematical models define transient flow behaviour and have been receiving research interests. Earlier, Bisgaard, Sorensen and Spangenberg (1987) developed a mathematical model of partial differential equations for describing the unsteady flow of gas in pipelines using time-varying flow profile and pressure. Prior to this, Rudinger (1965) revealed a reduction in gas flow velocity during increase loading of particles in the flow domain. In line with Rudinger's suggestion, the formation of hydrate crystals in gas pipelines can aid the understanding of hydrates transportability.

The emphasis on a good correlation model is aimed at reducing dependence on laboratory predictions for higher temperatures and pressures, especially for high pressure high temperature (HPHT) flow scenario from reservoirs in deeper waters. There have been efforts in using machine learning such as

Support Vector Machine Regression (SVM) and Radial Basis Functions Neural Network (RBFN) in extrapolating the temperatures and pressures outside experimental results. These models have been used to predict results at temperatures of 299K to 340K outside experimental limitations (Ibrahim et al. 2016).

Mesbah, Soroush and Rezakazemi (2017) used the modified SVM – the Least Square Support Vector Machine (LSSVM), that was originally introduced by Suykens and Vandewalle (1999) to predict hydrates formation temperature (HFT). Genetic programming has also been used to aid prediction of HFT (Abooali and Khamehchi 2019). Similarly, there is growing interest in using mechanistic flow conservation equations in predicting the formation and growth of hydrates, as discussed extensively later.

For instance, Abbasi and Hashim (2014) obtained hydrates formation temperature and pressure through mathematical models that considered both convection and conduction heat transfer methods, and potential energy only. These approaches are mentioned here to underscore the growing research interest in hydrates prediction models in various fields of study. Recently, there has been a shift in interest from the above thermodynamic charts and analytical equations because they can only predict the temperatures and are unable to estimate transient growth of hydrates in pipelines. Thus, the emphasis on hydrates prediction multiphase studies in the literature will be discussed further.

2.6.1 Experimental Studies on Hydrate Prediction

Experiments remain the primary option for assessing the risk of hydrate formation under various operating scenarios, despite their limitations in terms of scope, size, and budget. Oduola et al. (2017) provided detail discussion on the series of flowloop experiments on the formation, agglomeration, and deposition of hydrates in gas-dominant systems.

The initial study in a series of recent flowloop experiments for the prediction of hydrates in gas-dominated systems is the study by Di Lorenzo et al. (2014a). During the experimental investigation, the growth rate of hydrates and the resulting frictional pressure drop were recorded on the Hytra gas-

dominant flowloop. The study involved six experiments at various subcooling temperatures within the 12 m length hydrate formation region. The feed into the loop consisted of natural gas, composed of 87.3% methane. All six experiments were conducted at gas superficial velocity of 8.7 m/s and water superficial velocity of 0.09 m/s. Water injection was maintained at 6% by volume. All experimental runs were halted at the set maximum threshold pressure drop designed for the flowloop.

Temperatures and pressures are measured at various points in the test section using intrusive resistance temperature detectors and pressure transmitters, which have been mounted inside measurement thermowells within the flowloop. Temperature and pressure measurement uncertainties are ± 0.27 °F and ± 3.9 psi, respectively. The results showed that the formation and deposition of hydrates increased the pressure drop between transducers located 33.4 m apart on the main test station. This was due to growing frictional resistance along the pipe wall as the flow became more viscous. Shear stress along the wall resulted in shedding and sloughing of hydrates until the line was packed with hydrate crystals.

The motivation for a similar experiment by Aman et al. (2016) was to explore the impact of lower gas flow velocity on the rate of hydrate formation. This need arose because Di Lorenzo et al. (2014a) had exclusively investigated hydrate formation and deposition at a higher velocity of 8.7 m/s. Understanding the parametric effect of lower gas velocity on hydrate formation and deposition in pipelines is crucial for enhancing flow assurance when gas production decreases, and the pipeline operates below its design capacity. Lowering gas velocity may result from integrity assessment studies on a pipeline to prevent pipe failure due to a reduction in wall thickness caused by internal corrosion.

The experimental setup mirrored that of Di Lorenzo et al. (2014a). Hydrate growth and particle deposition rates were investigated with variable liquid holdup ranging from 1% to 10% in volume and subcooling temperatures of 1-20°C. The findings revealed that reducing gas phase velocity from 8.7 m/s to 4.6 m/s at a constant subcooling temperature of 6°C led to a decrease in liquid entrainment and lowered the hydrate formation rate. Moreover, the

results indicated that the reduction in gas velocity increased the estimated rate of hydrate deposition on the pipeline wall by 50%.

As a follow-up on the work of Di Lorenzo et al. (2014a) and Aman et al. (2016), Ding et al. (2017) conducted a high-pressure flowloop experiment to investigate hydrate deposition mechanisms in different gas-liquid flow patterns. This flowloop was similar to the one discussed earlier by Di Lorenzo et al. (2014a). The test sections totaled 30 m in length, with an internal pipe diameter of 0.0203 m. The results indicated that annular-dispersed flow is more suitable for gas pipelines, as minimal hydrate formed in the bulk gas phase at the core. The authors concluded that hydrate deposition for all flow patterns follows the descending order: annular flow > slug flow > bubble flow > stratified flow. This finding aligns with the observations of Di Lorenzo et al. (2014a) and Aman et al. (2016), confirming that hydrates tend to form in an annular pattern in gas-dominated pipes.

In addition to the previous experiments, Zhang, Wu and Mu (2017) conducted some experiments to explain the influence of temperature on the spontaneous formation of methane hydrates under different stable temperature and pressure conditions. Subcooling occurred when vapour condensed on the outside wall of the pipe. Their observations aligned with the earlier findings of Turner et al. (2005), suggesting a direct connection between gas flow rate and gas consumption rate during hydrate formation in the fully condensed hydrocarbon phase. This observation facilitates the determination of the hydrate deposition rate on the pipe wall based on the density of hydrate in the hydrate-water composite, as applied in this study.

Again, the volume of the gas phase at standard temperature and pressure is concentrated in the deposited layer of hydrates by a factor of 180 (Sloan 2011). As a consequence, the density of gas increases towards the wall of the pipe where hydrates form. The results also indicate that the initial stage in hydrate formation involves nucleation and growth. It was reported that only the initial nucleation stage is positively influenced by the amount of pressurization in the system. Furthermore, hydrate deposition was found to be controlled by the system temperature, and the system temperature is

affected by heat transfer across the wall of the pipe into the surrounding environment through conduction.

In support of the findings from the aforementioned experiments, Odutola et al. (2017) conducted an investigation into hydrate formation in a gas-dominated system using a flowloop at the University of Port Harcourt, Nigeria. The flowloop comprised a 12 m length and 0.5-inch diameter, utilizing a 316 stainless steel pipe enclosed in an insulated 4-inch Polyvinylchloride (PVC) pipe to minimize heat loss to the environment. Their experimental pressure and temperature plots effectively illustrated the theory of hydrate formation and agglomeration. Additionally, this literature extensively discusses other existing flowloops used for hydrates and multiphase experiments.

In the experimental research conducted by Liu et al. (2020), the authors monitored variations in pressure drop from the initiation of hydrate formation to deposition and bedding. This was done across various liquid-water loadings and gas-water multiphase mixture velocities, while also observing the flow patterns throughout the experiments. The findings revealed that the flow of hydrate slurry may encompass four stages: hydrate formation, agglomeration, deposition, and bedding, preceding the eventual blockage of the pipeline. The work of Liu et al. (2020) served as the foundation for superimposing the pressure results onto the simulated hydrate profile graph in this PhD study, enabling the prediction of hydrate deposition.

In summary, the key findings from the above experiments are as follows: (i) Hydrates can form in gas pipelines under specific temperature and pressure conditions; (ii) The experiments yield numerical values that can serve as validation for both Computational Fluid Dynamics (CFD) and mathematical/analytical models predicting hydrate growth in gas-dominated pipelines; and (iii) Accurate calculation of hydrate growth relies on precisely estimating the total interfacial area between the continuous gas phase and the entrained water phase, as well as between the gas in the continuous phase and the water phase at the pipe wall.

2.6.2 Analytical Hydrates Prediction Models

Recent mathematical models on hydrate growth in gas-dominated systems have indicated the need for a more accurate model (Khan, Warriar and Koh 2023). Turner et al. (2005b) developed a hydrates kinetic model that demonstrated predictions of hydrate formation results closely matching experimental values more than any other previous model.

Wang et al. (2017) demonstrated the influence of entrained liquid in the gas phase on hydrate deposition in a gas-dominated system with free water. The rationale for the research was that previous mathematical models had primarily focused on hydrate formation and growth from the liquid film on the pipe wall. The proposed model comprises three sub-models: hydrate formation, hydrate deposition, and hydrate layer growth. These models were employed to analyze the annular-mist flow pattern in the gas pipeline, illustrating the relationship between hydrate formation and deposition. The level of liquid entrainment was estimated using the correlation developed by Pan and Hanratty (2002).

The findings indicate that the formation rate of hydrates is higher in the gas phase with entrained liquid than from the liquid film on the pipe wall. This was due to higher interfacial area of contact between the guest (gas) and the host (water), especially with liquid film atomization which create turbulence at the interface between the dispersed water in gas pipelines (Wang et al. 2017). Also, the hydrates formation sub-model was able to predict the experimental observations discussed earlier that the formation of hydrates increases as the subcooling temperature decreases. However, this study was only conducted for higher gas velocity of 8.6 m/s. There was still a gap to develop an analytical model that can compare with experimental outcomes at lower gas velocity. Already, Aman et al. (2016) had provided experimental results at low gas velocity of 4.6 m/s that can be used for the validation of analytical models for this gas velocity.

Di Lorenzo et al. (2018) developed another analytical model based on their earlier single pass gas-dominant flow loop experiments (Di Lorenzo et al. 2014a; Aman et al. 2016). This analytical model was aimed at predicting

hydrate deposition and sloughing in gas-dominated pipelines, as well as to predict pressure and temperature profiles along a horizontal pipeline during normal operation in the presence of a mono-ethylene glycol (MEG) inhibitor. A classical hydrate kinetic model was combined with a simplified two-phase flow model for pipelines to calculate the growth rate of hydrates in the gas pipelines. This model was able to predict hydrate formation and deposition at high and low gas velocities within 40% and pressure drop within 50% of experimental results over the same subcooling temperature ranges. Thus, there is need for a model that can improve on the above predictions and reduce the wide variation between experimental and model predictions for proactive plugging risk prevention intervention.

Wang et al. (2018) modelled the growth of hydrates in a horizontal gas-dominated pipeline with free water. Previous studies on the growth of hydrate layers focused enormously on a single-flow pattern which is predominantly gas and hydrates. The mechanistic flow patterns investigated in the study were considered as coexisting at different segments of the pipe: gas-liquid-hydrate; gas-hydrate; and water-saturated gas. Also, a key assumption was that the growth rate was uniform throughout the length of the hydrate formation section of the pipe for the three stages investigated. The weakness of this assumption is that it can lead to inaccurate estimation of the mass deposited at the initial point of deposition. The results show that accurate estimation of hydrate growth must consider the hydrate formation from both the water entrained in the continuous gas phase and the hydrate crystalizing from the liquid phase at the pipewall, else the hydrate calculated will be smaller than actual volume of hydrates in the pipeline. However, the three above phase change and flow pattern were not validated with experimental results.

A most recent analytical model discussed in this literature review was proposed by Liu et al. (2019). In this model, the effect of hydrate shedding was considered with the assumption that the shear rate of the hydrate bed along the wall of the pipe during sloughing is not constant. Earlier, Di Lorenzo et al. (2018) had proposed a model where the shear stress during hydrates sloughing was assumed to be constant. Also, the iteration method was

implemented to calculate temperature, pressure, and hydrate formation to enhance the accuracy of the results at a gas velocity of 8.6 m/s. The model was validated with existing gas-dominated pipeline experimental data from Di Lorenzo et al. (2014a), with hydrate formation volume deviation error of 0.01 L/min. However, the model was not validated for lower gas flow velocity.

In summary, accurate analytical models have been developed in line with the mass, momentum, heat transfer, and kinetic growth equations for predicting hydrate formation in gas pipelines. However, none of the above models directly incorporated the hydrate deposition rate in the pressure drop equation. This type of model can enhance the prediction of hydrate plugging risk by determining the expected volume of hydrates in the pipeline directly from pressure drop readings. Thus, a new analytical model addressing this need will be developed in this study.

Application of CFD Modelling in Hydrates Prediction

The complexity of multiphase flow assurance problems often requires the use of advanced computational and experimental methods to solve the equations that describe the flow mechanism. Davarnejad (2014) demonstrated that Hysys can predict corresponding hydrate formation temperatures over a range of experimental pressure values, with maximum absolute error of 1.07% for the Salman gas field. This was achieved by incorporating the Peng-Robinson equation of state as the steady state package in Aspen Hysys. Also, Odutola and Ugwu (2019) conducted a simulation in Aspen Hysys based on the experimental setup in Odutola et al. (2017). However, no hydrate was formed from their observation, as it was unable to predict the true state of the kinetics reaction to form hydrates in the flowloop.

Additionally, using OLGA® software multiphase simulator, Charlton et al. (2018) simulated hydrate growth and transportability in gas-dominant flow based on experimental findings of Di Lorenzo et al. (2014a). However, the results from the hydrate simulator in OLGA® under-predicted the average pressure drop by approximately 15% and did not compare favourably with experimental hydrate formation reports. An identified gap is the need for accurate internal convective and conductive heat transport coefficients that

account for hydrate growth on the pipe wall, which was not possible with OLGA®. One major outcome of this research was the development of an in-house kinetic growth model for hydrates.

Unlike CFD packages such as ANSYS, the simulator software packages above were unable to show transient hydrate formation contour along the pipe. Literature evidence demonstrates that CFD software can be used to model the conditions for multiphase flow through numerical volume cell computation. For instance, Balakin et al. (2016) investigated CFD modelling of hydrates in a turbulent oil-dominated flow.

A population balance method (PBM) was used to establish the rate of hydrate agglomeration and deposition. The methods adopted comprised of the following stages: (i) determination of the apparent viscosity of the hydrate-water-oil interface using the Colorado School of Mines Hydrate Kinetics (CSMHyK) rheological model; (ii) determination of the effective volume fraction of hydrate agglomeration; and (iii) development of the Eulerian-Eulerian model for the three equations of continuity, momentum, and energy, and coupled with the PBM model solved numerically in "STAR-CCM" (a commercial CFD package). Good meshing and 25% refinement near the wall were to ensure early prediction of formation from the hydraulics simulation at the viscous sublayer. The model was validated with experimental data sets from the literature. A major finding is that agitation and turbulence reduced the formation of hydrates, also corroborated in Sule et al. (2015). Similarly, the findings reveal that while heating tends to reduce hydrates formation, it increases the adhesive force between hydrate crystals. However, this CFD model is for oil-water system, but indicates the possibility of using CFD in modelling hydrates formation.

In gas-dominated pipelines, hydrate deposition on the pipeline wall has been confirmed based on the earlier experimental observations. This is because the annular flow pattern of the gas-water interface promotes the formation of hydrates from 85 mole % water and 15 moles % gas (Sloan 2011). Thus, for a gas-dominant pipeline, the formation of hydrates stops in the absence of water. This occurs because gas hydrate nucleation is consistently observed at the vapour-liquid interface (Khan, Warriar and Koh 2023). The annular-

dispersed multiphase flow for gas-dominant system is modelled using the Eulerian-Eulerian frame and a finite volume method discretization.

A review of research effort on hydrates prediction using CFD software up to 2015 is discussed extensively in the literature (Balakin et al. 2016; Neto et al. 2016), indicating that no CFD model is yet to accurately replicate experimental data for hydrate deposition rates. The review below focuses on research publications on CFD application in hydrate prediction for gas-dominated systems from 2016 to 2019. Earlier, Naseer and Brandstätter (2011) modelled hydrate formation in a gas pipeline using ANSYS fluent, a commercial CFD package. The model was also not validated because of lack of relevant experimental data as at the time until the experimental reports of Di Lorenzo et al. (2014a).

Neto et al. (2016) developed a CFD hydrate prediction model using ANSYS CFX with a 5 m length and 0.381 m diameter straight pipe, with mixed flow of methane gas and water at a subcooling temperature for hydrate formation equilibrium based on the selected operating pressure obtained from the correlation proposed in Sloan and Koh (2007). Adopting the stoichiometric reaction equation, hydrate formation was assumed to stop once the gas becomes the limiting reactant in the presence of excess water. The contour CFD profiles indicates that hydrates were crystalized from the liquid phase which settled at the bottom of the pipe wall due to density difference and gravity. Also, due to the presence of turbulence, the liquid phase spread evenly circumferentially around the inner pipe wall with some entrained water droplets in the gas phase, hence showing that flow is combined annular and dispersed pattern prior to pipe plugging by hydrates. This CFD model was not validated with existing empirical results.

Moreover, the findings that hydrates formation was limited by gas (methane) availability is in line with the experimental findings of Aman et al. (2016), discussed earlier. Hence, this work shows that ANSYS CFD can be used to model hydrate formation in transient flow condition. Recently, Ma et al. (2024), simulated a CFD deposition modeling experiment involving the use of hydrates as a discrete phase. However, there remains a requirement for

a deposition rate without the use of an externally injected discrete phase. With no success yet in using CFD to accurately predict hydrate deposition rates, current interest has shifted to using CFD to model hydrate slurry transportation in water-dominated gas pipelines (e.g., Berrouk et al. 2020).

2.6.3 Regression Modelling of Hydrates Deposition Rate

Experimental, analytical and CFD approaches have provided the basis for understanding the flow parameters influencing the deposition rates of hydrates in gas pipelines through parametric analysis of the influence of subcooling temperature, water volume fraction, gas velocity and pipeline diameter on hydrates deposition rate. Therefore, it is possible to formulate a multiple linear regression model where hydrates deposition rate is the dependent variable. Although, no previous hydrates-related regression models studies have predicted hydrates deposition rates, there are literature evidence of employing machine learning regression modelling to predict hydrate formation equilibrium temperature and pressure (e.g., Baghban et al. 2016; Ibrahim et al. 2016; Mesbah, Soroush and Rezakazemi 2017; Aboali and Khomehchi 2019; Landgrebe and Nkazi 2019; Cao et al. 2020). The multiple regression approaches implemented in the cited literature include the use of support vector machine (SVM), least square support vector machine (LSSVM), and genetic algorithm (GA).

Recently, hydrate volume fraction was predicted using regression modelling (Qin et al. 2019). Again, Yu and Tian (2022) adopted Random Forest, Naive Bayes, and Support Vector Regression to determine hydrates formation condition for pure and mixed hydrates forming gases. Also, the accuracy of machine learning classification models requires huge amount of data for testing and validation which is difficult to achieve. However, no regression modelling approach has been adopted to predict deposition rate of hydrates in gas pipeline. Regression modelling is implemented when the data to be observed cannot be easily measured from the field, and this is applicable to measuring the deposition rate of hydrates in industry scale gas pipeline.

The deposition of hydrates have been reported in gas pipelines that were shut down due to unforeseen operational problems without the need to depressurise the line (Jamaluddin, Kalogerakis and Bishnoi 1991; Bai and Bai

2005; Ballard, Shoup and Sloan 2011), at the point of excess water at the low-lying point of the pipeline where the injected methanol can become diluted leading to formation of hydrates (Sloan, Koh and Sum 2011b). However, it is not possible to simulate this condition using CFD by making the gas flow velocity “zero.” Hence, with a multivariate regression model including velocity as an independent variable, the deposition rate can still be predicted by zeroing the velocity term.

2.6.4 Prediction of Hydrates Plugging Event Location

The detection of blockages along pipelines is a challenging problem and has received considerable attention in literature (e.g., Adeleke, Ityokumbul and Adewumi 2013; Besancon et al. 2013; Srour, Saber and Elgamal 2016; Stewart and Jack 2017; Jafarizadeh and Bratvold 2019; Yang et al. 2019; Abdullahi 2020; Razvarz, Jafari and Gegov 2020). However, blockage location detection techniques from flow transients using time domain or frequency domain analysis proposed in the above literature are not suitable for real-time detection of hydrate plugs in gas pipelines for the following reasons.

The first approach is the pressure wave using time domain analysis, which depends on the determination of acoustic velocity from the time of flight of the pressure disturbance in the fluid medium (Chen et al. 2007; Adeleke, Ityokumbul and Adewumi 2013; Stewart and Jack 2017). In this approach, gas is propagated from the receiving facility, located downstream of the blockage, to the surface of the blockage. The time of flight is the total time from when the pressure signal was sent to when the reflected signal from the surface of the blockage was received. However, the acoustic velocity is affected by the pipeline internal diameter and wall thickness. During hydrates deposition the pipeline hydraulic diameter varies linearly along the hydrates section, hence the uniform ratio of pipeline internal diameter to the wall thickness in the acoustic velocity equation proposed by Stewart and Jack (2017) is not suitable for the detection of hydrate plug location.

In a similar pressure-time approach (Besancon et al. 2013), the detection of plug location is based on finite difference discretization of the velocity field, where the time to experience the first significant pressure fluctuation is

related to the fluid velocity to obtain the distance of the blockage from the inlet. The length of the blockage is estimated from the time when the first transient rise in pressure was detected to when the signal decayed to "zero." The model was developed for liquid flows and did not consider the temperature and pressure dependent fluid parameters such as density and viscosity of gas. Viscosity effects influences the prediction of blockage severity in gas pipelines (Adeleke, Ityokumbul and Adewumi 2013).

A second approach is the pressure wave that uses frequency domain analysis method (e.g., Mohapatra et al., 2006). By assuming a sinusoidal behaviour of the pressure and flow velocity, the time domain in the pressure wave analysis method above is converted into frequency domain to estimate the blockage location from the observed amplitude of the disturbance injected into the fluid domain. The blockage location is estimated from a relationship of the fluid velocity, frequency, number of peaks, and length of the pipe (Chaudhry 1979; Mohapatra et al. 2006; Datta, Gautam and Sarkar 2018). Again, the frequency domain approach requires an external fluid disturbance to create a reflected signal off the surface of the partial blockage. An approach that can lead to accidents in locating hydrates plugs if the pipeline pressure is not adequately depressurised before injecting the flow disturbance.

A third approach is based on the detection of blockage location from the prediction of wall shear stress (Srouf, Saber and Elgamal 2016). In this approach, a small sinusoidal disturbance is introduced to the original flow from an external source at the inlet to create time changes in the velocity field and wall shear stress. This nature of sinusoidal disturbance will have little effect in detecting hydrates plug location because of the higher pressure and non-steady flow in gas pipelines. However, the approach of identifying blockage from pipewall shear stress was adopted in this work to determine the effect of pipewall shedding stress during hydrates deposition.

The experimental and computational fluid dynamics (CFD) model by Yang et al. (2019) suggests that pressure drop increases as the blockage location increases along the pipeline. Transient pressure-drop fluctuations during hydrates deposition and pipe plugging can lead to pipeline rupture (Di

Lorenzo et al. 2014a; Aman et al. 2016; Zhang et al. 2019). Therefore, accurate prediction of the hydraulic effect of hydrate deposition and plug location is critical to the safety and operability of natural gas transport pipelines, especially for subsea gas transport pipelines where maintenance and intervention activities are more difficult. One of the limitations of existing blockage location models is based on the need to introduce a pressure signal downstream of the blockage from an external source (Adeleke, Ityokumbul and Adewumi 2013). An approach that is not suitable for hydrates forming pipelines because of possible accidents that can occur when the upstream and downstream pressures are not balanced.

Another limitation of existing pressure-wave blockage location models is that the reflected pressure wave from the surface of the hydrates is affected by the viscosity of the gas phase because of the drop in temperature, thus affecting the time of flight used in estimating the location of the hydrates plug from the acoustic velocity of the gas (Adeleke, Ityokumbul and Adewumi 2013; Abdullahi 2020). Consequently, for hydrate forming pipelines where the temperature at the hydrates surface is colder, the time of flight will be affected by the return pressure wave.

2.7 Hydrates Plugging Risk

The consequences of hydrates plugging in pipelines are always high, hence the plugging risk mitigation is only addressed by assessing the likelihood of occurrence. Three risk levels have been suggested in the literature (Zerpa et al. 2012), based on the ease of transportability to the riser as follows: (i) low-risk (easy flowing slurry), when the pressure drop is less than 2 MPa (300 psi), hydrate volume fraction is less than 0.10 and when the hydrates slurry viscosity is less than 10; (ii) intermediate-risk (slurry flow can be hindered by restrictions or change in pipe geometry leading to line plugging), when the pressure drop is less than 3.45 MPa (500 psi); hydrate volume fraction is greater than 0.1 but less than 0.40 and the hydrates slurry viscosity is greater than 10 but less than 100; (iii) high-risk (highly viscous flow and easily plugs line) - when the pressure drop is greater than 3.45 MPa (500 psi); and (iv) hydrate volume fraction is greater than 0.40 and the hydrates slurry viscosity is greater less than 100.

The definition of risk in the literature is for oil and condensate lines and the need to expand hydrates blockage predictions to gas transport pipelines is still being advocated (Zhang et al. 2022b). A recent investigation suggests that increase in slurry flow velocity increases the wavy flow pattern in the pipeline (Lv et al. 2023). This suggests the difficulty of flowing hydrate slurry at higher velocities, ultimately resulting in a significant reduction in the economic capacity of the pipeline. Another recent study (Zhang et al. 2023), equally concentrated on depositional profile and not the deposition rate.

Consequently, the current study has improved on the above approach by considering the effect of hydrates-induced transient pressure drop on the design pressure of the pipeline to prevent pipeline burst. Classifying plugging risk based on the above three conditions can be addressed from the estimation of plugging flowtime and the first significant transient pressure drop for the specific gas pipeline. Thus, both flowtime and pressure drop estimation forms the basis for the risk regime adopted in this work.

2.8 Computer Program for Predicting Hydrates Plugging Risk

Merey and Sinayuc (2016) developed a MATLAB code for easily predicting the properties of hydrates using the formulas of Mann et al. (1989). The code was developed for each of the properties investigated (e.g., molecular weight, density, enthalpy of hydrate dissociation) using reservoir condition. The results revealed the ease of using computer programming codes such as MATLAB in modelling hydrate prediction equations with reliable accuracy. The study have also adopted this line of reasoning in providing a MATLAB program for predicting hydrates plugging risk from the equations developed in this study. He (2022) developed extremely randomized stochastic hydrate formation temperature prediction model using 1000 experimental data points. However, this model is unable to predict the expected hydrates plugging time, pressure drop and transportability.

Other recent studies where computer programming was adopted in the prediction of hydrates formation conditions include neural network modelling in the literature (El-hoshoudy et al. 2021; Nasir et al. 2022). As a gap, there is no computer program developed for estimating the plugging risk of

hydrates in gas-dominated pipelines by combining the flowtime for hydrates plugging event, pressure drop and the transportability of hydrates. This kind of approach can provide a detailed report of hydrates plugging risk and the urgency of intervention.

2.9 Theoretical Implications for Current Study

The modelling of hydrates formation in gas pipelines is governed by theoretical assumptions. The knowledge of the physics of fluid mechanics and various mechanistic flow pattern and regimes are important in explaining the process of formation, deposition, sloughing, and pressure drop. Hydrates formation is a multiphase phenomenon under certain conditions which can be modelled based on the crystallization theory, two-film theory for the gas absorption into the liquid phase (Englezos et al. 1987) and nucleation theory (May et al. 2018). The gas pipeline system creates the necessary reactor, and the turbulent flow is likened to a continuous stirring of the gas and water mixture for hydrate formation (Meindinyo et al. 2015). Other flow parameters are explained from the physics of Newtonian and non-Newtonian fluids, pressure drop due to obstruction, and pipewall shear stress and friction.

Though, experimental models explains the theory of hydrates formation, sloughing and pipe blockage, they are limited to the size of pipe used and results can hardly be extrapolated for other sizes of pipelines. Equally, as seen in the discussion on analytical models, the results are yet to accurately agree with experimental data, though able to represent theory mathematically. CFD software are coded from analytical models, however the ability of computers to handle high volume of discretisation is exploited to provide results that can possibly match experimental outcomes. Until now, there is no CFD model as at the time of this study that has accurately predicted experimental hydrates deposition rates for gas pipelines at lower gas flow velocity. This is critical to pipeline safety as more wells are quitting and pipelines are operated below design capacity.

In all, the theory of hydrates formation in gas system is well represented in all the hydrates prediction models. What is left is how both analytical models

and CFD models can accurately predict experimental results. This PhD work closes the gap identified above by providing a CFD model that improves hydrates deposition rates prediction when compared with existing analytical models and an analytical model to predict pressure drop and hydrates plug time by directly incorporating the CFD predicted hydrates deposition rates. Other outcomes of current research include clearly explaining pipewall shedding by hydrates, regression modelling of the deposition rates of hydrates, plugging risk definition based on pipeline design pressure and a MATLAB program for estimating the plugging risks of hydrates from the mathematic relations developed in this study.

The summary of the theories developed from this literature review and employed in this research is presented below.

- a. Gas solubility in water increases below the hydrate equilibrium temperature (Lekvam and Bishnoi 1997; Pruteanu et al. 2017). Hydrates are formed at the gas-water interface (Sloan 2011), hence the cooling effect of water on the gas at the pipe wall encourages the formation of more hydrates. This provides the basis for understanding the effect of subcooling temperature on hydrates formation.
- b. The presence of water in gas, and the deposition of hydrates results in dispersed annular flow pattern (Di Lorenzo et al. 2014b, 2014a). A tapering annular flow pattern was one of the observations expected from the CFD contour temperature profiles needed to validate the simulation.
- c. Higher hydrates formation risks are possible in gas-dominant pipelines because of lower volume fraction of liquid water (Sloan, Koh and Sum 2011a). The experiments used for validation used 6% water volume fraction and was adopted in the CFD model for this study.
- d. Increase in turbulence increases hydrates formation rate (Carroll 2014; Aman et al. 2016). It is expected in this study that as the flow velocity increases, the CFD model should predict increasing hydrates formation and deposition rates.
- e. Hydrates formation, agglomeration and deposition are instantaneous at the right temperature, pressure and flow condition (Lingeleem, Majeed and Stange 1994; Turner et al. 2005). Thus, the formation

and agglomeration of hydrates are characterised by phase change and can be measured by the gas flowrate in the fluid domain. Hence, the CFD model developed in this study should record increase in pressure and a lowering of the temperature early in the simulation.

- f. Eulerian-eulerian CFD framework is most adequate for accurate interfacial interaction (Neto et al. 2016; Berrouk et al. 2020). This theory was adopted in this study to enhance gas-liquid interfacial interaction for hydrates formation at the core and at the pipewall.
- g. Hydrates concentrates the volume of the gas phase by a factor of 180 relative to the volume at standard temperature and pressure (Sloan 2011). Hence, the density of gas is expected to increase towards the wall of the pipe where the hydrates are formed and deposited in this study. This also explains why hydrate layers grows from the wall towards the core of the pipe.
- h. Experimental results suggest an increase in gas flowrate during hydrate formation because of the increase in gas consumption rate (Turner et al. 2005; Odutola et al. 2017). Also, the gas flowrate is relatively stable during agglomeration (Odutola et al. 2017) and decreases during hydrates deposition because of the reduction in pipe hydraulic diameter (Aman et al. 2016). This understanding aided the identification of hydrates formation rate, agglomeration rate and deposition rate. The superimposition of the pressure profile on the experimental temperature will be compared with the outcome in Liu et al. (2020) for a close match as evidence for validating the CFD model.

Thus, the CFD and analytical modelling approach adopted in the current study is premised on the work of Neto et al. (2016) and Di Lorenzo et al. (2018), respectively.

2.10 Gaps in Current Knowledge and Justification for Research Objectives

The contributions to knowledge in this work are based on addressing the literature gaps identified in the literature review.

- i. Existing analytical hydrates deposition rate model is not sensitive to low gas velocity, hence exposing the pipeline under this operating scenario to hydrates plugging risk. This gap was closed using CFD modelling approach. Details are presented in chapter 4.
- ii. Shear stress profile along the pipe during hydrates formation and deposition not available in existing literature. This kind of profile can help to map the section of severe internal corrosion along the pipeline. This gap was also closed using CFD modelling approach and discussed in chapter 5.
- iii. There is no model yet for predicting hydrates deposition rates during shutdown scenario. Predicting hydrates deposition during shutdown can provide the optimum time for intervention before start-up to prevent hydrates from plugging the pipeline. This gap was closed using regression modelling approach in chapter 6.
- iv. There are no existing predictive models for detecting the location of hydrate plug in gas pipelines. The proactive detection of plugging event location through pressure drop can inform the decision for early intervention and prevent damage from hydrate-induced accidents to the pipeline and topside/surface facilities. This gap was closed using analytical modelling approach. Details of the approach adopted in this study is presented in chapter 7.
- v. There are no plugging risk criteria for gas lines with emphasis on the maximum operating pressure of the pipeline. This risk classification can be helpful in determining the pipewall thickness to overcome the pressure rise in the pipeline during intermittent hydrates plugging events. The detail of this study is presented in chapter 8.
- vi. There is need to develop a computer program that can estimate plugging risk based on hydrates deposition rates and pressure drop. The existing program can only estimate hydrate forming temperatures. This kind of program can provide a one-page handy report for intervention planning and schedules, and a means for ranking hydrates forming pipelines based on plugging severity. To close this gap, a MATLAB program has been developed in this study and presented in chapter 9.

Furthermore, the research objectives were formulated to address the abovecritical gaps identified in existing knowledge and practices related to hydrate management in subsea gas pipelines.

Objective i: Existing analytical models lack sensitivity at low gas velocities, leaving pipelines vulnerable to hydrate plugging under such conditions. This objective utilizes CFD modeling to address this gap and provide accurate hydrate deposition rate predictions under various velocities. This objective is fulfilled in chapters 4.

Objective ii: Existing literature lacks information on shear stress profiles during hydrate formation. By implementing CFD modelling (Chapter 5), this objective aims to identify sections prone to severe internal corrosion due to hydrate formation. No prior model exists to predict hydrate deposition rates during shutdown scenarios (critical for intervention planning). This objective fills this gap by developing a regression model (Chapter 6) to predict deposition rates during shutdown, enabling optimal intervention timing to prevent pipeline plugging. Current methods lack the ability to establish hydrate plug location. This was achieved using the developed pressure drop model in chapter 7.

Objective iii: Existing risk criteria do not consider maximum operating pressure for gas lines. Developing risk criteria based on this factor would inform pipe wall thickness design to withstand pressure fluctuations during hydrate plugging events. This was achieved in chapter 8.

Objective iv: While existing programs estimate hydrate formation temperature, a more advanced program could assess plugging risk based on deposition rates and pressure drop. Developing a MATLAB code user-friendly program could provide valuable insights for intervention planning and pipeline risk ranking. This was achieved in chapter 9.

2.11 Summary of Literature Review

The importance of predicting hydrate plugging risk, especially in gas-dominated pipelines, has been a major focus of research efforts, as highlighted in this literature review. This emphasis stems from the significant challenges hydrates pose for safe and efficient pipeline operation. This study

aims to bridge the gaps identified in current knowledge by setting clear objectives outlined in Chapter 1. Chapter 3 will then delve into the specific methodology employed to address these identified gaps. By detailing the approach taken, Chapter 3 will provide a roadmap for understanding how this study tackles the limitations in hydrate plugging risk prediction for gas pipelines.

CHAPTER 3: STUDY DESIGN/METHODOLOGY

3.0 Preamble

A positivist cause-effect quantitative study is adopted, involving three modelling methods: CFD, regression and analytical techniques. The regression and analytical techniques addressed the challenges of micro to macro scale CFD modelling to reduce computational demand and higher pressure drops in the CFD simulation of large-scale pipeline sizes. Adopting a 3D pipe configuration over 2D for the CFD model offers the opportunity to visualize the annular flow pattern of the gas-water interface, as suggested in the literature (Wang et al. 2017).

The adopted research approach is presented in **Figure 3.1**. For each approach, an overview of the methodology adopted will be provided, while detail methodology in each case will be discussed in chapters 4 and 5 (CFD modelling), chapter 6 (regression modelling) and chapter 7 (analytical modelling). The analytical and mathematical relations developed in the adopted methods above will be coded in MATLAB to provide a handy one-pager report on hydrates plugging risk. In this section, the analysis and discussion of the rationale for adopting this investigative methodology will focus on the theory, model development, data collected, and approach to data analysis. The modelling assumptions are provided for each section.

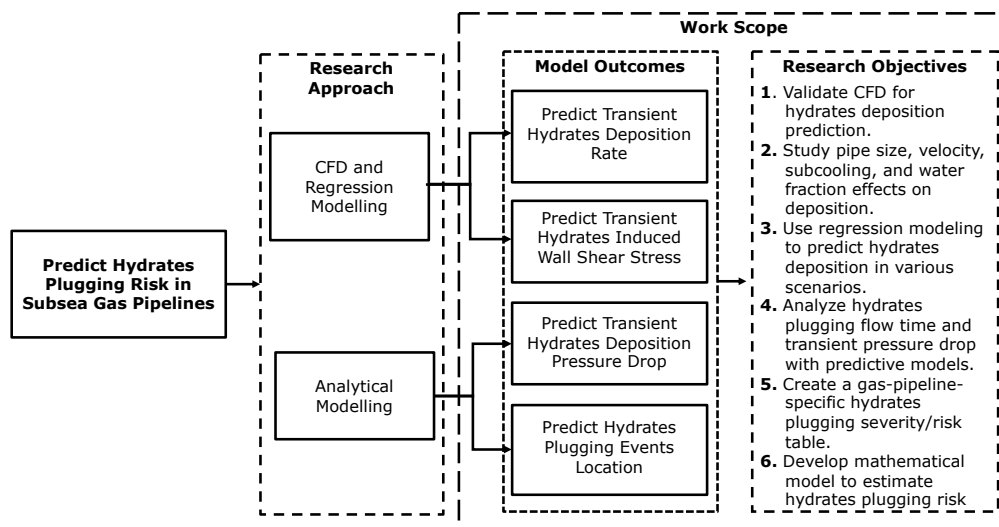


Figure 3.1: Research work scope and methodology

3.1 CFD Modelling Methodology

Theoretically, CFD models employ the principles of the Navier-Stokes equations and used to simulate the interaction of two or more matter existing together with thermodynamically different phases and their surfaces defined by boundary conditions. There are several CFD modeling software options available, such as OpenFoam, COMSOL Multiphysics, SimScale, and ANSYS Fluent.

In a comparative study of the performance of three CFD software packages—ANSYS Fluent, Star-CCM+, and OpenFOAM—against experimental results on water impingement flow from the literature (MacKenzie et al. 2015), the results suggest that OpenFOAM and ANSYS Fluent performed more favourably compared to Star-CCM+ when compared with the experimental result. In a different study (Li 2015) on simulating indoor thermal comfort using CFD software such as ANSYS Fluent, StarCCM+, and IESVE Microflo, the results indicated that IESVE Microflo demonstrates less precision, reduced accuracy, and increased simulation time for CFD modelling when contrasted with ANSYS Fluent and Star-CCM+. However, ANSYS Fluent was adopted in this study because the researcher is familiar with the software. Where applicable, the set up in the adopted software will be provided and explained.

This study simulates the thermodynamic interaction between natural gas and water under hydrates forming boundary conditions of temperature, pressure, flow velocity and water volume fraction. The flow-domain was set up to predict hydrates deposition rate based on the principle of increased solubility of methane gas in water at elevated operating pressure and lower temperatures. The main model is a horizontal pipe with diameter of 0.0204 m and length of 10 m. Parametric analysis was performed to investigate hydrate formation with extended pipe diameter by multiplying the original diameters with factors of 2 and 3 as the case requires. The stages adopted in the development of the CFD model is presented below, and the detail of each stage as applicable is discussed later.

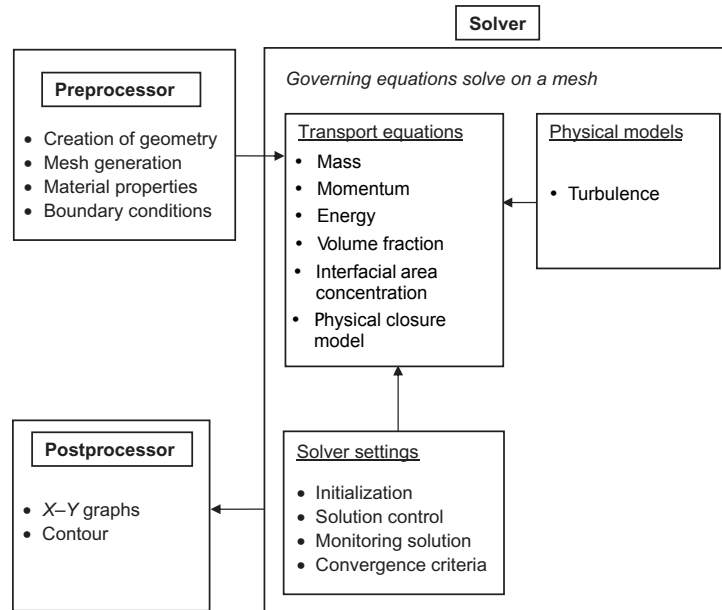


Figure 3.2: Adopted CFD framework (Adapted from Tu, Yeoh and Liu 2018, p.35)

The flowchart in **Figure 3.3** outlines the computational process for predicting hydrate deposition rates in a subsea pipeline using ANSYS FLUENT, incorporating a User-Defined Function (UDF) within a multiphase Eulerian-Eulerian framework and employing the pressure-velocity phase coupled SIMPLE algorithm.

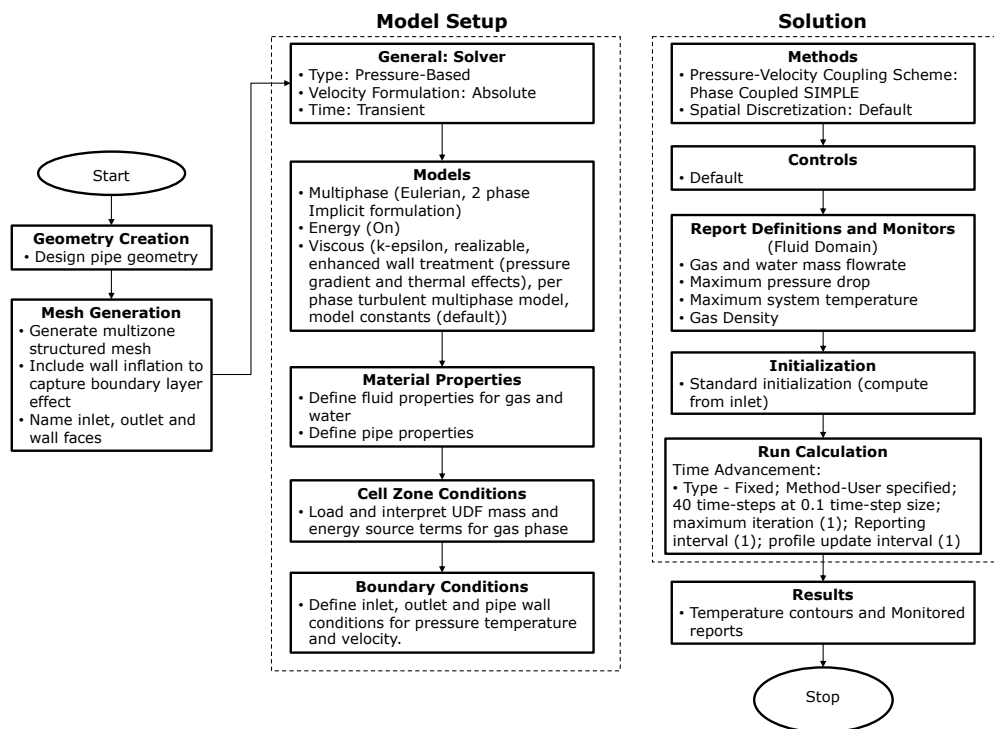


Figure 3.3: Computation Process

3.1.1 CFD Model Development

The main assumptions in the development of this model are as follows. (i) One simplifying assumption of the analytical model by Di Lorenzo et al. (2018) is that the compositional changes in the gas phase during the formation of hydrates was not considered. This can affect the prediction of hydrate deposition under different conditions of gas velocity and subcooling temperature. Instead, the authors adopted an empirical hydrate deposition tuning parameter which was not sensitive to changes in subcooling temperature at low gas velocity.

To overcome this challenge, this study introduced mass and energy UDF codes into the software to ensure that the gas flowrate in the fluid domain is related to the gas velocity and subcooling temperature; (ii) The accuracy of the model is dependent on the resulting increase in pressure drop during the agglomeration of hydrates. Since the model adopted a pressure-velocity coupling CFD simulation technique, the stability of the model at higher gas velocity was achieved by choosing a mesh size with the least pressure drop; and (iii) The interpretation of the contour profiles generated by the CFD model was based on an earlier assumption in the literature (Di Lorenzo et al. 2018), that hydrate deposits grows radially inwards in the pipeline.

Two approaches for predicting hydrate formation rates are the mass transport limited model (Skovborg and Rasmussen 1994) and kinetics models (e.g., Turner et al., 2005). Nevertheless, the outcomes of the kinetics model exhibited a more favourable comparison with the findings from the experiments documented in the literature (Di Lorenzo et al. 2014b; Aman et al. 2016; Wang et al. 2018), which were used for the validation of the CFD Model. Based on empirical observations, it is anticipated that there will be a relatively stable temperature and increasing transient pressure during the formation and agglomeration of hydrates. This occurs due to turbulent hydraulic loading of hydrates in the continuous gas phase and the deposition of hydrates on the wall (Turner and Talley 2008; Li et al. 2013; Zerpa et al. 2013; Odutola et al. 2017; Liu et al. 2020).

In this study, the UDF mass and energy sources control gas flowrate in the fluid domain under hydrates formation, agglomeration, and deposition conditions (see appendix C for UDF code). During the simulation, three parameters were monitored: the gas mass flow rate in the fluid domain, the increase in system absolute pressure drop, and a consistently stable lower gas temperature.

The steps utilized in constructing this model are illustrated in **Figure 3.4**, depicted below.

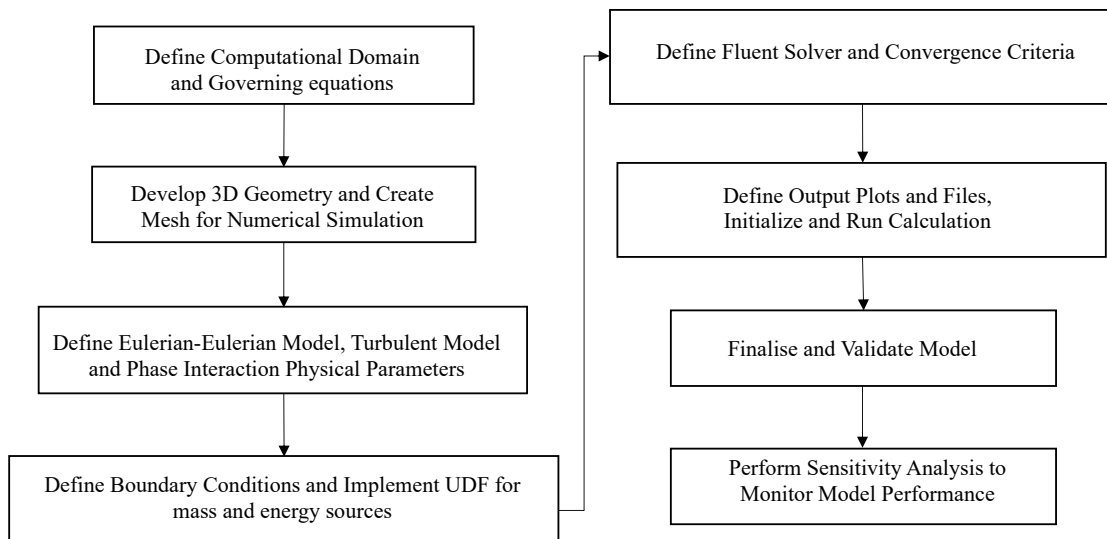


Figure 3.4: CFD model development stages

This research relies on the Eulerian-Eulerian multiphase framework, incorporating boundary conditions and physical flow parameters primarily to improve the interaction between gas and water at the interface. Earlier computational fluid dynamics (CFD) simulations of gas hydrates opted for the Eulerian-Eulerian approach, considering it the most suitable method for capturing interfacial gas-water interactions (e.g., Neto et al., 2016; Berrouk et al., 2020). The boundary conditions adopted in this investigation are derived from the experiments conducted by Di Lorenzo et al. (2014b, 2014a) and Aman et al. (2016), as detailed in **Table 3.4**: gas velocities of 4.7 m/s and 8.8 m/s, gas temperature of 292 K, operating pressure of 8.8 MPa and water volume fraction of 0.06.

The outcomes of the experiments were recently employed to confirm the validity of the analytical models by Wang et al. (2017), Di Lorenzo et al.

(2018) and Liu et al. (2019). The primary objective of this research is to expand the computational fluid dynamics (CFD) model to enhance its applicability in the design, operation, and maintenance planning of gas pipelines prone to hydrate formation.

3.1.2 Computational Domain

Two diagrams illustrating a 2D cross-section and 3D mesh cells of the computational domain for the CFD model is presented in **Figure 3.5** and **Figure 3.6**, respectively. The domain represents a 10 m length (L) pipe with a diameter (D) of 0.0204 m and a pipe wall thickness of 0.0012 m. To ensure flow stability in various practical turbulent flow scenarios, the entrance length (L_e) is estimated for a pipe of diameter (D) within the range of $20D < L_e < 30D$ (Munson et al. 2013). Taking $30D$ as the maximum, the computed L_e is 0.612 m, indicating that a 10 m length of a 0.0204 m diameter pipe is sufficient for the CFD simulation. The multiphase fluid comprises water and natural gas, with the inlet variable defined as velocity, and the monitored outlet variable as pressure.

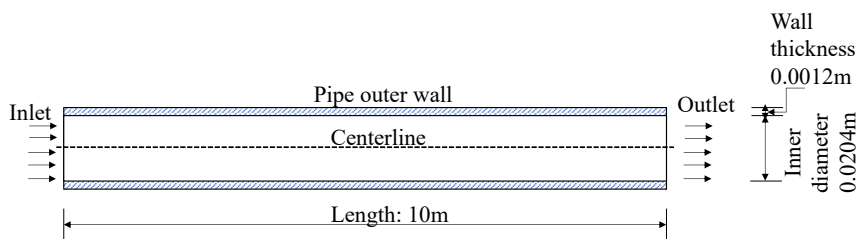


Figure 3.5: 2D representation of the computational domain (dimensions are not to scale)

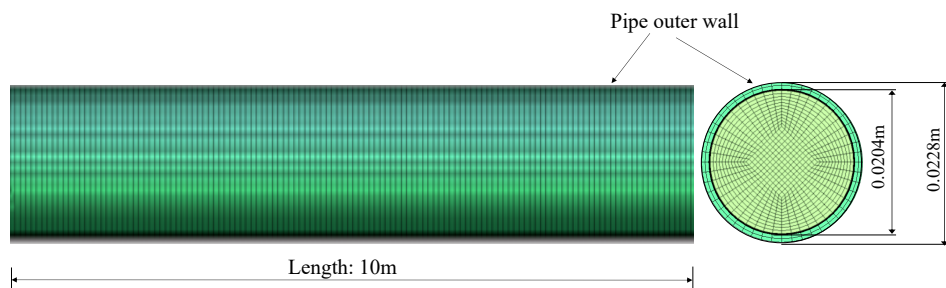


Figure 3.6: 900,000 cells 3D mesh computational domain (dimensions are not to scale)

However, the wall thickness was not used to model heat transfer in this study because the temperature was applied at the interface between the fluid and

the pipeline. However, it is included here as expected in the design of a typical pipeline for completeness.

3.1.3 Governing Equations

Gas hydrates form when the solubility of natural gas in water increases under specific temperature and pressure conditions conducive to hydrate formation, as previously explained. Consequently, employing Eulerian-Eulerian interfacial interaction between gas and water, the initial state of the model involves a two-phase flow. The adopted governing equations are discussed as follows.

Continuity Equation:

The following expression illustrates the mass continuity equation according to the literature (Fluent Theory, 2017):

$$\frac{\partial}{\partial t}(\alpha_q \rho_q) + \nabla \cdot (\alpha_q \rho_q \vec{v}_q) = \sum_{p=1}^n (\dot{m}_{pq} + \dot{m}_{qp}) + S_q \quad (3.1)$$

where, α_q represents the phase fraction; \vec{v}_q is the velocity (m/s) of the phase within the control volume; ρ_q is the density (kg/m³) of the respective phase; S_q represents the source/sink term, assumed to be "zero" for implicit multiphase flow modeling; \dot{m}_{pq} is the mass transfer rate from the p^{th} to the q^{th} phase and \dot{m}_{qp} is mass transfer (kg/s) from the q^{th} phase to the p^{th} phase.

$\sum_{p=1}^n (\dot{m}_{pq} + \dot{m}_{qp})$ is considered "zero" in this study, assuming no interphase mass transfer, as per the literature (Balakin et al. 2016). The gas consumption rate is exclusively dependent on the gas mass source, S_q .

The gas consumption rate (kg/s) aligns with the hydrate formation rate, as indicated in equation 3.2, by Turner et al. (2005). The authors established this correlation by assuming that hydrate formation exclusively occurred within the gas phase saturated with condensed water. In this investigation, there is a direct and proportional relationship between the gas consumption rate and the gas mass flow rate computed through CFD.

$$\dot{m}_{CH_4} = \frac{dm_g}{dt} = -k_1 \exp\left(\frac{k_2}{T_{sys}}\right) \cdot A_i \Delta T_{sub} \quad (3.2)$$

In the equation, \dot{m}_{CH_4} represents the gas consumption rate ($\frac{dm_g}{dt}$; kg/s); k_1 and k_2 are constants; and A_i stands for the interfacial area (m^2). For methane hydrates, the constants k_1 and k_2 are derived from experimental measurements by Vysniauskas and Bishnoi (1983) and found to be: $k_1 = 7.3548 \times 10^{17}$ and $k_2 = -13600K$ (Zerpa et al., 2013, p.301). The thermal driving force for hydrate formation as suggested by Turner et al (2005) , is denoted as the sub-cooling temperature ΔT_{sub} in Kelvin, expressed as:

$$\Delta T_{sub} = T_{eq} - T_{sys} \quad (3.3)$$

where T_{eq} represents the equilibrium temperature for hydrate formation, and T_{sys} is the system pipe wall temperature. The rate of hydrate deposition, measured in m^3/s , is determined by dividing the simulated gas mass flow rate, \dot{m}_{CH_4} (kg/s), by the hydrate density of $807.77kg/m^3$, a value adopted from the literature (Balakin et al., 2016).

$$\dot{m}_{CH_4} \left(\frac{m^3}{s}\right) = \frac{\dot{m}_{CH_4} \left(\frac{kg}{s}\right)}{807.77 \left(\frac{kg}{m^3}\right)} \quad (3.4)$$

The estimation of the interfacial area (A_i) was derived by summing the entrained droplets and the liquid film present at the wall. This approach was chosen because hydrates are formed through both the annular wetting film along the pipe wall and the entrained droplets, as highlighted by Wang et al., (2017). The approximation of the interfacial area for this particular study was based on the results obtained in Aman et al. (2016) and is expressed as:

$$A_i = (2.941v_g - 8.824)LD \quad (3.5)$$

where L represents the length (m) of the pipe occupied by dispersed liquid and the liquid film along the pipe wall; D is the Diameter(m) of the pipe section susceptible to hydrate formation; and v_g denotes the velocity (m/s)

of the primary continuous gas phase. The interfacial area (A_i) is expressed in m^2 . The mass source for equation 3.1, as per equation 3.2, is incorporated using a User-Defined Function (UDF). The mass source is exclusively implemented as a sink for the gas phase, as the hydrate formation is estimated based on the gas consumption rate, as developed by (Turner et al., 2005).

Momentum Equation:

When hydrates form, the two-phase flow behaves like an incompressible flow due to rising gas density and liquid loading. Consequently, the flow relies on the averaging of flow parameters to account for turbulent fluctuations. The momentum equation (Equation 3.6) in Fluent Theory (2017) defines the Reynolds-Averaged Navier-Stokes (RANS) in this context.

$$\frac{\partial}{\partial t}(\overline{\alpha_c \rho_c \tilde{u}_c}) + \nabla \cdot (\overline{\alpha_c \rho_c \tilde{u}_c} \otimes \tilde{u}_c) = -\overline{\alpha_c} \nabla \tilde{p} + \nabla \cdot \overline{\alpha_q} \rho_q \left(\frac{2}{3} k - 2 \frac{\mu_{tq}}{\rho_q} \cdot \nabla \cdot \tilde{u}_c \right) \quad (3.6)$$

where the subscripts "c" and "q" denote the carrier (gas) and qth phase respectively. The common interfacial momentum velocity governing hydrate formation is determined by the velocity of the gas stream (Bendiksen et al. 2004). Thus, the exclusion of drag force on the primary phase is because the dispersed phase is interconnected with the primary phase, and the driving force in the process is the velocity of the gas. Wall lubrication by the gas is assumed to be "zero" since the pipe wall is wetted solely by the water phase. No external body force affects the fluid domain. The phase-averaged variables denoted with tilde, such as \tilde{u}_c (averaged velocity) and \tilde{p} (averaged-density) for both phases, are defined as follows: $\tilde{u}_c = \frac{\overline{\alpha_c U}}{\alpha_c}$ (where U is the free stream velocity); $\tilde{p} = \frac{\overline{\alpha_c \rho}}{\alpha_c}$, where ρ is the free stream density; ρ_c is the density of the gas phase and ρ_q is the density of the qth phase. The turbulent viscosity of the qth phase, μ_{tq} , is defined according to Fluent Theory (2017) as:

$$\mu_{tq} = \rho_q C_\mu \frac{k_q^2}{\varepsilon_q} \quad (3.7)$$

where all variables maintain their previously defined meanings, and C_μ represents the turbulent viscosity constant calculated by Fluent for the realizable $k - \varepsilon$ turbulence model, which is utilized in this study as elaborated later. The μ_{tq} term establishes the connection between the RANS momentum equation and the turbulence $k - \varepsilon$ transport equations (Equations 3.10 and 3.11). The neglect of the lift force on water droplets on the pipe wall is based on the assumption that water deposits on the wall as a film to create hydrates. Additionally, it is assumed that the maximum shear stress on the pipe wall caused by the deposited hydrate layer is where the wall shedding of the deposited hydrates occurs (Liu et al., 2019).

Energy Equation:

The energy equation for a multiphase fluid can be expressed in a general form as:

$$\frac{\partial}{\partial t}(\alpha_q \rho_q h_q) + \nabla \cdot (\alpha_q \rho_q \vec{v}_q h_q) = -\alpha_q \frac{\partial p_q}{\partial t} + \bar{\tau}_q \cdot \nabla \vec{v}_q - \nabla \cdot \vec{q}_q + S_q + \sum_{p=1}^n (Q_{pq} + \dot{m}_{pq} h_{pq} - \dot{m}_{qp} h_{qp}) \quad (3.8)$$

where the specific enthalpy of the q^{th} phase is denoted as h_q , while h_{pq} represents the interphase enthalpy. The source energy from hydrate formation, denoted as S_q , is further detailed in equation 3.9. The heat flux is represented by \vec{q}_q and $\frac{\partial p_q}{\partial t}$ denotes the transient system pressure (Pa/s). Q_{pq} denotes the intensity of heat exchange between phases when a dispersed secondary phase exists in a primary phase. The heat generated from hydrate formation is exothermic and serves as an external energy source in the gas phase, thus $Q_{pq} = 0$. Assuming no interphase mass transfer, the product of mass transfer rate and interphase enthalpy, $\dot{m}_{pq} h_{pq} = 0$ and $\dot{m}_{qp} h_{qp} = 0$. All other parameters retain their earlier definitions. The source energy results from the exothermic heat of hydrate formation, as described in Meindinyo et al. (2015), below:

$$S_q = \frac{dm_g}{dt} \cdot \Delta H_{Hyd} \quad (3.9)$$

Where the gas consumption rate $\frac{dm_g}{dt}$ (kg/s) as specified in equation 3.2, represents the rate at which gas is consumed in kilograms per second. The enthalpy of hydrate generation ΔH_{Hyd} (J/kg), is also a contributing factor. The energy source is incorporated into a user-defined function (UDF) as a positive driving force exclusively for the gas phase, given that the dispersed water phase is interconnected with the gas phase. It is important to note that there is no slip velocity observed at the interfacial contact point where hydrates are being formed (Zerpa et al. 2013).

3.1.4 Turbulence Models

Turbulence models play a crucial role in multiphase CFD simulations, as highlighted by Fox (2014). The induction of hydrate formation is facilitated by flow agitation, a significant factor emphasized by Carroll (2014). Consequently, experimental reaction cells for hydrate formation, as demonstrated in the literature (Meindinyo, Svartas and Svartås 2015), are consistently stirred to promote optimal hydrate development. This research employs the realizable $k - \varepsilon$ two-equation turbulence models to improve the modeling of near-wall viscosity for accurate prediction of hydrate deposition, as reiterated in the literature (Wang et al., 2018). Here, ' k ' represents turbulent kinetic energy, and ' ε ' denotes turbulent dissipation. The transport equations are individually solved for each phase to incorporate depositional drift velocity.

Kinetic Equation:

$$\frac{\partial}{\partial t}(\alpha_q \rho_q k_q) + \nabla \cdot (\alpha_q \rho_q \vec{v}_q k_q) = \nabla \cdot \left(\alpha_q \left(\mu_q + \frac{\mu_{tq}}{\sigma_{kq}} \right) \nabla k_q \right) + \alpha_q G_{kq} - \alpha_q \rho_q \varepsilon_q + \alpha_q \rho_q \Pi_{kq} \quad (3.10)$$

Dissipation Equation:

$$\frac{\partial}{\partial t}(\alpha_q \rho_q \varepsilon_q) + \nabla \cdot (\alpha_q \rho_q \vec{v}_q \varepsilon_q) = \nabla \cdot \left(\alpha_q \left(\mu_q + \frac{\mu_{tq}}{\sigma_{\varepsilon q}} \right) \nabla \varepsilon_q \right) + \alpha_q \frac{\varepsilon_q}{k_q} (C_{1\varepsilon} G_{kq} - C_{2\varepsilon} \rho_q \varepsilon_q) + \alpha_q \rho_q \Pi_{\varepsilon q} \quad (3.11)$$

where the source terms for turbulence interactions between the entrained water phase and the primary gas phase are denoted as Π_{kq} and $\Pi_{\varepsilon q}$, while G_{kq} represents the turbulent kinetic energy production term for the q^{th} phase. The turbulent viscosity μ_{tq} (Pa.s) of the q^{th} phase is also considered. Buoyancy effect and fluctuating dilatation are omitted in equation 3.10 due to the incompressible nature of the gas-water multiphase flow. In the current study, both equations are solved per phase to improve the prediction of hydrates at the wall. $C_{1\varepsilon}$, $C_{2\varepsilon}$ and $C_{3\varepsilon}$ are constants. The terms σ_{kq} and $\sigma_{\varepsilon q}$ are the turbulent kinetic energy (TKE) and turbulent dissipation rate (TDR) Prandtl numbers, set at 1 and 1.2, respectively, based on literature recommendations (Theory 2017).

The terms σ_{kq} and $\sigma_{\varepsilon q}$ are related to the dimensionless ratio of temperature-dependent kinematic eddy viscosity between the continuous gas phase and the dispersed liquid phase. The value of the turbulent Prandtl number σ_{kq} is set to ensure that the ratio of momentum diffusivity to thermal diffusivity equal to 1. This assumption is aimed at balancing the thermal diffusivity between gas and liquid phases at the wall during hydrate formation based on the Reynolds analogy (Li 2019). This is essential for enhancing hydrate stability and minimizing advection (Tu, Yeoh and Liu 2018). For the realizable $k - \varepsilon$ model, $C_{1\varepsilon}$ is computed during the simulation by the software. The values for the constants used in this study are: $C_{2\varepsilon}$ (1.9) and $C_{3\varepsilon}$ (1.3). Additionally, closure parameters Π_{kq} and $\Pi_{\varepsilon q}$ for each phase are determined using the closure model developed by Simonin and Viollet (1990), as modified in Fluent Theory (2017):

For the primary continuous phase:

$$\text{Kinetic source: } \Pi_{kq} = C_s \alpha_q K_{pq} \vec{v}_{pq} \cdot \vec{v}_{dr} \quad (3.12)$$

$$\text{Dissipation source: } \Pi_{\varepsilon q} = C_{3\varepsilon} \frac{\varepsilon_k}{k_q} \Pi_{kq} \quad (3.13)$$

For the dispersed secondary phase:

$$\text{Kinetic source: } \Pi_{k_p} = C_s \alpha_p K_{pq} \vec{v}_{pq} \cdot \vec{v}_{dr} \quad (3.14)$$

$$\text{Dissipation source: } \Pi_{\varepsilon_p} = C_{3\varepsilon} \frac{\varepsilon_k}{k_p} \Pi_{k_p} \quad (3.15)$$

where the constants $C_{3\varepsilon} = 1.3$ and $C_s = 1$; K_{pq} is the covariance of the phase velocities. The drift velocity between the gas and liquid phase is expressed as, \vec{v}_{dr} , while \vec{v}_{pq} is the relative velocity between the phases. The calculation of drift velocity follows the formulation presented by Simonin and Viollet (1990), as shown below:

$$\vec{v}_{dr} = -\frac{D_{t,pq}}{\sigma_{pq}} \left(\frac{\nabla \alpha_p}{\alpha_p} - \frac{\nabla \alpha_q}{\alpha_q} \right) \quad (3.16)$$

where the binary diffusivity, denoted as $D_{t,pq}$ is expressed as $D_{t,pq} = \frac{1}{3} K_{pq} \tau_{t,pq}$. $\tau_{t,pq}$ represents the interaction time of the eddy particle. The variations in gas and liquid phase concentrations are denoted as $\nabla \alpha_p$ and $\nabla \alpha_q$, respectively. The dispersion Prandtl number σ_{pq} is typically set to 0.75 to enhance thermal diffusivity in incompressible flow (Theory 2017).

However, for all simulations in this study, the turbulent dispersion is intentionally set to "none" to restrict dissipation and subsequent conversion of kinetic energy into thermal internal energy. It is important to note that in incompressible flow, the dissipation term can be disregarded, especially when aiming to prevent flow-induced mechanical deformation of a viscous fluid, which is relevant in the prediction of hydrates deposition, as indicated in the literature (Tu, Yeoh and Liu 2018). Theoretically, the appropriate turbulence conditions create the necessary interfacial area for the stoichiometric reaction involved in hydrate formation.

3.1.5 Wall shear stress

The turbulent stress τ_c^t acting on the hydrates at the pipe wall, influenced by the carrier (gas) phase, is determined by the stress term on the right-hand side (RHS) of equation 3.6 as:

$$\tau_c^t = \bar{\alpha}_c \rho_c \left(\frac{2}{3} k - 2 \frac{\mu_{t_c}}{\rho_c} \cdot \nabla \cdot \tilde{u}_c \right) \quad (3.17)$$

The parameters in equation 3.17 maintain their previously assigned definitions.

3.1.6 Enhanced near wall effects

3.1.6.1 Pressure Gradient Effect

The near wall pressure predictions can be unreliable due to boundary layer separations when the pipe wall is subjected to severe pressure gradients as a result of turbulence (Mottaghian, Yuan and Piomelli 2018). This can occur during hydrate deposition on the wall since the surface of the hydrate layer creates a wavy stratified annular profile (Aman et al. 2016; Di Lorenzo et al. 2018), hence the need to ensure that Reynolds number is in the transition zone by preventing turbulent dispersion as explained earlier. The effect of turbulence on near wall pressure predictions is minimised by enhanced wall treatment with the pressure gradient effects activated under realizable $k - \varepsilon$ turbulence model in ANSYS Fluent.

3.1.6.2 Thermal Effect

Hydrate deposition is dependent on thermal gradient between the fluid and the pipe wall (Turner et al., 2005). Near wall turbulence affects the thermal profile (Kader 1981). Also, with increasing thermodynamic mixing (Abbasi and Hashim 2014), there is a reduction in the temperature of the gas at the core, leading to further hydrates generation. Hence, to solve the near wall thermal heat transfer accurately, there is the need to consider the varying near wall eddy viscosity. As the hydrates profile grows, the near wall thermal effect also varies (Aman et al., 2016; Di Lorenzo et al., 2018). Thus, the lower turbulent kinetic energy Prandtl number of 1, used in the simulations

was done to enhance the stability of hydrates on the wall of the pipe by enhancing the thermal cooling of the gas. Consequently, thermal effect was activated as enhanced wall treatment on the realizable $k - \varepsilon$ turbulence model in this study.

3.1.7 Mesh Grid Sensitivity and UDF Performance

The computational geometry is 3D representation of a 10 m length and 0.0204 m diameter pipe. This diameter is the same used in the experimental setups, where the generation of hydrates occurs at a 12 m section of the experimental flowloop (Aman et al. 2018). The use of 10 m length CFD model was premised on the fact that hydrates are produced at a section of the pipeline and transported downstream where it plugs bends or areas of constriction as indicated in the flowloop experiments (Di Lorenzo et al. 2014a; Aman et al. 2016, 2018). Also, pipelines can span lengths of up to 100 km and above, which is difficult to model using CFD because of computer processing time.

As a result, it was important to ascertain if a shorter length than the 34 m used in the above experimental setups can accurately predict the deposition rates of hydrates and flow behaviour, especially when the hydrates were generated in a 12 m section of the test flowloop. Flow materials are methane gas and water, with defined properties in the literature (Di Lorenzo et al., 2018). Inlet velocities range from 2.0 m/s to 8.8 m/s at various sub-cooling temperatures ranging from 2.5K to 8.0K.

To enhance multiphase flow in the oil and gas industry, pipelines are designed to reduce the pressure drop by minimising friction loss and pipewall erosion. Hence, the stability of the CFD simulation was improved by choosing a mesh size with the least significant pressure drop through a mesh grid sensitivity analysis in **Figure 3.7**. The mesh sensitivity was carried out at the inlet velocity of 10 m/s (flowrate of 3.3 kg/s), temperature of 292 K, and pressure of 8.8 MPa.

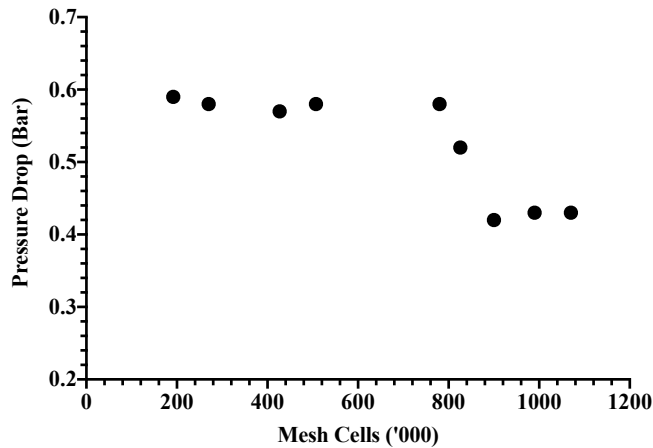


Figure 3.7: Mesh sensitivity

From **Figure 3.7**: the mesh size of 900,000 cells resulted in the lowest pressure-drop of 0.42 bar and was selected as the model mesh size. The effect of the mass and energy source UDFs on the primary phase using this grid size is presented in **Figure 3.8**, below. Implying that the UDF codes resulted in shorter flowtime. Also, the slight increase in pressure at 8.8 m/s on the UDF curve in **Figure 3.8** is due to accurately metered gas mass flowrate based on the kinetics model. Without the UDFs, the software underpredicted the deposition rates of hydrates and extended the simulation flowtime. Hence, with the UDFs, a proactive higher hydrates deposition rates reduction was achieved.

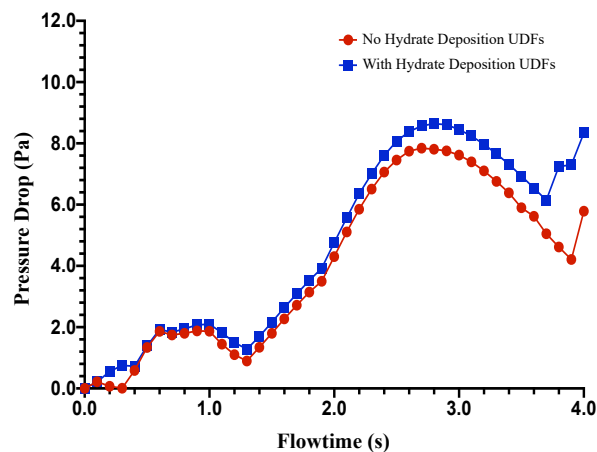


Figure 3.8: Comparison of pressure drop (with and without hydrate deposition UDFs) at gas flow velocity of 8.8m/s

The flow behaviour captured by the pressure profile indicates that the UDFs resulted in a better prediction of hydrate deposition, as explained later in

Figure 4.18. The UDF codes also incorporated a conditional statement using equation 3.18, as proposed by Sloan and Koh (2007, p. 193) for methane hydrates at 0 to 25°C to calculate the resulting equivalent system pressure at the hydrate formation temperature. The peak pressure at 3.0 s indicates full agglomeration of hydrates filling the pipe annulus, and the drop in pressure after 3.0 s represent the deposition of hydrates, allowing for ease of fluid flow at the core until the line is plugged with hydrates beyond 3.8 s.

$$P_{eq} = \exp\left(38.98 - \frac{8534}{T_{eq}}\right) \quad (3.18)$$

where P_{eq} is the hydrate formation equilibrium pressure (KPa). This calculated equivalent pressure must be equal or less than the system pressure for the hydrates to be stable in the pipeline because hydrate formation and stability is favoured at high pressure and low temperature. The fluid properties and input parameters for the simulations are presented in **Table 3.1 - 4** below.

Table 3.1: Natural gas properties (Ansys Fluent Version 2020 R1)

Natural Gas Properties	Value
Gas density (kgm-3)	Peng Robinson (real gas)
Molecular weight of natural gas	18.043
Viscosity (Pa.s)	Kinetic theory
Thermal conductivity (W.m-1K-1)	0.0332
Constant pressure heat capacity (J·K-	Kinetic theory
Critical pressure (MPa)	4.6
Critical temperature (K)	191
Critical specific volume (m3/kg)	6.15x10-3
Reference temperature (K)	298.15
Energy parameter (k)	148.6
Degrees of freedom	0
Characteristics length (angstrom)	3.758
Standard state enthalpy (J.kg-1mol-1)	-7.49x10-7
Standard state entropy (J.kg-1mol-1)	1.86x105
Acentric factor	0.01

[†]Gas molecular weight from Di Lorenzo et al (2018), based on the gas composition

Table 3.2: Liquid water properties (Ansys Fluent Version 2020 R1)

Liquid Water Properties	Value
Water density (kgm^{-3})	998.2
Molecular weight (kg.kmol^{-1})	18.0152
Viscosity (Pa.s)	1.0×10^{-3}
Thermal conductivity ($\text{W.m}^{-1}\text{K}^{-1}$)	0.626
Constant pressure heat capacity ($\text{J.K}^{-1}\text{kg}^{-1}$)	4182
Interfacial tension with gas phase (N.m^{-1})	0.0721
Standard state enthalpy ($\text{J.kg}^{-1}\text{mol}^{-1}$)	-2.858×10^8
Reference temperature (K)	298

Table 3.3: Gas hydrate properties

Gas Hydrate Properties	Value
Hydrate density (kgm^{-3}) [†]	807.77
Hydrate enthalpy of formation (Jkg^{-1}) ^{††}	6.4×10^5

[†](Balakin et al. 2016); ^{††} (Di Lorenzo et al., 2018)

Table 3.4: Input parameters/boundary conditions (Di Lorenzo et al, 2018)

Input Variables	Value
Velocity (m/s)	4.7; 8.8
Inlet operating pressure (MPa)	8.8
Inlet operating temperature (K)	292
Inlet water volume fraction	0.06
Pipe wall temperature (K)	Operating temperature less subcooling temperature
Pipe internal wall surface roughness (dimensionless) [†]	0 (Smooth pipe)
Gauge pressure (Pa)	101325

[†](Jassim, Abdi and Muzychka 2010)

The Peng and Robinson equation of state (EOS) is used to calculate gas density (**Table 3.1**), as it is widely used in gas pipeline hydraulic calculations, because the equation expresses the compositional properties of natural gas in terms of both critical properties and acentric factor (Peng and

Robinson 1976). Also, the gas viscosity and heat capacity were calculated by the kinetic theory to account for the effect of turbulence on the thermodynamics of the system. During simulation, the pipeline temperature in the fluid domain is reduced from the inlet value of 292K by the subcooling temperature at the pipe wall to lower temperatures favouring hydrate formation and stability, as indicated in **Figure 4.6**, and the temperature contour maps (**Figure 4.10** and **Figure 4.11**).

3.1.8 Fluent solver configuration

Pressure-based fluent solver is activated to combine the continuity and momentum equation. Such that, in the discretization of mass conservation equation when the velocity gradient is already derived from the momentum equation at the cell centre, there is also implicit incorporation of the resultant pressures at the cell centres (Ashrafizadeh, Alinia and Mayeli 2015; Vakilipour et al. 2019). The " $k - \varepsilon$ " turbulent equation was set to realizable to ensure the positivity of normal stresses when the strain rate is large as suggested by Shih et al. (1995), because of near-wall turbulent shear stress effect. Also, activating thermal effects enables the modelling of the thermal transfer on the near-wall viscous layer between the fluid and pipe wall based on the subcooling temperature gradient, which is important in prediction of hydrates deposition rates (Turner et al. 2005; Lim et al. 2020).

3.1.9 Solution Method

The solution method is Phase coupled SIMPLE to avoid instabilities because of the incompressible nature of the flow and the pressure build up during phase change; especially for transient time-dependent problems where computer CPU time is a concern for convergence (Theory 2017). Here, due to pressure-velocity coupling, the pressure and velocity are stored at cell centres (Ferreira et al. 2019). Relaxation factor is set to 0.75. Under-relaxation factors were set to appropriate values for the simulation, as they suppresses the oscillations between time steps so that convergence is achieved (Barron and Neyshabouri 2003).

For optimum result, both pressure under-relaxation factor (ϕ_p) and velocity under-relaxation factor (ϕ_u) must sum up to 1 and it was ensured that $\phi_u >$

ϕ_p (Demirdzic et al. 1987; Min and Tao 2007). Gradient is set to Least Square Cell Based (LSCB), because it is time saving and can achieve a minimum of first order accuracy (Mishriky and Walsh 2017). Furthermore, pressure is solved through second order upwind scheme, thus providing a better accuracy through multidimensional linear reconstruction (Shyy, Thakur and Wrightt 1992). Also, cell face fluxes for solved parameters are cell-averaged values and assumed to hold for all cells (Ferreira et al. 2019). At the outlet, the “radial equilibrium pressure distribution” option was activated to further enhance annular hydrate deposition prediction, because hydrates are deposited on the wall by radial velocity (Wang et al., 2018). Backflow is not anticipated since it is a continuous pipeline with exit.

However, for incompressible flows the time steps was not considered as a major criterion for convergence because it is not limited by Courant Friedrich Levy (CFL) criterion in implicit functions (Bendlksen et al. 2004). The CFD software solved six equations: mass, momentum, volume fraction, energy, turbulence (kinetic and dissipation) and interfacial area concentration. Calculation for each case was completed in 4.0 seconds with fixed time advancement, 40-time steps, and time step size of 0.1 seconds. The 0.1 seconds time step size was adopted after comparing various time step sizes at 4.7 m/s in **Figure 3.9**, because the hydrates curve was more stable and realistic with experimental results.

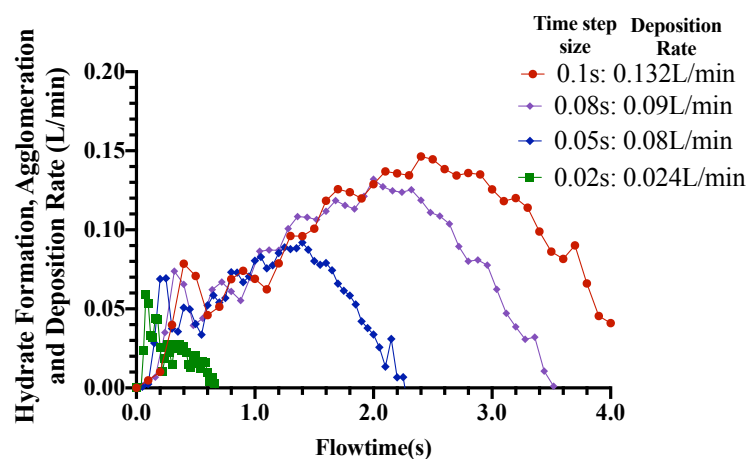


Figure 3.9: Comparing average hydrate deposition curves at a velocity of 4.7 m/s (7.0K) for various timestep sizes. The identification of hydrates

formation, agglomeration and deposition sections are provided later in Figure 4.7.

The simulation was achieved with a computer of 2.10GHz quad-core Intel Xeon Gold 6230 CPU and RAM size of 16GB. The results, validation and discussions are presented next in section 4.1.

3.1.10 Approach to CFD Results Analysis and Model Validation

The transient data collected were from the fluid domain during the experimental CFD simulation, and include absolute pressure, gas and pipewall temperatures, gas density, gas flowrate, and minimum gas and water volume fraction. The gas flowrate was the accumulated gas in the fluid domain, which represent the extent of gas consumed to hydrates in the literature (Turner et al, 2007) and was converted to hydrates formation, agglomeration, and deposition rates in litre per minutes. Temperature contour of the gas phase was retrieved for flow velocities of 2-10 m/s, at subcooling temperatures of 2-8K. The density contour for the gas phase was also presented to show how the gas density increased towards the pipe wall in an annular pattern as a confirmation of increasing deposition of gas at the wall and the resulting increases in hydrates deposition at the wall.

The results were interpreted using the experimental pressure and temperature profile in the literature (Liu et al. 2020). The model prediction was monitored to produce the pressure and temperature profile in **Figure 3.10**. The positions I, II, III, and IV in the experimental result represent hydrate formation, agglomeration, deposition, and bedding leading to pipeline blockage by hydrates (Liu et al. 2020). Thus, the basis for the interpretation of the CFD model results and the average deposition rate was estimated from stage III, as presented in **Figure 3.10**.

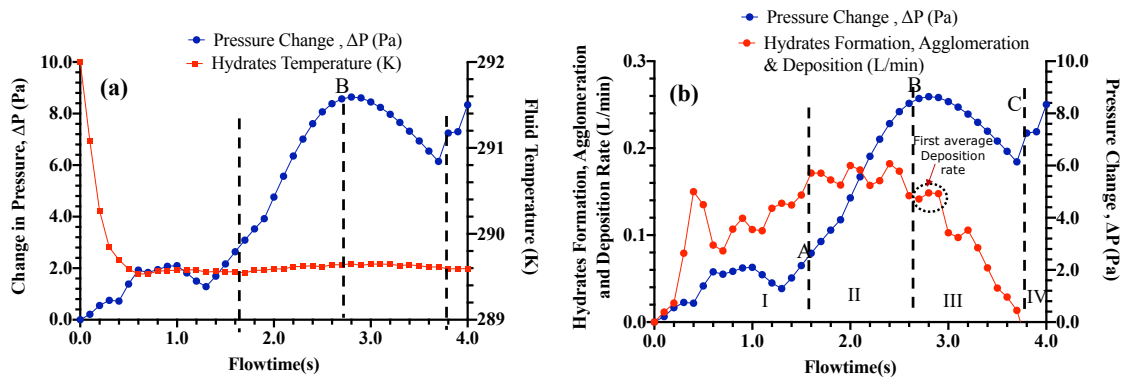


Figure 3.10: CFD simulation result at 8.8m/s and 7.1K. (a) CFD replication of the experimental hydrates pressure and temperature curve by Liu et al. (2020). (b) Superimposition of the CFD pressure curve on the simulated hydrates profile.

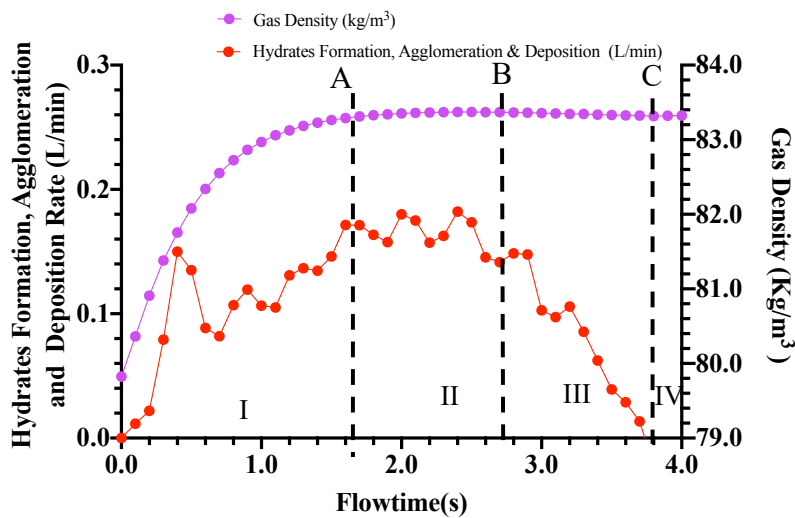


Figure 3.11: CFD simulation result for the gas density at a velocity of 8.8m/s and subcooling temperature of 7.1K.

By superimposing the simulated gas density profile on the hydrate curve, the result shows that the gas density is relatively stable from point A at full agglomeration to point B and C during the deposition of hydrates on the wall of the pipeline section. The stable value of gas density is an indication that the flow is increasingly viscous and approximating to an incompressible multiphase flow. Hence, the experimental pressure and temperature curves provided by Liu et al. (2020) provided a means for interpreting the CFD results and the deposition rates of the hydrates were validated with empirical results in Aman et al (2016) and Di Lorenzo et al (2014).

3.2 Regression Modelling Methodology

The purpose of this modelling approach is to predict the deposition rate of hydrates based on the observed linear relationship between the deposition rate of hydrates and the gas velocity, subcooling temperature, pipeline diameter and water volume fraction during the CFD simulation. This approach is important in predicting the deposition of hydrates in shutdown scenario. A multiple linear regression approach was adopted using the machine learning regression learner in MATLAB® version 2021a. A classification approach was not adequate since the modelling intention was to estimate a value of the dependent variable rather than to determine a class.

Machine learning (ML) and deep neural network (DNN) are two main approaches to artificial intelligence in data modelling. While ML requires only input and output data, DNN includes a hidden set of data and require more data than regression modelling approach using ML. In this study, 81 data sets made up of 4 input predictors and 1 output was trained in MATLAB® machine learning regression app. Since the observed relationship between the deposition rate of hydrates and each of the input variables was linear from the parametric analysis presented in chapter 4, only linear regression applications have been considered. The linear models include the standard linear, robust linear, stepwise linear and interaction linear regression applications.

A further simulation using the support vector machine (SVM) linear regression application was conducted, but the result did not yield a good fit, hence it was discarded in favour of the above linear models. Model validation was achieved through experimental results and parametric analyses were carried out to determine the out of data performance of the final model. The choice of the final model was informed from statistical model fit analyses criteria in the literature as discussed below.

This study develops an approximating function for the deposition rate of hydrates in gas-dominant subsea pipelines, operating in environmental temperature conditions that favours hydrates formation. The main assumption in this study is that the deposition rate of hydrates in the pipeline

can be accurately predicted by the gas velocity, water volume fraction, subcooling temperatures and pipeline diameter from evidence in the literature (Di Lorenzo et al. 2014b, 2014a, 2018; Aman et al. 2016; Umuteme et al. 2021, 2022).

Stable hydrates form when the system temperature is below the hydrating equilibrium condition for stable hydrates. The equilibrium hydrates formation pressure equation for methane temperature ranging from 0-25°C by Sloan and Koh (2007) is adopted to compute the minimum pressure required for hydrates formation. Stable hydrates are formed at temperatures below 292K from the hydrates loci for methane discussed in chapter 4 (**Figure 4.1**). Hence, the regression model is for natural gas with methane gas above 82% by composition.

The model is based on the parametric simulations conducted using the validated model CFD model for predicting the deposition rates of hydrates developed in chapter 4. The data is made up of 81 x 5 matrix data table with a total of 405 data. The basis for the selected variables is discussed as follows based on evidence in the literature (Di Lorenzo et al. 2014b, 2014a, 2018; Aman et al. 2016; Umuteme et al. 2021): (i) gas velocity defines the nature of fluid flow – laminar, transitional, or turbulent. The developed regression model was validated with experimental. The stages of the adopted method in the development, validation and application of this regression model are presented in **Figure 3.12**, below.

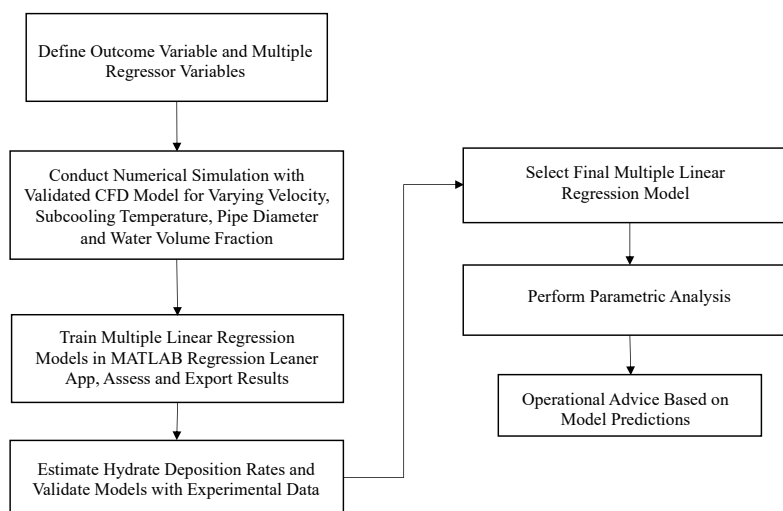


Figure 3.12: Stages of the adopted methodology

Hydrates formation, agglomeration and deposition are affected by gas velocity. (i) increase in gas velocity under the same pressure and subcooling temperature, increases the deposition rates of hydrates; and (ii) increasing the subcooling temperature of the pipeline at constant gas velocity also increases the deposition rate of hydrates. Also, the outcome of the CFD simulations in chapter 4 proposes that: (i) increase in pipeline diameter under the same gas flow condition increases the deposition rate by similar factor; and (ii) increase in water volume fraction reduces the deposition rate of hydrates. The subcooling temperature reduces the gas temperature by the subcooling value into the hydrates stable zone of the hydrate loci in **Figure 4.1**. The equilibrium pressure must be lower than the operating pressure of 8.0 MPa and the pipeline temperature must be less than 292K to ensure that hydrates are forming before using this regression model.

3.2.1 Defining Variables and Data Generation

The data for the development of the regression model was obtained from the validated CFD model for predicting the deposition rates of hydrates in gas pipelines discussed in section 3.1 earlier. The validated CFD model is a 10 m length by 0.0204 m diameter pipe. Initial multiphase flow is made up of natural gas and water. Input variables are operating pressure, temperature, water volume fraction and gas velocity (**Table 3.5**). A eulerian-eulerian multiphase scheme was adopted to enhance interfacial interaction. The simulation was conducted for different ranges of pipe diameter, gas velocity, subcooling temperatures and water volume fraction. A total of eighty-one (81) deposition rates of hydrates were predicted from 81 simulations.

The sample size was determined as per the recommendation in the literature (Cohen 1988; Cohen et al. 2003) using G*Power software, version 3.1 (Faul et al. 2007), with a conservative effect size of 0.30 because the CFD model is already validated with experimental results, and statistical power of 95% which yields a minimum sample size of 72. Detail documentation on the development and validation of the CFD model is already discussed in section 3.1. The input variables for the CFD simulations are defined in **Table 3.5**, as follows.

Table 3.5: Range of input data for the CFD simulations

Variables	Range
Gas Velocity (m/s)	2.0 - 8.8
Subcooling Temperature (K)	1.0 - 9.0
Water Volume Fraction (-)	0.02 - 0.12
Pipe Diameter (m)	0.0204 - 0.0612
Hydrates Deposition Rate (L/min)	0.0370 - 0.7030

3.2.2 Regression Model Development

The regressor variables are as defined earlier, including the subcooling temperature (ΔT), pipeline diameter (D), water volume fraction (α_w) and gas velocity (V) as predictors, while the deposition rates of hydrates (\dot{Q}_{hd}) is the outcome variable. This is represented in **Figure 3.13**, below.

Hence,

$$\dot{Q}_{hd} = f(V, \Delta T, D, \alpha_w)$$

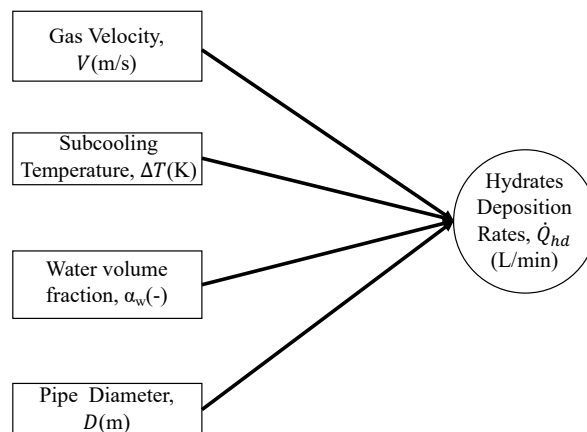


Figure 3.13: Interaction of regressor variables with the deposition rate of hydrates

Selecting a multiple regression model with the most appropriate explanatory and predictive power is difficult and depends on selecting appropriate set of variables that defines the expected response. In MATLAB, multiple regression modelling can be achieved by the standard linear regression, robust linear regression, interaction linear regression, and stepwise linear regression. The standard linear model is also known as ordinary least square (OLS) estimation of the intercept and coefficients to minimize the error sum of the squares, SS_E (Cohen et al. 2003).

However, there are instances where the data sets contain values that have high discrepancy from the expected outcome, also known as outliers. When this occurs, as with some experimental outcomes, an alternative approach using robust linear regression may be adopted. The robust linear regression modelling approach minimises the effect of outliers on the regression model by minimizing the weights given to outlying cases when calculating the regression coefficients to produce improved estimates (Cohen et al. 2003). By modelling with robust linear regression algorithms, it is possible to rule out the presence of outliers in the data sets when the outcome compares favourably with the predictions of the OLS model.

In this study, both approaches were adopted to rule out the presence of outliers in the data sets generated for the study. Both models have been represented in equation 6.1, while neglecting the error term in the general multiple regression equation. Also, the stepwise linear regression modelling approach was considered to enhance the predictability of hydrates deposition rates in MATLAB. In stepwise regression approach, one variable at each stage is selected from a group of predictors that produces the highest coefficient of determination (R^2).

The selected variable is the regressor that produces the largest value of F-statistic (Montgomery and Runger 2014). Implying that variables are either added or removed at each step leading to an iterative sequence of regression models. However, one problem with this approach is the high dependence on chance and the likely underestimation of predictive confidence intervals (Cohen et al. 2003). Equation 6.2 is the stepwise regression model with the variables defined for this study. In the equation, two sets of interactions between two regressors were included with the four additive regressors in the OLS. The last approach adopted is the interaction linear regression model. In the interactions approach, additional sets of interacting variables are added to the additive models of the original regressors as in the OLS. Here the interaction predictors are products of the original predictors (Cohen et al. 2003). Equation 6.3, represents the outcome of the interactions model based on data training in MATLAB.

This study acknowledges that while dimensional homogeneity is desirable for both physical understanding and broader applicability, achieving it with regression equations can be challenging and not always straightforward. To ensure dimensional homogeneity, a mathematical relationship was derived based on the understanding of the relationship captured by the adopted regression equation in Chapter 6.

3.2.3 Model Selection Criteria

The adopted model for the parametric studies was based on a combination of five model selection criteria, including the error sum of squares (SS_E), adjusted R-squared ($R^2_{adj.}$), standard F test; root of mean square error (RMSE) and the Akaike information criterion (AICc). Each criterion is discussed further below to provide insight into the parameters influenced the predictive power of the chosen model.

Error Sum of Squares (SS_E): In regression analysis, the sum of squares is used to explain the dispersion of the data sets around a mean. The error sum of squares or residual sum of squares, as used in this study is based on the residual after the model-fitting process. SS_R represent the regression sum of squares of the data set that predicted the model-fit regression line. The total variability in the data is described by the total sum of squares (SS_T). The estimation of SS_E , SS_R , and SS_T are defined in equations 3.19, 3.20 and 3.21, below.

$$SS_E = \sum_{i=1}^n (y_i - \hat{y}_i)^2 \quad (3.19)$$

$$SS_R = \sum_{i=1}^n (\hat{y}_i - \bar{y})^2 \quad (3.20)$$

$$SS_T = SS_R + SS_E = \sum_{i=1}^n (y_i - \bar{y})^2 \quad (3.21)$$

where SS_R is the regression sum of squares; \hat{y}_i , is the predicted value per data point; y_i , is the original target value; \bar{y} is the mean of the data set

representing the regression line prediction, and $y_i - \bar{y}$, is the deviation of each data from the mean.

Adjusted R-Squared (R^2_{adj}): The coefficient of determination (R^2) is determined from the ratio of the SS_E and SS_T (Equation 3.22). Since it is a ratio where the denominator is always higher or equal to the numerator, the value is from 0 to 1. The value of R^2 indicate the extent by which the variance in the predicted variable is dependent on the predictor variables. However, because the value of R^2 increases as new variables are added to the regression equation, it is seldom problematic in determining model fit when comparing models. To overcome this weakness, the R-squared is adjusted (R^2_{adj}) as in equation 3.23. to compensate for this effect such that the R^2 value decreases as more predictor variables are added to the regression model (Montgomery and Runger 2014), thus guarding against overfitting. Thus, it is important to select the predictors that have higher effect on the variance of the response variable.

$$R^2 = \frac{SS_E}{SS_T} \quad (3.22)$$

$$R^2_{adj} = 1 - (1 - R^2) \frac{n - 1}{(n - k - 1)} \quad (3.23)$$

where, $n - k - 1$ is the degree of freedom for the denominator, k is the number of predictor variables, and n is the total data points.

Standard F Test: Another statistical measure for model selection is the standard F test which tests the significance of the obtained value of the R^2 . It is used to determine if the set of predictor variables statistically explain a significant amount of the outcome. Higher values of F indicate better model performance. F-test is estimated from equation 3.24.

$$F = \frac{R^2(n - k - 1)}{k(1 - R^2)} \quad (3.24)$$

where, k is the number of predictor variables and $n - k - 1$ is the degree of freedom.

Root of mean square error (RMSE): This model selection measure is the standard deviation of the prediction errors or residuals. The RMSE provides insight into how far the errors are from the predictions. Models with lower RMSE have higher predictive power. The RMSE is estimated from equation 3.25 below, where the symbols n , \hat{y} , and y_i are as defined earlier.

$$RMSE = \sqrt{\frac{1}{n} \sum_{i=1}^n (\hat{y}_i - y_i)^2} \quad (3.25)$$

Akaike Information Criterion (AICc): This measure estimates the prediction error and relative quality of a statistical model for a given set of data. It provides a means for model selection because it compares the quality of each model against the other models. The smaller case "c" in equation 3.27 indicates that the calculated AIC value has been corrected for smaller samples to prevent overfitting because of the inclusion of both stepwise and interaction models in this study. The AIC criteria is generally an estimation of the information loss because of the presence of the likelihood function, \hat{L} . This index also take into account the number of regression coefficients being tested (Cohen et al. 2003). When the experimental data sets for cross-validation is sparse, the AICc have been found to be more reliable than the F-test (Kletting and Glatting 2009). The smaller the value of AICc the better the model fit achieved. AIC is estimated using equation 3.26.

$$AIC = 2k - 2\ln(\hat{L}) \quad (3.26)$$

$$AICc = AIC + \frac{2k^2 + 2k}{n - k - 1} \quad (3.27)$$

where, \hat{L} is the likelihood function, and k is the number of predictor variables and $n - k - 1$ is the degree of freedom. Implying that the higher the variables the higher the AIC value. Thus, from the discussion above the model selection criteria are defined as follows.

Table 3.6: Criteria for model selection

Parameter	Criteria
R^2_{adj} .	Higher
SS_E	Lower
RMSE	Lower
AICc	Lower
F-Test	Higher

A simple ranking method was adopted, where the most favourable of the four models was awarded a score of 4 and the least favourable model was awarded a score of 1 on each selection parameter. The model with the highest sum was finally adopted.

3.3 Analytical Modelling Methodology

The driver for developing this model is to have a validated analytical model that directly incorporates the hydrates deposition rate for gas-dominated pipeline in one mathematical relation. Two equations were developed to predict the plugging flowtime and the resulting pressure drop. To achieve this, the general frictional pressure drop equation was modified with the Lagrangian particle velocity differential equation to capture the first pressure spike after the onset of hydrates deposition, as indication of the commencement of hydrates plugging the pipeline.

A linear growing hydrates deposit profile on the pipe wall was assumed in calculating the volume of the deposited hydrates and the time to plug the pipe at the first significant pressure spike. The model prediction was guided by the principle that, as a proactive hydrate plugging preventive analytical tool, it is essential that the model can “underpredict” the plugging flowtime and “overpredict” the transient pressure drop when compared with experimental data in the literature. The basic assumption behind the transient pressure drop model is that as a precautionary measure, it is important to stop gas flow once the first spike in pressure drop is recorded.

Implying that the effect of hydrates sloughing is neglected in the modelling philosophy.

The analytical model was validated with experimental data from the literature. The model was finally implemented in the prediction of the location of hydrate plugging events by developing a mathematical relation for estimating the density and viscosity of hydrates. Also, the effect of bulk modulus, shear strain and shear stress were investigated and how these parameters influence the transportability of hydrates in the pipeline section experiencing hydrates formation. Details of the methodology is provided below.

3.3.1 Model Development Stages

The study assumed a hydrates-prone gas pipeline flow computational domain, with annular and linearly growing hydrates deposit profile (**Figure 3.15**). A 2-fluid multiphase flow pressure drop equation due to friction was adopted for this domain with temperature, pressure, velocity, viscosity, and friction factor as input variables. Furthermore, the time to plug the pipeline from the onset of hydrates deposition was developed from the computational domain. Details of the model development stages are discussed further in the sections that follows. A schematic of the stages adopted is presented in **Figure 3.14**.

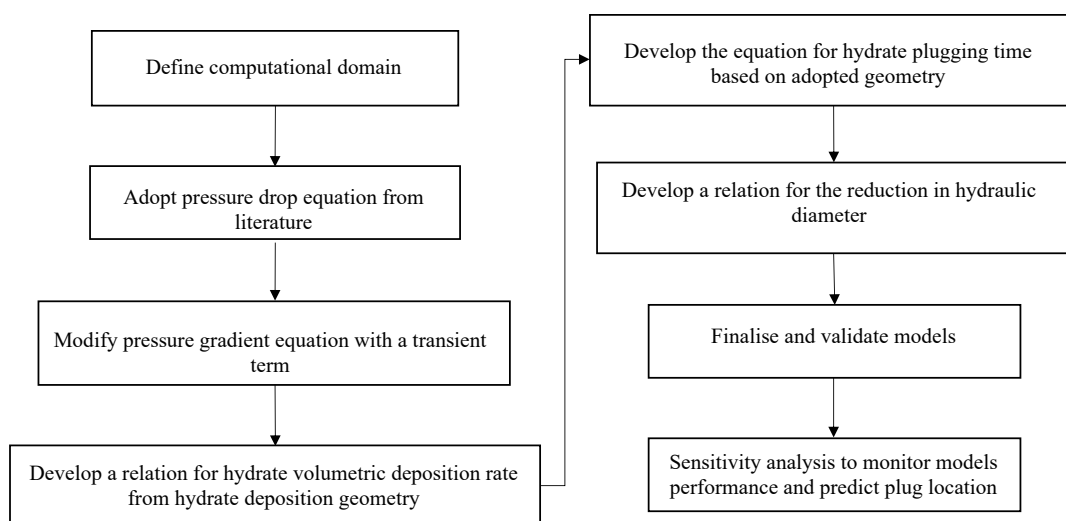


Figure 3.14: The development stages of plugging flowtime and transient pressure drop models

3.3.2 Equations and Derivations

The following basic assumptions have been made in the development of the transient pressure drop model in this work: (i) the fluid flow behind the hydrate plug is single phase because the flow is driven by the gas phase; (ii) the flow is isothermal with negligible temperature change once hydrates are formed and deposited; (iii) viscous effect in the hydrates forming section increases the resistance to flow; and (iv) there is a linear annular growing symmetrical hydrate deposits on the wall of the pipe which reduces the hydraulic diameter in relation to the hydrates deposition rate.

Based on the fact that the pressure drop rises during hydrates plugging, the focus of this work is to develop a transient pressure drop model that directly incorporates the hydrate deposition rate into one equation to account for the viscous changes during hydrates formation through a modification of the two-phase gas-liquid steady-state pressure gradient equation (Beggs and Brill 1973). Such a modelling framework is relatively lacking in existing hydrate-induced pressure drop predicting analytical models. Another separate model was developed to predict the plugging flowtime, which is also lacking in existing literature. The results from both models have been used to provide insight into the location of hydrates plugging event in a gas pipeline.

To validate the models developed in this study, hydrate deposition rates are obtained from experimental models by Di Lorenzo et al. (Di Lorenzo et al. 2014a) and Aman et al. (Aman et al. 2016) to predict the plugging flowtime and transient pressure drop at both high and low velocity scenarios. The computational domain is represented in **Figure 3.15**. The geometry will be used to derive the plugging flowtime for hydrates deposition and the resulting transient pressure drop. The gas flowtime (t_0) and line pressure (p_0) at the onset of hydrates formation and deposition are advanced by equal partitioning of the hydrates forming section (L) by change in time (dt), until the pipeline diameter (D) is plugged by hydrates at time t_{plug} as the hydraulic diameter D_h reduces along the hydrates deposition profile. Hence, the

transient pressure drop (Pa) at the hydrate deposition flowtime (t_1, t_2, \dots, t_n) are represented as dp_1, dp_2, \dots, dp_n .

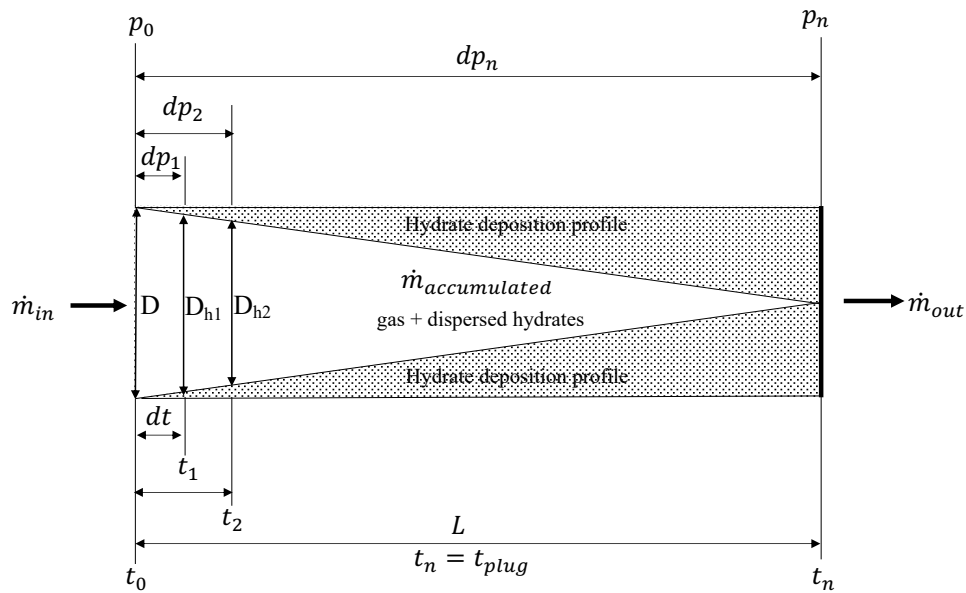


Figure 3.15: Computational fluid domain

Since the deposition of hydrates is a complicated process and depends on the carrier gas, among other factors (Jassim, Abdi and Muzychka 2010), the mixture velocity of the dispersed hydrate and the gas phase have been assumed to be the same as the gas velocity. This is because this model assumes that the hydrates are deposited on the wall with no sloughing and wall shedding, and that there is no-slip between the continuous gas phase and dispersed phase.

The assumption of no sloughing allows for a proactive prediction of early pipeline plugging. However, since it is difficult to account for how much hydrates and water are dispersed in the gas stream, and because the flow is principally driven by gas, the fluid density is approximated to the temperature and pressure dependent density of the gas phase equation 3.36. The lower temperature of the gas phase is enhanced by the fact that water is a poor conductor of heat and because the solubility of methane gas increases at lower temperatures and higher pressure condition, as applicable during hydrates formation (Lekvam and Bishnoi 1997; Odutola et al. 2017; Pruteanu et al. 2017).

To adjust for the effect of the density of the dispersed phase, a multiplying factor will be included in the transient pressure model. For calculating hydrate deposition rates, we will adopt the regression equation discussed in the previous section. In the following derivations, the effect of hydrates sloughing and wall shedding by hydrates is neglected to enhance proactive prediction of the models.

3.3.3 Mass Conservation Equation

Considering a hydrate forming pipeline section of length (L) and diameter (D) originally transporting gas and some entrained water, some of the accumulated mass of gas in the pipeline from the commencement of hydrate deposition to when the pipeline is plugged is related to the mass of gas consumed by the water phase to form hydrates. Hence, from our computational geometry we derive the following equations.

$$\dot{m}_{in} = \dot{m}_{out} + \dot{m}_{accumulation} \quad (3.28)$$

Once the pipeline is plugged, $\dot{m}_{out} = 0$, and equation 3.28 becomes:

$$\dot{m}_{in} = \dot{m}_{accumulated} \quad (3.29)$$

This can be expressed in differential form as:

$$\frac{d}{dt} \rho_g V_g = \frac{dm_g}{dt} \quad (3.30)$$

Expanding the LHS of equation 3.30 using partial differentiation technique, yields:

$$\rho_g \frac{d}{dt} V_g + V_g \frac{d}{dt} \rho_g = \frac{dm_g}{dt} \quad (3.31)$$

During hydrates deposition leading to the reduction of the hydraulic diameter of the pipeline section where hydrates are formed, the gas density is relatively constant because of the uniform hydrate temperature and

pressure, hence $\frac{\partial}{\partial t}\rho_g = 0$ and equation 3.31 reduces to the form in equation 3.32.

$$\rho_g \frac{d}{dt}V_g = \frac{dm_g}{dt} \quad (3.32)$$

re-arranging gives:

$$\frac{d}{dt}V_g = \frac{1}{\rho_g} \cdot \frac{dm_g}{dt} \quad (3.33)$$

where V_g , is the volume of gas; ρ_g (m/s) is the density of gas; $\frac{d}{dt}V_g$, is related to the hydrates deposition rate from the gas consumption rate during the formation of hydrates (Turner et al. 2005); and $\frac{1}{\rho_g} \cdot \frac{dm_g}{dt}$, is the volumetric rate of gas (m³/s) accumulating in the pipeline after hydrates plugging which is responsible for the transient pressure rise. We will now establish the pressure drop due to hydrates deposits plugging the pipeline from the momentum equation.

Momentum Equation

The single-phase momentum equation is adopted because the flow is driven by the continuous gas phase along the pipeline is stated as follows.

$$\frac{d}{dt}\rho_g v_g + \frac{d}{dL}\rho_g v_g^2 = -\frac{dp}{L} + \frac{dp_{wall\ friction}}{L} \quad (3.34)$$

Once the line is plugged, the convective term $\frac{d}{dL}\rho_g v_g^2 = 0$. Other forces resulting from the shear stress, lift force, drag force, and gravitation force have been neglected because the derivation assumes no sloughing and wall shedding events, and there is no influence of gravity since the pipeline is horizontal. $\frac{dp_{wall\ friction}}{dL}$ is the pressure drop due to irreducible friction losses (Teixeira, Secchi and Biscaia 2015). The Darcy pressure drop due to friction equation (Munson et al. 2013), is given below:

$$\frac{dp_{wall\ friction}}{L} = \frac{1}{2} \cdot f \cdot \rho \frac{v^2}{D} \quad (3.35)$$

During hydrates generation in a gas-dominated pipeline, the multiphase flow is approximated to a single-phase flow since the hydrates are deposited on the wall and the flow along the hydraulic diameter is driven by the gas phase. Hence, the diameter (D) term in the pressure gradient due to friction in equation 3.35 can be modified with the hydraulic diameter (D_h) due to the deposition of hydrates (Di Lorenzo et al. 2018).

$$\frac{dp_{wall\ friction}}{L} = \frac{1}{2} \cdot f \cdot \rho_g \frac{v_g^2}{D_h} \quad (3.36)$$

Inserting equation 3.36 into equation 3.34 will give:

$$\frac{d}{dt} \rho_g v_g = -\frac{dp}{L} + \frac{1}{2} \cdot f \cdot \rho_g \frac{v_g^2}{D_h} \quad (3.37)$$

Expanding the LHS using partial differentiation, yields:

$$\rho_g \frac{d}{dt} v_g + v_g \frac{d}{dt} \rho_g = -\frac{dp}{L} + \frac{1}{2} \cdot f \cdot \rho_g \frac{v_g^2}{D_h} \quad (3.38)$$

During hydrates formation, the gas density is assumed to be constant, hence $v_g \frac{d}{dt} \rho_g = 0$. Also, there is no acceleration of the fluid in the hydrate forming section once the pipeline is plugged, implying that $\frac{d}{dt} v_g = 0$. The gas pressure continues to rise due to gas accumulation and compression behind the hydrate plug. This is possible because it has been assumed in this derivation that there is no sloughing and wall shedding, which represent a worst-case scenario. Consequently, equation 3.38 becomes:

$$\frac{dp}{L} = \frac{1}{2} \cdot f \cdot \rho_g \frac{v_g^2}{D_h} \quad (3.39)$$

In this study, the hydraulic diameter D_{h_n} varies with time t_n , hence equation 3.39 can be re-arranged and written by replacing D_h with D_{h_n} as:

$$dp_n = \frac{1}{2} \cdot f \cdot \rho_g \frac{v_g^2 L}{D_{h_n}} \quad (3.40)$$

where the subscript $n = 1, 2, 3, \dots, n$, representing the location indicators from hydrates equilibrium point to hydrates plug along the pipeline. Where dp (Pa) is the transient pressure rise because of hydrates formation and deposition as the hydraulic diameter D_h (m) reduces; L (m) is the length of the hydrates forming and plugging section; v_g is the gas velocity from the discharge compressor station at the instant of plugging; and f is wall friction factor because of hydrates deposition.

The pressure drop along the pipeline is because of the increase in gas viscosity during hydrates formation, and can be explained from the standpoints of both force and energy balance (Munson et al. 2013). From the perspective of force balance, the pressure force in the pipeline will balance the viscous force generated during the flow. For energy balance in the flow domain, the work done by the pressure force must overcome the energy dissipation due to the viscous effect from hydrate formation (Beggs and Brill 1973). The hydrates deposition induced transient pressure drop can be obtained by estimating the volume of hydrates deposited from the geometry in **Figure 3.15**.

3.3.4 Volume of Hydrates Deposited

The above derivations have been based on the following five assumptions: (i) hydrates deposition along a pipeline are unevenly distributed (Zhang et al. 2019). The volume of deposited hydrates is estimated experimentally from the pressure gradient in equation 3.39, by calculating the reduction in pipeline hydraulic diameter from the beginning of gas and water injection into the experimental loop until the end of the experiment (Di Lorenzo et al. 2014b); (ii) the pipeline hydraulic diameter is related to the growth of hydrates film layer along the pipe using a constant growth rate (Di Lorenzo et al. 2018). However, this constant growth rate is dependent on the subcooling temperature and the gas flow velocity, hence can only be determined accurately through experimental observations.

In developing the current model, the constant growth rate of hydrates layer is represented by the ratio of the pipe diameter to the plugging flowtime of hydrates in the pipe, as presented later in equation 3.49; (iii) the plugging flowtime t_{plug} , is positively related to the deposition rate of hydrates (Aman et al. 2016), as represented in equation 3.43; (iv) by assuming that one-third of the hydrates generated are deposited on the wall and form in an annular linear growth profile along the pipeline based on the geometry in the literature (Di Lorenzo et al. 2018) and in a nonuniform diameter in the pipeline as suggested in Wang et al. (2017), a modified computational domain incorporating the hydrate profile in a horizontal gas pipeline of diameter D , hydraulic diameter D_h and hydrate deposition sectional length L , has been described for the purpose of this study in **Figure 3.15**; and (v) although sloughing and wall shedding occurs during hydrates deposition (Di Lorenzo et al. 2018; Liu et al. 2019), this effect is neglected. This is partly because of lack of established relative studies on the effect of sloughing on hydrates layer growth and thickness (Wang et al. 2018), and also because of the intended practical application of this model, which is to capture the first peak in transient pressure drop for the purpose of developing a proactive and preventive hydrate intervention program for gas pipelines.

For industry application, the hydrates growth sectional length (L) can be determined from the pressure and temperature gradient profile generated in a hydraulic simulator; from where the pressure and temperature correspond with the hydrates equilibrium condition determined from a phase envelop. This is because, hydrates are generated at the horizontal section of the pipeline and transported downstream to a point of obstruction or change in flow configuration (McMullen 2011; Di Lorenzo et al. 2014a). Based on this profile, the maximum time from the onset of hydrate deposition to the point where the pipeline becomes plugged can be estimated as a function of the hydrate deposition rate and the pipe diameter. The change in gas volume during hydrates formation can be explained by the mass continuity equation in equation 3.33. In this study, the relation for the deposited volume of hydrates will be developed by taking a 3D geometry of the computational domain in **Figure 3.15**, as:

$$V_H = \frac{\Pi \cdot D^2 \cdot L}{6} \quad (3.41)$$

The hydrates deposition rate can be obtained by dividing both sides of equation 3.41 with the time to plug the pipeline section.

$$\frac{V_H}{t_{plug}} = \frac{\Pi \cdot D^2 \cdot L}{6t_{plug}} \quad (3.42)$$

$\frac{V_H}{t_{plug}}$ is the hydrates deposition rate \dot{Q}_{H-d} . Therefore, the time taken to fill the volume in equation 3.41 at the hydrate deposition rate can be derived as:

$$t_{plug} = \frac{\Pi \cdot D^2 \cdot L}{6\dot{Q}_{H-d}} \quad (3.43)$$

This can be re-arranged as:

$$L = \frac{6\dot{Q}_{H-d}t_{plug}}{\Pi \cdot D^2 \cdot L} \quad (3.44)$$

where t_{plug} , is the flowtime (s) from the beginning of hydrates deposition to the time to record the first significant peak in transient pressure drop, indicating the presence of hydrates plug in the pipe. In this study, the first significant transient pressure spike is when the upstream pressure is above the pipeline design pressure. Substituting L from equation 3.44 into L in equation 3.40, yields:

$$dp_n = \frac{1}{2} \cdot f \cdot \rho_g \cdot \frac{v_g^2}{D_{hn}} \cdot \frac{6\dot{Q}_{H-d}}{\Pi \cdot D^2} \cdot t_{plug} \quad (3.45)$$

where the gas density ρ_g (kg/m³) is estimated from (Di Lorenzo et al. 2018) as follows:

$$\rho_g = -1.27 \times 10^{-7} PT + 0.49T + 4.79 \times 10^{-5} P - 156 \quad (3.46)$$

Since there is no lubrication of the pipe wall by the gas, it is assumed that the gas is flowing over a smooth layer of hydrates and the friction factor is estimated from the equation for smooth round pipe (Drew, Koo and McAdams

1932). During hydrates deposition, the flow is assumed to be frictionless because the depositing hydrate is over a thin layer of water on the wall of the pipeline (McMullen 2011).

$$f = 0.0056 + 0.5Re^{-0.32}; 3000 < Re < 3 \times 10^6 \quad (3.47)$$

The Reynolds number is defined as: $Re = \frac{\rho_g v_g D}{\eta_g}$

where η_g is the gas viscosity (Pa. s) as defined by (Di Lorenzo et al. 2018), below.

$$\eta_g = 6.45 \times 10^{-9} T + 7.36 \times 10^{-13} P + 5.555 \times 10^{-6} \quad (3.48)$$

where T is Temperature (K); and P is Pressure (Pa).

3.3.5 Pipeline Hydraulic Diameter

The hydraulic diameter D_h (m), in equation 3.39 will be derived in this section. This was achieved by replacing the constant hydrate growth rate in the derivation for the reduction in pipe hydraulic diameter in (Di Lorenzo et al. 2014b) by the ratio of the pipe diameter to the hydrates plugging flowtime in the pipe, as represented below:

$$D_{h_n} = D - \frac{D \cdot t_n}{t_{plug}} \quad (3.49)$$

D_{h_n} is the hydraulic diameter varying with time t_n . Which is simplified as:

$$D_{h_n} = D \left(\frac{t_{plug} - t_n}{t_{plug}} \right) \quad (3.50)$$

where $\frac{t_{plug} - t_n}{t_{plug}}$, is the pipe annulus reduction factor due to the deposition of hydrates. Submitting for t_{plug} from equation 3.43, yields equation 3.51. This representation allows for a gradual linear reduction in hydraulic diameter as represented in **Figure 3.15**.

$$D_{h_n} = D \left(\frac{\Pi \cdot D^2 L - 6 \dot{Q}_{H_d} t_n}{\Pi \cdot D^2 L} \right) \quad (3.51)$$

3.3.6 Final Models

The final transient pressure drop model during hydrates deposition can be derived by substituting D_{h_n} from equation 3.51 into equation 3.45 yields:

$$dp_n = \frac{K_H}{2D} \cdot f \cdot \rho_g \cdot \frac{6v_g^2 L \dot{Q}_{H_d}}{(\Pi \cdot D^2 L - 6 \dot{Q}_{H_d} t_n)} \cdot t_{plug} \quad (3.52)$$

The time to plug t_{plug} , has been modified with a factor K_{ft} (Equation 3.53). The value of K_{ft} is taken as 0.8 to approximate the total hydrate deposited on the pipe wall to 26.4% of the hydrates formed as suggested in the literature (Wang et al. 2017). Also, for the purpose of computation, this factor will also prevent the final plugging pressure drop from being infinite when the line is totally plugged.

$$t_{plug} = K_{ft} \frac{\Pi \cdot D^2 \cdot L}{6 \dot{Q}_{H_d}} \quad (3.53)$$

where:

dp_n = Pressure Drop (Pa) at time t_n (s)

t_{plug} = Time to plug the pipeline (s)

dt = Time step obtained by dividing t_{plug} into n equal sections.

$K_H = 0.0188v_g + 4.392$; is a dimensionless empirical model fit constant

$K_{ft} = 0.8$; is a dimensionless empirical approximation constant

f = dimensionless friction factor for gas flowing inside a pipe with hydrate deposition; calculated from equation 3.47.

ρ_g = gas density (kg/m³, calculated from equation 3.46).

V_g = gas velocity (m/s)

t_n = instantaneous flowtime (s): computed from equation 4.43, based on the algorithm in **Figure 3.16**, below.

\dot{Q}_{H_d} = Hydrate deposition rate predicted from experimental, CFD model (m³/s), or predicted from the regression/mathematical model developed in chapter 6 later.

L = hydrates formation and deposition pipeline section (as defined in **Figure 3.15**)

D = Pipe internal diameter (m)

Π = The ratio of the circumference of the pipe annulus to the diameter of that pipe, taken as 3.142.

Equation 3.52 above is the pressure drop model incorporating the hydrate deposition rate. The inclusion of hydrates deposition rate in the model already contained the influence of the subcooling temperature. At the current hydrates deposition rate, the model predicts the first spike in pressure at the pipeline condition. The pressure drop is estimated as the difference between the first pressure spike and the hydrates formation equilibrium condition.

To solve the above model, we developed the computational algorithm presented in **Figure 3.16**.

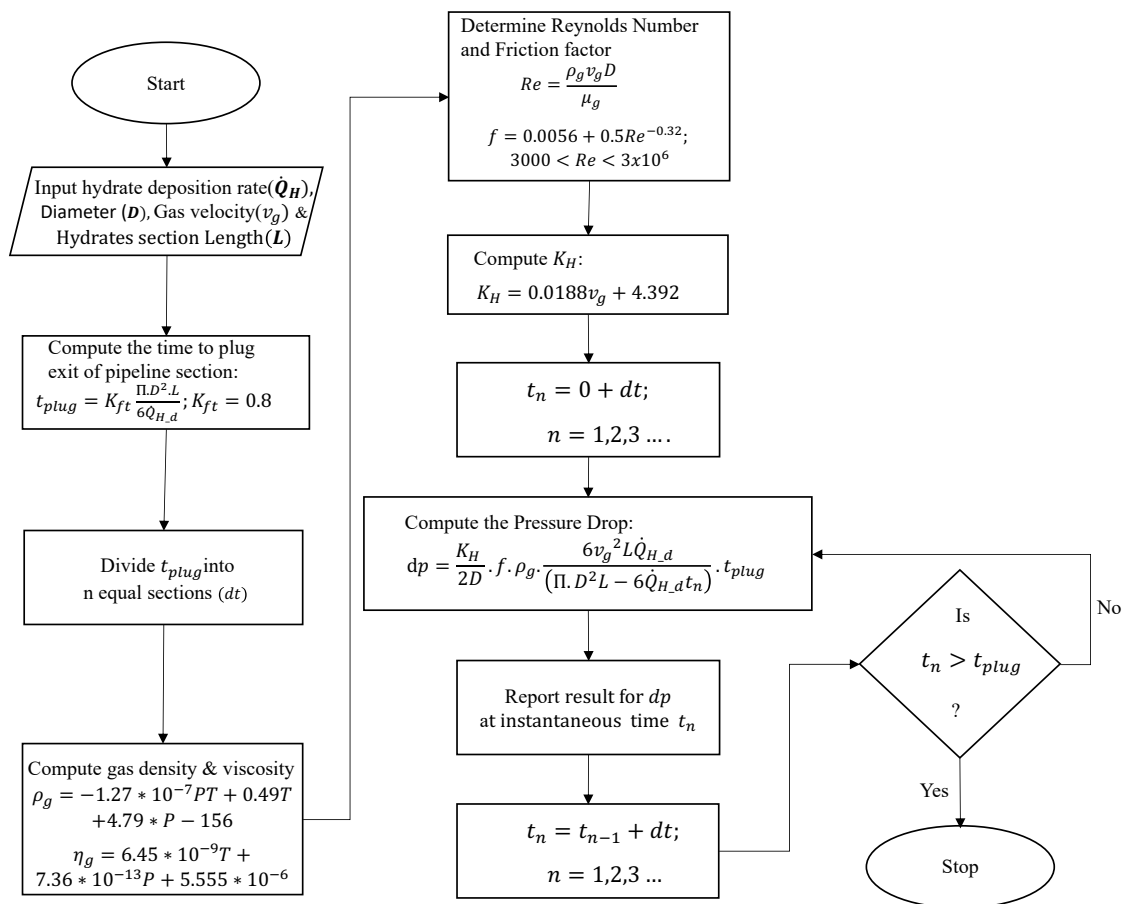


Figure 3.16: Solution Algorithm

When the model is implemented to locate hydrate plug in the line, different lengths can be iterated until the flowtime matches the recorded operational flowtime between the onset of hydrates and the first pressure spike. Ballard et al. (2011) recommended the installation of pressure transmitters along the pipeline to monitor hydrates formation, as a spike in pressure is an indication of hydrates forming downstream of the pressure transmitter. Our model can be implemented with this kind of installation to predict real-time hydrates deposition rate. The above algorithm is explained in the following steps:

Step 1: Input data for hydrate deposition rate (\dot{Q}_H), Length of hydrate deposition pipe section, which is also the location of the hydrates plug (L), Diameter of pipe (D), and gas velocity (v_g), are entered into the model.

Step 2: The expected time to plug the exit of the pipe based on the deposition rate is calculated.

Step 3: The timestep is also calculated by dividing the time calculated in step 2 into n equal sections

Step 4: Computes the pressure and temperature dependent gas stream density and viscosity.

Step 5: Computes the Reynolds number (Re) and friction factor (f)

Step 6: Computes the empirical factor K_H

Step 7: Computes the first computational instantaneous time

Step 8 & 9: Evaluates the pressure drop with the inputs and calculated variables from steps 1-8 and reports the pressure drop.

Step 10: Advances the timestep by adding the timestep to the previous computational instantaneous time.

Step 12: Executes a conditional statement that determines if the computation should proceed or terminate.

3.4 Hydrate Plugging Risk Table

Estimating the risk of plugging and mitigating it is not a straightforward science. Whereas other researchers have estimated this risk in aiding the planning of intervention programs, none had addressed this risk based on plugging flowtime and the safety of the pipeline from the resulting pressure drop in comparison with the pipeline design pressure. Hence, a hydrate

plugging risk table was developed from the perspective of plugging flowtime and if the resulting pressure drop is lesser or greater than the maximum allowable operating pressure of the pipeline (MAOP). Details of the risk table development and a case study that connects the deposition rate of hydrates and the resulting pressure drop in providing guidance on a proposed new 30km offshore pipeline are provided in chapter 8.

3.5 MATLAB® Programming

The use of MATLAB® was adopted to perform the programming of the outcome of this study to predict hydrates deposition rate, pressure drop and time to plug the hydrate forming pipeline section. The program calculates the pressure drop and time to plug the line based on the indicated length of the hydrate forming section, hence by plotting the pressure drop against the hydrate forming section, a linear graph of the relationship can indicate possible position of a plug, since the pressure drop increases the further the obstruction is located from the pipeline inlet because of the increase in compressed gas volume behind the plug. The MATLAB® code is provided in Chapter 9.

3.6 Chapter Summary

This chapter presented the multiple methodologies adopted in this study as dictated by the scope of this research in **Figure 3.1**. The details of each methodology will be provided in subsequent chapters. Every chapter after now starts with a introduction, that provide insights into the problem solved, the methodology, the results, and implications. This is followed with the methodology, results and validation, parametric analysis, and chapter summary.

CHAPTER 4: CFD MODELLING OF HYDRATES DEPOSITION RATES AND PIPEWALL SHEAR STRESS IN SUBSEA GAS PIPELINES¹

4.0 Introduction

The need for a specific gas-hydrate predicting model for gas-dominated systems has been stressed in the literature (Charlton et al. 2018a). In 2020, global demand for natural gas was estimated as 4.4 trillion cubic meters (BP 2020). As the world move into a fully digital economy, the dependence on natural gas will continue to increase. Hence, while waiting for other competitive sources of energy that can meet global energy demand in the coming years, it is important to enhance the flow assurance of natural gas pipelines through proactive intervention measures that can manage the formation and deposition of hydrates. Gas hydrates are still operational pipeline plugging risk in the transportation of natural gas.

For offshore gas pipelines buried or lying on the seabed, subcooling temperatures around the pipeline can lead to gas-pipewall thermal gradient that can increase the formation and deposition of hydrates. This occurrence can hinder gas availability to costumers. Also, pipeline plugging and reduction of hydraulic diameter during hydrates deposition can lead to pipeline failure through over-pressurisation (Jassim, Abdi and Muzychka 2010; Sloan, Koh and Sum 2011b).

Thus, hydrate deposition in gas-dominated pipelines is one of the prevailing safety and economic concerns in the oil and gas industry (Koh and Creek 2011; Kinnari et al. 2015). This has led to increase in research activity in this area to improve the knowledge of how hydrate formation and deposition can affect flow assurance in gas pipelines. Currently, three approaches to hydrates management are implemented in the industry, including hydrate prediction, prevention and problem solving (Kinnari et al. 2015). Firstly,

¹ The results in this chapter are published in the Journal of Natural Gas Science and Engineering: Umuteme, O. M., Islam, S.Z., Hossain, M. and Karnik, A., 2022. An improved computational fluid dynamics (CFD) model for predicting hydrate deposition rate and wall shear stress in offshore gas-dominated pipeline. *Journal of Natural Gas Science and Engineering*, 107 (2022). Doi: 10.1016/j.jngse.2022.104800.

hydrate prediction is related to how hydrates are formed and the related safety concerns, such as pressure rise and pipeline rupture (Di Lorenzo et al. 2014a; Kinnari et al. 2015). Secondly, hydrate prevention in gas pipelines is possible by modifying the flow parameters and conditions, such as temperature, pressure and gas flowrate (Lederhos et al. 1996; Li et al. 2013; Carroll 2014; Lim et al. 2020). Thirdly, problem solving approach to hydrate management in the oil and gas industry is cost intensive and not usually recommended for effective hydrate control (Jassim, Abdi and Muzychka 2010; Kinnari et al. 2015).

Hydrate formation kinetics and growth models provides the foundational knowledge for understanding the flow behaviour of hydrates in pipelines, and are discussed extensively in the literature (Sloan, Koh and Sum 2011a; Carroll 2014; Yin et al. 2018). Recent advances exist in experimental research (Li et al. 2013; Di Lorenzo et al. 2014a, 2014b; Aman et al. 2016; Ding et al. 2017; Odutola et al. 2017; Zhang, Wu and Mu 2017; Liu et al. 2020) and analytical models (Wang et al. 2017, 2018; Di Lorenzo et al. 2018; Liu et al. 2019) on hydrate formation and deposition rates in gas pipelines.

The experimental study of hydrates in gas pipelines is usually a difficult task (Lim et al. 2020) and expensive because, changing the experimental pipe geometry, such as length and diameter, requires new or modified experimental set up. Thus, increasing the difficulty in extrapolating experimental results for large scale field application.

Consequently, analytical models have gained research attention lately leading to the following significant findings: (i) sloughing and shedding of the deposits of hydrates is responsible for the fluctuation in the shear strength of hydrates (Liu et al. 2019) and transient pressure drop in the pipe (Di Lorenzo et al. 2018; Liu et al. 2019); (ii) hydrate deposition and growth generate the following multiphase flows, including: 3-phase gas-water-hydrates; 2-phase gas-hydrate; and 2-phase water-saturated gas. The authors suggested that the plugging risk of hydrates is more likely in the 3-phase gas-water-hydrates flow (Wang et al. 2018); (iii) the thickness of hydrates along the pipe wall follows a non-uniform pattern, and about fifty-percent (50%) of the hydrates deposited are formed at the dispersed water

in the gas phase (Wang et al. 2017); and (iv) increasing the gas velocity increases the depositional distance from the point of hydrates generation along the pipeline (Jassim, Abdi and Muzychka 2010).

However, only the analytical models developed by Di Lorenzo et al. (2018) and Wang et al. (2018) focused on hydrates deposition rates in gas dominated pipeline at different subcooling temperatures, which is relevant for estimating the plugging flowtime of hydrates and the resulting transient pressure drop. Both models predicted deposition rates of hydrates comparatively with experimental results. However, only the model by Di Lorenzo et al. (2018) considered hydrates deposition rates at low gas velocity of 4.7m/s, yet the tweaking of the model through multiplier parameters to predict experimental results is a concern for scalability and extension for industrial size pipelines.

Consequently, the model underpredicted all the experimental results of Aman et al. (2016) at the gas velocity of 4.7m/s and subcooling temperature range of 4.5-7.5K. After predicting the first experimental result of 0.055L/min as 0.04L/min at the subcooling temperature of 4.5K, the model predicted the hydrates deposition rate of 0.07L/min against the experimental value of 0.105L/min at 7.5K subcooling temperature under the same gas velocity of 4.7m/s. This imply that the model is unreliable at higher subcooling temperature and low gas productivity, which is a concern raised in the literature (Li et al. 2021). Thus, the extension of this model for industrial application can underpredict hydrate plugging risk under similar flow condition, with attendant consequences that were discussed earlier.

Therefore, the increasing availability of various CFD software necessitated the need for a validated CFD model that can accurately predict hydrate deposition rate in gas pipelines. Progress in CFD modelling of hydrates in gas pipelines has focused on the deposition and transportability of hydrates, and not on hydrates deposition rates. A CFD model capable of accurately predicting hydrates deposition rates and wall shear stress during hydrates deposition can provide additional insights into hydrates plugging risks in gas pipelines. However, progress in related CFD models is relatively lacking. Recent advancement in CFD modelling are discussed as follows. Balakin et

al. (2016) developed a CFD model for the agglomeration and deposition of hydrates using the population balance method (PBM) in oil-dominated pipelines.

Though the results were validated with experimental data, the model was developed for oil-dominated pipelines and did not predict hydrates deposition rates by direct simulation of hydrates temperature and pressure conditions. Other oil-dominated hydrate deposition CFD models reported in the literature (e.g., Lo, 2011; Neto et al., 2015; Song et al., 2018a), are not suitable for predicting hydrates deposition in gas pipelines because of the difference in multiphase flow in oil-dominated pipeline (oil-gas-water) and gas-dominated pipeline (gas-water). For gas-dominated pipelines, Jassim et al. (2010) developed a CFD model that determines the distribution of fluid properties in the flow domain during the formation and deposition of hydrates to calculate the particle size distribution and depositional distance of hydrates along the pipeline.

The hydrates deposition CFD model by Neto et al. (2016) provided insight into the nature of hydrates slurry settling at the bottom in a gas pipeline, but the model was not validated. Also, the model did not simulate the annular effect of hydrate growth on the pipe wall reported from experimental observations (Di Lorenzo et al. 2014b; Aman et al. 2016). Other CFD models for hydrates studies in gas pipelines neglected the formation of hydrates but focused on the agglomeration, deposition, rheology, and transportability of hydrates by injecting hydrates into the flow domain as a discrete phase (e.g., Berrouk et al., 2020; Jujuly et al., 2017; Li et al., 2019; Song et al., 2018; Sule et al., 2015).

Thus, the CFD model developed in this doctoral work is timely for the following reasons. First, the predictions of the only analytical model that predicted hydrates deposition rates at lower velocity of 4.7m/s underpredicted experimental result at higher subcooling temperatures of 7.5K by 33%, thus exposing the pipeline under this condition to underpredicted hydrate plugging risk. Second, existing CFD models injected hydrates into the flow domain as a discrete phase.

While this approach predicts hydrate velocity distribution, deposition, agglomeration, and transportability of hydrates, it is not adequate for transient simulation prediction of hydrate plugging risk based on the temperature and pressure conditions in the pipeline. Third, this CFD model simulation aim to clarify the disagreement in the literature on whether the wall shear stress varies (Liu et al. 2019) or is constant (Di Lorenzo et al. 2018) during the deposition of hydrates along the pipeline. This is important for future studies that aim to model the impact of gas and water-induced shear stress on the plugging risk of hydrates in gas pipelines.

Although there are currently no validated CFD models to predict the depositional rates of hydrates, research evidence indicates that CFD transport and energy equations, and other physical models that defines the intensive and extensive properties of the fluid medium can be implemented in CFD modelling of hydrate deposition in gas pipelines. The CFD model developed in this study for predicting hydrate deposition rates in a gas pipeline is based on the conditions for hydrate formation in the literature (Carroll, 2014): (a) adequate combination of low temperature and high pressure based on the composition of the natural gas; (b) availability of gas hydrate formers (e.g., methane, ethane, and carbon-dioxide); and (c) presence of water in sufficient amount.

The formation of hydrates is equally enhanced by flow and physical parameters such as turbulence and agitation, hydrate nucleation sites (elbows, Tees, and valves) and water-gas interface (Carroll, 2014). Furthermore, the gas consumption rate during hydrate formation is dependent on the increasing solubility of methane gas in water at higher pressure and lower temperatures below the equilibrium point on the hydrate formation loci (Lekvam and Bishnoi 1997).

Additionally, experimental results suggests that the growth of hydrates is dependent on the temperature driving force and gas–water interfacial area (Aman et al., 2016; Di Lorenzo et al., 2014b, 2014a; Ding et al., 2017; Turner et al., 2005; Zhang et al., 2017).The thermal gradient between the temperature of the wet gas and pipe wall influences the induction time during the initiation and growth of hydrates (Lim et al., 2020). Also, the pipeline

environment creates the sub-cooling temperature, which results in the thermal transfer by convection during the turbulent interaction between the water phase and the continuous gas phase. Thus, the increase in the solubility of natural gas in water is initiated by the thermal cooling at the pipe wall due to increasing sub-cooling temperatures from the environment.

In their flowloop experiment, Odutola et al. (2017) reported that at the commencement of hydrate formation, the temperature decreased until it was stable during the agglomeration and deposition of hydrates. This position is also corroborated in an earlier experiment by Li et al. (2013) and recently by Liu et al. (2020). Furthermore, Ding et al. (2017) reports a range of 771-830kg/m³ as the density of hydrates during deposition. Earlier, Li et al. (2013) reported a range of 805-825kg/m³. From both studies, an average value of 807.75kg/m³ is obtained as the density of hydrates. However, this study adopted a similar hydrate density of 807.77kg/m³ used in the CFD-PBM simulation in Balakin et al. (2016). Furthermore, visual inspection during experimental runs indicates an annular-dispersed flow pattern during hydrate formation and deposition (Di Lorenzo et al. 2014a, 2014b; Aman et al. 2016; Ding et al. 2017).

Therefore, this section of this thesis report is on the results and validation of a CFD model for predicting hydrate deposition rates and the resulting wall shear stress in the horizontal section of an offshore hydrate-forming gas pipeline by simulating the thermo-mechanistic multiphase (methane and water) flow conditions for the formation of hydrates. Through the implementation of user defined function (UDF) codes for the mass and energy sources in a commercial CFD software package (ANSYS Fluent), metered gas injection into the computational domain was controlled to mimic the gas consumption rate during hydrate formation. This effect was enhanced by the increasing density of gas towards the pipe wall by momentum and thermal diffusivity, as the solubility of methane in water increases at the simulation subcooling temperatures and pressure.

Using a mathematical relation, the resulting simulated average gas mass flowrate was converted to average deposition rates of hydrates in L/min. The final results are validated with experimental and analytical results available

in the literature (Di Lorenzo et al. 2014b, 2018; Aman et al. 2016). Sensitivity analyses was carried out to improve the understanding of the effect of velocity and temperature on the depositional rates of hydrates, the resulting transient pressure drop and wall shear stress, and to establish the predictability of the CFD model based on parameter variability. Thus, the focus of this research in this chapter is to accurately predict hydrate deposition rate and the resulting pipe wall shear stress, as both are important flow assurance phenomenon for gas pipelines in the oil and gas industry. The rest of the chapter is structured as follows – a detailed discussion of the results and validations in section 4.1. Parametric analysis is presented in section 4.2. The chapter summary is also presented in section 4.3.

4.1 Model Validation and Discussion

The empirical results of this CFD model at 4.7 m/s and 8.8 m/s predicted within $\pm 10\%$ uncertainty bound of the quantile-quantile slope plots (**Figure 4.2** and **Figure 4.3**) for both experimental results (Di Lorenzo et al. 2014b; Aman et al. 2016) and analytical model results (Di Lorenzo et al. 2018). At lower gas velocity of 4.7 m/s, the model overpredicted the hydrates deposition rates of the experimental results in Aman et al. (2016) by a range of 9-25.7%, whereas the analytical model of Di Lorenzo et al. (2018) underpredicted the same experimental results by a range of 27-33% (**Figure 4.4**). Consequently, the CFD model can improve proactive hydrate plugging risk predictions earlier than the analytical model.

Similarly, at a velocity of 8.8 m/s and subcooling temperatures of 2.5K, 7.1K and 8.0K, the CFD model underpredicted the hydrate deposition rates of the regressed experimental results in Di Lorenzo et al. (2014a) by 14%, 6% and 4% respectively, and overpredicted the results by 1% at a subcooling temperature of 4.3K (**Figure 4.5**). In comparison, the hydrate deposition rate predictions of the analytical model in Di Lorenzo et al. (2018) at a velocity of 8.8 m/s and increasing subcooling temperatures were inconsistent with theorized linear regression trend, as the model prediction at the subcooling temperature of 2.5K was higher than subsequent predictions at higher subcooling temperatures (**Table 4.2**). Finally, the CFD model

predicted the locations and corresponding phase change during hydrate formation, agglomeration, and deposition.

Especially, the CFD model also captured hydrate formation, agglomeration, deposition and plugging through pressure and temperature curves as reported in the literature (Liu et al. 2020). Under similar subcooling temperature (e.g., 4.5/4.3), doubling the velocity also doubles the deposition rate, which is also consistent with the experimental report in Aman et al. (2016).

From the model results we suggest that hydrate sloughing shear stress is relatively constant, and the wall shedding shear stress by hydrates vary during deposition. Again, in all the temperature contour maps generated (**Figure 4.10-18**), there is a reducing temperature profile towards the wall and the annular flow pattern observed is consistent with experimental visual observations (e.g., Ding et al., 2017; Di Lorenzo et al., 2014b). The gas density also increases from the pipe core towards the wall (**Figure 4.14**), which also resonates with reported experimental observations (Di Lorenzo et al., 2014b; Aman et al., 2016; Ding et al., 2017).

All simulations were carried out within the temperature and pressure corridor for the experimental observations of Di Lorenzo et al. (2014a, b) and Aman et al. (2016) as shown in the hydrate loci curve in **Figure 4.1**. Thus, confirming that the CFD results presented in detail hereafter predicted the formation and deposition of hydrates.

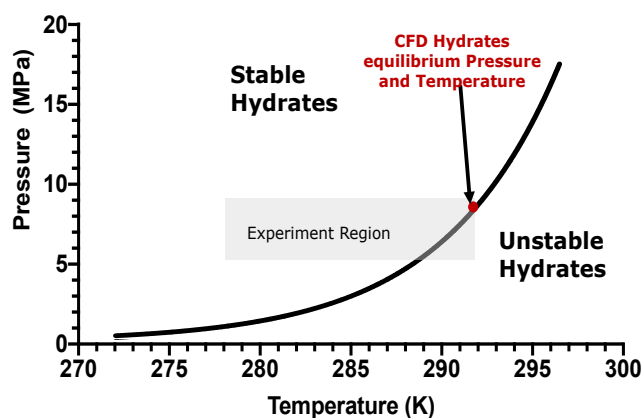


Figure 4.1: Methane hydrate loci showing experimental region

As indicated in **Figure 4.1**, at the system inlet operating pressure of 8.8 MPa, the stability of hydrates is at temperatures lower or equal to 290K. The details of the model validation are discussed in section 4.2.1.

4.1.1 CFD Model Validation

In this section, the predicted deposition rates of hydrates are validated with both experimental and analytical results in the subsections that follows.

4.1.1.1 Hydrate Deposition Rates

The deposition rate results have been validated with both experimental (Di Lorenzo et al. 2014b; Aman et al. 2016) and analytical results (Di Lorenzo et al., 2018) in **Table 4.1** and **Table 4.2**. The average deposition rates of hydrates for all subcooling temperatures from **Figure 4.19** and **Figure 4.20** are computed during hydrates deposition as indicated in section III of **Figure 4.7**, identified as first average deposition rate.

In **Figure 4.2** and **Figure 4.3**, the graphical comparison of the predicted deposition rates by the CFD model with experimental and analytical results are presented. Aman et al. (2016) mentioned the presence of uncertainties in the estimated deposition rates of hydrates in their experiment at 4.6 m/s. For instance, at gas velocity of 4.6 m/s and subcooling temperature of 7.0K, Aman et al. (2016) reported 0.004 L/min as the average hydrates deposition rate.

Since hydrates deposition increases with subcooling temperature, this value was considered an outlier and not included in the graph for Aman et al. (2016) in **Figure 4.2** below. Also, at 8.8 m/s and a subcooling temperature of 2.5K, the analytical model of Di Lorenzo et al. (2018) predicted a value of 0.34 L/min and followed with lower values as the subcooling temperatures increased. As a result, this value was considered an outlier because it did not represent the theorized regression trend of lower deposition rate as subcooling temperature reduces.

Table 4.1: Hydrate deposition rate validation at 4.7m/s

Velocity (m/s)	Sub-Cooling Temp.(K)	Average Hydrate Deposition Rate (L/min)		
		Aman et al., 2016 (Exp.)	Di Lorenzo et al., 2018 (Analytical)	CFD Model
4.7	4.5	0.055	0.04	0.060
	6.0	0.078	0.06	0.097
	7.0	0.004 ^{††}	0.07	0.121
	7.5	0.105	0.07	0.132

^{††} Experimental data considered an outlier because it did not agree with the expected outcome of higher deposition rate as subcooling temperature increases.

Table 4.2: Hydrate deposition rate validation at 8.8m/s

Velocity (m/s)	Sub-Cooling Temp.(K)	Average Hydrate Deposition Rate (L/min)		
		Di Lorenzo et al., 2014a (Exp.) [†]	Di Lorenzo et al., 2018 (Analytical)	CFD Model
8.8	2.5	0.073	0.34 ^{††}	0.063
	4.3	0.124	0.12	0.125
	7.1	0.150	0.14	0.141
	8.0	0.191	0.24	0.183

[†]The experimental deposition rates are regressed from the uninhibited results in Di Lorenzo et al. (2014a) at subcooling temperatures of 4.5K, 4.7K, 6.8K and 8.8K. ^{††} Analytical data was considered an outlier because it did not agree with the expected outcome of lower deposition rate as subcooling temperature reduces

As indicated in **Table 4.1** and **Table 4.2**, the hydrate deposition rate values obtained by this CFD model compared favourably with both experimental and analytical results. Again, the CFD simulated hydrate deposition rate of 0.125 L/min at 8.8 m/s and 4.3K compared favourably with 0.15 L/min reported in the analytical model of Wang et al. (2018). For similar lower subcooling temperatures (e.g., 4.5K/4.3K) doubling the velocity also doubled the deposition rate of hydrates.

As the subcooling temperature increased, this effect also reduced; for instance, doubling the velocity at subcooling temperature of 7.0K/7.1K only increased the deposition rate by approximately 16.5%. Implying that subcooling temperatures plays a significant role in hydrates plugging risk prediction. The quantile-quantile (Q-Q) plot in **Figure 4.2** and **Figure 4.3** below compares the CFD model result with both experimental and analytical

hydrate deposition rates within 90% confidence interval, to investigate the consistency of the results predicted by the CFD model across the subcooling temperatures.

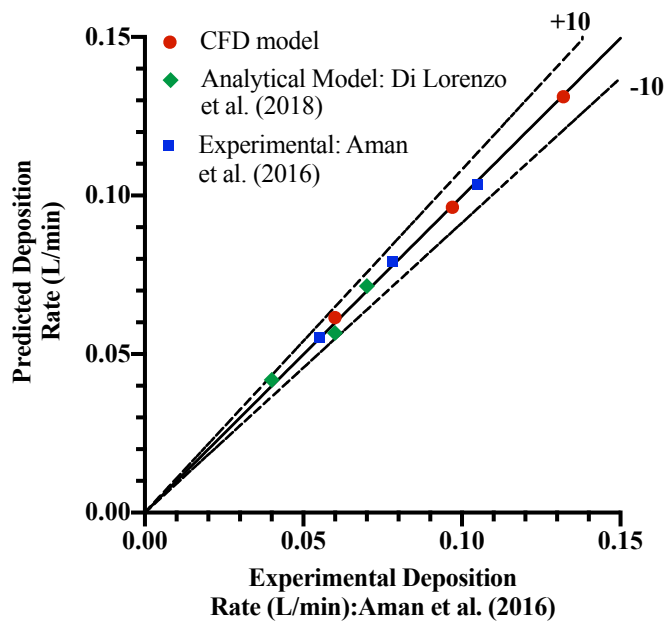


Figure 4.2: 10% bound Q-Q plot comparison of CFD model prediction of hydrate deposition rates at a gas velocity of 4.7 m/s with experimental and analytical model results

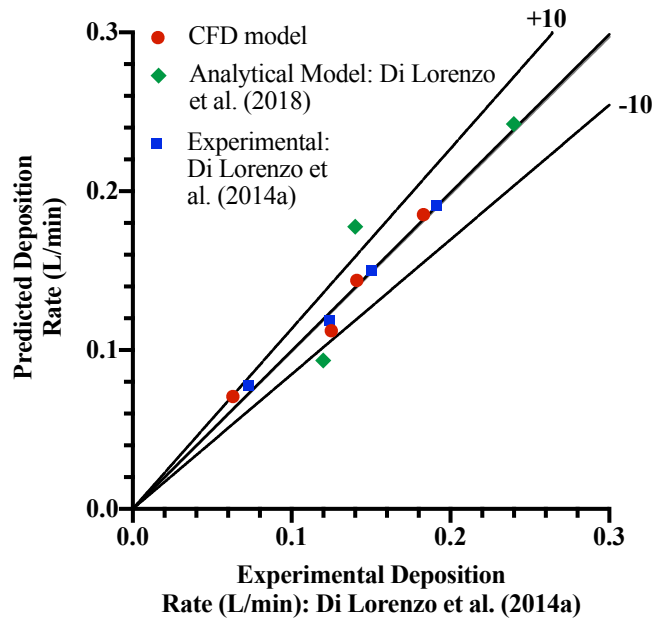


Figure 4.3: 10% bound Q-Q plot comparison of CFD model prediction of hydrates deposition rates at a gas velocity of 8.8 m/s with experimental and analytical model results

The dotted linear lines in **Figure 4.2** and **Figure 4.3**, represent the consistency of the CFD model predictions within $\pm 10\%$ uncertainty bound compared with experimental and analytical results. The deviation of the CFD model predictions from experimental results is discussed further. The observation from **Table 4.1**, suggests that the CFD model at low gas velocity of 4.7 m/s is a better alternative compared to the analytical model.

At lower velocity of 4.7 m/s (**Figure 4.4**), the CFD model results overpredicted the experimental results by a range of 9-25.7%, whereas the analytical model of Di Lorenzo et al. (2018) underpredicted the same experimental results by a range of 27-33%. Hence, the risk of underpredicted hydrate plugging risk is expected using the analytical model, especially at higher subcooling temperatures and lower gas velocity. In practice this can occur in under-capacity utilization flow regime in gas pipelines.

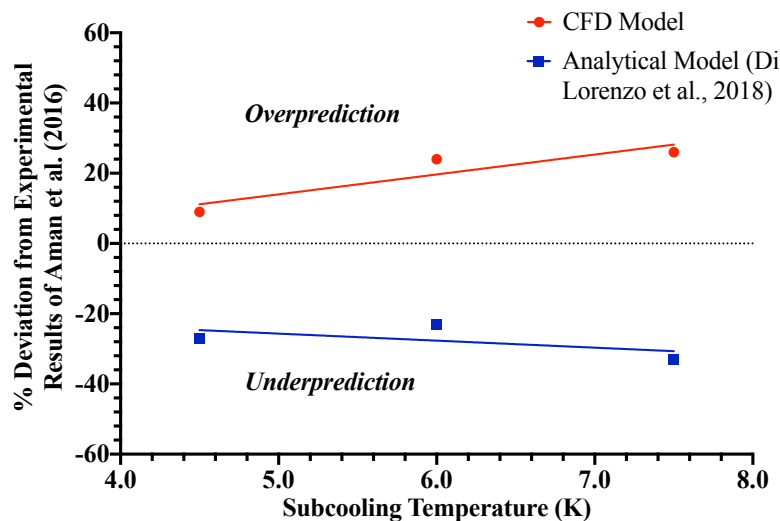


Figure 4.4: Comparing % deviation from experimental results at gas velocity of 4.7 m/s

As seen from **Figure 4.4**, the predictions of the CFD model at low gas velocity can lead to a proactive hydrates control intervention under low gas productivity, while the predictions from the analytical model can lead to delayed intervention with attendant pipeline failure risk from overpressurisation.

Furthermore, at a higher velocity of 8.8 m/s the regressed experimental data in **Table 4.2** at subcooling temperatures of 2.5K, 7.1K and 8.0K were underpredicted by the CFD model by 14%, 6% and 4% respectively (**Figure 4.5**). Also, the CFD model overpredicted the same experimental results by 1% at a subcooling temperature of 4.3K. However, aside the hydrate deposition rate prediction by the analytical model of 0.34 L/min against the regressed experimental value of 0.073 L/min at the subcooling temperature of 2.5K in **Table 4.2**, the hydrate deposition rate predictions of the analytical model indicates underprediction of experimental results by 3% and 7% at subcooling temperatures of 4.3K and 7.1K, respectively and overpredicted the same experimental results by 26% at the subcooling temperature of 8.0K, which is appropriate for a proactive hydrate deposition rate predicting model.

From the linear trend in **Figure 4.5**, there is the tendency that the CFD model will overpredict the experimental hydrate deposition rates as the subcooling temperatures increases beyond 8.0K. The risk of hydrate plugging is reduced at higher gas velocity (Aman et al. 2016), hence, the observation from the results (**Table 4.2** and **Figure 4.5**) indicates that the predictions from the CFD model is a consistent linear representation of the theorized positive regression trend of increasing hydrate deposition rates as the subcooling temperatures increases at constant gas velocity.

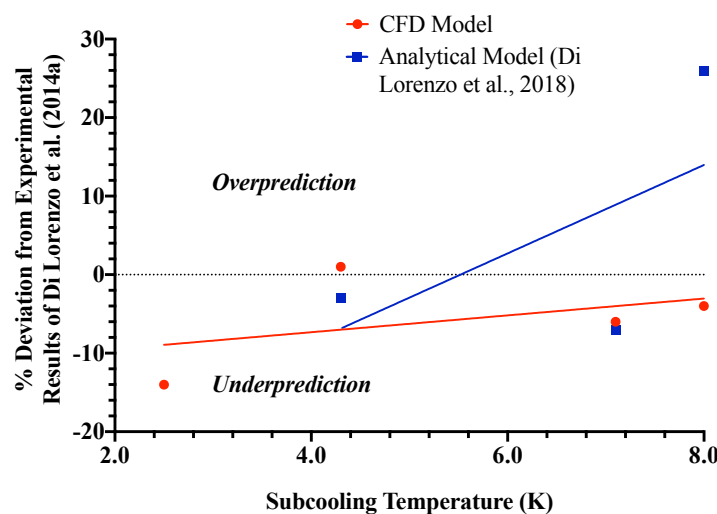


Figure 4.5: Comparing % deviation from experimental results at gas velocity of 8.8 m/s

Therefore, the outcomes of the validation above implies that the CFD model prediction is more proactive in hydrates plugging risk prediction, and an improvement over the predictions by the analytical model of (Di Lorenzo et al. 2018) at simulation conditions of low gas velocity. At higher velocities of 8.8 m/s, the predictions of both models are relatively the same except at lower subcooling temperatures of 2.5K considered as outlier earlier where the analytical model prediction was not consistent with expected reduction in the deposition rates of hydrates compared with values obtained at higher subcooling temperatures.

Figure 4.6 and **Figure 4.7** below present the graphical representations of the relationship between hydrate formation, agglomeration, and deposition rates, fluid temperature and pressure drop, and are used to describe the process of phase change in hydrate-forming gas pipeline (**Figure 4.24**). From **Figure 4.6**, the hydrates were stable after a flowtime of 0.3 s. The descriptions and indications compare favourably with experimental observations, as discussed further.

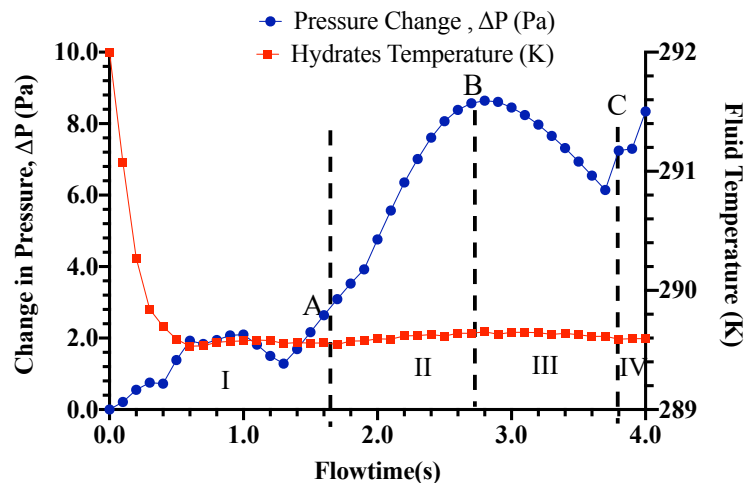


Figure 4.6: Relationship between pressure and temperature variation at 8.8 m/s and subcooling temperature of 7.0K

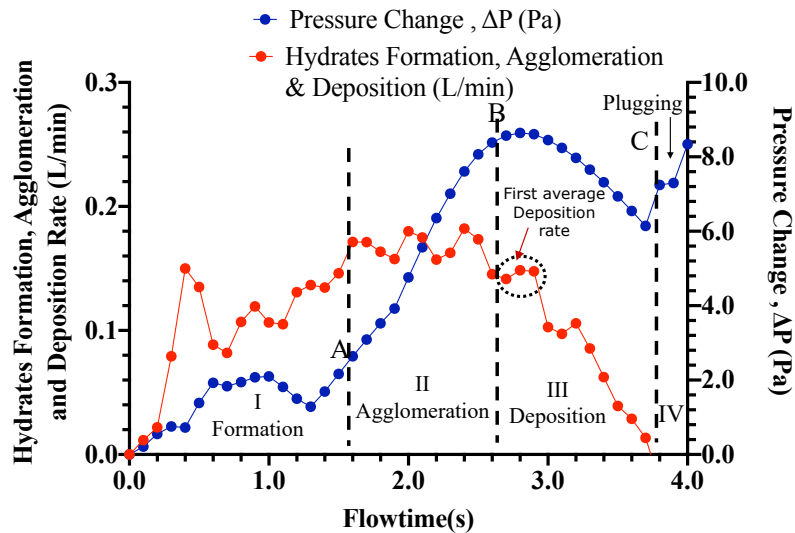


Figure 4.7: Relationship between pressure drop and hydrate deposition rate at 8.8 m/s and subcooling temperature of 7.0K

In **Figure 4.6** and **Figure 4.7**, hydrate formation, agglomeration, deposition and pipe plugging are represented in sections I, II, III and IV respectively as indicated in (Liu et al. 2020). Higher hydrates formation risks are possible in gas-dominant pipelines because of lower volume fraction of liquid water (Sloan, Koh and Sum 2011a). The formation and agglomeration of hydrates are characterised by phase change and can be measured by the gas flowrate in the fluid domain. Experimental results suggest an increase in gas flowrate during hydrate formation because of the increase in gas consumption rate (Turner et al. 2005; Odutola et al. 2017).

Also, the gas flowrate is relatively stable during agglomeration (Odutola et al. 2017) and decreases during hydrates deposition because of reduction in pipe hydraulic diameter (Aman et al. 2016). As discussed later in section 4.2.1 (**Figure 4.24**), hydrate formation and agglomeration in gas-dominant pipeline occur during 3-phase flow of gas, water, and hydrates (section I) and 2-phase flow of gas and hydrates (section II), respectively. Consequently, the formation of hydrates is not possible in section II, because of the absence of water in the fluid domain.

The rates of hydrate formation, agglomeration, and deposition are indicated on the left-hand side of the vertical axis in **Figure 4.7**, and can be obtained from the curve. Full agglomeration of hydrates was achieved in stage II at

an average rate of 0.17 L/min in **Figure 4.7**. The transient pressure drop was superimposed to explain the effect of these stages on the pressure drop in the pipeline. The temperature is relatively stable during full agglomeration of hydrates (section II), and hydrate deposition (section III) which is similar to indications in the literature (Turner and Talley 2008; Li et al. 2013; Odotola et al. 2017; Liu et al. 2020).

In section III, there is a continuous decline in hydrate deposition rate (**Figure 4.7**), which is consistent with observations in literature (Liu et al. 2019). Also evident from the graph is the sharp rise in the system pressure during the agglomeration of hydrates, which is also consistent with experimental observations (e.g., Di Lorenzo et al., 2014a; Aman et al., 2016). By comparing the transient temperature curves at subcooling temperature of 7.0K at gas velocities of 4.7 m/s and 8.8 m/s (**Figure 4.8**), the observation suggests that hydrates are more stable at lower flow velocities. This observation is consistent with indications in the literature (Aman et al. 2016).

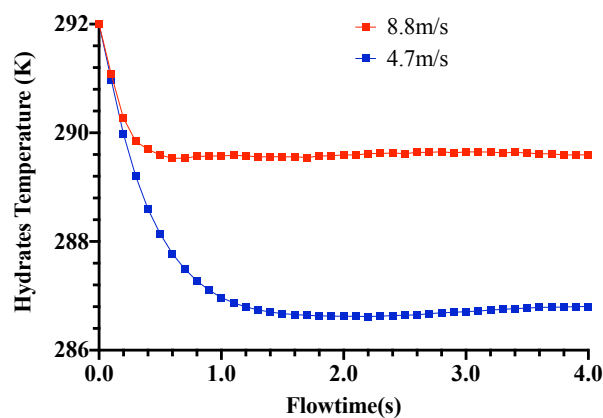


Figure 4.8: Comparing hydrate temperatures at subcooling temperature of 7.0K with gas flow velocities of 4.7 m/s and 8.8 m/s

The indication in **Figure 4.8** explains why the plugging of pipelines by hydrates is severe at low gas velocities. Whereas the deposition rates of hydrates increases at higher gas velocities under the similar subcooling temperatures (Aman et al. 2016), the increase in gas velocity enhances the interaction of the hydrates at the wall with the gas at the core, thus increasing the near wall temperature at the velocity of 8.8 m/s. This explains why there are lower sloughing of hydrates events at low flow velocity

(Aman et al. 2016). Hydrates were unstable at the core as indicated from the temperature profile in **Figure 4.9**.

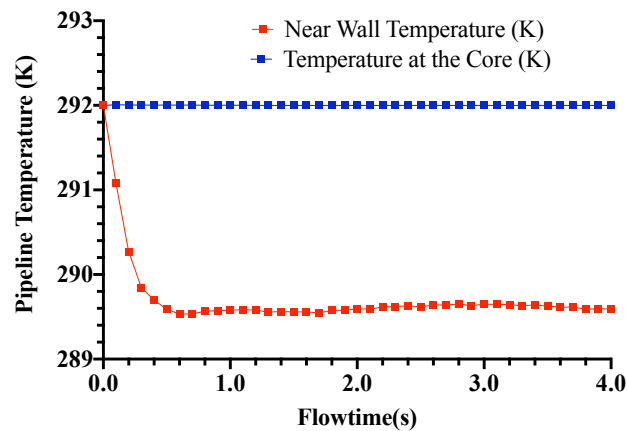


Figure 4.9: Comparing the stability of hydrate near the pipe wall and at the core at subcooling temperature of 7.0K with gas flow velocity of 8.8 m/s

Details of the results from the CFD model simulations are discussed further in sections 4.1.1.2 to 4.1.1.5.

4.1.1.2 Temperature contours showing the effect of changes in velocity and subcooling temperatures during hydrate deposition

The temperature contours in **Figure 4.10-12**, represent the thermal behaviour of hydrate formation because of the temperature-dependent solubility of the gas in water. By varying the gas velocity while keeping the subcooling temperature constant at 7.0K, 2D cross-sectional slices of gas temperature contour maps along the horizontal section of the pipe are obtained and presented in **Figure 4.10**. From the contour maps with a cut-off minimum temperature of 287.6K for the purpose of comparison, annular layers of temperature variations indicates that the temperature at the pipe wall is lower than that at the core.

Severe cases of hydrate deposition in the pipeline occurs at lower gas velocities (e.g., 2.0m/s) and higher subcooling temperatures (e.g., 7.0K). Also indicated in **Figure 4.10** is a tapering effect of the gas core along the pipe and from bottom (highest velocity) to top (lowest velocity) for the range of flow velocities simulated. The diameter of the gas at the core at the

temperature of 292K indicates availability of gas for the formation and sloughing of hydrates. A reduction in gas volume and quality also occurs as the gas core reduces along the pipe due to hydrate formation and deposition. As a result, the gas-water-hydrate flow during the formation of hydrates is relatively incompressible. Also, from **Figure 4.10** a comparison of the profiles at the range of gas velocities from 2.0-8.0 m/s explains the effect of increasing velocity on the depositional distance of hydrates (Jassim et al., 2010).

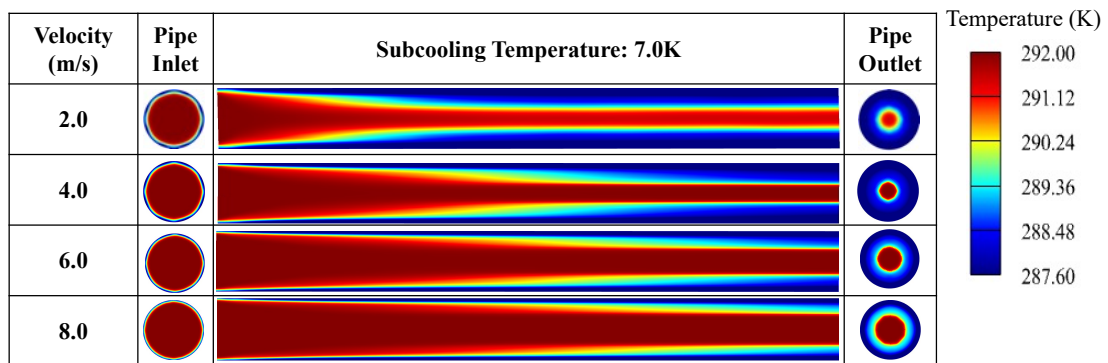


Figure 4.10: Temperature contour at varying velocities and constant subcooling temperature of 7.0K for the gas phase

Figure 4.10 suggests a strong correlation between flow velocity and hydrate plugging risk at constant subcooling temperature. The temperature contours reveal earlier hydrate deposition at lower velocities. For example, at 2 m/s, the blue contour representing 287 K indicates hydrate formation starting near the pipe inlet. This is in contrast to higher velocities where the red contour, signifying the primary gas phase, remains dominant throughout the pipe core. Although more hydrates are formed at higher velocities of 6.0 m/s and 8.0 m/s due to the increase turbulence of dispersed water droplets (Aman et al., 2016) and the increased solubility of gas, the hydrates are deposited farther downstream of the point of hydrate nucleation (Jassim, Abdi and Muzychka 2010).

Thus, higher velocities increase hydrate loading into the continuous gas phase, until the gas is totally consumed in the water phase to form hydrates. Again, the variation of temperature across the 2D cross-sectional slices at constant velocity was investigated as shown in **Figure 4.11**, to explain the

thermal effect of varying the subcooling temperature at constant flow gas velocity on hydrate formation and deposition.

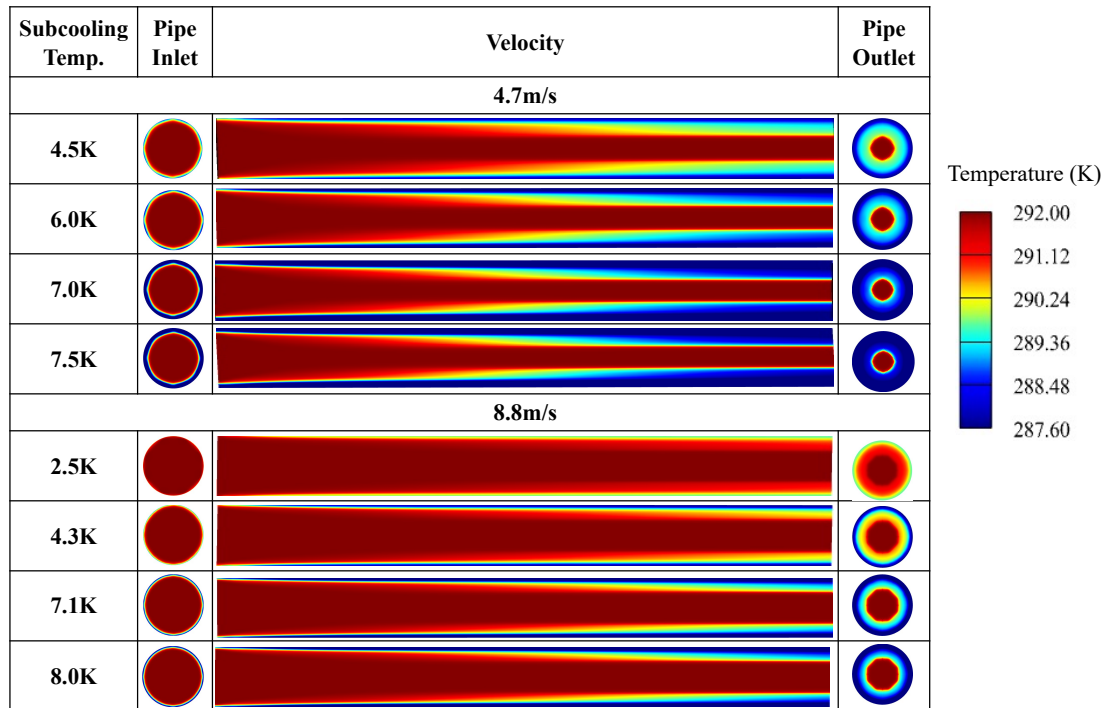


Figure 4.11: Temperature contour at varying subcooling temperatures and constant velocities of 4.7 m/s and 8.8 m/s for the gas phase

The contour maps in **Figure 4.11** suggests increasing hydrate formation and deposition as the subcooling temperature increases. As the subcooling temperature rises, the risk of plugging intensifies for both gas velocities (4.7 m/s and 8.8 m/s). Interestingly, at the lower velocity of 4.7 m/s, a subcooling temperature of 7.0 K presents a higher plugging risk compared to the same temperature contour observed at the higher velocity (8.8 m/s).

This indication provides insight into the behaviour of gas flow in hydrate-forming pipelines during temperature changes from summer to winter, for instance. This can also occur when the thermal integrity of the external pipe insulation is compromised and allows the conduction of the ambient temperature in an offshore environment across the wall of the pipe to the fluid domain. From both **Figure 4.10** and **Figure 4.11**, it is advisable to investigate the optimum velocity that can decrease the concentration of hydrates (Yongchao et al. 2019), without adversely compromising gas quality and transportability, especially during seasonal temperature changes.

One clear inference from **Figure 4.10** and **Figure 4.11**, is the tapering effect observed along the pipeline from the inlet as indicated in **Figure 4.12** below, which can lead to plugging of the horizontal section or riser base of subsea pipelines with hydrates (Aman et al. 2018).

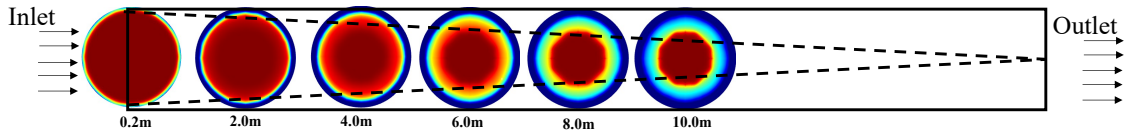


Figure 4.12: Temperature contour tapering effect of hydrate deposition along the pipe at a velocity of 8.8 m/s and subcooling temperature of 7.1K

The pattern in **Figure 4.12**, agrees with experimental observations in the literature. The tapering effect from the inlet at 0.2 m to 10 m shows that hydrates will eventually plug the pipeline at a distance from the inlet. Again, the presence of hydrates as dispersed phase is possible because of the dispersed water phase in the gas stream in **Figure 4.13**.

The higher gas temperature of 292K indicates that the hydrates at the core will not be stable until the entire gas is consumed. From **Figure 4.13**, the maximum temperature of the water phase which is 290K will continue to enhance the cooling of the gas for more stability of hydrates, since the gas temperature of 292K is already at the hydrate equilibrium temperature point. Eventually, the pipe core will be filled with hydrates once the entire gas is consumed.

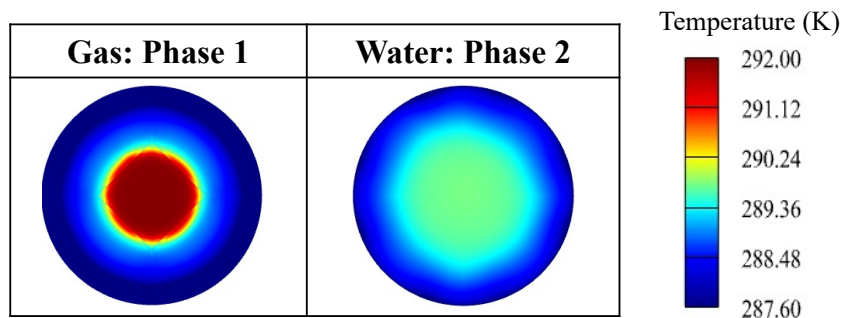


Figure 4.13: Temperature contours of gas and water phase at gas velocity of 8.8 m/s and subcooling temperature of 7.1K indicating the formation of Hydrates as dispersed phase and deposition on the wall of the pipe.

4.1.1.3 Gas density contours showing cross-sectional increase in gas density towards the wall of the pipe

A cross-sectional density profile at the subcooling temperature of 7.0K and velocities of 4.7 m/s and 8.8m/s, indicates how the gas density varies across the section in a reducing core phenomenon (**Figure 4.14**). This observation is consistent across all the subcooling temperatures simulated.

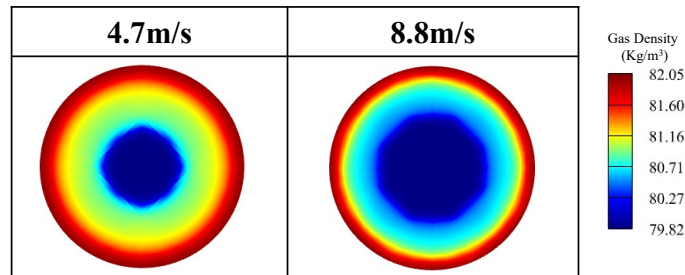


Figure 4.14: Gas density contour increasing towards the wall of the pipe at subcooling temperature of 7.0K.

The higher gas density at the wall is because methane solubility in water increases at lower temperatures (Lekvam and Bishnoi 1997). Again, hydrates concentrates the volume of the gas phase by a factor of 180 relative to the volume at standard temperature and pressure (Sloan 2011). This phenomenon is also related to hydrate formation and deposition. With increase in density, gas compressibility reduces, and the flow become increasingly viscous resulting in increasing pressure drop.

4.1.1.4 Pressure drop during hydrate formation, agglomeration and deposition with change in velocity and subcooling temperature.

Transient pressure drop graphs can provide insight into how change in velocity and subcooling temperatures affects hydrates-induced flow hydraulics in gas pipelines. The effect of varying gas flow velocity on pressure drop during the CFD simulation is presented in **Figure 4.15**.

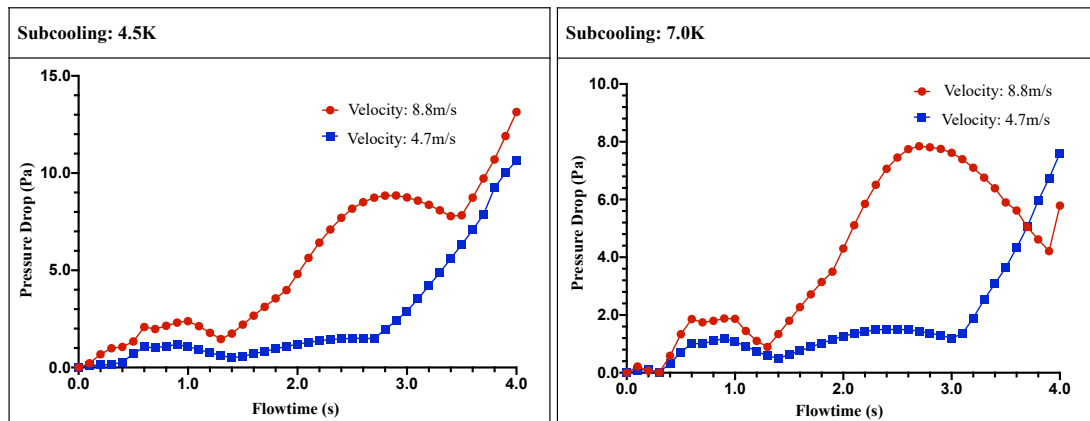


Figure 4.15: Effect of velocity change under constant subcooling temperature on pressure drop during hydrate formation, agglomeration, and deposition

From **Figure 4.15**, at a subcooling temperature of 4.5K and same pressure drop, for instance, the simulation at a velocity of 8.8 m/s attained pressure drop value of 9.0 Pa at 2.9 s earlier than the simulation at 4.7 m/s which attained this same transient pressure drop of 9.0 Pa at 3.9 s. This observation is similar with the empirical remark by Aman et al. (2016) - that the experimental time to attain the maximum transient pressure drop of the flowloop facility was shorter at higher gas velocity than at lower gas velocity.

As the subcooling temperature increases from 4.5K to 7.0K, the pressure drop reduces because of higher gas consumption rate to form more hydrates. Also, the flow is more viscous at 4.5K with higher pressure drop because of higher tendency for plugging because lower hydrates loading capacity by the flowing gas stream. The practical implication of this indication is that hydrates plugging risk should be anticipated earlier at higher gas velocity, especially at the riser base.

Following the observations in **Figure 4.6** and **Figure 4.7** discussed earlier, the two dips on the pressure curves in both plots at subcooling temperatures of 4.5K and 7.0K at 8.8 m/s in **Figure 4.15** indicates the onset of the agglomeration of hydrates (first dip), and the second dip is hydrates deposition. Also, for both velocities the maximum pressure-drop observed at 7.0K is greater than that at 4.5K for the same flowtime. As seen in **Figure 4.15** above, the transient pressure drop increases as the velocity increases

because of increase in hydrate formation by the increasing turbulence in the pipeline.

In **Figure 4.16**, it is observed that increase in subcooling temperatures did not imply a significant increase in the transient pressure drop along the pipe at constant velocity, which also agrees with experimental observations. At a constant gas velocity of 4.6 m/s, Aman et al. (2016) observed similar behaviour from their experiments.

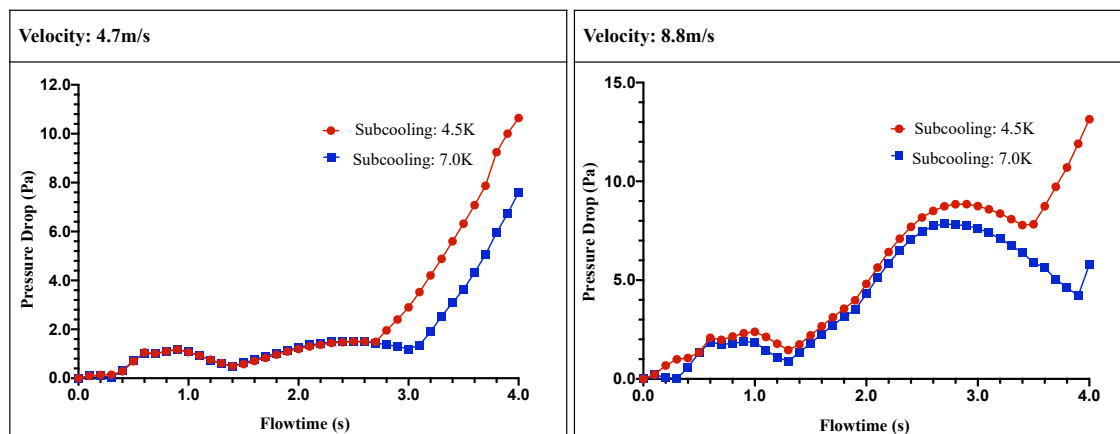


Figure 4.16: Effect of change in subcooling temperature at constant velocity on pressure drop during hydrate formation, agglomeration, and deposition.

Furthermore, the extended position of the second dip at both subcooling temperatures in **Figure 4.16**, implies increased hydrates deposition rate when the gas velocity was increased from 4.7 m/s to 8.8 m/s. Higher deposition is obtained at higher subcooling temperatures. Also, the viscous loading of agglomerating hydrates at 4.5K was higher leading to an early rise in pressure.

4.1.1.5 Quantitative measurement of hydrate deposition rates

The hydrate deposition graphs presented in this section are based on the mass of gas flow rate in the fluid domain, as a representation of the gas consumption rate during hydrate formation, agglomeration and deposition discussed earlier. A sample plot of the gas flowrate versus the simulation flowtime at 8.8 m/s and the subcooling temperature of 7.0K without the UDF codes implemented is presented in **Figure 4.17**, below.

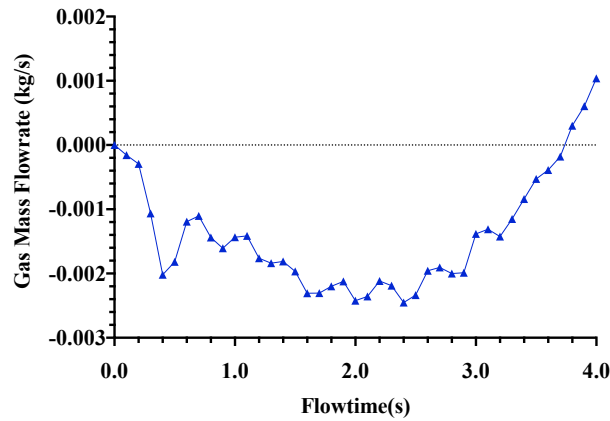


Figure 4.17: Gas mass flowrate during hydrate formation, agglomeration, and deposition

Turner et al. (2005) suggests that the formation of hydrates is instantaneous at the right pressure and subcooling temperature. Also, hydrate deposition velocity is assumed to be constant for a fully developed turbulent flow in the pipeline (Jassim et al., 2010). Therefore, the average gas consumption rate (kg/s) is expected to be the best approximation of hydrate deposition (Turner et al. 2005; Di Lorenzo et al. 2014a; Aman et al. 2016; Liu et al. 2019). Based on the eulerian-eulerian model and the assumption of no interphase mass transfer, the right-hand side of equation 3.1, reduces to the mass source term S_q only, which is implemented in a gas injection UDF. The energy source term in equation 3.9, is also implemented in another UDF. The plot for both UDF and no UDF simulation at a velocity of 8.8 m/s and subcooling temperature of 7.1K are compared in **Figure 4.18**, below.

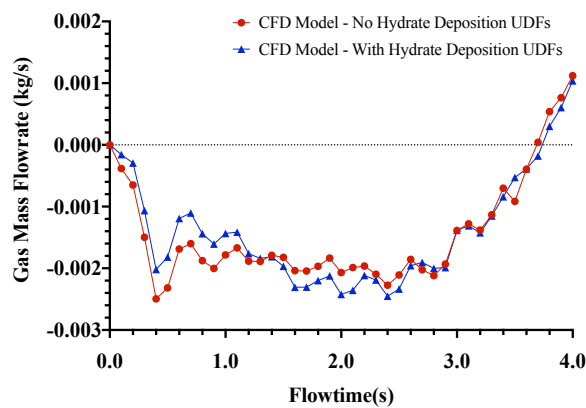


Figure 4.18: Comparison of gas mass flowrate 'with' and 'without' hydrate deposition UDFs. Higher agglomeration of hydrates at 1.6 s to 2.6 s is observed when the UDFs were implemented.

As indicated in **Figure 4.18**, ANSYS Fluent can produce similar gas mass flowrate results without the UDFs for a model length of 10.0 m, provided the boundary conditions for the formation of hydrates are the same. For the UDFs curve, the initial gas consumption rate was lower up to 1.1 s but increased slightly thereafter until 2.6 s. From this point both curves reduced gas mass flow rates along the same curve.

Moreover, while the non-UDFs curve maintained a seemingly stable horizontal profile during the hydrate agglomeration period (1.0 – 2.8s), the UDFs curve maintained a non-uniform trough with a vertical dip at 2.0 s within this same period, suggesting more agglomeration of hydrates. The implementation of the UDF codes in this research is to ensure that the energy source term is based on experimental correlations in equation 3.9), and the make-up gas supplied into the domain is in the is proportional with empirical predictions in equation 4.1. The hydrate deposition rates in **Figure 4.19-21** are estimated from equation 4.1, below.

$$Q_{H_d} = \frac{-60000\dot{m}_{CH_4}}{\rho_{H_hwc}} \quad (4.1)$$

where Q_{H_d} is hydrate deposition rate, L/min; \dot{m}_{CH_4} is gas mass flowrate, kg/s; ρ_{H_hwc} is the density of hydrate (807.77kg/m³). For validation, the recorded hydrate formation data at 4.7 m/s and 8.8 m/s are plotted for different subcooling temperature simulations and presented hereafter in **Figure 4.19** and **Figure 4.20**.

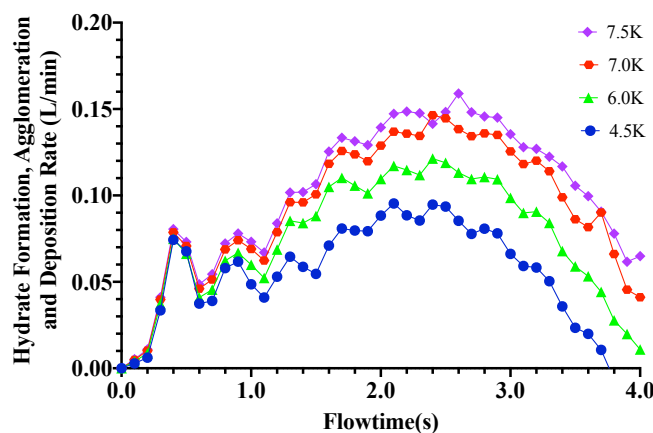


Figure 4.19: Comparing hydrate deposition curves at a velocity of 4.7 m/s for various subcooling temperatures.

The comparisons of the curves in **Figure 4.19** indicate an increasing deposition rate of hydrates as the subcooling temperature increases. This is because of the increased solubility of methane gas in water at lower temperatures below the hydrate formation condition (Lekvam and Bishnoi 1997).

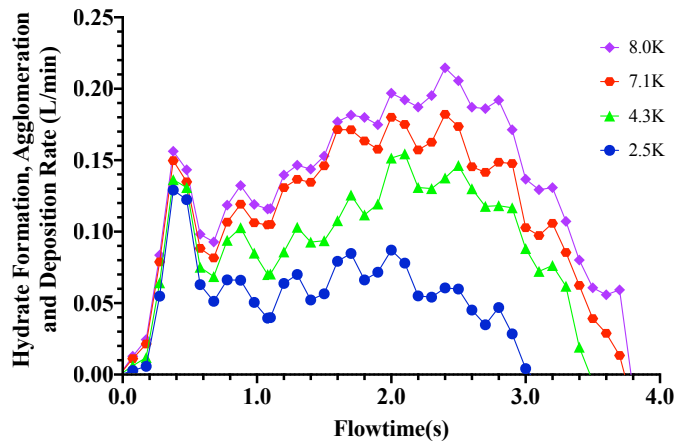


Figure 4.20: Comparing hydrate deposition curves at a velocity of 8.8 m/s for various subcooling temperatures.

The UDFs simulated hydrate curves in **Figure 4.19** and **Figure 4.20** attains a hydrate agglomeration/growth rate peak before a deposition (decline point on the curves). The simulated deposition rates as indicated in stage III of **Figure 4.7** are computed from equation 4.1 and presented in **Table 4.3**, below.

Table 4.3: CFD model predicted hydrate deposition rates

Velocity (m/s)	Sub-Cooling temp.(K)	CFD Model Predicted Average Hydrate Deposited Rate (L/min)
4.7	4.5	0.060
	6.0	0.097
	7.0	0.121
	7.5	0.132
8.8	2.5	0.063
	4.3	0.125
	7.1	0.141
	8.0	0.183

In **Table 4.3**, there is an increasing trend of hydrate deposition rates as the subcooling temperature increases at a gas velocity of 4.7 m/s and 8.8 m/s

for all subcooling temperatures. This trend is due to methane solubility as explained earlier, hence deposition rate of hydrates is positively related with subcooling temperatures. This observation agrees with the experimental report in Aman et al. (2016), that hydrates deposition rate is positively influenced by increase in gas velocity.

To estimate the deposition rates of hydrates at different gas flowrates, the gas flowrates are entered as constant negative source mass for the gas phase. So that the CFD software computes the added flowrates as externally controlled gas input into the control system. **Figure 4.21** indicates the effect of injecting various gas mass flowrate per volume from the range of 0.15-0.50 kg/m³-s into the computational domain on hydrate deposition at 8.8 m/s and a subcooling temperature of 8.0K.

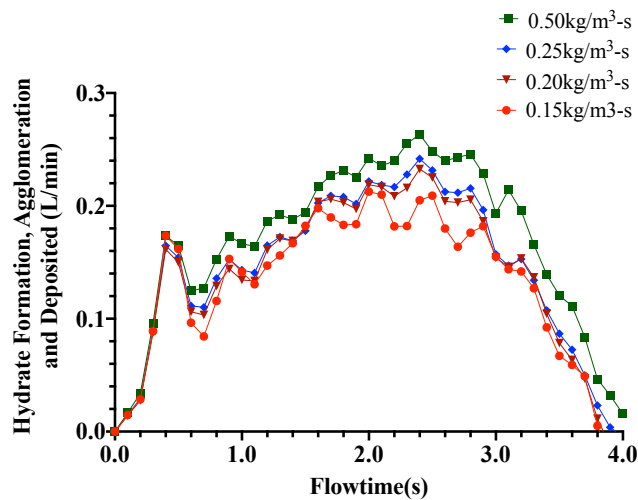


Figure 4.21: Comparing hydrate formation for various gas supply rate at a velocity of 8.8 m/s and constant subcooling temperature of 8.0K

The results in **Figure 4.21** indicate that increasing the gas supply into the fluid domain increases hydrate deposition rates, provided the conditions for the formation of hydrates are met. This observation is important in managing hydrates. Furthermore, as gas supply is cut off, the growth of hydrates is also stopped (Neto et al., 2016). In operations and maintenance, once hydrates start forming in a pipeline, the first technical advice is to stop the flow of gas (Li et al., 2013). Again, if hydrates deposition rates are estimated during design, the operations of hydrate-forming pipelines can be optimised based on routine cleaning operations and maintenance planning. It is also

important to estimate the equivalent gas supply rate to the rate of hydrates deposited by superimposing the graph at 8.8 m/s and 8.0K subcooling temperature in **Figure 4.20** on **Figure 4.21** as presented in **Figure 4.22**.

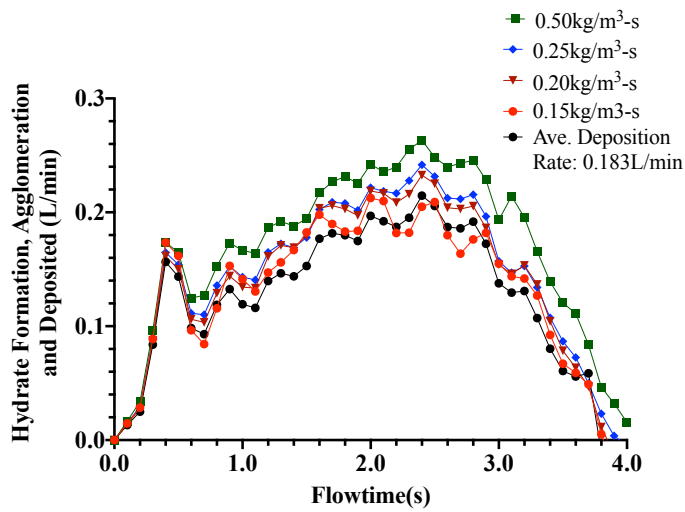


Figure 4.22: The relationship between hydrate deposition rate and gas supply rate at a velocity of 8.8 m/s and subcooling temperature of 8.0K

From **Figure 4.22**, the relationship between gas consumption rate and hydrate deposition rate was set at: 0.183 L/min (black curve) of hydrates deposited is equivalent to 0.20 kg/m³-s of gas injected. Implying that 1.1 kg/m³-s of consumed gas deposited 1 L/min of hydrates. Again, at lower velocity of 4.7 m/s and subcooling temperature of 7.0K, this relationship also holds (**Figure 4.23**).

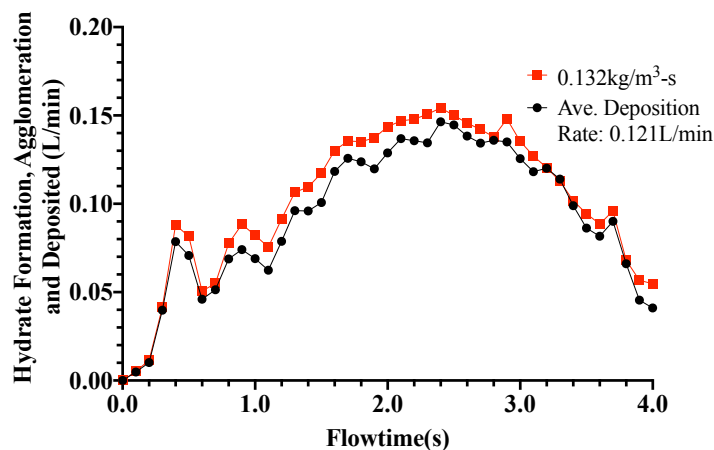


Figure 4.23: Relationship between hydrate deposition rate and gas supply rate at a velocity of 4.7 m/s and subcooling temperature of 7.0K.

Thus, by converting to mol/min of gas supplied based on the volume of the pipe and molecular weight of the gas (**Table 3.1**), it is estimated that 12

mol/min of gas deposited 1 L/min of hydrates. The above indication shows that gas availability in the pipeline is the determining factor for hydrate formation and deposition.

4.2 Parametric Analysis

4.2.1 Effect of Hydrates on Volume Fraction of Gas and Water

The sum of the volume fractions is equal to 1. The volume fraction of gas and water will reduce during hydrate formation. Hydrate volume fraction α_h , was estimated by subtracting the sum of the minimum transient volume fraction of gas and water from 1 (Equation 4.3).

$$\sum \alpha_q = 1 \quad (4.2)$$

$$\alpha_h = 1 - (\alpha_g + \alpha_w) \quad (4.3)$$

where α_q , the volume fraction of each phase and subscripts, g , w , and h represent gas, water, and hydrate phase respectively. From 2.0 s of flowtime, both gas and water phase formed a viscous flow that mimicked the flow of hydrate slurry in gas pipeline.

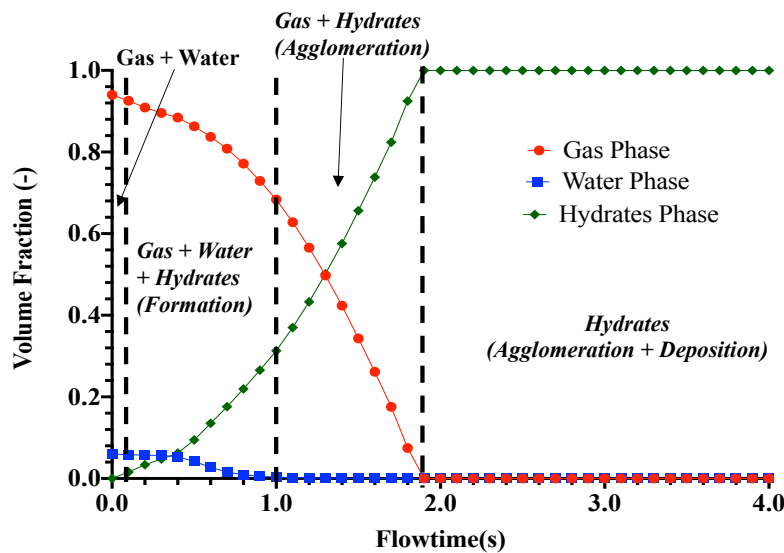


Figure 4.24: Phase change during hydrate formation, agglomeration, and deposition at gas velocity of 8.8 m/s and subcooling temperature of 7.0K

The volume fractions in **Figure 4.24**, are the minimum values obtained in the fluid domain of the pipe section. This was appropriate to ensure that the

values computed by the software was representative of reality. As indicated in **Figure 4.24**, the transient multiphase flow phase change during hydrate formation, agglomeration and deposition are: (i) 2-phase flow of water and gas between 0.0s to 0.1s; (ii) 3-phase flow of gas, water, and hydrates between 0.1s to 1.0s; (iii) 2-phase flow of gas and hydrates between 1.0s to 1.9s; and (iv) agglomeration and deposition of hydrates beyond the flowtime of 1.9s to 4.0s.

At full occlusion, the volume fraction of water ranges from 0.000029 to 0.000011 respectively, whereas the volume fraction of gas beyond the flowtime of 1.9s was relatively "zero." This insignificant volume fraction of water after the expiration of the gas phase beyond 1.9s indicates the presence of slight hydrates slurry (agglomeration) and high deposition on the wall, which led to a drop in transient pressure between the flowtime of 2.8 s and 3.8 s (**Figure 4.6**). This is because, as the hydrates were deposited on the wall, there was a slight increase in hydraulic diameter for the light hydrate slurry to flow. Later in **Figure 4.28**, it will be noticed that the tangential velocity of the hydrates slowed down, implying a gradual reduction in deposition as more hydrates are deposited on the wall. However, not all the hydrates are stable as the temperature of the hydrates at the core is 290K (**Figure 4.13**).

As indicated earlier in **Figure 4.6** and **Figure 4.7**, agglomeration occurred after 1.0 s. The inlet temperature of 292K was reduced to hydrate-forming temperature in 0.1 s (**Figure 4.6**). This observation is supported in the literature (Turner et al. 2005), that the formation of hydrates is instantaneous at the right subcooling temperature. Again, the observation of 3-phase flow (gas, water, and hydrates) followed by 2-phase flow (hydrates and gas) in **Figure 4.24** is consistent with the suggestion in the literature (Wang et al. 2018).

The plugging risk of Hydrates increases at lower near wall temperatures as indicated by the hydrate volume fraction (**Figure 4.25**), hence at lower gas flow velocity hydrate plugging risk is higher in agreement with earlier indications in **Figure 4.8**.

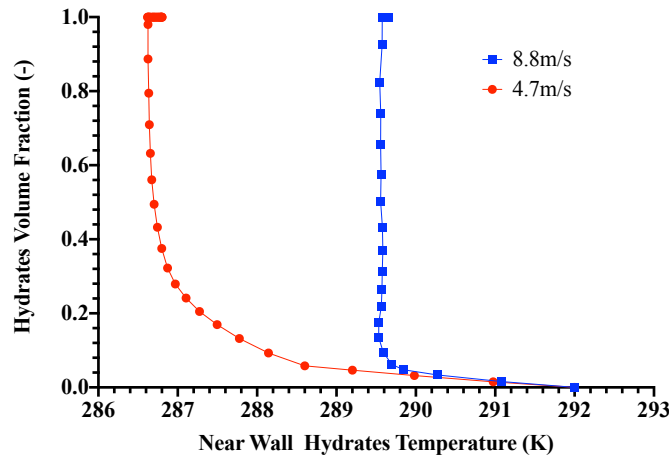


Figure 4.25: Effect of temperature on hydrate plugging risk at subcooling temperature of 7.0K.

A decrease in the deposition rates of hydrates was observed when the water volume fraction was increased (**Figure 4.26**). Implying that reducing the water volume fraction leads to decrease in liquid loading by the carrier phase and increases hydrate plugging risk. This observation is also corroborated in another study (Chaudhari, Zerpa and Sum 2018). Increase in water volume fraction also encourages the sloughing of hydrates (Di Lorenzo et al. 2014a).

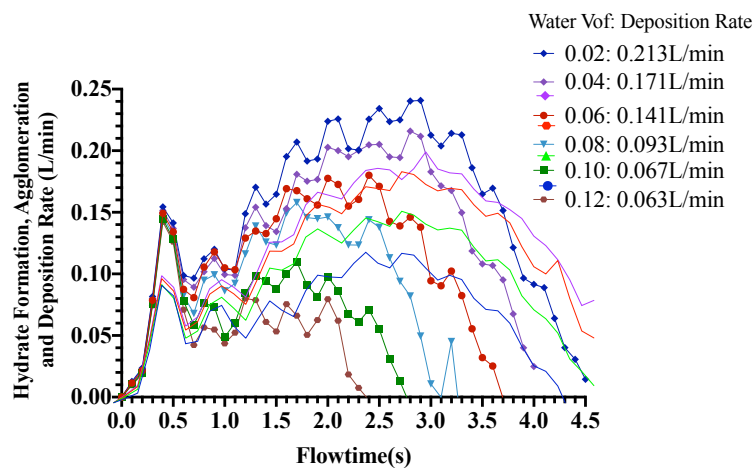


Figure 4.26: Effect of water volume fraction on hydrate deposition rates at subcooling temperature of 7.0K and gas velocity of 8.8 m/s.

4.2.2 Effect of Turbulence and Tangential Velocity on Hydrate Deposition

The deposition of hydrates is controlled by the source mass. From equation 3.1, the source mass is expected to be the dependent variable. Since the gas

phase is treated as sink, with increase in gas density towards the wall because of the subcooling temperature at the wall, the only variable that will adjust to accommodate the mass flowrate of the injected gas based on the law of mass conservation is the gas velocity, hence treated as the subject dependent variable. Hydrate deposition is favoured in laminar and transition flow regimes. Hence, the velocity of the gas and water will reduce under the above scenario. Laminar flow occurs in the pipeline if the turbulent Reynolds number is less than 2100, and turbulent, if the Reynolds number is greater than 4000 (Munson, Young and Okiishi 1994).

Between these two values, the flow is transitional, implying intermittent switch between laminar and turbulent flow. Turbulence is present at the gas-liquid interface (Di Lorenzo et al. 2014b), and enhances hydrate formation. The turbulent Reynolds number, Re_y (Theory 2017) is given as:

$$Re_y = \frac{\rho y \sqrt{k}}{\mu} \quad (4.4)$$

where y is the distance to the nearest wall (m); ρ , is the density of the fluid domain (kg/m^3); k , is turbulent kinetic energy per unit mass (J/kg); and μ , is the fluid viscosity (Pa.s). The curves in **Figure 4.27**, are plots of maximum turbulent Reynolds number, Re_y , at the subcooling temperature of 7.0K and gas velocities of 4.7m/s and 8.8m/s.

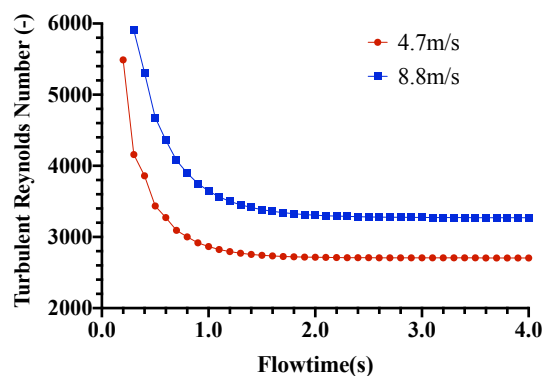


Figure 4.27: Effect of hydrate formation, agglomeration, and deposition on turbulent Reynolds number at subcooling temperature of 7.0K.

The Re_y value explains the flow in the viscosity-affected-near-wall region (Theory 2017), and important here because the deposition of hydrates is a

near-wall phenomenon. From equation 4.4, increasing the viscosity of hydrates reduces the Reynolds number as the density is relatively stable (Li et al. 2013; Ding et al. 2017). Hence, the Re_y represent the Reynolds number of hydrates in the pipe. Both simulations at 4.7 m/s and 8.8 m/s are within the transition flow zone during agglomeration and deposition. The higher turbulence at the Re_y values of 4000-6000, enabled good temperature mixing leading to the formation of hydrates. During the transition flow, hydrates deposition is enhanced. The tangential velocity of hydrates also enhances hydrates agglomeration in readiness for deposition (**Figure 4.28**).

The agglomeration of hydrates commenced at 1.0s and deposition commenced at 2.8s as discussed earlier in **Figure 4.6** and **Figure 4.7**. At 4.7 m/s, the hydrates remained in the gas phase until 2.0 s before drifting towards the wall when the flow was relatively steady (**Figure 4.27**). At higher gas velocity, the hydrates tangential velocity is higher, implying a much farther depositional distance as seen in the temperature contour profile at 8.8 m/s and subcooling temperature of 7.0K in **Figure 4.10**.

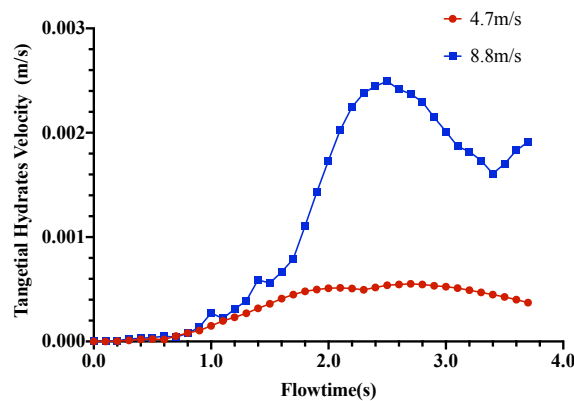


Figure 4.28: Tangential velocity of hydrates at subcooling temperature of 7.0K

During agglomeration (1.0s – 2.8s), the tangential velocity increases and drop during deposition (2.8s to 3.5s) at both 4.7 m/s and 8.8 m/s. At 3.4 s and velocity of 8.8 m/s, the tangential velocity started rising because more hydrates are depositing father away from the point of agglomeration. This observation is why hydrates plugging events are higher at lower gas velocities.

4.2.3 Effect of Pipe Length on Hydrate Deposition Rate

Two model lengths of 10m and 1m and same pipe diameter of 0.0204m were simulated in this analysis. The inlet and outlet surface of the pipe were meshed to the same mesh cells. The results are presented in **Table 4.4**.

Table 4.4: Comparison of hydrate deposition rates for CFD model lengths

Velocity (m/s)	Sub-Cooling temp.(K)	Average Hydrate Deposited Rate (L/min)	
		CFD Model (1.0m length)	CFD Model (10.0m length)
4.7	4.5	0.058	0.060
	6.0	0.065	0.097
	7.0	0.072	0.121
	7.5	0.071	0.132
8.8	2.5	0.151	0.063
	4.3	0.133	0.125
	7.1	0.133	0.141
	8.0	0.117	0.183

As indicated in **Table 4.4**, the 1.0m length model did not agree with the expected increasing trend of hydrate deposition rates as subcooling temperature increases at the higher velocity of 8.8 m/s. This is because the entry length for this diameter is 0.612m resulting in a highly unstable flow in the 1m length pipe at 8.8 m/s. Thus, substantiating the use of a higher length of 10 m for this study.

4.2.4 Effect of Pipe Diameter on Hydrate Deposition Rate

This sensitivity investigates the need of developing new horizontal geometry with changing diameter and mesh sizes for each flow case when the pipe diameter varies. The hydrates deposition rates at a velocity of 8.8 m/s and subcooling temperature of 7.1K are plotted for pipe dimeters of 0.0204 m, 0.0408 m and 0.0612 m in **Figure 4.29**. The outcome is represented in a linear relationship in **Figure 4.30** for the purpose of deriving a linear mathematical relation that can aid in the extrapolation of the deposition rates of hydrates for any diameter of pipe.

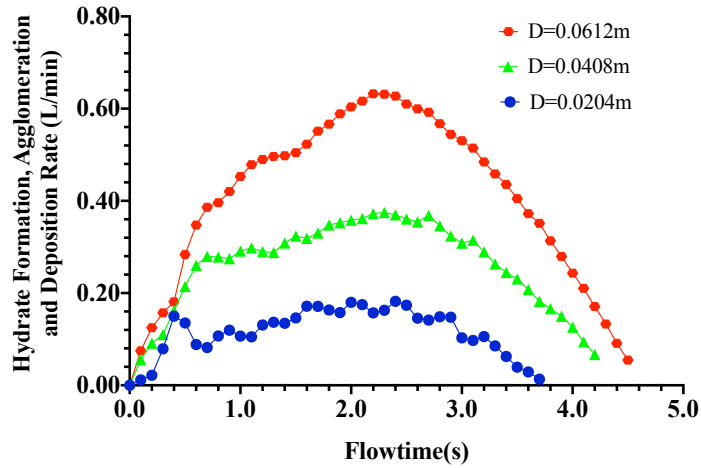


Figure 4.29: Impact of change in pipe diameter on hydrate deposition rate at 8.8m/s and 7.1K subcooling temperature.

Figure 4.29 shows that increasing the pipe diameter also increases the rates of hydrates deposition because of increase in gas volume. The hydrate deposition rates in L/min for each pipe diameter were plotted in **Figure 4.30**, below.

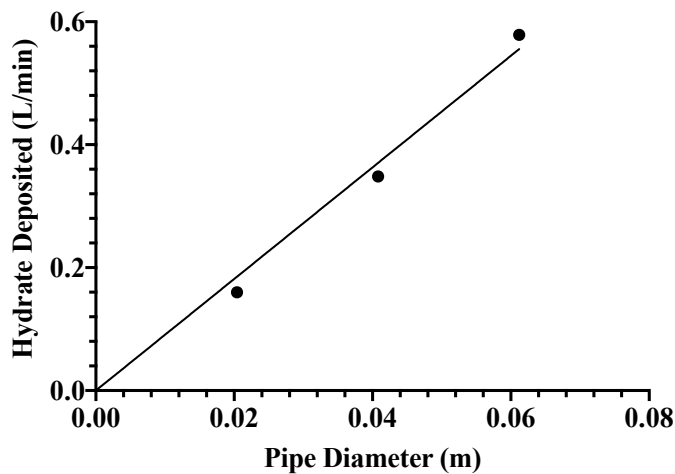


Figure 4.30: Relationship between hydrate deposition rate and pipe diameter at constant flow velocity. Higher diameter at constant velocity implies higher flowrate.

Thus, as indicated in **Figure 4.30**, increasing the pipe diameter at the same velocity and subcooling temperature increases the volume of gas, which is a determining factor in hydrate formation and deposition as observed earlier in **Figure 4.22**. Also, increase in pipe diameter imply increase in the volume of free water. The observation in **Figure 4.30** is supported by Aman et al. (2016), that increase in the amount of entrained water increases hydrate

formation and deposition. From the linear graph in **Figure 4.30**, a relationship between the deposition rate of hydrates and pipe diameter is stated as:

$$Q_{h,d} = 9.075D \quad (4.5)$$

where $Q_{h,d}$ retains the earlier definition in equation 4.5. Therefore, the corresponding diameter can be written as:

$$D = \frac{Q_{h,d}}{9.075} \quad (4.6)$$

To find the approximate hydrate deposition rate for a higher diameter by extrapolation, we can use the ratio of the pipeline diameters as shown below:

$$\frac{D_1}{D_2} = \frac{Q_{h,d1}}{Q_{h,d2}} \quad (4.7)$$

This can be modified with an extrapolation factor (K_{ex_factor}) as:

$$Q_{h,d2} = K_{ex_factor} \cdot \frac{D_2}{D_1} \cdot Q_{h,d1} \quad (4.8)$$

where $Q_{h,d1}$ is the hydrate deposition rate predicted by this CFD model, L/min; $Q_{h,d2}$ is the hydrate deposition rate estimated for actual design pipe, L/min; D_1 is the pipe diameter of this CFD model, 0.0204 m; D_2 is the pipe diameter of the actual pipeline, m; and K_{ex_factor} is the extrapolation factor (dimensionless), given a value of 1.1.

Equation 4.8, indicates that increasing the diameter by a factor also increases the deposition rate by 1.1 times the same factor. For field application, the value of K_{ex_factor} can be modified based on field experience to estimate actual deposition rates of hydrates. Hence, by first entering the gas and water properties into this CFD model of diameter 0.0204 m and 10 m length, the hydrates deposition rate can be obtained, and is extrapolated for the purpose of design for the new pipeline using equation 4.8.

4.2.5 The Relationship between Velocity and Shear Stress on Hydrate Deposition

The fluctuating gas shear stress on the pipe wall because of hydrate formation and deposition is important in providing insight into the possibility of hydrates deposition resulting in pipeline vibration (Jujuly et al. 2017). For the transportation of natural gas, the shear stress is defined by the Darcy friction factor and accounted for in the momentum equation (Coelho and Pinho 2007).

In multiphase turbulent flow computations, the primary carrier (gas) phase shear stress is related to the turbulent (eddy) viscosity ($\mu_{tc} = \rho_c C_\mu \frac{k_c^2}{\varepsilon_c}$) discussed in equation 3.7. Earlier, the turbulent shear stress on the pipewall by the continuous carrier (gas) phase is mathematically defined as: $\tau_c^t = \bar{\alpha}_c \rho_c (\frac{2}{3} k - 2 \frac{\mu_{tc}}{\rho_c} \cdot \nabla \cdot \tilde{u}_c)$, in equation 3.17. By modifying this equation with the turbulent viscosity term above, we can have equation 4.9.

$$\tau_c^t = \bar{\alpha}_c \rho_c (\frac{2}{3} k - 2 C_\mu \frac{k_c^2}{\varepsilon_c} \cdot \nabla \cdot \tilde{u}_c) \quad (4.9)$$

From the above mathematical relation, the shear stress can be influenced by turbulent kinetics (k), the phase volume fraction and density. Hence, decrease in turbulent kinetics of the of the carrier phase (k_c), on the wall results in higher resisting shear within the water-hydrate composite. Hence, a reduction in the volumetric flow of gas in a hydrates forming pipeline is an indication of high resisting hydrates thickness on the wall.

In this study, dissipation term is neglected to enhance deposition of hydrates at the wall. Implying, the water-induced shear stress on the deposited hydrates is expected to be higher than that of the gas within the hydrates (Charlton et al. 2018b). However, the increase in density of the gas phase from 79-83kg/m³ during the formation of hydrates can increase the shear stress of the gas phase slightly as indicated in **Figure 4.32** and **Figure 4.33**. As explained in the turbulent Reynolds number plots (**Figure 4.27**), it was essential to achieve a $y^+ < 5$ for the flow of hydrates at 4.7 m/s and 8.8 m/s. This ensures that the shear stress of the deposited hydrates is equivalent to

the wall shear stress, aiding a no-slip condition due to the viscous force of the deposited hydrates at the wall (**Figure 4.31**). The maximum y^+ at 4.7 m/s (2.5) and at 8.8 m/s (4.0) indicates that the water-induced shear stress on the layer of hydrates is equivalent to the pipe wall shear stress (Tu, Yeoh and Liu 2018). The y^+ is defined in the literature (Theory 2017; Tu, Yeoh and Liu 2018), as indicated below.

$$y^+ = \frac{\rho y u_\tau}{\mu} \quad (4.10)$$

where ρ , y and μ , retains their earlier definitions. u_τ , is related to wall shear stress and hydrates density as defined in the literature (Theory 2017; Tu, Yeoh and Liu 2018).

$$u_\tau = \sqrt{\frac{\tau_w}{\rho}} \quad (4.11)$$

Hydrates-induced wall shear stress can be defined from equations 4.10 and 4.11 as:

$$\tau_w = \frac{1}{\rho} \left(\frac{y^+ \mu}{y} \right)^2 \quad (4.12)$$

From equations 4.10 and 4.11, the high viscosity of hydrates is responsible for the $y^+ < 5$. In equation 4.12, the increase in the viscosity of hydrates has a power of 2 effect, leading to high wall shedding shear stress by the deposited hydrates. The main assumptions in deducing the predictions of the shear stress in this study are as follows: (i) the estimated shear stress is based on hydrate deposition only, and not on the pipe wall roughness because the pipe internal wall surface is assumed to be smooth; (ii) the gas-induced shear stress is the sloughing shear stress because it is the carrier phase; and (iii) the water-induced shear stress on the hydrates is the wall shedding shear stress by the hydrate deposits because of the direct contact with the pipe wall. Determining the shear stress during hydrate sloughing and wall shedding is still an active area of research, with no consensus among scholars on the nature of the shear stress during hydrate sloughing and wall shedding by hydrates.

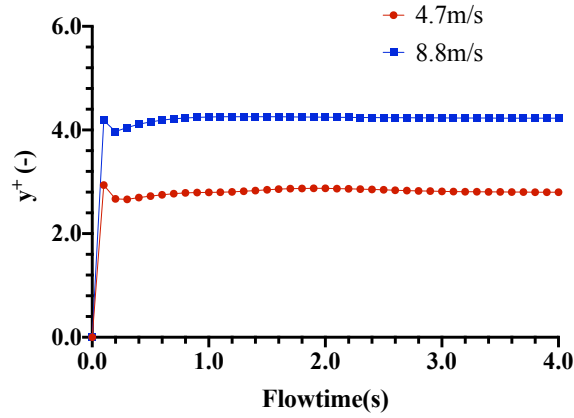


Figure 4.31. Maximum y^+ plot at subcooling temperature of 7.0K indicating that the simulation is dominated by viscous forces.

Two shear stress regimes are proposed in this study – a gas-induced shear stress responsible for hydrate sloughing, $\sigma_{sloughing}$, and water-induced shear stress leading to wall shedding by hydrates $\sigma_{shedding}$, such that $\sigma_{shedding} > \sigma_{sloughing}$. This study defines a new operating shear stress ratio, σ_{op_ratio} , as follows.

$$\sigma_{op_ratio} = \frac{\sigma_{shedding}}{\sigma_{sloughing}} \quad (4.13)$$

This ratio is similar to the ratio of maximum to minimum shear stress proposed in (Aman et al. 2018). Liu et al. (2019) had argued in their paper that the position of Di Lorenzo et al. (2018) was inadequate in modelling hydrate rheology in the pipeline. However, the understanding posited in this paper clarifies why Di Lorenzo et al. (2018) assumed a constant shear stress in their analytical model on hydrate sloughing and Liu et al. (2019) assumed a fluctuating shear stress in their wall shedding analytical model. From this study, the constant shear stress is the gas shear stress for sloughing and the fluctuating shear stress is the water-induced shear stress for wall shedding by hydrates. **Figure 4.32** and **Figure 4.33** present the shear stress plots at gas velocities of 4.7 m/s and 8.8 m/s.

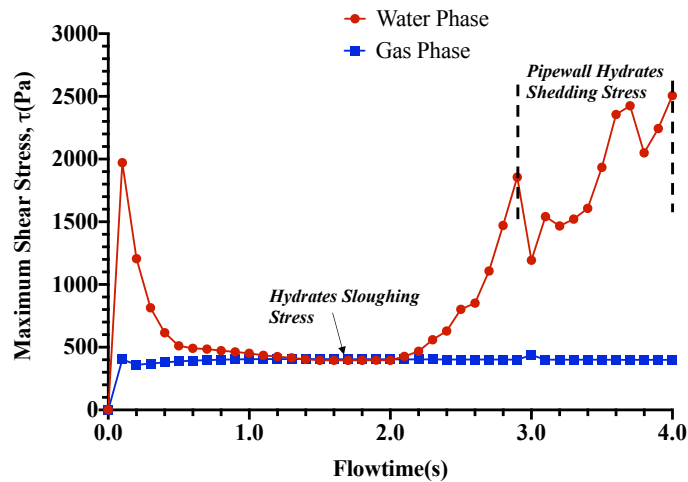


Figure 4.32: Maximum shear stress on hydrate deposits at subcooling temperature of 7.0K and at velocity of 8.8 m/s.

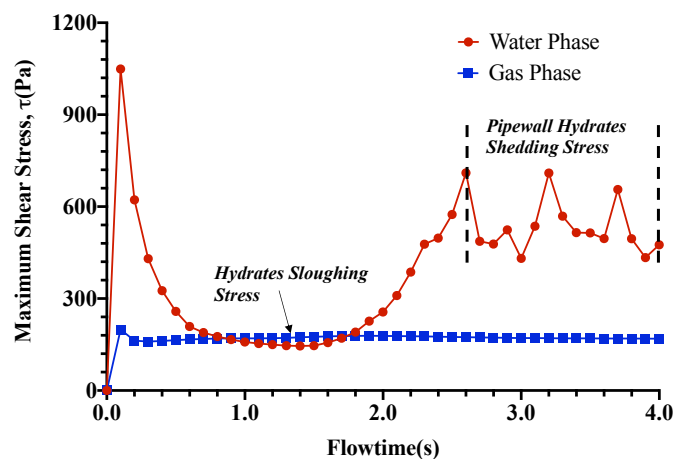


Figure 4.33. Maximum shear stress on hydrate deposits at subcooling temperature of 7.0K and at velocity of 4.7m/s

From **Figure 4.32** and **Figure 4.33**, there is a steep rise in shear stress after 2.0 s, after the formation of hydrates. The shear stress induced from the water phase on the hydrate deposits from the flowtime of 2.5 s, increases at 8.8 m/s and fluctuates around 400 Pa at 4.7 m/s (**Figure 4.33**). As the gas velocity increases from 4.7 m/s to 8.8 m/s, the gas shear stress also increased relatively by a factor of 1.5. This is as a result of increase in tangential velocity (Andreussi, Asali and Hanratty 1985).

The curves of the water-induced shear stress on the layer of hydrates in both velocity scenarios, agrees with the position of Liu et al. (2019) that the shear

stress on hydrate deposit is not constant. Higher wall shedding of hydrates can be noticed at 8.8 m/s, while the wall shedding of hydrates at 4.7 m/s is relatively stable. Thus, assuming a uniform shear stress at lower velocity can be acceptable, but not at higher velocities.

Although, sloughing has been studied in the literature with no concrete conclusion on the location of occurrence along the pipeline (Wang et al. 2018), the initial investigation by Aman et al. (2016) suggests that the ratio of the resisting water-hydrate composite shear stress to the flowing gas shear stress is 4.8. From **Figure 4.32** at 8.8 m/s, the average resisting shear stress is that of the water-hydrate composite (1934Pa) and the flowing gas shear stress is 400 Pa, hence the ratio is 4.84. Similarly, at 4.7 m/s (**Figure 4.33**) the ratio of the average resisting shear stress of the water-hydrate composite of 655 Pa to the corresponding flowing gas shear stress of 172 Pa is 3.81.

The higher wall shear stress at 8.8 m/s implies a higher resistance to shear. Whereas there is a linearly growing hydrate layer at 8.8 m/s before wall shedding (**Figure 4.32**), there is a uniformly stratified growing layer at 4.7 m/s before subsequent wall shedding (**Figure 4.33**). However, this study suggests that higher minimum values of shear stress than the 100-200 Pa suggested in the literature (Aman et al. 2018; Di Lorenzo et al. 2018) is expected during sloughing at a higher gas velocity, as the range stated in the literature only agree with this CFD model prediction of 172 Pa at lower velocity of 4.7 m/s.

Similarly, from the indications in **Figure 4.32** and **Figure 4.33** this study suggests the following.

- (a) At higher velocity of 8.8 m/s the operating shear stress ratio (Equation 4.9) is relatively equal to 1 ($\sigma_{op_ratio} = 1$) during sloughing of hydrates, corresponding to the flowtime of 1.0-2.0 s when there was 2-phase gas and hydrates flow dominated by hydrate agglomeration. The rise in water-induced shear stress beyond 2.0 s until 2.8 s was to initiate the first wall shedding of hydrates as the hydrates agglomerates until the first deposition occurred at 2.8 s. Beyond this point, $\sigma_{op_ratio} > 1$,

encouraging wall shedding by hydrates. The shear stress fluctuates and increased in a linear order as more hydrate deposits from 2.8 s to the end of simulation flowtime.

- (b) at lower velocity of 4.7 m/s, $\sigma_{op_ratio} = 1$ during hydrate sloughing, corresponding to the flowtime of 1.0-1.9 s when there was 2-phase gas and hydrate flow dominated by agglomeration of hydrates. The rise in water-induced shear stress beyond 1.9 s until 2.5 s was to initiate the first wall shedding of hydrates as the hydrates agglomerates until the first deposition occurred at 2.5 s. Beyond this point, $\sigma_{op_ratio} > 1$, leading to wall shedding by hydrates. The shear stress fluctuates in a relatively stable manner as more hydrate deposits from 2.5 s to the end of simulation flowtime. Hence, this research proposes that the hydrate layer at the velocity of 8.8 m/s is a linearly growing annular profile, while the layer of hydrates at 4.7 m/s were deposited in a stratified annular pattern.

4.2.6 Change in Pipeline Geometry: Effect of 90-degree riser on hydrates formation

The simulation results discussed above are for the horizontal section of the pipeline where hydrates usually formed and are accumulated at sections where the pipeline changes geometry such as bends, sag points and risers. Usually, the subsea is undulating but not enough to lead to flow assurance issues. However, sag points can occur along the route, but do not constitute hydrate forming sections except during shutdown. During installations bends are avoided along the pipeline route as much as possible to prevent flow assurance issues, except at subsea manifold and jumpers. Hydrates deposition on the base of the riser (**Figure 4.34**) was further investigated at low velocity of 2.5 m/s and subcooling temperature of 7.0 K. This flow condition provided a higher hydrate plugging risk during the simulation of the horizontal section.

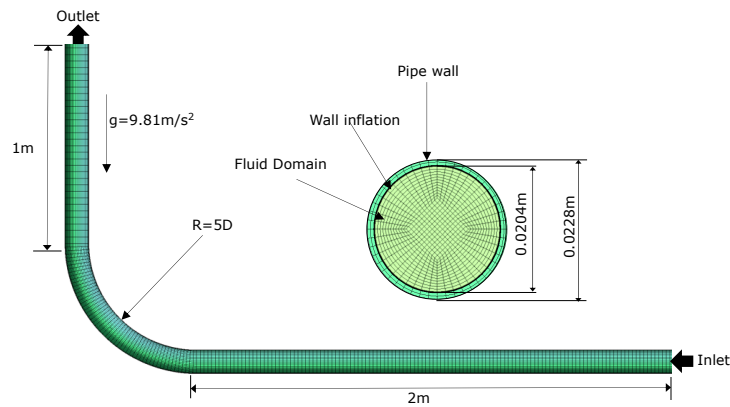


Figure 4.34: A 90-degree riser base section with diameter of 0.0204m (654,624 mesh cells).

The density contour in **Figure 4.35**, provides insight into the simulation results. Though the density increased, the change was minimal (maximum of 0.6), compared with the change in density at the horizontal section discussed earlier which was 3.0. This further illustrate the fact that hydrates are not deposited at the riser because the temperature and turbulence do not favour hydrates agglomeration and deposition.

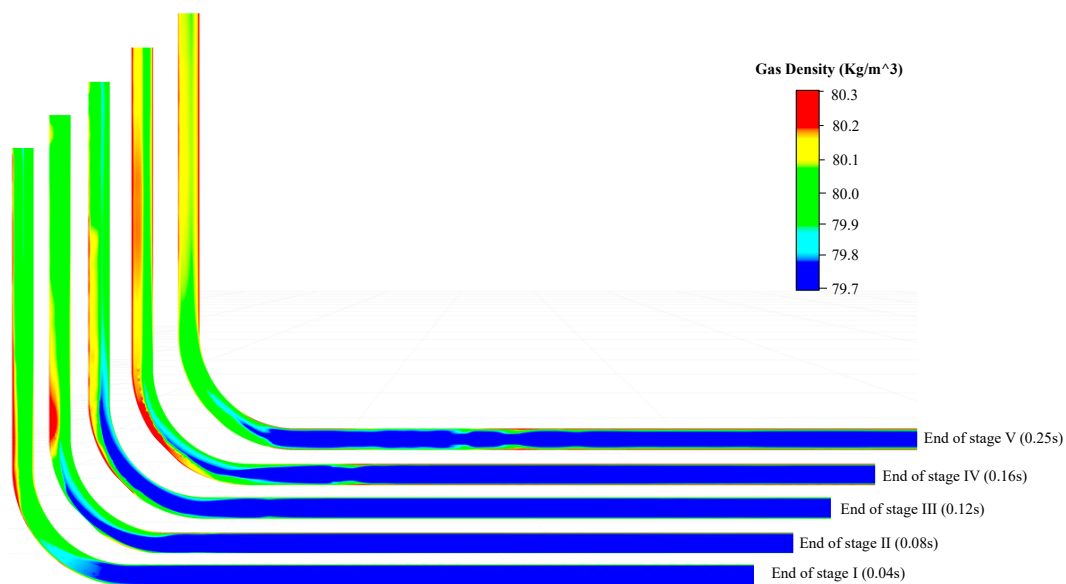


Figure 4.35: Change in gas density contour map during the growth, erosional and transportation of hydrates in the riser at 2.5 m/s and subcooling temperature of 7.0 K

The gas temperature was relatively stable at 292K throughout the simulation and the temperature contour was unable to capture the stages explained in

Figure 4.36 for the horizontal section. Hence, the option of displaying the observed changes using the gas density contour above. As seen in **Figure 4.36a** below, hydrates formation occurred in stages II and IV, and a slight agglomeration in between stages IV and V, before deposition in stage V after 0.20 s. A corresponding rise in pressure is observed in **Figure 4.36b**. The stable temperature in stage IV can be accepted as the onset of agglomeration and deposition. However, the result from the density contours in **Figure 4.35** suggests that the hydrates are not stable. Implying that the rise in pressure is due to increasing loading of a dense hydrate forming phase in the riser section.

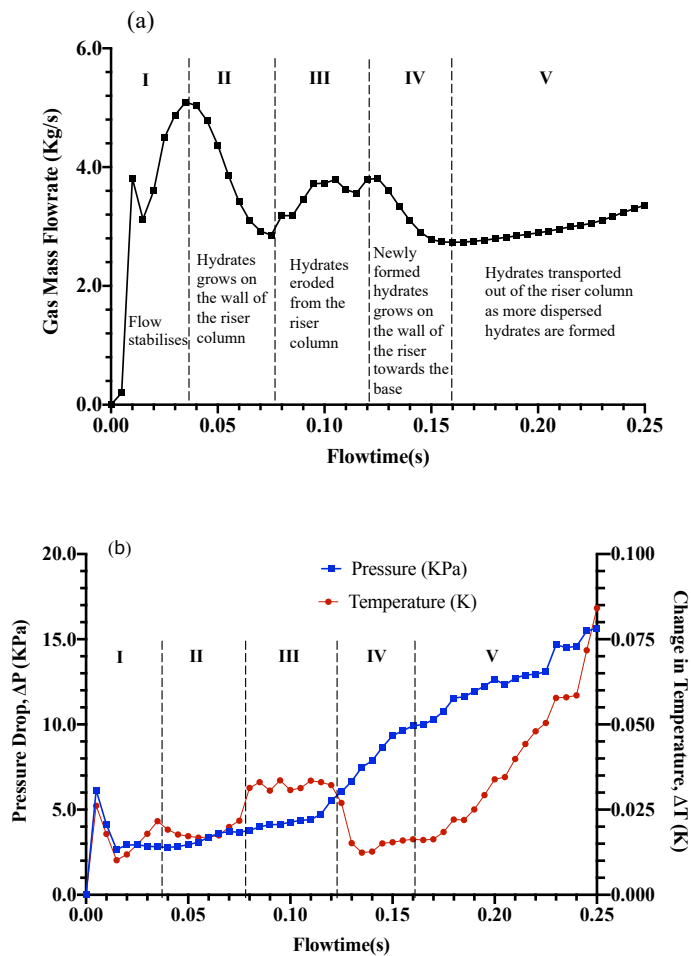


Figure 4.36: (a) Change in gas mass flowrate and (b) change in pressure and temperature, in the fluid domain during the growth, erosional and transportation of hydrates in the riser at 2.5 m/s and subcooling temperature of 7.0K

Also, there was no drop in the pressure curve, which is an indication of hydrates deposition as observed for the horizontal section (**Figure 4.6**). Hence, it is emphasised that during normal operation of gas pipelines, hydrates do not deposit at the riser when a hydrate forming gas is transported but are accumulated from the horizontal section and pushed into the riser base as hydrate plugs. This also agrees with the indication of the temperature of the dense gas at the wall (**Figure 4.37**), as the hydrates formed under this condition are not stable.

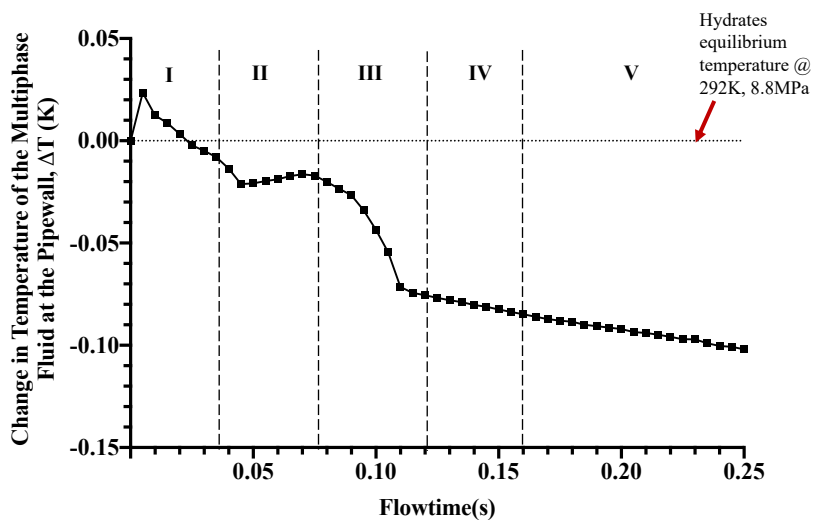


Figure 4.37: The gas temperature at the pipewall dropped below the hydrate equilibrium temperature of 292K to 291.9K, indicating a relatively stable temperature, hence the hydrates were not stable.

4.3 Chapter Summary

The need for a specific gas-hydrates predicting model for gas-dominated systems has been stressed in the literature (Charlton et al. 2018a). Currently, both experimental and analytical research reports indicate the occurrence of hydrate deposition and gas shear stress on the pipe wall during hydrate sloughing and shedding along the pipe. However, this present work has developed a validated CFD model based on the fact that: (i) experiments are expensive and can hardly be extrapolated for actual field application; and (ii) the need to improve on the predictions of the existing analytical model of Di Lorenzo et al. (2018). Based on the outcome of the analysis, the CFD model was able to accurately predict experimental and analytical results

comparatively. The empirical results of this CFD model at 4.7 m/s and 8.8 m/s predicted both experimental and analytical model results within $\pm 10\%$ uncertainty bound. Consequently, the unique contributions of this work to knowledge include:

- a. This novel CFD modelling approach improved hydrates deposition rate predictions at lower gas flow velocity of 4.7 m/s when compared with the only analytical model that predicted the deposition rates of hydrates at this velocity in gas-dominated pipeline.
- b. As a proactive predictive tool, this CFD model can predict the deposition rates of hydrates using the system gas flow velocity, pressure, and temperature as inputs. Thus, serving as a real-time predictive tool for monitoring the plugging risk of hydrates in gas pipelines, unlike existing CFD modelling of the deposition of hydrates in the literature that requires external injection of hydrates into the flow domain.
- c. The model also predicted the phase changes during the formation, agglomeration and deposition of hydrates, which is consistent with results from the analytical model of Wang et al. (2017) of 3-phase (gas, water and hydrates flow) and 2-phase (gas and hydrates flow).
- d. The model simulation results using different pipe diameter led to a new proposition that the deposition rate of hydrates increases as the diameter of the pipe increases under the same boundary conditions. No prior study has reported this observation. This is useful in extending the CFD model for industrial application using a scaling factor.
- e. In previous studies, Di Lorenzo et al. (2018) assumed a constant flowing shear stress, while Liu et al. (2019) assumed a varying shear stress value in their analytical models. This CFD model clarifies the disagreement as follows: (i) that the water-induced shear stress along the pipe fluctuates during wall shedding of hydrates as assumed in Liu et al. (2019); and (ii) the gas-induced shear stress on the hydrates layer during hydrates sloughing is relatively constant as assumed in Di Lorenzo et al. (2018).

By proposing a new ratio for the operating shear stress during sloughing and wall shedding, the model results compares favourably with the ratio of the resisting hydrates-water composite shear stress to the flowing gas shear stress on the deposit of hydrates suggested in Aman et al. (2016). The proposed 100-200Pa shear stress during sloughing (Di Lorenzo et al. 2018) agrees with the predictions of this model at lower velocity of 4.7 m/s. However, this study suggests that higher values of shear stress than the value of 100-200Pa suggested in the literature might be expected during sloughing at higher velocities.

- f. This study proposes that the deposit of hydrates at the velocity of 8.8 m/s is a linearly growing annular profile, while the hydrates layer at 4.7 m/s were deposited in a stratified annular pattern.
- g. Finally, the flow condition at the riser base do not favour hydrates agglomeration and deposition, but hydrates are deposited at the horizontal section of the pipeline and pushed into the riser base, where they are accumulated to form hydrate plug.

The need to provide further insights into hydrates pipewall shedding stress is discussed next in chapter 5. A regression model that can be implemented to predict the deposition rates of hydrates in shutdown scenario is provided in chapter 6. While the CFD model can predict transient pressure drop during hydrates deposition and the resulting pipeline plugging flowtime, it is difficult to estimate both the actual transient pressure drop and plugging flowtime for an industry scale gas pipeline using the CFD model. Therefore, the need to combine the deposition rate of hydrates predicted in this model with an analytical model for estimating the actual plugging flowtime and resulting transient pressure drop for an industry size pipeline is identified as a gap that will be closed in chapter 7.

CHAPTER 5: CFD PREDICTION OF HYDRATES SLOUGHING AND PIPEWALL SHEDDING BY HYDRATES IN SUBSEA GAS PIPELINES²

5.0 Introduction

The knowledge of the shear stress profile along the pipeline during hydrate sloughing and pipewall shedding by hydrates is helpful in determining accurate flow velocities in gas pipelines. The CFD simulation adopted in this study mimicked hydrates deposition by applying a subcooling temperature to the pipe wall at hydrates formation condition to increase the density of the gas at the wall and enhance the viscous interaction of the gas with the water at the annular water layer on the pipewall. The simulated temperature contour profile compared favourably with hydrate deposit geometry in the literature (Di Lorenzo et al. 2018).

Also, the shear stress plot indicated a dip which corresponds with the relative location of shedding events from the inlet of the pipeline in the literature (Liu et al. 2019). Increasing flowing shear stress leads to higher corrosion rate by wearing off the corrosion protective film (Nyborg and Dugstad 2003; Obanijesu 2009). The CFD model can provide further insight into the shear stress profile resulting from hydrates related flow in offshore gas pipelines. This can further enhance the determination of pipeline sections prone to higher internal corrosion rates because of pipewall shedding by hydrates.

Hydrate sloughing and wall shedding are essential in the study of hydrate deposition, transportability and pipeline plugging by hydrates. However, evidence in the literature suggests the difficulty in modelling sloughing events because of the complicated nature of the deposition of hydrates in gas-dominant pipelines as a result of flow turbulence (Charlton et al. 2018b). Transient sloughing events are responsible for the fluctuating pressure drop during the operation of gas-dominant pipelines (Di Lorenzo et al. 2014a), while the shedding of hydrates creates a uniform internal diameter at the

² The results in this chapter are published in Gas Science and Engineering: Umuteme, O. M., Islam, S.Z., Hossain, M. and Karnik, A., 2023. Computational fluid dynamics simulation of natural gas hydrate sloughing and pipewall shedding temperature profile: Implications for CO₂ transportation in subsea pipeline. *Gas Science and Engineering*, 116(2023). Doi: 10.1016/j.jgsce.2023.205048.

section where it occurs leading to sharp decrease in total pressure drop (Liu et al. 2019). Thus, the study of hydrate sloughing and shedding is important to provide insight into the application of hydraulic flow control measures in monitoring the plugging of pipeline by hydrates. Moreover, the presence of hydrates in gas pipelines has continue to attract research interest among academic and industry researchers in the last decade as evident from literature search.

Related studies in gas pipelines, include hydrates nucleation, agglomeration, deposition and plugging, which can be explained by both hydrate formation kinetic and hydraulic flow models. Kinetic models provide insights into the nucleation and agglomeration of hydrates, while hydraulic models explain deposition and plugging. The kinetic model by Turner et al. (2005) has gained increased acceptance in the modelling of hydrate growth kinetics by researchers with results that compares favourably with experimental outcomes (Zerpa et al. 2013; Charlton et al. 2018a; May et al. 2018; Liu et al. 2019). Also, the CFD model developed earlier in chapter 4, implemented the kinetic model in the UDF codes for both mass and energy sources in Ansys Fluent.

Furthermore, studies on the agglomeration, deposition, and plugging of hydrates have led to the following propositions. Jassim et al. (2010) suggests that agglomeration leads to the growth of hydrates up to a critical size before they are deposited, and that the depositional distance is a function of pipe diameter. Hydrates smaller than the critical size are transported with a drift velocity farther away from the source of formation (Jassim, Abdi and Muzychka 2010).

Research outcomes suggests that the deposition of hydrates on the pipe wall leads to plugging and this has been studied with the propositions that hydrates deposition: (i) increases with velocity at constant subcooling temperatures; and (ii) increases with subcooling temperatures at constant gas velocity (Di Lorenzo et al. 2014a; Aman et al. 2016). The four stages of hydrates formation, agglomeration, deposition and plugging can be observed through both temperature and pressure curves, where the pressure increases during formation and agglomeration, reduces during deposition

and increases again during plugging (Liu et al. 2020). Theoretically, a drop in pressure is observed at the onset of deposition and a steady rise in pressure is observed until the line is fully plugged.

Hydrates shedding at the pipe wall and sloughing occurs alongside deposition and leads to the transport of hydrates downstream until the hydrates are closely packed at locations of reduced pipe annulus or at the base of offshore pipeline riser. Therefore, sloughing and wall shedding are related to the hydraulic effects of hydrates transportability. Both concepts are important in the study of hydrates and lead to fluctuating transient pressure spikes. In some cases, the pipe can rupture before the safe-trip valves are activated because of pressure spikes beyond the pipeline incidental pressure.

Analytical models in the literature have been conservative in predicting the transient pressure drop and plugging flowtime (e.g., Wang et al, 2017; Di Lorenzo et al., 2018, Liu et al., 2019), as these models have been unable to accurately predict hydrates sloughing and wall shedding sites along the hydrates forming sections of the pipeline. A better understanding of how both concepts occur can provide further insights into the relationship between hydrates plugging flowtime and overall flow dynamics that for understanding the transportability of hydrates and the planning of mechanical pigging activities.

The literature on the mechanism of hydrates sloughing and shedding are not exhaustive (Aman et al. 2018). Specifically, experimental observations suggest the following theoretical position: (i) the minimum shear stress for hydrates shedding in gas-dominated pipelines is 20 times that for water dominated pipelines (Aman et al. 2018); (ii) hydrates deposition is primarily a pipewall phenomenon (Aman et al. 2018); (iii) hydrates flowing shear stress increases with increasing deposit of hydrate under the same flow velocity and subcooling temperature; (iv) hydrates flowing shear stress is about 4.8 times the wall shear stress prior to the deposition of hydrates (Aman et al. 2018); and (v) the value of the pressure drop in the pipeline reduces during hydrates sloughing (Di Lorenzo et al. 2014a).

Consequently, there are still gaps in the study of hydrates sloughing and wall shedding as the extant literature are not conclusive in providing the needed information to understand how both events occur in gas pipelines. Three basic factors have been identified as responsible for the increasing hydrates formation and deposition in gas-dominated pipelines.

These scenarios are encountered during: (i) seasonal temperature changes influencing the subcooling temperature at the same gas flowrate; (ii) operational need to increase gas production into the pipeline because of the development of new wells and the increasing demand for gas at a constant subcooling temperature; and (iii) the need to cut gas supply at a constant subcooling temperature. Thus, in this study hydrates sloughing/shedding are assumed to occur within the hydrates by removing top layers of deposited hydrates, while pipewall shedding by hydrates is explained with the understanding of pipewall erosion.

Therefore, the purpose of this chapter is to enrich the literature on hydrates sloughing and shedding by studying pipewall shedding as a new concept different from sloughing and shedding. Thus, pipewall shedding by hydrates is caused by dispersed hydrates in the multiphase flow behind the location of hydrates sloughing/shedding events and is critical to pipewall erosion. By plotting the hydrates-induced shear stress profile along the pipeline, higher shear stress zones were identified as locations of pipewall erosion and internal corrosion. Previous studies reports a positive relationship between flowing shear stress and increasing internal corrosion rate in a gas pipeline (Obanijesu 2009). The strain rate of the water phase and the molecular viscosity of the resulting multiphase flow have been studied in this chapter to provide insight into hydrates-induced shear stress on the pipewall.

A eulerian-eulerian multiphase CFD model developed in the last chapter was used for the simulations in this study. The results were recorded at the velocity range of 2-8 m/s and subcooling temperature range of 2-8K. The conceptual framework is based on the parameters influencing sloughing and wall shedding during hydrates formation. To achieve the objectives of this study, the following two assumptions have been made: (i) pipewall shedding

depends on the magnitude of the wall shear stress and the strain rate of the hydrates; and (ii) hydrates sloughing depends on the shear stress of the gas on the deposited hydrates and the resisting shear strength of the hydrate phase. Hence, three parameters have been investigated, including molecular viscosity, strain rate and shear stress.

These parameters were measured in this study because: (i) the resisting shear strength of the hydrate layer depends on the molecular viscosity of the multiphase flow and the strain rate on the secondary water phase; (ii) the shear stress induced by the primary gas phase on the hydrates layer is dependent on the pressure drop along the hydraulic profile created by the depositing hydrates; and (iii) the wearing effect of the resulting multiphase flow on the protective corrosion film on the wall of the pipe increases internal corrosion rate as the shear stress increases. The remaining sections of this chapter will discuss details of the results and summary of findings.

5.1 Results and Discussion

Temperature, molecular viscosity, and density contour maps were extracted to define the predicted deposit of hydrates profile (Umuteme et al. 2023a). Based on the hydrates profile, the *sweep length* is a new concept introduced in this study to understand the effect of velocity on the deposition of hydrates. It is the difference between the length of the pipe and the section of hydrate deposits. The sweep length section is the area prone to the effect of pipewall shedding. The termination of the sweep length section is the onset of hydrates sloughing. The strain rate was studied as indication of the severity of sloughing and wall shedding in relation to changes in velocity and subcooling temperatures, which affects the deposition rates of hydrates. The results and discussions are provided as follows.

5.1.1 Mist-Annular Flow Pattern During Hydrates Formation and Deposition

Profile of hydrates along the hydrates forming section of the pipeline is related to the concept of mist-annular flow pattern. To provide a substantive hydrates profile, the pattern of the contour maps for the temperature and density of the gas phase was investigated. The temperature contours in

Figure 5.1 and **Figure 5.2** suggests dispersed annular flow as the core contains unstable hydrates dispersed in the primary gas phase and the wall is layered with deposited hydrates. The increasing deposition of hydrates farther away from the inlet creates a subcooling effect for hydrates formation at the core.

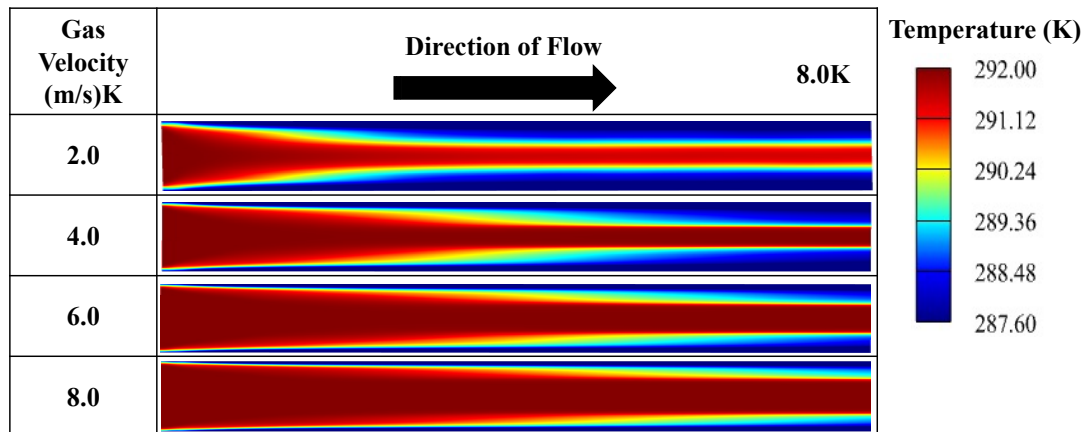


Figure 5.1: Temperature profile of hydrates at constant subcooling temperature of 8K and varying gas velocity. Deposited hydrates are stable below 290K. Unstable hydrates are formed at 292K at the core of the pipe.

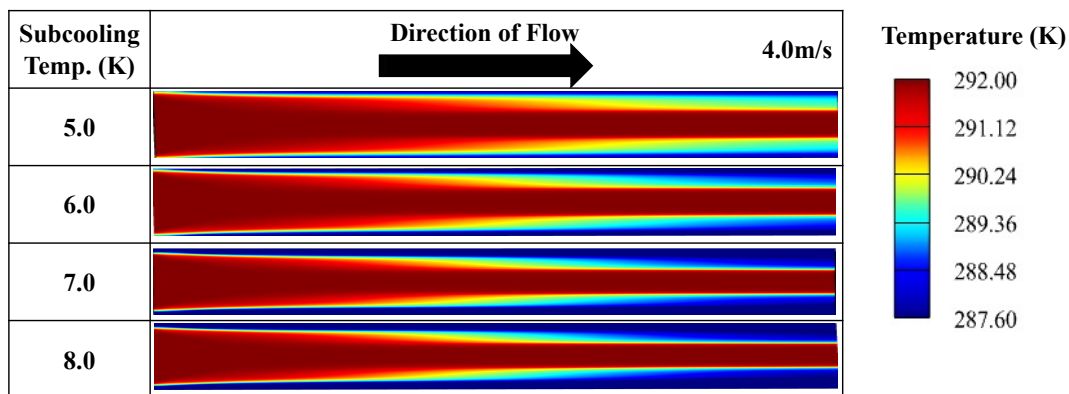


Figure 5.2: Temperature profile at constant gas velocity of 4.0 m/s and varying subcooling temperature. Deposited hydrates are stable below 290K. Unstable hydrates are formed at 292K at the core of the pipe.

Both figures reveal a critical trend: a gradual decrease in gas temperature towards the pipe wall at the core. This is corroborated with the position in the literature (Wang et al. 2017), of the importance of considering the hydrates formed at the core during the analytical modelling of hydrates formation in gas-dominant system. The gas density of the hydrate profile in **Figure 5.3** was generated at 4.0 m/s and subcooling temperature of 7.0K

to demonstrate the effect of annular flow pattern during hydrates formation and deposition.

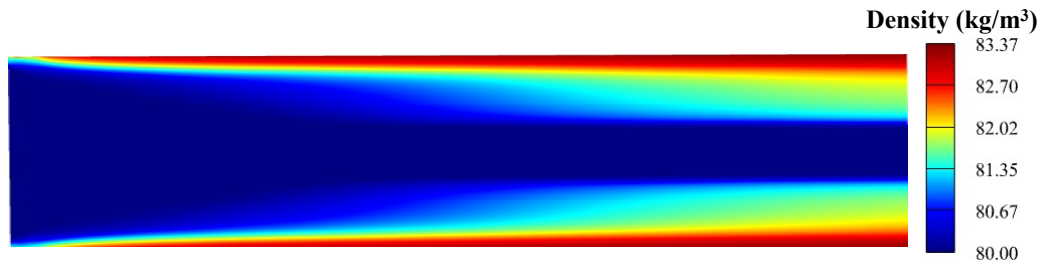


Figure 5.3: Hydrates profile obtained from the gas density. The higher gas density at the wall indicates hydrates deposition.

From **Figure 5.3**, it is observed that the gas density is dependent on pressure and temperature and increases towards the wall which is at a lower temperature than the core. As indicated earlier in **Figure 5.1** and **Figure 5.2**, at lower gas velocity there is higher tendency of early plugs of hydrates forming in the pipeline. Also, at higher subcooling temperature, the layers of deposited hydrates create a narrow annulus at the outlet of the pipe, and an indication of increased in deposition at higher subcooling temperatures in **Figure 5.2**. The profile of the deposited hydrates was generated by limiting the contour map to a maximum temperature to 290K as indicated in **Figure 5.4**. From the temperature hydrate contours, the mechanism of shear and sloughing is described in **Figure 5.4**, below.

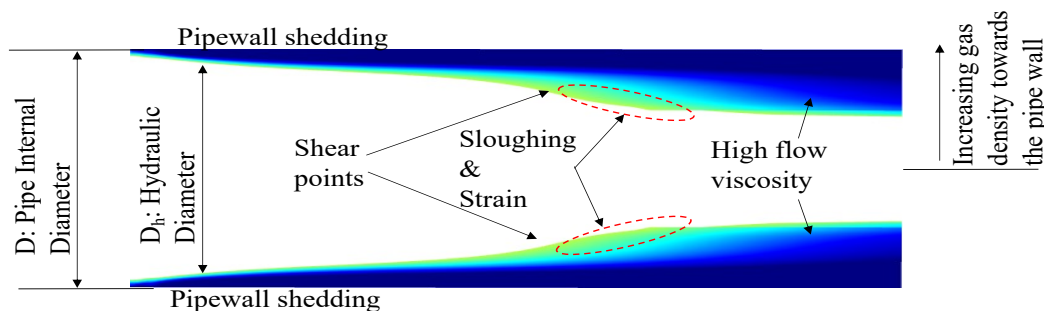


Figure 5.4: Labelled profile of deposited hydrates

The above profile in **Figure 5.4** agrees with the one proposed and discussed elsewhere (e.g., Di Lorenzo et al., 2018). The pipe's hydraulic diameter narrows towards the exit, further constricting the flow. This constriction creates shear points, particularly near the identified sloughing locations. These shear points likely contribute to the strain placed on the deposited

hydrates, potentially leading to their detachment. Additionally, the viscosity of the fluid also increases towards the pipe wall, further hindering flow and potentially influencing hydrate formation and stability. The location of sloughing is identified based on the hydrate profile suggested in the literature because these are likely sites where the hydrates push-off can increase the hydraulic diameter and lead to momentarily decrease in pressure drop (Di Lorenzo et al. 2014a). It is possible to establish a relationship between the sloughing points and velocity or subcooling temperatures as the reduction in pipe hydraulic diameter. Increase in hydrates deposition can increase the shear stress at the sloughing site (Charlton et al. 2018b).

In offshore gas lines, sloughing is responsible for delayed plugging at higher flow velocity, until the hydrates plugged the base of the riser. In chapter 4, it was suggested that the shear stress varies along the pipe length at higher gas velocity instead of having a fixed value as assumed in Di Lorenzo et al. (2018). Pipewall shedding by hydrate deposits occurs upstream of the sloughing location.

5.1.2 Variation of Hydrates Thickness with Velocity and Subcooling Temperature

By reconstructing the contour profiles in **Figure 5.1** and **Figure 5.2**, the thickness of the deposited stable hydrates along the pipe when the temperature is below 290K indicates that the thickness decreases as the velocity increases at constant subcooling temperature. By considering the deposited hydrates profile at varying gas velocities, it is possible to understand the effect of sloughing on hydrate deposits as indicated in **Figure 5.5**.

Whereas higher velocities lead to higher hydrates deposition rates, most of the deposited hydrates are carried along with the flow until they are deposited at the riser base. At lower gas velocity (e.g., 2.0m/s), the risk of hydrates plugging the horizontal section of the pipeline is higher. **Figure 5.5** indicates that the thickness of hydrates increases along the length of the pipeline from inlet to outlet. At a constant subcooling temperature of 8.0K, the thickness (t) of hydrates increases as the velocity decreases.

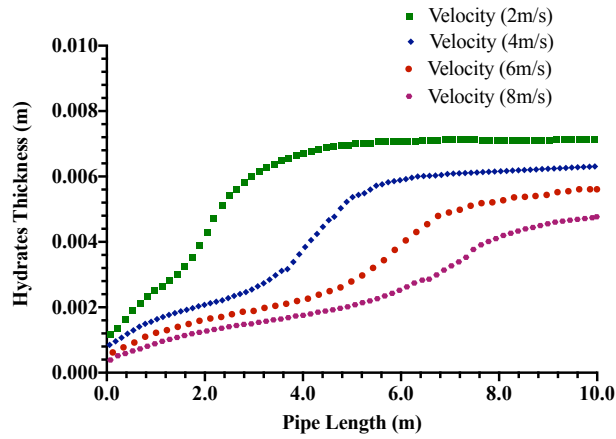


Figure 5.5: Hydrates profile at a subcooling temperature of 8.0K and varying gas flow velocity of 2-8 m/s

The area under each curve (AUC, m^2) is estimated from the approximation of trapezoidal method and is useful in determining the volume of deposited hydrates.

$$AUC = \frac{1}{2} \sum_0^n (t_n + t_{n-1}) \Delta L \quad (5.1)$$

where t , is the thickness of the hydrate layer and ΔL is the pipeline length where the hydrates are forming. The volume of the deposited hydrates V_H , can be estimated as follows.

$$V_H = \frac{2}{3} AUC \cdot \pi D \quad (5.2)$$

In equation 5.2, D is the pipe diameter (m) and π is a dimensionless constant (3.142). For the range of velocities considered in **Figure 5.5**, the volumes of hydrates deposited are presented in **Table 5.1**, with increasing reduction in hydraulic diameter as the velocity reduces. The force to push the hydrates out of the pipeline is directly related to the resisting shear stress between the hydrates and the pipewall. The discussion that follows investigates the relationship between the fluid properties and flow dynamics during hydrates deposition, sloughing and shedding further. The shear stress experienced by the deposited hydrate layer is dependent on the molecular viscosity of the multiphase mixture and the strain rate of the deposited hydrates layer. Also,

the pipewall skin friction influences the pressure drop and wall shedding by hydrates.

Table 5.1: Volumes of deposited hydrates at a subcooling temperature of 8.0K and varying gas flow velocity of 2-8 m/s

Gas Velocity, V_g (m/s)	Thickness of Hydrates Deposits (mm)	Area Under Curve, AUC (m^2)	Volume of Hydrates, V_H (m^3)	Reduction in Hydraulic Diameter
2	7.13	0.0585	0.0025	69%
4	6.31	0.0430	0.0018	62%
6	5.61	0.0324	0.0014	55%
8	4.77	0.0245	0.0010	47%

The plot of the deposited hydrate volumes and the respective gas velocities indicates that the deposited volume decreases as the gas flow velocity increases.

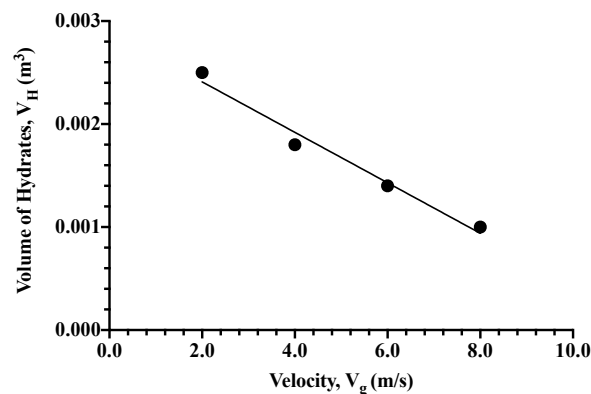


Figure 5.6: The effect of increasing gas velocity on volume of deposited hydrates at subcooling temperature of 8.0K.

The volume of hydrates along the pipe reduces with increasing velocity because of increased loading of hydrates in the primary gas phase at higher gas velocities. This is a concern for pipewall erosion because of increasing abrasive wear-off of the corrosion protective layer on wall. Implying that the need to transport hydrates at higher velocities must be weighed with the effect on internal pipewall corrosion. Empirical results suggests that the depositional distance of hydrates increases with increased Reynolds number (Jassim, Abdi and Muzychka 2010). From here, the effect of sloughing and wall shedding is seen as primarily related to the change in gas velocity.

5.1.3 Effect of Gas Velocity on Molecular Viscosity of the Multiphase

Previous studies suggest that the formation and deposition rates of hydrates increases with increasing velocity at constant subcooling temperature (Di Lorenzo et al. 2014b, 2014a; Aman et al. 2016). **Figure 5.7** provides a profile of the molecular viscosity of the multiphase flow during hydrates formation, agglomeration, and deposition.

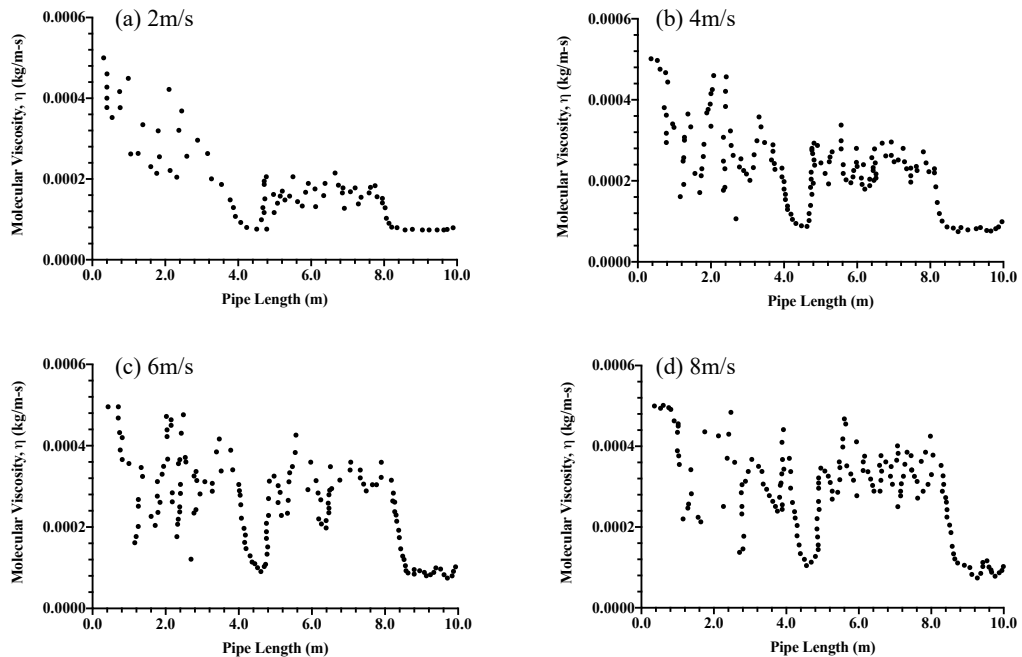


Figure 5.7: Increasing molecular viscosity of the multiphase flow during hydrates formation, agglomeration, and deposition.

During the simulation, the flow is driven initially by 94% gas volume fraction, which reduces as hydrates are formed and deposited. The increasing formation and agglomeration of hydrates increases the molecular viscosity. Thus, the fluctuating profile of the molecular viscosity the multiphase flow during the simulation in **Figure 5.7** indicates the presence of turbulence, deposition and sloughing of hydrates. Pipewall shedding by hydrates also occurs intermittently. The presence of these hydraulic occurrences along the hydrates forming section of the pipe is due to increasing loading of hydrates into the continuous gas phase as the velocity increases.

The initial gas viscosity at inlet condition was 0.000015 Pa-s, and the increasing viscosities in **Figure 5.7** are due to phase change under hydrates forming condition of temperature, pressure, and gas velocity. The increasing

viscosity as the gas velocity increases is evidence of dispersed hydrates in the flow due to sloughing and wall shedding. The dip at 4 m from the inlet is the onset of sloughing. However, this sloughing is more pronounced at lower gas velocity of 2 m/s. The molecular viscosity in the entire pipeline section is relatively uniform at higher gas velocities of 6 m/s and 8 m/s.

As indicated, sloughing occurred more rapidly as the flow velocity increases. The sharp drop in the value of the molecular viscosity of the multiphase flow (gas-water-hydrates) at the gas velocity of 2 m/s and 4 m from the inlet is because of agglomeration and deposition. Lower molecular viscosity is an indication of the onset of pipe plugging by hydrates. Thus, it is possible to identify the location of hydrates sloughing events along the pipeline as critical to hydrates plugging risk.

5.1.4 Effect of Pipewall Skin Friction

Skin friction affects flow by increasing the hydraulic pressure drop along the pipeline. Also, viscous effects create a restraining force that tend to balance the pressure force (Munson et al. 2013). As discussed in chapter 4, the turbulent Reynolds number throughout the simulation was within the transition zone where there is intermittent switch between laminar and turbulent flow. While deposition is enhanced in laminar regime, sloughing increases the turbulence in the multiphase flow.

The increasing viscosity of the flow after sloughing can lead to higher spike in pressure drop. As a consequence, the resistance along the flow path induces shear stress on the pipewall. Hence, the succeeding pressure spikes during sloughing were higher in the experiments. It is advisable to shut down the pipeline at the onset of the first significant pressure spike. Hydrates deposition, sloughing and pipewall shedding can be explained using the boundary layer phenomenon. This phenomenon of pipewall friction is related to the wall shear stress through the Darcy friction factor f , as follows.

$$f = \frac{8\tau_w}{\rho V^2} \quad (5.3)$$

where ρ is the density of the fluid, V is the velocity the fluid and τ_w is the wall shear stress. **Figure 5.8** provides the pipewall skin friction factor

during the simulation at the subcooling temperature of 8.0K. The average coefficient of friction C_f values reduce as the gas velocity increases, providing evidence of pipewall erosion at higher velocities.

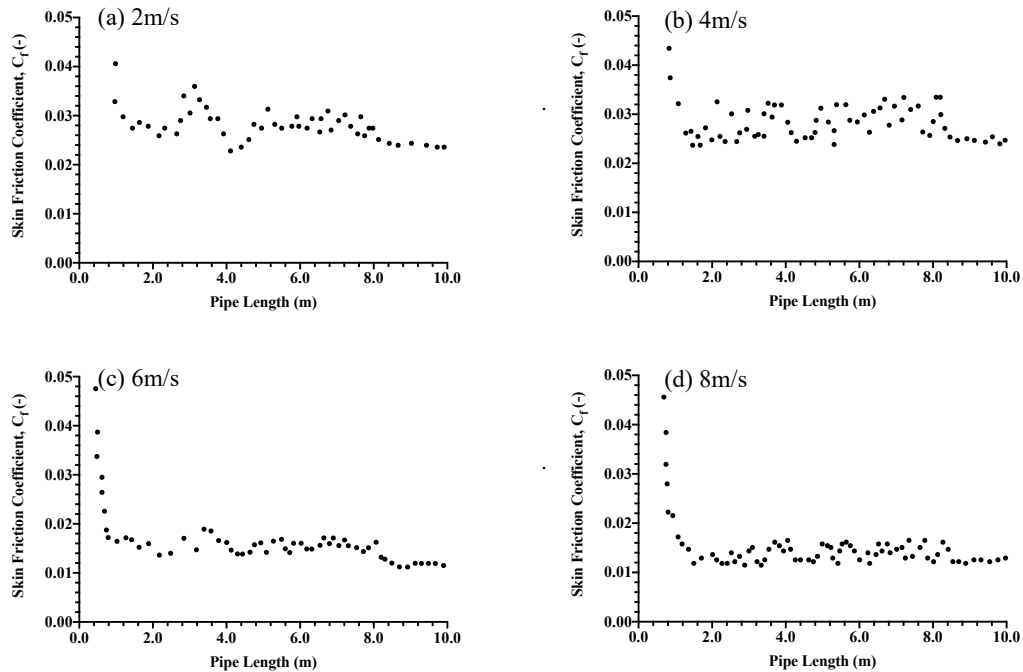


Figure 5.8: Increasing coefficient of pipe wall skin friction during hydrates formation, agglomeration, and deposition. The wall skin friction is obtained from the secondary water phase.

5.1.5 Effect of Velocity on the Strain Rate of Hydrate Deposits

The CFD simulation results mimicked the actual effect of velocity change on the strain rate of hydrate deposits on the pipe wall by obtaining the strain rate data of the secondary phase in the presence of the heavier gas. Earlier in **Figure 5.3**, it was shown that the density of the gas increased towards the wall of the pipe because of a sustained cooling effect from the annular profile of the secondary phase film on the pipewall. The influence of velocity on the deformation of the viscous phase by the heavier gas phase can provide insight on the carrying capacity of the gas phase and ability to transport hydrates out of the pipe as they are formed.

It is important to understand the effect of velocity on the strain rate of hydrates because hydrates shedding can damage of the passive wall film on

the pipe, leading to internal corrosion (Obanijesu et al. 2011). Higher strain rate indicates higher wall shedding by hydrate deposits and a reduction of the contraction rate of the pipeline diameter. In **Figure 5.9**, the strain rates of the deposited hydrates are compared for velocities of 2, 4, 6 and 8 m/s. In all the graphs, two zones are clearly indicated – the zone where wall shedding occurs (from inlet to 4m), and the zone where sloughing occurs (4m to 10m).

The strain rate drops at about 4m downstream of the inlet and rises again until 2 m to the pipe exit. The resistance to deformation of the hydrates deposits can be seen as positions of drops in strain rate where minimal pipewall shedding (0-4m) and hydrates sloughing (4-10m) occurred. Hence, the results shows that hydrates sloughing and wall shedding events are nonuniform but create a wavy profile of hydrate deposits along the pipe.

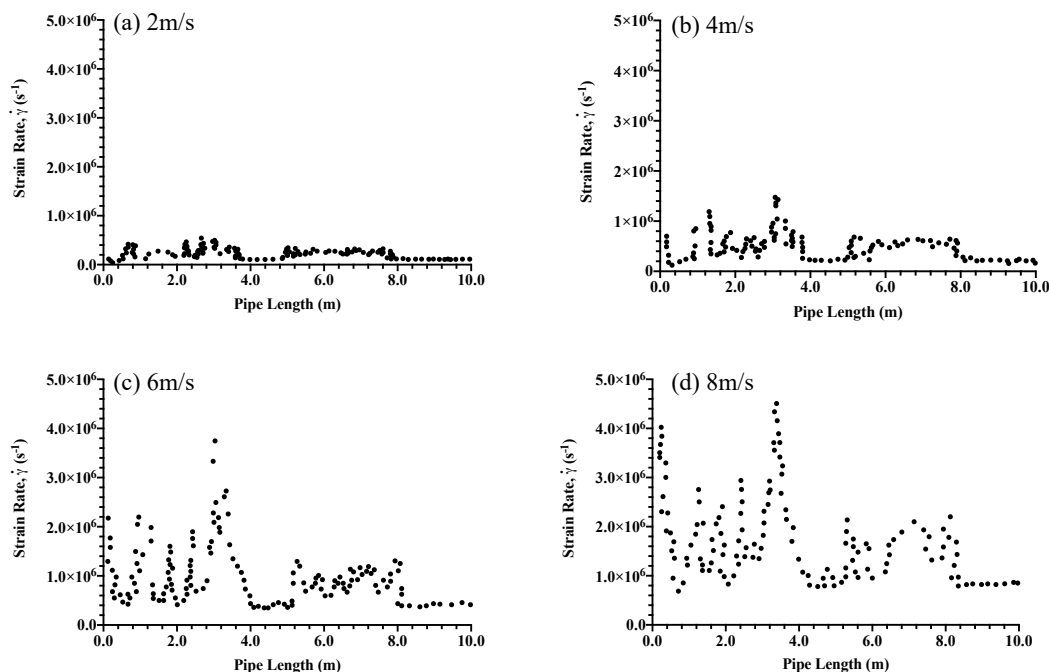


Figure 5.9: The strain rate of hydrate deposits on the pipe wall by obtaining strain rate data of the secondary phase in the presence of the heavier gas.

5.2 Hydrates Sloughing and Pipewall Shedding

This study differentiates between hydrates sloughing/shedding and pipewall shedding by hydrates. In previous studies, both hydrates sloughing/shedding which happens within the layer of the deposited hydrates was confused with

pipewall shedding which is critical to pipewall erosion. Internal corrosion because of the erosion of the pipewall by hydrates has been reported in the literature (Obanijesu 2012). Thus, by simulating the conditions for hydrates formation and deposition, the profile of the deposited hydrates was captured and compared with the resulting shear stress profile. In the CFD simulations, hydrates sloughing and pipewall shedding by hydrates can be studied from the profiles of the molecular viscosity, strain rate and shear stress.

As the gas density increased towards the wall of the pipe (**Figure 5.3**) and the molecular viscosity increases (**Figure 5.7**), the interaction of the heavier gas phase at the wall with the water film was used to mimic the hydraulic behaviour of hydrate deposits. The simulation effect on multiphase flow pattern during hydrates formation was shown as annular from the temperature profile in **Figure 5.1** and **Figure 5.2**. The locations of hydrates sloughing and pipewall shedding identified earlier in **Figure 5.4** are presented in **Figure 5.10** below.

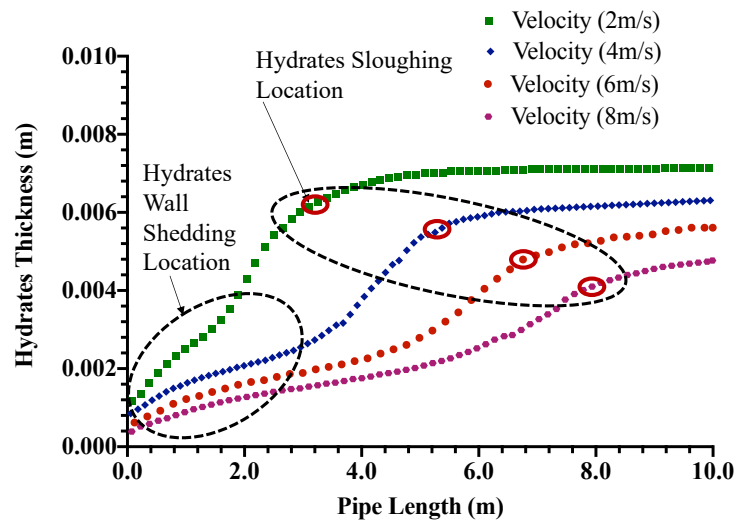


Figure 5.10: Locations of hydrates sloughing and wall shedding along the pipe

Increase in Reynolds number increases the depositional distance of hydrates along the pipe (Jassim, Abdi and Muzychka 2010). This is also evident as the profile for the gas velocity of 8 m/s indicates a farther depositional distance compared to the sloughing location at the gas velocity of 2 m/s.

5.2.1 Sloughing and Pipewall Shedding Shear Stress

As proposed in this study, pipewall shedding by hydrates occur at the proximity of the pipe wall, with higher shear stress than the sloughing zone which offer lesser resistance to flow. A closer synonym to shedding as implied in this study is "skinning." Thus, the discussion hereafter is how pipewall "skinning" is influenced by the shear stress on the deposited hydrates. The location for hydrates sloughing has been identified from the suggestion by Di Lorenzo et al. (2018). The shear stress plots in this section were obtained from the product of the molecular viscosity (**Figure 5.7**) and shear strain (**Figure 5.9**). The Shear stress along the pipe section has been compared with the respective hydrates temperature contour at gas velocity of 4 m/s and subcooling temperature of 8.0K and labelled as presented in **Figure 5.11**.

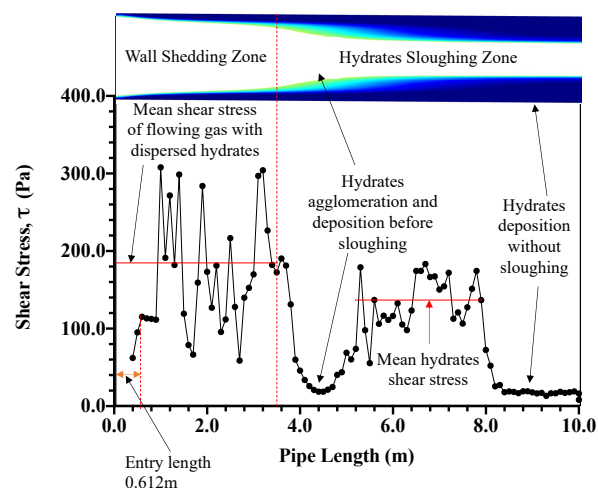


Figure 5.11: Representation of shedding and sloughing along the shear stress plot at 4 m/s and subcooling temperature of 8.0K

The plots that follow indicate the variation of shear stress with gas velocity. The reduction in wall shear stress at lower gas velocity is due to the thickening of the boundary layer and is associated with a decrease in velocity gradient at the surface (Kundu, Cohen and Dowling 2016). The thickening of the boundary layer is analogous to the increase in hydrate deposits, which is noticed at lower velocities. The shearing stress acts on a plane perpendicular to the radial direction (Munson et al. 2013), hence able to enhance wall shedding as the flow velocity increases.

Higher stresses are as a result of higher volume fractions of hydrates in the multiphase flow, which is also corroborated in another study elsewhere (Jujuly et al. 2020). Also, sloughing shear stress increases with increasing gas velocity.

The average pipewall shedding shear stress was obtained from between the distance of 1 m to 3 m along the pipe and increased in the following order: 2 m/s (71Pa), 4 m/s (167Pa), 6 m/s (259Pa) and 8 m/s (527Pa). The average resisting sloughing shear stress was measured from the distance of 5 m to 7 m along the pipe and increased in the order: 2 m/s (43Pa), 4 m/s (122Pa), 6 m/s (245Pa) and 8 m/s (487Pa). The maximum pipewall shedding shear strength by the hydrate layer on the pipewall recorded are above 100 Pa, in agreement with experimental predictions in Aman et al. (2018).

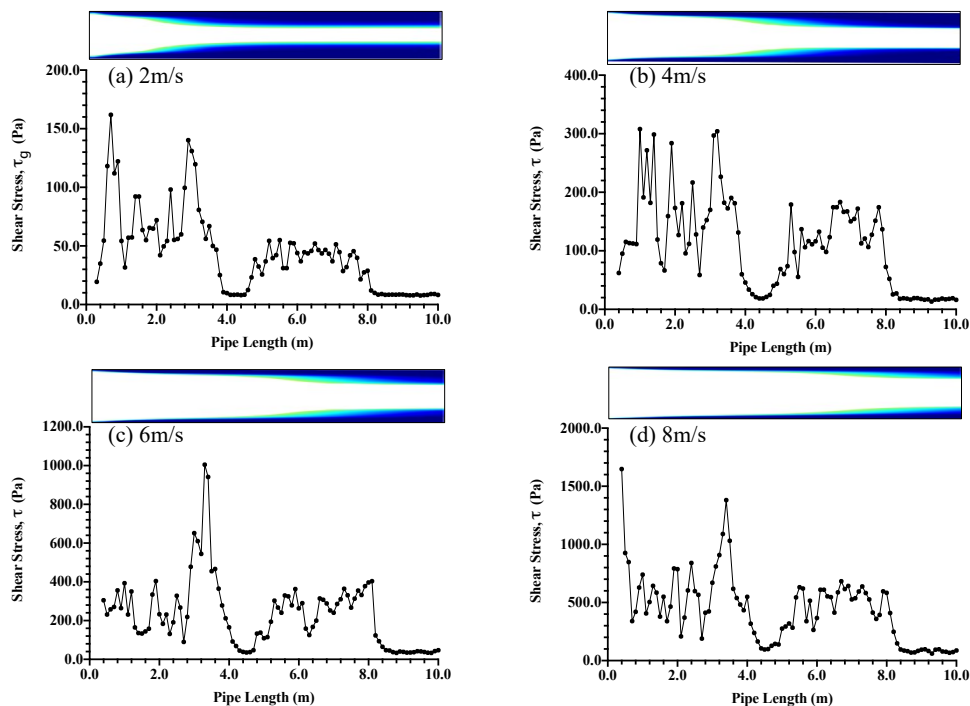


Figure 5.12: Variation of shear stress with gas velocity at constant subcooling temperature of 8.0K

More hydrates are forming at higher velocities increases hydrates loading and cohesiveness, with a consequent increase in flowing shear stress. The location of hydrates sloughing was estimated at approximately 0.4575L from the inlet of the pipeline (Liu et al. 2019). This corresponds to the point 4.5 m position along the pipe length in **Figure 5.11** and **Figure 5.12**. By

identifying the location of hydrates sloughing corresponding to the dip at 4.0 m along the pipe length above, the pipewall shedding stress is identified as occurring before this point in this study. Although this demarcation is present at higher velocities of 6 m/s and 8 m/s, the relatively uniform shear stress plots indicate the presence of pipewall erosion at higher flow velocities.

Hence, while it is advisable to increase gas velocities to enhance hydrates transportability, the increasing pipewall shear stress can lead to pipewall erosion. The minimum shear stress for pipewall shedding in gas-dominated pipelines is at least 100 Pa (Aman et al. 2018), and equally estimated elsewhere as 150-155 Pa (Di Lorenzo et al. 2018). Hence, with the CFD predictions above a more effective pipewall shedding is possible at higher flow velocities. This raises a concern for low flow conditions from aging producing fields or when processing units are down for turn-around maintenance.

The ratio of pipewall shedding shear stress to sloughing shear stress is in the order: 2m/s (1.7); 4m/s (1.4); 6m/s (1.1); and 8m/s (1.1). Thus, pipewall shedding and sloughing occur differently at lower gas velocities, and as the velocity increases, the gap between pipewall shedding and sloughing reduces. Implying that higher pipewall erosion by hydrates occurs at higher gas velocities. Earlier in chapter 4, the wall shedding stress was obtained from the water phase on the pipe wall, hence the higher value of 2500 Pa at the velocity of 8.8 m/s. Here, the wall shedding stress values are obtained by multiplying the shear strain of the water phase with the molecular viscosity of the gas-water multiphase and should be a more realistic outcome. However, this would have to be validated with field or experimental results in future.

5.2.2 Pressure Drop and Shedding Stress

The relationship between pressure drop and wall shear stress is given in the literature (Munson et al. 2013).

$$\tau_w = \frac{D\Delta p}{4L} \quad (5.4)$$

where D is the CFD model pipe diameter, L is pipe length, τ_w is the estimated wall shear stress and Δp is the pressure drop. However, this relation will not hold for pipe sections experiencing hydrates deposition because of the reduction in hydraulic diameter and the available pipe length. In the equation 5.4, the pressure drop reduces from the pipe inlet to the outlet. During hydrates formation, the pressure drop is transient and peaks during agglomeration, hence equation 5.4 is unable to provide the relationship between pressure drop and wall shear stress in a hydrate forming gas pipeline.

Transient variation in available length of the pipeline, the hydraulic diameter and transient pressure drop will be discussed further. The available length is hydrates forming section of the pipeline less the hydrates plugging section and have been identified as the sweep length in this study. In **Figure 5.13** the sweep length (L_{sw}) has been identified, indicating the section of the pipe where pipewall shedding is prevalent.

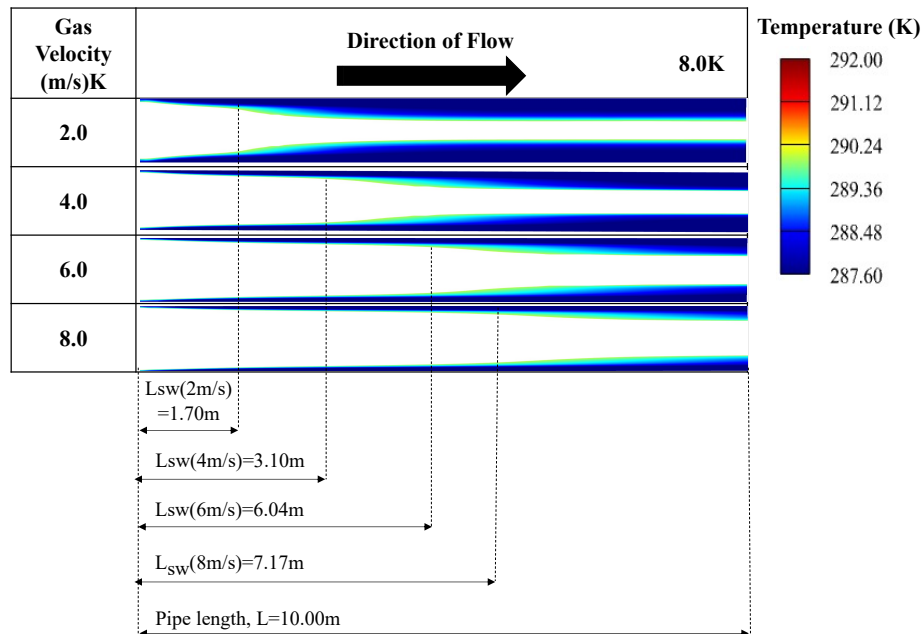


Figure 5.13: Variation of hydrates sweep length with gas velocity at constant subcooling temperature of 8.0K.

The sweep length represents the hydrates pipewall shedding section along the pipe. The sweep length terminates at the onset of hydrates sloughing. The sweep length increases with increasing velocity, suggesting that higher gas velocities can enhance hydrates transportability, but can also lead to

higher pipewall erosion. The hydraulic diameter for the sweep length section ($D_{h_{sw}}$), is uniform and creates a hydrates layer thickness that finally adheres to the wall of the pipe. The value of $D_{h_{sw}}$ in **Figure 5.13** at the termination of the L_{sw} , widens as the gas velocity increases. Another term, the sweep ratio (S_{sw_r}), was introduced to relate the sweep length, L_{sw} to the length of the hydrates forming section of the pipeline, L . As seen in **Table 5.2** and **Figure 5.14**, the S_{sw_r} increases with increasing gas velocity.

$$S_{sw_r} = \frac{L_{sw}}{L} \quad (5.5)$$

Table 5.2: Sweep length and sweep ratio at a subcooling temperature of 8.0K

V_g (m/s)	L (m)	L_{sw} (m)	S_{sw_r} (-)
2	10	1.70	0.17
4	10	3.10	0.31
6	10	6.04	0.60
8	10	7.17	0.72

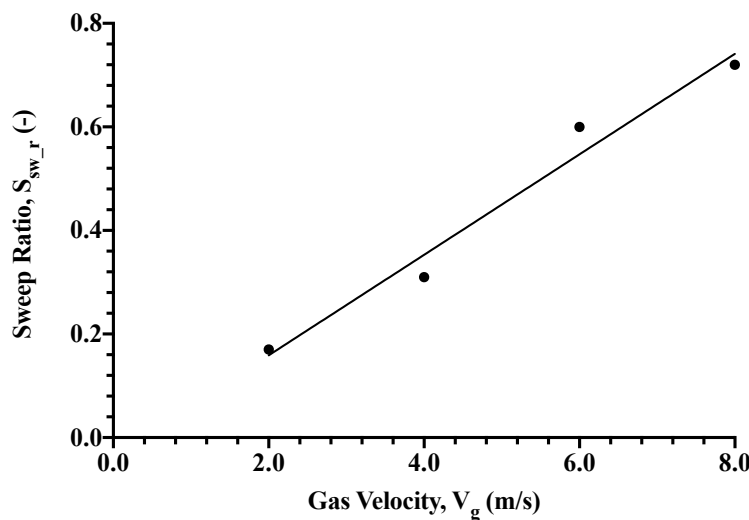


Figure 5.14: Effect of gas velocity on sweep ratio at a subcooling temperature of 8.0K.

For all simulations, the gas density was constant during hydrates agglomeration and deposition as presented earlier in **Figure 3.11**. The ratio of pressure drop is compared with the inertia force using the dimensionless

Euler number ratio (Eu) in equation 5.6. In **Figure 5.15**, $Eu < 1$ for all gas velocities, showing that pipewall shedding and sloughing are driven by inertia force rather than the pressure drop. A more resisting flow is observed at 2 m/s, suggesting higher plugging risk at lower gas velocities.

$$Eu = \frac{\Delta p}{\rho V_g^2} \quad (5.6)$$

where Δp , ρ , and V_g retains their earlier definitions.

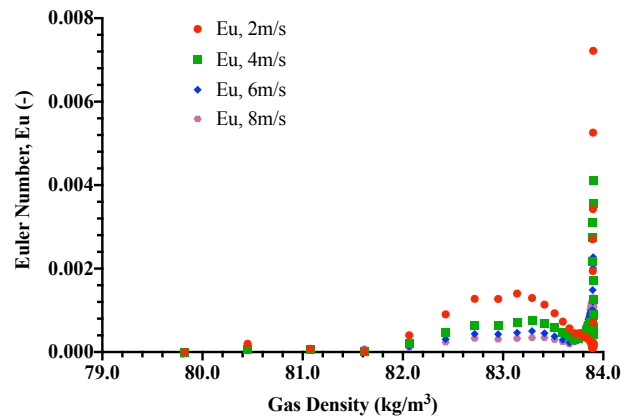
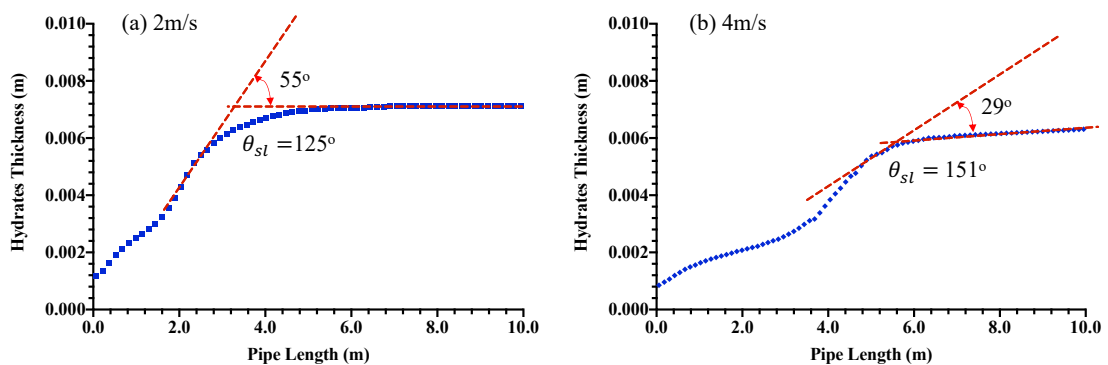


Figure 5.15: Effect of change in the density of the gas on the Euler number at a subcooling temperature of 8.0K.

A further analysis of **Figure 5.10** by defining the 'sloughing angle (θ_{sl})' as a new term suggests the sloughing angle increases with increasing velocity. This can be inferred from the deposition rate as the gas velocity increases under the same subcooling temperature.



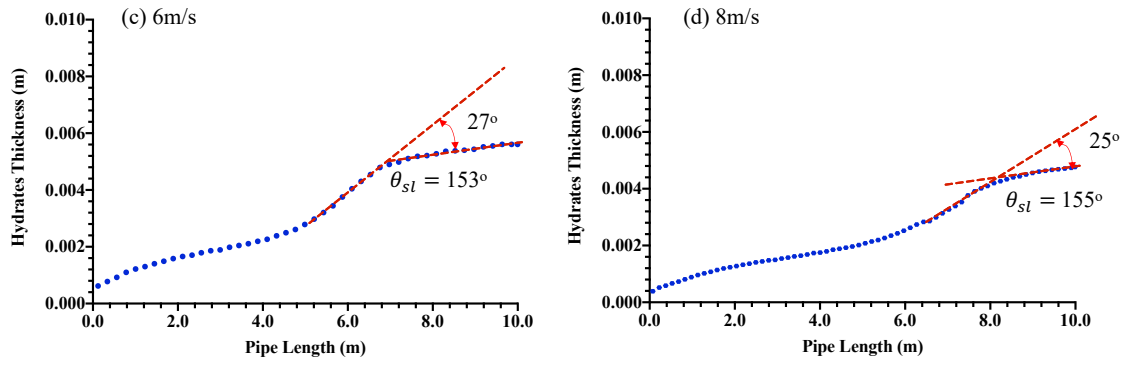


Figure 5.16: Hydrates profile at a subcooling temperature of 8.0K and varying gas flow velocity. (a) 2 m/s – sloughing angle of 125°. (b) 4 m/s – sloughing angle of 151°. (c) 6 m/s – sloughing angle of 153°. (d) 8 m/s – sloughing angle of 155°.

Thus, the steepness of the deposited hydrates profile increases with increasing velocity and can lead to early plugging of the pipeline. Furthermore, by constructing a linear regression line of the sloughing profile to forecast the possible plugging location when the hydraulic diameter is “zero”, the plugging distance for the pipe diameter of 0.0204 m for the different gas velocities at a subcooling temperature of 8.0K are: 72 m (2 m/s), 42 m (4m/s), 31 m (6m/s) and 15.8 m (8m/s). Whereas a higher reduction of 69% in hydraulic diameter was earlier at the velocity of 2 m/s (**Figure 5.18**), the plugging of the horizontal section of the pipeline is earlier at higher velocities if the riser base or the location of change in pipeline geometry is near the equilibrium point of hydrates formation (**Figure 5.17**).

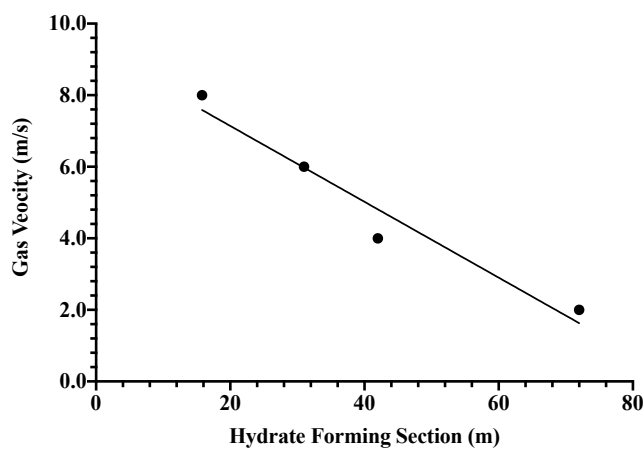


Figure 5.17: Effect of sloughing on hydrates plugging distance at a subcooling temperature of 8.0K and varying gas flow velocity.

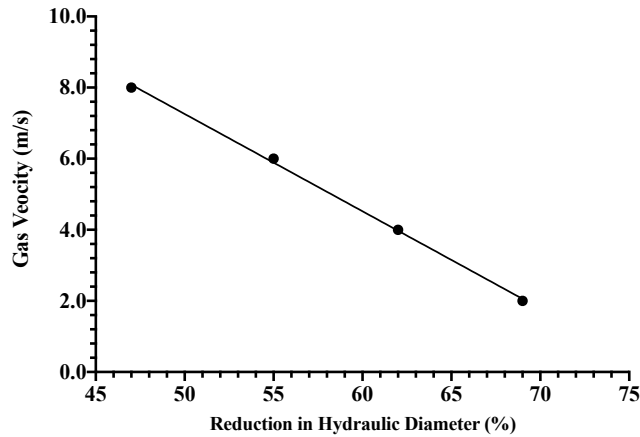


Figure 5.18: Effect of sloughing on pipeline hydraulic diameter at a subcooling temperature of 8.0K and varying gas flow velocity.

Finally, the effect of sloughing and wall shedding shear stress in a hydrate forming pipeline can be inferred from the simulation results for the velocities of the gas and water phase at 8.8 m/s and subcooling temperature of 7.0K (**Figure 5.19**).

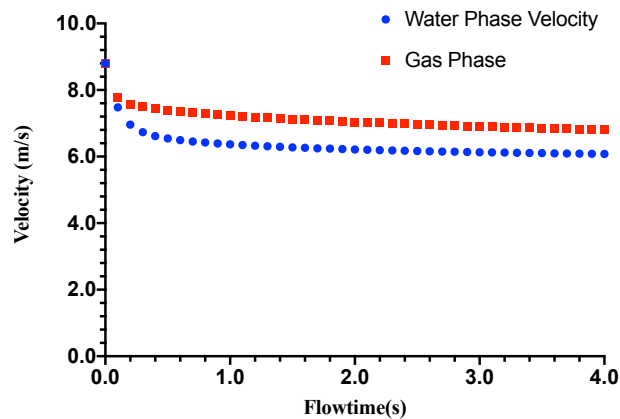


Figure 5.19: Velocity profile of gas and water phase during hydrates formation at a subcooling temperature of 7.0K.

The velocity of the water phase is below the primary gas phase, suggesting an increasing resistance to flow by the water phase. The drop in the velocity of both phases is due to reduction in volume and obstruction to flow because of increase in viscosity. Implying that as the viscosity increases due to more deposition of hydrates, there will be a decrease in both sloughing and pipewall shedding events, and the pipeline will finally get plugged by hydrates.

5.3 Chapter Summary

This study simulated the conditions necessary for hydrates formation and deposition in a gas pipeline using the validated CFD model that was developed earlier in chapter 4. The need for this study was premised on enriching the literature on hydrates sloughing/shedding and pipewall shedding by hydrates. Previous research confused hydrates shedding with pipewall shedding by hydrates, hence shedding was seen as hydrates “falling off” the pipewall under the influence of a viscous force.

The geometry of hydrate deposits (Di Lorenzo et al. 2018) and the plot of the thickness of hydrates deposits along the pipeline (Liu et al. 2019), indicates that a three phase gas, water and dispersed hydrates multiphase flow upstream of the hydrates sloughing point exists. Hence, there it is important to emphasize the effect of a dispersed hydrates phase on the pipewall. The shear stress profile along the pipeline provide insight on the effect of pipewall shedding by hydrates on pipewall erosion.

The CFD simulation adopted in this study mimicked hydrates deposition by applying a subcooling temperature to the pipe wall at hydrates formation condition to increase the density of the gas at the wall and enhance the viscous interaction of the gas with the water at the annular water layer at the wall. The simulated temperature contour profile captured the expected cooling effect on the gas phase similar to the hydrates deposit geometry in the literature (Di Lorenzo et al. 2018). The plots of molecular viscosity of the multiphase mixture and strain rate of the secondary phase indicated a dip which agrees with the relative location of sloughing events in the literature from the inlet of the pipeline (Liu et al. 2019). This study proposes that:

- a) Hydrates sloughing is predominant at lower gas velocities, happening over a longer distance along the hydrates forming section until the pipeline is plugged.
- b) Whereas a higher reduction in hydraulic diameter is earlier at a lower velocity, the plugging of the horizontal section of the pipeline is earlier at higher velocities if the riser base or the location of change in pipeline geometry is near the equilibrium point of hydrates formation.

- c) The profile of the deposited hydrates is steeper at higher velocities than at lower velocities as indicated by the sloughing angle, which is a new term developed in this study. The lower the sloughing angle the longer the sloughing event along the pipeline and can lead to a gentle profiling of hydrates layer over a longer section of the pipeline. Thus, hydrates plugs are longer at lower velocities than at higher velocities. Implying a higher plugging risk at lower velocities.
- d) At lower gas velocities pipewall shedding leads to higher shear stress values when compared with the shear stress at the sloughing location. This observation occurred at velocities of 2.0 m/s and 4.0 m/s.
- e) Pipewall shedding and sloughing occurs simultaneously at higher gas flow velocities. This was observed at velocities of 6.0 m/s and 8.0 m/s.
- f) The fluctuating plots of shear stress suggests that hydrates sloughing events and pipewall shedding by hydrates occurs intermittently and can lead to flow induced vibration along the pipeline. This proposition is also corroborated in a previous study (Jujuly et al. 2017).
- g) The location of hydrate sloughing is nearer the inlet of the pipeline in all flow scenario simulated, which also agrees with the indication in the literature (Liu et al. 2019).
- h) The shear stress profile along a hydrate forming gas pipeline can enhance the determination of locations prone to higher corrosion rates.
- i) Hydrates sloughing and pipewall shedding are driven by inertia force, instead of pressure force.

CHAPTER 6: MULTIPLE REGRESSION MODELLING OF HYDRATES DEPOSITION RATE IN SUBSEA GAS PIPELINE IN OPERATING AND SHUTDOWN SCENARIOS³

6.0 Introduction

This chapter developed a multiple regression model to predict the deposition rates of hydrates in subsea gas pipelines. Whereas there are regression models for estimating the pressure and temperature conditions for hydrates formation, these models do not consider the impact of flow velocities on the formation of hydrates in gas pipelines. Also, there is no regression model that considers the deposition of hydrates on the wall of the pipeline, especially during shut down periods. The data used for this study originated from 81 simulations performed in a validated computational fluid dynamics (CFD) model we earlier developed for this purpose. The data set were used to train 4 linear regression models in MATLAB regression learner app.

The model predictions were cross validated using experimental data, and based on the criteria set for model selection in the literature, the standard linear regression model was the most suitable for this study. The parametric studies conducted fulfilled the theoretical positions on the conditions for hydrates deposition in gas pipelines. With all predictions within 10% uncertainty bound, this study has provided a regression model for predicting the deposition rate of hydrates where gas flow velocity, water volume fraction, subcooling temperature and pipeline diameter plays significant roles in determining hydrates plugging risk in subsea gas pipelines.

The formation of hydrates in subsea gas-dominant pipelines continue to obstruct the safe flow of gas to processing plants. Hydrates deposition occurs very fast within the first hour of hydrates formation, and can plug the pipeline more quickly when large mass of hydrates are detached from the wall by

³ The results in this chapter are published in the Journal of Sustainability (Switzerland): Umuteme, O. M., Islam, S.Z., Hossain, M. and Karnik, A., 2023. Modelling Hydrate Deposition in Gas-Dominant Subsea Pipelines in Operating and Shutdown Scenarios. *Sustainability (Switzerland)*. Doi: 10.3390/su151813824.

sloughing events (Marques et al. 2022). Therefore, estimating the deposition rate of hydrates allow for the estimation of the volume of hydrates deposited and the severity of hydrates plugging events within a given period of pipeline operation. The emphasis on predicting hydrates deposition rates have been studied using experiments (Di Lorenzo et al. 2014a, 2014b; Aman et al. 2016) and analytical models (Wang et al. 2017; Di Lorenzo et al. 2018).

These experiments have provided the basis for understanding the flow parameters influencing the deposition rates of hydrates in gas pipelines through parametric analysis, including subcooling temperature, water volume fraction, gas velocity and pipeline diameter. Therefore, it is possible to formulate a multiple linear regression model where hydrates deposition rate is the dependent variable. Previous studies adopted machine learning regression modelling of hydrate formation equilibrium temperature and pressure (Baghban et al. 2016; Ibrahim et al. 2016; Mesbah, Soroush and Rezakazemi 2017; Aboali and Khomehchi 2019; Landgrebe and Nkazi 2019; Cao et al. 2020).

The multiple regression approaches implemented in the cited literature include the use of support vector machine (SVM), least square support vector machine (LSSVM), and genetic algorithm (GA). Recently, hydrate volume fraction was predicted using regression modelling (Qin et al. 2019). Again, Yu and Tian (2022) adopted Random Forest, Naive Bayes, and Support Vector Regression to determine hydrates formation condition for pure and mixed hydrates forming gases. However, no regression modelling approach has been adopted to specifically predict the deposition rate of hydrates in gas pipeline.

Regression modelling is implemented when the data to be observed are not easily accessible and measured from the field, and this is applicable to measuring the deposition rate of hydrates in industry scale gas pipeline. This study proposes a regression model with subcooling temperature (ΔT), pipeline diameter (D), water volume fraction (α_w) and gas velocity (V) as predictors, while the deposition rates of hydrates (\dot{Q}_{hd}) is the dependent variable. This is to further ensure that the prediction of hydrates deposition rate is handy in the field, so that the model can be used as a quick predictor

of the risk of pipeline plugging by hydrates. The predictions of hydrates deposition rates by the CFD model was more representative of experimental predictions than existing analytical model at lower velocity of 4.7 m/s. Hence, the data used in developing the multiple regression model have been simulated from the validated CFD model for predicting the deposition rates of hydrates developed in chapter 4.

Another driver for this study is the need to estimate the deposition rates of hydrates when the pipeline is shut down without depressurisation. The deposition of hydrates have been reported in gas pipelines shut down due to unforeseen operational problems without the need to depressurise the line ((Jamaluddin, Kalogerakis and Bishnoi 1991; Bai and Bai 2005; Ballard, Shoup and Sloan 2011). However, it is not possible to simulate this condition using CFD by making the gas flow velocity "zero." Hence, with a multivariate regression model, the deposition rate can still be predicted by zeroing the velocity term.

Usually, cooldown time are up to 24 hours (Bai and Bai 2005) or 48 hours (Jamaluddin, Kalogerakis and Bishnoi 1991), and it is important to estimate the amount of hydrates deposited within this shutdown period (Umuteme et al. 2023c). Multiple regression modelling is implemented to identify the best combination of the predicting variables (Mertler and Reinhart 2016), when the independent variables are more than one (Montgomery and Runger 2014). In this study, the combination of the predictor variables has been selected based on the parametric sensitivity simulations conducted in chapter 4.

6.1 Result, Validation and Model Selection

6.1.1 Results

The data retrieved from the CFD simulation was trained in the regression learner application in MATLAB version R2020a and the coefficient for each predictor variable was recorded as presented in **Table 6.1**, for each investigated regression model. The p-value for each coefficient is also indicated as defined below (**Table 6.1**).

Table 6.1: Coefficients of predictor variables for each regression model

Parameter Estimates	Standard Linear Regression	Robust Linear Regression	Stepwise Linear Regression	Interaction Linear Regression
β_0	-0.0845*	-0.0615	-0.4770***	-0.0129
β_V	0.0163***	0.0131***	0.0156***	-0.0105
$\beta_{\Delta T}$	0.0252***	0.0240***	0.0531***	-0.0268
β_{α_w}	-3.4127***	-3.3872***	2.5804	2.2833
β_D	7.3412***	7.5444***	12.3156***	7.0976***
$\beta_{\Delta T}.\beta_{\alpha_w}$	-	-	-0.4020*	-0.0372
$\beta_{\alpha_w}.\beta_D$	-	-	-77.0638***	-80.6991***
$\beta_V.\beta_{\Delta T}$	-	-	-	0.0049
$\beta_V.\beta_{\alpha_w}$	-	-	-	-0.2666
$\beta_V.\beta_D$	-	-	-	0.2793
$\beta_{\Delta T}.\beta_D$	-	-	-	0.5397*

* $p < 0.1$; ** $p < 0.05$; *** $p < 0.01$

At alpha (α) level of 0.05, all the predictor variables have coefficients with high level of significance for both the standard linear and robust linear regression models. For the stepwise linear regression model, the coefficient for the water volume fraction was not statistically significant. For the interaction Linear regression model, only the coefficients for pipeline diameter and the interaction between water volume fraction and pipeline diameter were statistically significant. The corresponding regression equations based on the coefficients in **Table 6.1** are of the forms stated in equations 6.1, 6.2, and 6.3, below. All coefficients are standardised.

Standard and Robust Linear Regression

$$\dot{Q}_{hd} = \beta_0 + \beta_V V + \beta_{\Delta T} \Delta T + \beta_D D + \beta_{\alpha_w} \alpha_w \quad (6.1)$$

Stepwise Linear Regression

$$\dot{Q}_{hd} = \beta_0 + \beta_V V + \beta_{\Delta T} \Delta T + \beta_D D + \beta_{\alpha_w} \alpha_w + \beta_{\Delta T} \beta_{\alpha_w} \Delta T \alpha_w + \beta_{\alpha_w} \beta_D D \alpha_w \quad (6.2)$$

Interaction Linear Regression

$$\begin{aligned} \dot{Q}_{hd} = \beta_0 + \beta_V V + \beta_{\Delta T} \Delta T + \beta_D D + \beta_{\alpha_w} \alpha_w + \beta_{\Delta T} \beta_{\alpha_w} \Delta T \alpha_w + \beta_{\alpha_w} \beta_D D \alpha_w \\ + \beta_V \beta_{\Delta T} VT + \beta_V \beta_{\alpha_w} V \alpha_w + \beta_V \beta_D VD + \beta_{\Delta T} \beta_D TD \end{aligned} \quad (6.3)$$

where, β_0 is the intercept of the model and β_v , $\beta_{\Delta T}$, β_D and β_{α_w} are the partial regression coefficients of the respective regressor variables – gas velocity ($V, m/s$), subcooling temperature ($\Delta T, K$), pipe diameter (D, m) and water volume fraction (α_w , dimensionless), as defined earlier. The regression graphs in **Figure 6.1** are the outcome of each model predictions compared with the original CFD hydrates deposition rates. As seen from the regression graphs, the R-squared values for interaction linear regression model and the stepwise linear regression model could be error of overfitting because of the increase in predictor variables.

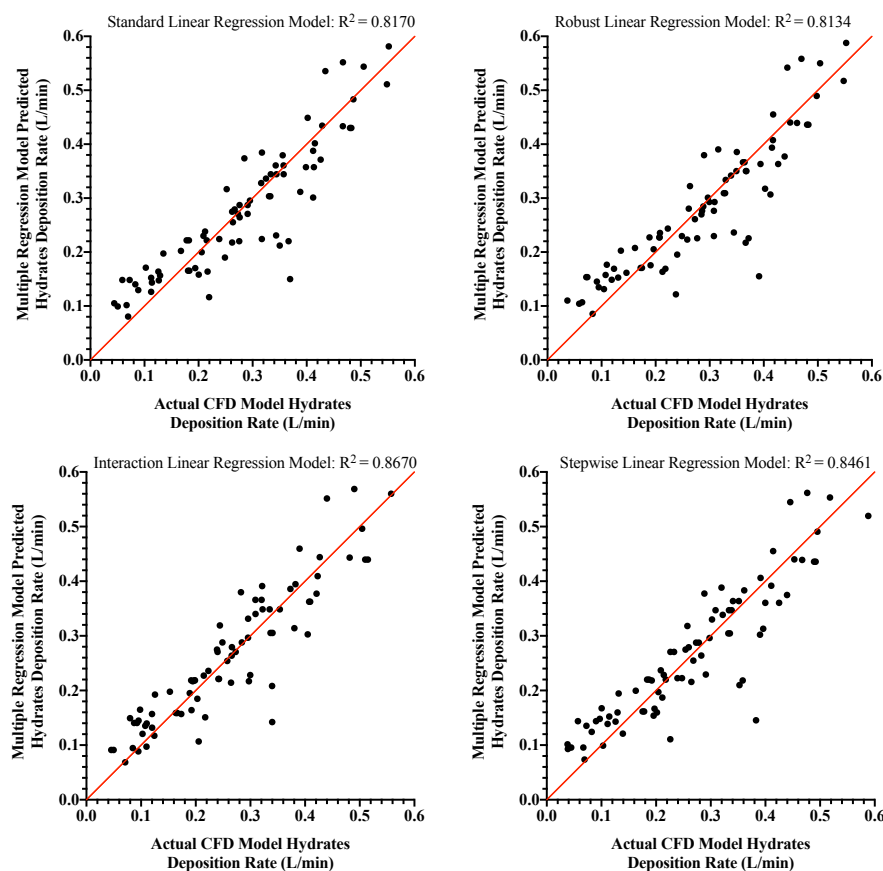


Figure 6.1: Comparing plots for each regression modelling approach

The absence of outliers is confirmed from the standard and robust regression models as the calculated R-squared have approximately similar values of 0.8170 and 0.8134 respectively. In **Figure 6.2**, the residual plots indicate that the residuals reduced as the hydrates deposition rate increased for both the standard linear and robust linear regression models.

The residuals for the interaction linear and stepwise linear regression models are spread across the deposition rates compared to the standard linear and robust linear regression models. The reduction in prediction error as the deposition rate increases for both standard linear and the robust models suggests that the predictor coefficients can account for a higher variance in the deposition rate when the pipeline is most vulnerable. Implying that both models are highly suitable in capturing higher risks of hydrates plugging events from deposited hydrates.

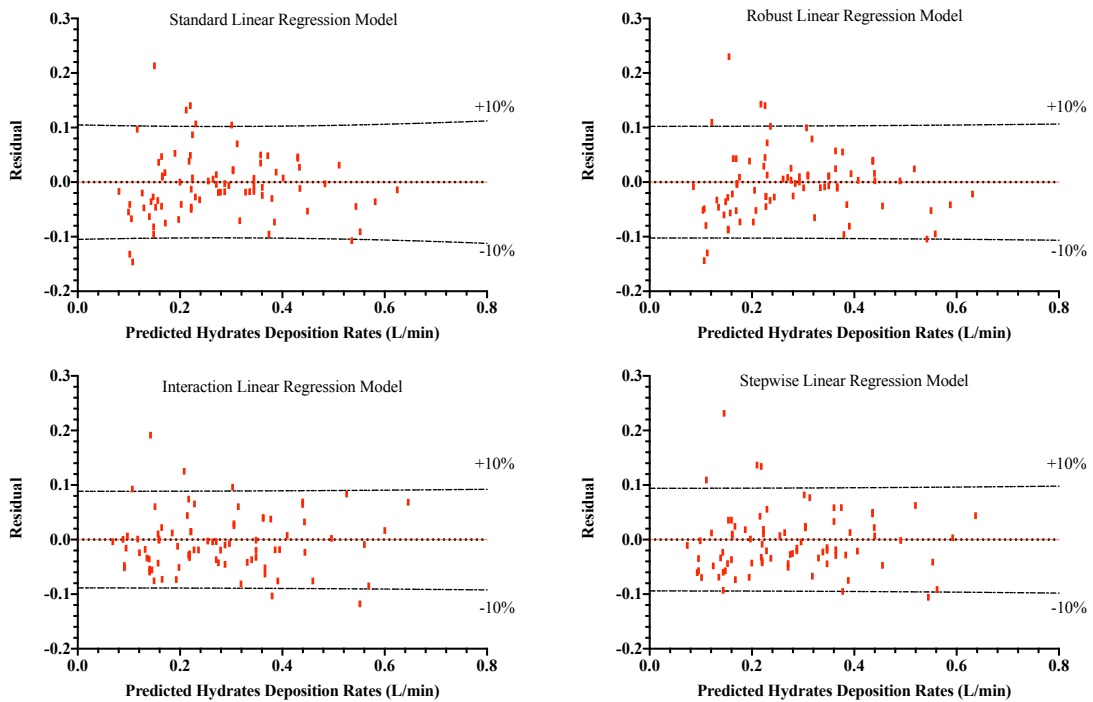


Figure 6.2: Residuals plots for each regression modelling approach

The most suitable model will be selected after validation with experimental results

6.1.2 Validation with Experimental Data

In **Table 6.2**, the predictive power of each model was validated with experimental data at low and higher gas velocities. Most importantly, the sensitivity of the regression models to changes in subcooling temperature at a lower velocity of 4.6 m/s compared more favourably with experimental outcomes than the analytical model of (Di Lorenzo et al. 2018).

Table 6.2: Validation of regression models with experimental data

Input Data				Experimental Hydrates Deposition Rates (L/min)	CFD Model Hydrates Deposition Rates (L/min) Umute et al., (2022)	Predicted Hydrates Deposition Rate (L/min) by Regression Models				Experiment References
Gas Velocity - V(m/s)	Subcooling Temperature - $\Delta T(K)$	Water Volume Fraction - $\alpha_w (-)$	Pipe Diameter - D(m)			Standard Linear Model	Robust Linear Model	Interaction Linear Model	Stepwise Linear Model	
4.6	4.5	0.06	0.0204	0.06	0.06	0.05	0.06	0.09	0.04	Aman et al. (2016)
4.6	6.0	0.06	0.0204	0.08	0.10	0.09	0.09	0.10	0.08	
4.6	7.5	0.06	0.0204	0.11	0.13	0.12	0.13	0.11	0.12	
8.8	2.5	0.06	0.0204	0.07	0.06	0.07	0.06	0.05	0.04	Di Lorenzo et al. (2014b)
8.8	4.3	0.06	0.0204	0.13	0.13	0.11	0.11	0.10	0.10	
8.8	7.1	0.06	0.0204	0.15	0.14	0.18	0.17	0.17	0.18	
8.8	8.0	0.06	0.0204	0.19	0.18	0.21	0.20	0.19	0.20	

In **Figure 6.3**, the outcome of the predictive regression models was compared and the R^2 value of the standard linear model was the highest. However, the closeness of the R^2 value for the standard linear model to the R^2 values for the other regression models suggests that the R^2 is not independently suitable to defend the choice of the final selected model, as the predictor variables in all the models were able to account for more than 80% variance in the deposition rates of hydrates.

The predictions goodness of fit is in the following ascending order: interaction linear regression (0.01349)>standard linear regression (0.01336)>stepwise regression (0.01078)>robust linear regression (0.006881). However, only two coefficients of the equation for the interaction linear model were significant at $p < 0.05$. Hence, the most appropriate model is the standard linear regression model with the highest goodness of fit value of 0.01336.

A further investigation of the predictive power of the regression models along the experimental data sets suggest close predictions by all models at lower and higher deposition rates of hydrates (**Figure 6.4**). The final model will be selected after considering other criteria discussed in **Table 3.6**. However, as the experimental deposition rate increased to 0.24 L/min, only the standard linear model was able to indicate the capability of higher out-of-data predictive power. The assumption of homoscedasticity and normality must be fulfilled in linear regression modelling, else a non-linear approach is adopted (Cohen et al. 2003). The test for normality and the consistency of the prediction of the models by fulfilling homoscedasticity was investigated using the normal probability plot (Q-Q plot) in **Figure 6.5**.

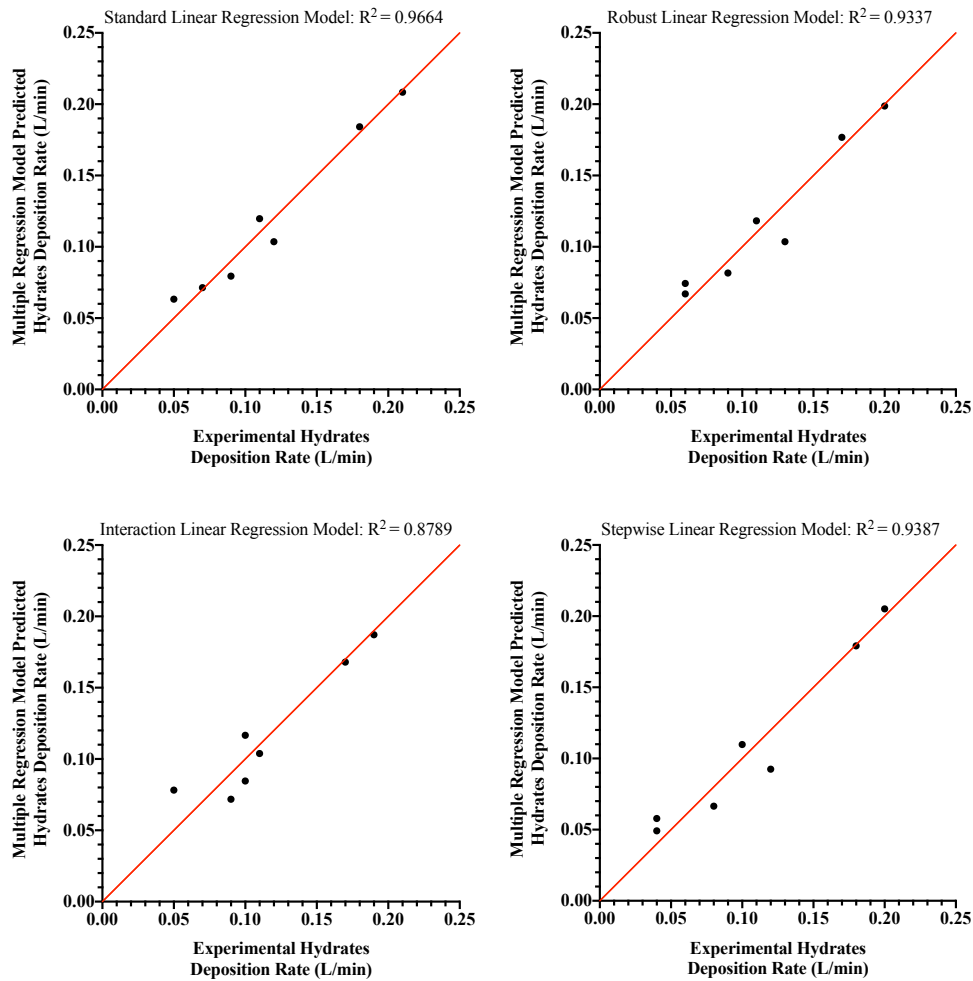


Figure 6.3: Prediction of experimental results by each regression modelling approach

The Q-Q plot normality test suggest that the predicted results are from the same population if the plot resembles a straight line (Mertler and Reinhart 2016), The linear nature of all the predicted results also aligned with experimental outcome, indicating the ability of the models to predict hydrates deposition rates beyond the training data from the CFD model. The certainty of accurate predictions was observed at 90% confidence interval on the Q-Q plot in **Figure 6.5a**, and indicate higher predictive power at higher deposition rates above 0.15 L/min. All the predictions are within 10% prediction band of the normal probability plot as indicated in **Figure 6.5b**.

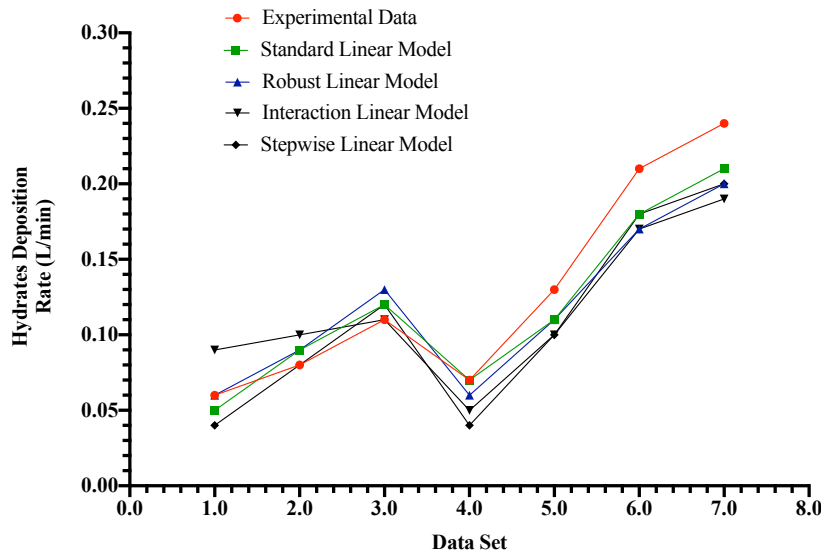


Figure 6.4: Comparing predictions by each regression modelling approach with experimental results

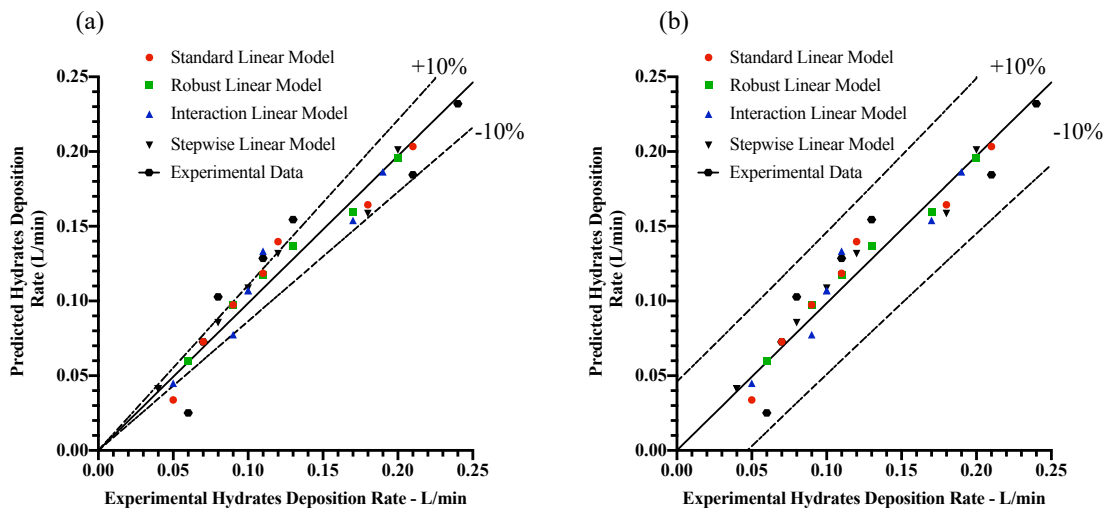


Figure 6.5: Normal probability plots (Q-Q plots). (a) with 90% certainty band. (b) with 10% prediction band

6.1.3 Model Selection

The close competition among the model predictions as discussed in section 6.1.2 above, show that the data generated using the CFD model are of experimental quality. In this section, the preferred regression model was selected using the criteria discussed in section 3.2.3. In **Table 6.3**, a comparison of the values for each model fit selection criteria are presented. The model selection criteria are based on a combination of adjusted R-

squared, error sum of squares, RMSE, AICc criteria and F-Test, as defined in **Table 3.6**.

Table 6.3: Comparing values of each model selection criteria for all regression models

Parameter	Standard Linear Regression	Robust Linear Regression	Stepwise Linear Regression	Interaction Linear Regression
R ² adj.	0.9597	0.9204	0.9264	0.8547
SSE	0.0007	0.0011	0.0015	0.0017
RMSE	0.0106	0.0138	0.0156	0.0168
AICc	-50.730	-47.080	-45.300	-44.300
F-Test	5.752	2.817	3.063	1.452

In **Table 6.4**, the model selection parameters have been ranked in the order that aligns with the criteria for model selection (**Table 3.6**), where 4 is given to the regression model that is most representative of the set criteria and 1 for the least representative regression model for each model fitness selection criteria.

Table 6.4: Parameter ranking based on fitness of each regression model to experimental results

Parameter	Standard Linear Regression	Robust Linear Regression	Stepwise Linear Regression	Interaction Linear Regression
R ² adj.	4	2	3	1
SS _E	4	3	2	1
RMSE	4	3	2	1
AICc	4	3	2	1
F-Test	4	2	3	1
Total Score	20	13	12	5

The standard linear model with the highest sum of model fit score in **Table 6.4** is selected. Again, a comparison of the normalized violin plots indicates that the shape of the standard linear model is a close match to the experimental data.

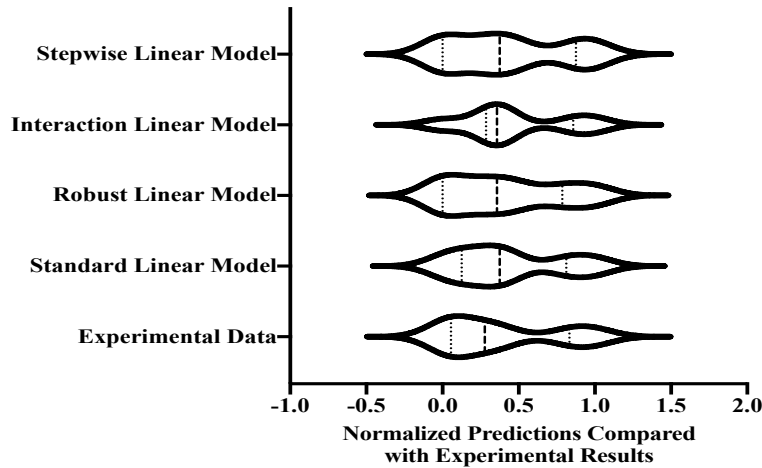


Figure 6.6: Normalized violin plots

Therefore, the representative equation for the standard linear model based on the coefficients in **Table 6.1** are presented below.

$$\dot{Q}_{hd} = 0.0163V + 0.0252\Delta T - 3.4127\alpha_w + 7.3412D - 0.0845 \quad (6.4)$$

The relative impact of each predictor variable on the hydrates deposition rate can be inferred from equation 6.4 as presented in **Table 6.5**.

Table 6.5: Relative impact of each predictor variable on hydrates deposition rate

Predictor Variable	Sensitivity (other variables held constant)	Impact on Hydrates Deposition Rate
Gas Velocity	Increase	Increase
	Decrease	Decrease
Subcooling Temperature	Increase	Increase
	Decrease	Decrease
Pipeline Diameter	Increase	Increase
	Decrease	Decrease
Water Volume Fraction	Increase	Decrease
	Decrease	Increase

As suggested in **Table 6.5**, velocity, subcooling temperature and diameter have increasing effect, while water volume fraction has a reducing effect on the deposition rate of hydrates. Hence, increasing the velocity while keeping

other variables constant will increase the deposition rate of hydrates. Again, at constant velocity, increasing the subcooling temperature increases the deposition rate of hydrates. Similarly, keeping other variables constant, increasing the pipeline diameter increases the deposition rates of hydrates, because of increasing gas volume.

Finally, as other variables are constant, increasing the water volume fraction enhances transportability while reducing deposition. Again, as hydrates deposition rate increases, the gas velocity, water volume fraction and pipe annulus approach zero and the stability of hydrates in the pipe becomes solely dependent on the subcooling temperature. Implying that increasing the temperature of the pipeline can reduce the mass of deposited hydrates. Another important feature of this model is the ability to predict hydrates deposition when the velocity is set to "0," as applicable during pipeline shutdown scenario. Thus, this regression model satisfies the theoretical position on hydrates deposition and transportability in subsea gas pipelines (e.g., Aman et al., 2016; Berrouk et al., 2020; Sule et al., 2015).

As indicated earlier, the use of the regression model is based on the gas temperature below the hydrate equilibrium temperature of 292K for natural gas with predominant methane compositional value above 80%. The operating pressure for the CFD model was set at 8.8 MPa for all simulations. Lower pressures predicts lower deposition rates (Jamaluddin, Kalogerakis and Bishnoi 1991). Hence, the prediction of this model is proactive and represents the worst-case scenario at the model operating pressure.

6.2 Dimensionally Homogenous Deposition Rate Model

Based on the difficulty in providing a dimensionally homogenous regression equation for equations 6.1-6.4, a mathematical relationship has been developed from the adopted regression equation (Equation 6.4), because it most accurately predicted experimental outcomes when compared with Equations 6.2-6.4. The dimensionally homogenous equation is now provided as follows. Based on the relationship in **Table 6.5**, the Q (m³/s) is provided as follows:

$$\dot{Q}_{hd} = C \frac{vD\Delta T}{\alpha_w} \quad (6.5)$$

where C is an experimental tuning parameter which is related to the pipe wall temperature (T_w), creating the temperature gradient. Increasing the pipewall temperature reduces the deposition rate, and a decrease in the pipewall temperature increases the hydrates deposition rate. The initial gas temperature is 292K, which is the onset of hydrates formation for methane hydrates which is the predominant constitute of natural gas at greater than 80% in the gas composition. To achieve dimensional homogeneity, D has been modified with the surface area of the pipewall (A). Using experimental data, C was calculated as $0.000014/T_w$. The final dimensionally homogenous equation is:

$$\dot{Q}_{hd} = \frac{0.000014vA\Delta T}{\alpha_w T_w} \text{ (m}^3\text{/s)} \quad (6.6)$$

In litres per minutes (L/min), which is the unit used in the experimental quantification of hydrates deposition rates, the equation becomes:

$$\dot{Q}_{hd} = \frac{0.82vA\Delta T}{\alpha_w T_w} \text{ (L/min)} \quad (6.7)$$

where T_w is the pipeline wall temperature in Kelvin and $A = \pi D$ (m^2). Thus, the this new model incorporates the pipe wall temperature, with a higher temperature leading to a slower deposition rate. The model also considers the internal cross-sectional pipe surface area. The final equation 6.6 and 6.7 is provided in both meters cubed per second ($\text{m}^3\text{/s}$) and liters per minute (L/min) for easy comparison with experimental data.

A comparison of the estimated hydrate deposition rate with both regression and the dimensionally homogenous analytical model is provided in **Table 6.6**. This model is applicable for natural gas hydrates with methane $\geq 80\%$ in composition, pressure within stable hydrate loci for methane, and temperatures lower than 292K.

Table 6.6: Comparing the predicted hydrates deposition rate by the dimensionally homogenous model with experiential and CFD results

Input Data				Experimental Hydrates Deposition Rates (L/min)	CFD Model Hydrates Deposition Rates (L/min) - Umuteme et al., (2022)	Predicted Hydrates Deposition Rate (L/min)		Experiment References
Gas Velocity - V(m/s)	Subcooling Temperature - $\Delta T(K)$	Water Volume Fraction - $\alpha_w (-)$	Pipe Diameter - D(m)			Standard Linear Regression Model	Dimensionally Homogenous Model	
4.6	4.5	0.06	0.0204	0.06	0.06	0.05	0.06	Aman et al. (2016)
4.6	6.0	0.06	0.0204	0.08	0.10	0.09	0.08	
4.6	7.5	0.06	0.0204	0.11	0.13	0.12	0.11	
8.8	2.5	0.06	0.0204	0.07	0.06	0.07	0.07	Di Lorenzo et al. (2014b)
8.8	4.3	0.06	0.0204	0.13	0.13	0.11	0.12	
8.8	7.1	0.06	0.0204	0.15	0.14	0.18	0.19	
8.8	8.0	0.06	0.0204	0.19	0.18	0.21	0.22	

As stated earlier, the advantage of a dimensionally homogenous mathematical equation for predicting the deposition rate of hydrates compared to a similar regression equation lies in its focus on physical relationships and broader applicability.

6.3 Practical Application of Regression Model

The parametric analysis in this section were done to investigate the practical application of the selected regression model. The analysis include: (i) the prediction of the deposition rates of hydrates in pipeline shutdown scenario, (ii) predicting the influence of change in environmental temperature on the deposition of hydrates, when the integrity of the pipeline coating and heating system is questionable, (iii) predicting the effect of change in gas velocity based on change in actual gas production especially at low flow velocity and constant subcooling temperatures, (iv) the influence of pipeline size on hydrates deposition rate during pipeline sizing in design phase, and (v) the influence of water volume fraction on the deposition rate of hydrates.

6.3.1 Pipeline Shutdown Planning

Estimating the deposition rate of hydrates at zero gas velocity can assist in determining how long a gas pipeline experiencing hydrates formation should be shut down during the maintenance of surface processing facilities. The change on the deposition rate of hydrates was predicted by the model in **Figure 6.7** at the subcooling temperature of 7.0K, water volume fraction of 0.06 and pipeline diameter of 8 inches (0.204m).

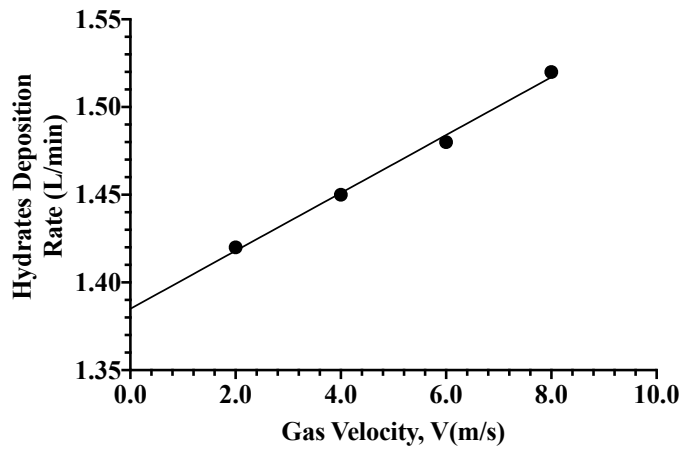


Figure 6.7: Change in the deposition rate of hydrates as the gas velocity increases at constant subcooling temperature of 7.0K, water volume fraction of 0.06 and pipeline size of 8inches (0.204m)

Increase in velocity at the same subcooling temperature increases hydrates deposition rate. From **Figure 6.7**, at the subcooling temperature of 7.0K and “zero” gas flow velocity which is the scenario when the line is shut down, the gas pipeline will still experience hydrates formation and deposition at the rate of 1.385L/min. Hence, the deposition of hydrates is expected if the line is shut down at the pressure and temperature condition that encourages hydrates formation. This model provides a means to study hydrates deposition when the pipeline is shut-down due to process failure or for other maintenance within the gas plant or subsea production facilities.

Depressurising the pipeline outside the hydrate formation temperature and pressure zone is advised in this instance. However, if it is impossible to keep hydrates out of the line, the total deposition can be estimated by multiplying the deposition rate with the duration that the line was shut down to estimate the expected hydrate deposits in the line. The total expected volume of hydrates is the sum of the deposited and dispersed hydrates. From the indication in the literature (Di Lorenzo et al. 2014b; Wang et al. 2017), about 33.3% of hydrates formed are deposited in the wall. Hence, an approximate total expected hydrate in the pipeline can be obtained by multiplying the deposition rate estimated by this model under shutdown scenario by a factor

of 3. Thus, the predicted deposition rate of hydrates by the model can be a guide for pigging or chemical injection. Hydrates growth during shut down is relatively slow (Jamaluddin, Kalogerakis and Bishnoi 1991; Bai and Bai 2005), leading to lower deposition rates as observed in the model predictions in **Figure 6.7**.

6.3.2 Effect of change in Subcooling temperature on Hydrates Deposition

This sensitivity is important in determining the cool-down temperature during shutdown scenario to prevent hydrates formation and deposition. Also, during change in the surrounding subsea temperature, the effect on the deposition of hydrates can be estimated from the model. The velocity was set to 4 m/s, 0.06 water, diameter of 0.204 m and the subcooling temperature was varied from 3K to 9K. From **Figure 6.8**, the deposition rate of hydrates increases as the subcooling temperature increases and vice versa, in agreement with experimental results.

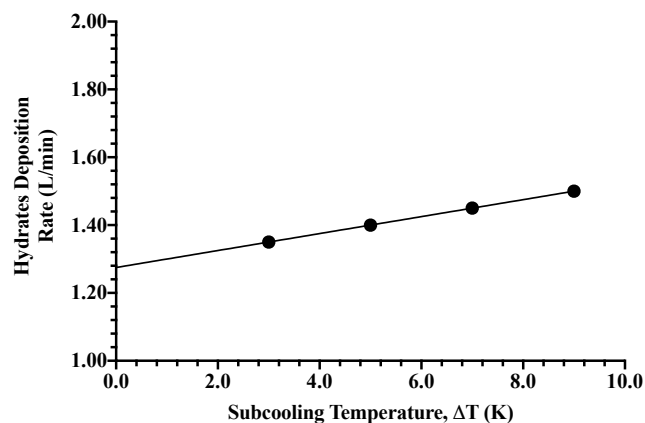


Figure 6.8: Change in the deposition rate of hydrates as the subcooling temperature increases at constant gas velocity of 4m/s, water volume fraction of 0.06 and pipeline size of 8 inches (0.204m)

6.3.3 Effect of Change in Water Volume Fraction on Hydrates Deposition

In this sensitivity analysis, the water volume fraction of the gas stream in the pipeline was varied to study the effect of increasing water volume fraction on the deposition rate of hydrates on the pipe wall. In theory, deposition rate

of hydrates reduces but form hydrates slurry instead, which can enhance transportability. At a constant velocity of 4 m/s, subcooling temperature of 7.0K and pipeline diameter of 0.204 m, the water volume fraction was varied from 0.06 to 0.12 to obtain the regression plot in **Figure 6.9**.

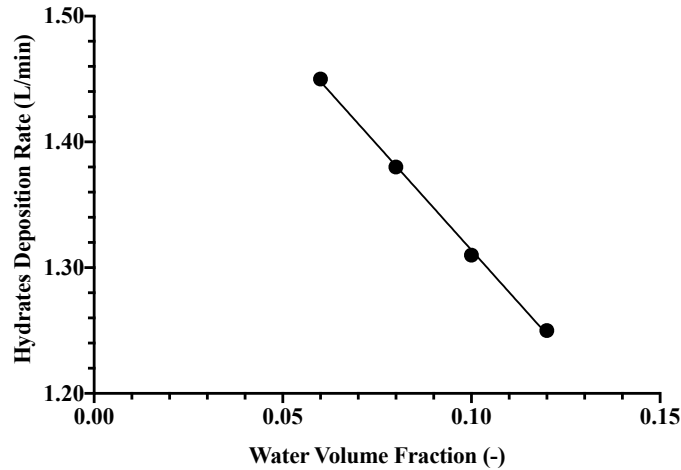


Figure 6.9: Change in the deposition rate of hydrates as the water volume fraction increases at constant gas velocity of 4 m/s, subcooling temperature and pipeline size of 8 inches (0.204m)

As expected from theory, increasing the water volume fraction in **Figure 6.9**, decreases the deposition rate of hydrates. Implying that in gas lines with high water volume fraction, the probability of hydrates depositing on the wall of the pipeline is minimal. This effect was studied in Berrouk et al. (2020), where the flow of hydrate slurry was enhanced by increasing the water volume fraction. Most importantly, the model developed in this study can provide insight into the maximum water volume fraction to prevent the deposition of hydrates, which would have required much computer simulation effort to estimate using CFD models.

6.3.4 Effect of Change in Pipeline Size on Hydrates Deposition in Design Phase

This effect was predicted by keeping the gas velocity at 4 m/s, subcooling of 7.0K and water volume fraction of 0.06 while changing the pipeline diameter from 4 inches (0.102m) to 16 inches (0.408m). The change in pipeline diameter increases the deposition rate of hydrates because of the availability of more gas in the pipeline. Implying also that if the flowrate was kept

constant and the pipe diameter increased, there will be a reduction in flowing pressure leading to early plugging of the line.

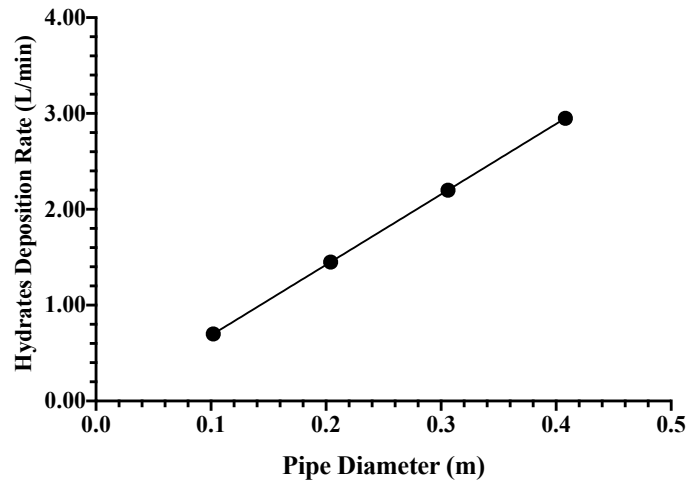


Figure 6.10: Change in the deposition rate of hydrates as the pipe diameter increases at constant gas velocity of 4 m/s, subcooling temperature and water volume fraction.

6.4 Chapter Summary

The need for applying regression modelling in predicting the formation and plugging risk of hydrates in gas pipelines is event from the lack of one in the extant literature on this subject. Aside the experimental, analytical and CFD approaches, previous studies have adopted machine learning regression modelling of hydrate formation equilibrium temperature and pressure. However, there has been no regression model that can predict the deposition rate of hydrates in gas pipelines, especially to predict hydrates deposition during gas pipeline shut down scenario.

This study closed this gap by adopting a multiple linear regression modelling approach using MATLAB regression learner app to train 81 data sets generated by CFD simulation. Four different regression models were developed and the outcome of the cross-validation using experimental data led to the choice of the standard linear regression model, with predictions that compared more favourably with the experimental validation data. The focus of this model prediction was to a maximum pressure of 8.8 MPa, which is within the maximum operating envelop of most gas pipelines.

Since lower operating pressures leads to lower formation rates (Jamaluddin, Kalogerakis and Bishnoi 1991), the deposition rates predicted by this model is proactive and represents the worst-case scenario at the model operating pressure of 8.8 MPa. The specific contributions of this study to knowledge are as follows:

- a. The possibility of quantifying and estimating the risk of hydrates in a gas pipeline during shut down period.
- b. The regression model reduces the rigour of computer CFD and analytical simulations to predict hydrate deposition rates in field situation where a quick approximation of hydrates plugging risk is required for early intervention.
- c. The predicted results by this model can serve as advisory input during pipeline sizing in design phase by considering the implication of the selected pipeline diameter on hydrates formation and deposition.
- d. As a handy tool, the model serves the purpose of determining the level of water volume fraction that can enhance the transportability of hydrates.
- e. Finally, the model can be used to easily estimate the expected volume of hydrates after a long period of operation, when the deposition rate is multiplied with the operating timeline of the pipeline since start-up.

CHAPTER 7: ANALYTICAL MODELLING OF HYDRATE-INDUCED PRESSURE DROP AND LOCATION OF HYDRATE PLUGGING EVENT IN SUBSEA GAS PIPELINE⁴

7.0 Introduction

Accurate prediction of the hydraulic effect of hydrate deposition and plug location is critical to the safety and operability of natural gas transport pipelines, especially for gas-dominant subsea pipelines where maintenance and intervention activities are more difficult. To achieve this, the present work improved an existing 2-phase pressure drop relation due to friction, by incorporating the hydrates deposition rate into the equation. In addition, a model has been developed to predict the pipeline plugging time. The transient pressure drop predictions in the present study for all six cases at high and low velocities are within 4% mean relative error.

Similar predictions by Di Lorenzo et al. (Di Lorenzo et al. 2018) are within 40% maximum relative error, while the mean relative error of the transient pressure drop predictions by Zhang et al. (Zhang et al. 2019) was 7.43%. In addition, the plugging flowtime model underpredicts the plugging time by a mean relative error of 9%. To enhance pipeline design for effective operability and prevent excessive transient pressure-drop that can lead to pipeline failure, it is important to identify possible sources of time-varying disturbances along the pipeline. Restriction to flow due to blockages in gas pipelines are responsible for time-varying pressure fluctuations during operation (Carroll 2014). As a result, accurate prediction of the pressure drop along the pipeline is an important aspect of design and operation in gas pipelines flow assurance.

The main source of blockage in gas pipelines is the formation of hydrate beddings and plugs (McMullen 2011; Carroll 2014). Removing hydrate plugs

⁴ The results in this chapter are published in Proc IMechE Part C: J Mechanical Engineering Science: Umuteme, O. M., Islam, S.Z., Hossain, M. and Karnik, A., 2023. Analytical modelling of the hydraulic effect of hydrate deposition on transportability and plugging location in subsea gas pipelines. *Proc IMechE Part C: J Mechanical Engineering Science*. Doi: 10.1177/09544062231196986.

in a pipeline can lead to accidents where the plugs behave like projectiles at high speed due to the higher pressure upstream of the plugs.

For aging gas pipelines, pipe burst from overpressurisation due to blockages are possible because of the reduction in pipe wall thickness from internal corrosion (Obanijesu et al. 2011). For surface pipelines, infrared temperature gun is used to identify cold section(s) where hydrates plugs are located, but for buried and offshore pipelines this approach is not feasible (Carroll 2014). Flow modelling, where the operating temperature crosses the hydrates curve have been applied in locating the section(s) where hydrates are formed in buried or subsea pipelines, although this approach cannot locate plugging sections because hydrates are formed and moved downstream to form beds and plugs (Carroll 2014).

Suspected hydrate plug locations are valves, low points along the pipeline/dents, or riser base. However, at low flow scenario hydrate plugs can form along the horizontal section of the pipe (Aman et al. 2016). Although it is impossible to locate the precise position of hydrate plugs along the horizontal section of the pipeline, other approaches that have been applied in locating hydrates plugs are reported in the literature (McMullen 2011).

These include the use of mechanical device such as coil tubing for wells, injection of thermodynamic inhibitor into gas pipelines to observe the pressure response, gamma ray densimeter provided the plug location can be accessed, hoop strain gage installed around the pipe by a remotely operated vehicle (ROV) to report change in hoop dimension, and the simulation of temperature, pressure, and other process data. Simulation approach is cost effective and can predict accurate hydrates plugging location (McMullen 2011).

The detection of blockages along pipelines is a challenging problem and has received considerable attention in literature (Adeleke, Ityokumbul and Adewumi 2013; Besancon et al. 2013; Srour, Saber and Elgamal 2016; Stewart and Jack 2017; Jafarizadeh and Bratvold 2019; Yang et al. 2019; Abdullahi 2020; Razvarz, Jafari and Gegov 2020). However, blockage

location detection techniques from flow transients using time domain or frequency domain analysis proposed in the above literature are not suitable for real-time detection of hydrates plugs in gas pipelines for the following reasons. The first approach is the pressure wave (time domain analysis), which depends on the determination of acoustic velocity from the time of flight of the pressure disturbance in the fluid medium (Chen et al. 2007; Adeleke, Ityokumbul and Adewumi 2013; Stewart and Jack 2017). In this approach, gas is propagated from the receiving facility (downstream of the blockage) to the surface of the blockage.

The time of flight is the total time from when the pressure signal was sent to when the reflected signal from the surface of the blockage was received. However, the acoustic velocity is affected by the pipeline internal diameter and wall thickness. During hydrates deposition the pipeline hydraulic diameter varies linearly along the hydrates section, hence the uniform ratio of pipeline internal diameter to the wall thickness in the acoustic velocity equation proposed by Stewart and Jack (Stewart and Jack 2017) is not suitable for hydrate plug location detection.

In a similar pressure-time approach (Besancon et al. 2013), the detection of plug location is based on finite difference discretization of the velocity field, where the time to experience the first significant pressure fluctuation is related to the fluid velocity to obtain the distance of the blockage from the inlet. The length of the blockage is estimated from the time when the first transient rise in pressure was detected to when the signal decayed to "zero." The model was developed for liquid flows and did not consider the temperature and pressure dependent fluid parameters such as density and viscosity of gas. Viscosity effects influences the prediction of blockage severity in gas pipelines (Adeleke, Ityokumbul and Adewumi 2013).

A second approach is the pressure wave (frequency domain) analysis method Mohapatra et al.(Mohapatra et al. 2006). By assuming a sinusoidal behaviour of the pressure and flow velocity, the time domain in the pressure wave analysis method above is converted into frequency domain to estimate the blockage location from the observed amplitude of the disturbance injected into the fluid domain. The blockage location is estimated from a relationship

of the fluid velocity, frequency, number of peaks, and length of the pipe (Chaudhry 1979; Mohapatra et al. 2006; Datta, Gautam and Sarkar 2018). Again, the frequency domain approach requires an external fluid disturbance to create a reflected signal off the surface of the partial blockage. An approach that can lead to accidents in locating hydrate plugs if the fluid pressure is not adequately depressurised before injecting the flow disturbance.

A third approach is based on the detection of blockage location from the prediction of wall shear stress (Srour, Saber and Elgamal 2016). In this approach, a small sinusoidal disturbance is introduced to the original flow from an external source at the inlet to create time changes in the velocity field and wall shear stress. This nature of sinusoidal disturbance will have little effect in detecting hydrates plug location because of the higher pressure and non-steady flow in gas pipelines. To close the above gap, this study suggests a cause-effect analytical modelling approach for the transient pressure drop (dependent variable) to locate the position of a single hydrate plug from the inlet of the gas pipeline. The independent variables are the hydrates deposition rate, the gas velocity, and pipeline pressure and temperature. The discussion that follows will explain the theoretical framework adopted in developing this model.

The experimental and computational fluid dynamics (CFD) model by Yang et al. (Yang et al. 2019) suggests that pressure drop increases as the blockage location increases along the pipeline. Transient pressure-drop fluctuations during hydrates deposition and pipe plugging can lead to pipeline rupture (Di Lorenzo et al. 2014a; Aman et al. 2016; Zhang et al. 2019). Therefore, accurate prediction of the hydraulic effect of hydrate deposition and plug location is critical to the safety and operability of natural gas transport pipelines, especially for subsea gas transport pipelines where maintenance and intervention activities are more difficult.

Hydrates morphology, properties and growth kinetics have been discussed extensively in the literature (Turner et al. 2005; Sloan and Koh 2007; Sloan 2011; Carroll 2014; Yin et al. 2018), and forms the basis for studying hydrates formation in pipelines using analytical and numerical models.

Hydrates are formed at low temperatures and higher gas pressures, a condition that exist in pipelines on the seabed due to low temperatures (Li et al. 2013). For subsea gas flowlines and pipelines, the presence of hydrates has been reported to cause line plugging and other related hazards (Koh and Creek 2011; Carroll 2014). Therefore, to proactively prevent pipeline failures from hydrate plugs there is the need to predict the time for hydrates to plug the pipeline and the resulting transient pressure spikes. However, evidence from the literature indicates that more studies are needed to accurately and proactively predict both plugging flowtime and transient pressure drop of hydrates deposition in a gas-dominant pipeline.

Thus, the purpose of this study is to develop an improved analytical modelling approach to predict the effect of hydrates deposition on the plugging flowtime and transient pressure drop in a subsea gas pipeline (Umuteme et al. 2023b). To achieve this, current pressure drop analytical model directly incorporates the hydrates deposition rate in predicting the transient pressure-drop through a modification of the general two-phase gas-liquid steady-state pressure gradient in horizontal pipeline (Beggs and Brill 1973). The corresponding plugging flowtime was estimated from the volumetric hydrates depositional growth geometry proposed in the literature (Di Lorenzo et al. 2018).

The formation and prediction of hydrates in gas pipelines has gained scholarly and industrial attention from several published related papers and textbooks. These include experimental flow-loop models (Li et al. 2013; Di Lorenzo et al. 2014a; Aman et al. 2016; Odutola et al. 2017; Liu et al. 2020), analytical models (Di Lorenzo et al. 2018; Wang et al. 2018; Liu et al. 2019) and computational fluid dynamics (CFD) models (Lo 2011; Balakin et al. 2016; Neto et al. 2016; Song et al. 2018b).

Experimental models for gas hydrates studies in pipelines are usually limited by scalability for real-life application because gas pipelines can span several kilometres which is difficult to setup in a laboratory experiment. However, experimental results have provided data for the validation of both analytical and CFD models. To overcome the limitation of experimental studies of gas hydrates in pipelines, analytical models have been developed. The results of

the analytical models for hydrates studies in gas-dominated pipelines have provided compelling evidence that analytical modelling can predict the plugging flowtime and transient pressure drop during hydrates deposition, as discussed further.

Jassim, Abdi and Muzychka (2010) described the near-wall behaviour and deposition spots of hydrate particles using Lagrangian particle deposition velocity theory. It was observed that increasing the Reynolds number increases the distance of deposition from the point of hydrates generation in the pipeline, except when the hydrate particles agglomerates to a critical size that becomes independent of the flow field velocity and are deposited *in situ*. Their work is important as it creates a picture of hydrates profile in a gas pipeline and the reason for pressure build-up during hydrates deposition and pipe plugging. In this model, we used this understanding in the determination of the volume of pipe occupied by deposited hydrates and the resulting reduction in pipe hydraulic diameter.

Wang et al. (2018) adopted the hydrates drift velocity proposed by Jassim et al.(Jassim, Abdi and Muzychka 2010) and developed an analytical model that can predict the risk of hydrates plugging in gas-dominated pipelines. Three stages of flow pattern were investigated: gas-water-hydrates; gas-hydrate; and water-saturated gas flow. From the model prediction, the first stage is more likely to plug the pipeline and was identified as the most vulnerable. While neglecting the effect of sloughing based on lack of established relative studies on the effect of sloughing on hydrates layer growth, the estimated hydrate thickness also increased almost linearly during this stage.

Though, it was anticipated that the estimated hydrates thickness can be overpredicted when compared to actual pipeline in the field, yet the model prediction was adequate for early hydrate management intervention to prevent associated risks of pipeline failures from hydrates plugging. In the development of the model in this study, this line of reasoning in the prediction of pipe plugging time and pressure drop was adopted. Earlier, Wang et al. (2017) developed an analytical model to capture hydrates formation from water droplets in the gas phase and to predict the most

vulnerable sites for hydrates deposition. The model also predicted the plugging flowtime and transient pressure drop. However, the hydrates deposition rates predicted by the model was only for a higher velocity of 8.7 m/s, hence the accuracy of the model in predicting the plugging flowtime and transient pressure-drop at lower gas flow velocities could not be ascertained.

Di Lorenzo et al. (2018) developed an analytical model with emphasis on hydrates sloughing to demonstrate that the hydrate deposited at the pipe wall is not stable. The authors argued against the immobility of the deposited hydrates at the pipe wall as this can lead to overestimation of the pressure drop. However, in their conclusion the authors indicates that their model was still unable to predict when and where hydrates sloughing can likely occur along the pipeline.

In overcoming the limitation of the model by Wang et al. (2017) identified earlier, the study results presented the depositional rate of hydrates at lower velocity of 4.7 m/s as well as at higher velocity of 8.8 m/s developed. However, the transient pressure-drop prediction was up to -40% relative error from experimental results at lower velocities. Also, the predicted hydrates deposition rate by the model underpredicted the experimental outcome at 4.7 m/s. The hydrates deposition rate was estimated by adjusting the pipeline volumetric change rate with different multiplier factors at various subcooling temperatures and constant gas flow velocity.

The use of different depositional multiplying factors can limit the application of the model for large size pipelines. Hence, in this new model I have neglected the effect of sloughing, but the model incorporates a multiplying factor to address the effect of any uncertainty in the predictions because of this key assumption. Also, as a worst-case scenario, the current pressure drop prediction model assumes that the deposited hydrates are relatively stable, and that the growth is linear around the annulus of the pipe until the pipe is plugged.

Again, to overcome the above limitations, the plugging flowtime and transient pressure drop models concentrated on having the hydrates

depositional rate as direct input. The results of the CFD model by Umuteme et al. (Umuteme et al. 2021) for predicting hydrates deposition rates in gas pipelines, compared more favourably with experimental results at lower velocity of 4.7 m/s than the predictions of Di Lorenzo et al. (2018). However, the CFD model was limited by pipe length, resulting in a gap to develop an analytical model that can predict plugging flowtime, transient pressure drop, and locate the position of hydrates plugging in industry size pipeline.

Liu et al. (2019) developed an analytical model to predict the deposition of hydrates with emphasis on the shedding of hydrates at the wall. This model was aimed at addressing the limitation of constant gas shear stress adopted in the model by Di Lorenzo et al. (2018), which is believed by the authors to have resulted in the high percentage relative error (up to -41%) recorded in their pressure drop predictions at lower gas flow velocity. The plugging flowtime and transient pressure drop model predictions by Liu et al. (2019) indicated a good match with the experimental results of Di Lorenzo et al. (2014a). However, for real life application it is difficult to locate the positions along the pipe where hydrates sloughing and wall shedding occurs, except special instruments will be installed to monitor this variation along the pipeline.

In summary, one of the limitations of existing blockage location models is based on the need to introduce a pressure signal downstream of the blockage from an external source (Adeleke, Ityokumbul and Adewumi 2013). An approach that is not suitable for hydrates forming pipelines because of possible accidents that can occur when the upstream and downstream pressures are not balanced. Another limitation of existing pressure-wave blockage location models is that the reflected pressure wave from the surface of the hydrates is affected by the viscosity of the gas phase because of the drop in temperature, thus affecting the time of flight used in estimating the location of the hydrates plug from the acoustic velocity of the gas (Adeleke, Ityokumbul and Adewumi 2013; Abdullahi 2020).

Consequently, for hydrates forming pipelines where the temperature at the hydrates surface is colder, the time of flight will be affected by the return pressure wave. Also, existing hydrates plugging pressure drop estimating

analytical models underpredicted experimental results at low flow velocity by up to 40%. Hence, the need to develop an analytical model for accurate prediction of hydrate-induced pressure drop at low gas flow velocity.

This study closes the identified gaps above with the specific aim to provide an industry fit-for-purpose semi-empirical analytical models that can be used in conjunction with the validated hydrates deposition rates prediction models, with the objectives to predict the: (a) time from initial hydrates deposition to near “no-flow” constriction or line plugging; (b) transient pressure drop due to increasing hydrates deposition on the pipe wall at both low and high gas flow velocity; and (c) location of hydrates plugging section of the pipe. By incorporating the hydrates deposition rate into the models, the predictions capture real-time plugging events in a curve.

The rest of the chapter is organised as follows. The validation of the model with experimental results is provided in section 7.1. Sections 7.2, 7.3, 7.4, 7.5 and 7.6 discusses hydrates transportability and extends the transient predictive models for predicting hydrates plug location along the pipeline. Finally, section 7.7 ends the chapter with the summary of the major findings.

7.1 Model Validation and Discussion of Results

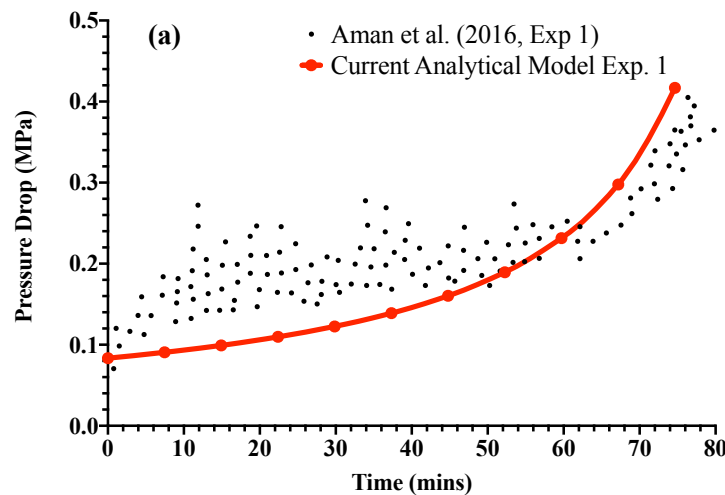
This model incorporates the hydrates deposition rate for gas-dominated pipeline in one mathematical relation. Two main equations were developed earlier in section 3.3; to predict the plugging flowtime (Equation 3.53) and the associated transient pressure drop formulation (Equation 3.52). The point of hydrates generation can be obtained from a phase envelop, and pressure and temperature gradient plot from a hydraulic simulator, or directly from subsea pressure and temperature transmitters installed on the flowline or pipeline. Also, the actual sectional length (L) experiencing hydrates growth can be obtained in like manner. In all the six cases considered from experimental data in (Di Lorenzo et al. 2014b) and (Aman et al. 2016), the plugging flowtime and transient pressure drop were dependent on the hydrate deposition rates.

As a proactive hydrate plugging preventive analytical tool, it is essential that the model can “underpredict” the experimental plugging flowtime at the experimental transient pressure drop in the literature. The basic assumption behind the transient pressure drop model is to stop gas flow once the first spike in pressure drop is recorded as a precautionary measure. **Figure 7.1**, compares the model performance with experimental data in the literature at both low and high velocities of 4.6 m/s and 8.7 m/s respectively.

From both figures, the analytical model predictions at both high and low velocity compared favourably with the experimental plots in the literature. By using only one multiplier factor, which is a function of the gas velocity, this model is an improvement over the analytical model of Di Lorenzo et al. (2018) since it proves to be more adaptable for industry application without adjusting the multiplier factor under various flow velocity. The relative error from the experimental results is calculated as in equation 7.1.

$$\% \text{ relative error} = \frac{\text{Model Result} - \text{Experimental Result}}{\text{Experimental Result}} \times 100 \quad (7.1)$$

The transient pressure drop predictions from experimental results for all six cases at both low and high velocities is at a maximum of 6% relative error.



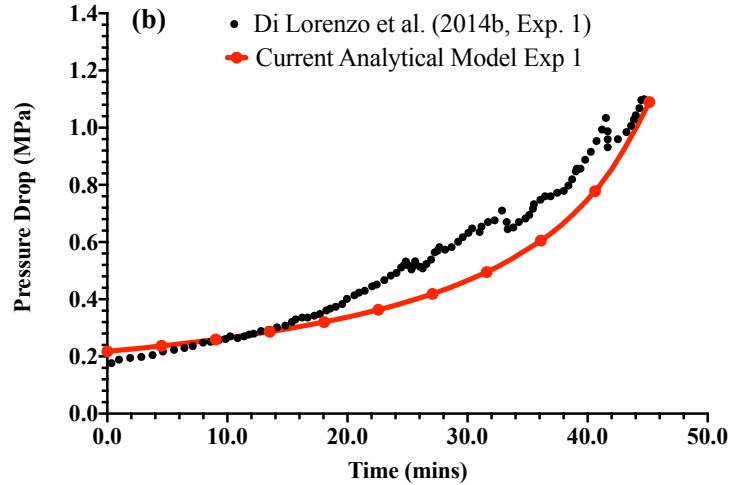


Figure 7.1: Comparing model predictions of first significant spike in transient pressure drop with experimental results: (a) Experiment 1 - hydrate deposition rate of 0.078 L/min at 4.6 m/s (Aman et al. 2016); (b) Experiment 1 - hydrate deposition rate of 0.129 L/min at 8.7 m/s (Di Lorenzo et al. 2014b).

Similar predictions by (Di Lorenzo et al. 2018) were within 40% relative error. Also, the mean relative error of the transient pressure drop predictions by (Zhang et al. 2019) was 7.43%. Hence, the current pressure drop model is an improvement over existing analytical hydrates plugging pressure drop prediction models. Again, the plugging flowtime for all cases was underpredicted within mean relative error of 9%, suggesting the plugging flowtime model can proactively predict hydrates plugging. More importantly, because the current model directly incorporates the hydrates deposition rate it is invaluable in real-time tracking of hydrates deposition rates when the pipeline is fitted with temperature and pressure transmitters. Further details on the validations of both models are presented in section 7.1.1.

7.1.1 Input Data

The hydrate deposition pipe length is 33.4m and 0.0204m in diameter as in the flowloop experiment information reported in (Di Lorenzo et al. 2014b) and (Aman et al. 2016). In both experiments, the hydrates were generated at a 12m inlet section of the pipe and deposited downstream along the pipe. Flow velocities are 4.6 m/s and 8.7 m/s (Aman et al. 2016). The input parameters used are presented below.

Table 7.1: Input Parameters

Input	Value	Source
Velocity (m/s)	4.6; 8.7	Aman et al. (2016)
Hydrates section length (m)	33.4 (except stated otherwise)	Aman et al. (2016) and Di Lorenzo et al. (2014b)
Pipeline diameter (m)	0.0204 (except stated otherwise)	
Average operating pressure (MPa)	Table 7.2 and Table 7.3	
Average operating temperature (K)	Table 7.2 and Table 7.3	
Hydrate deposition rate (L/min)	Table 7.2 and Table 7.3	
Gas density (kg/m ³)	Equation 3.46	Di Lorenzo et al. (2018)
Gas viscosity (Pa. s)	Equation 3.48	
Pipe friction factor	Equation 3.47	Drew et al. (1932)

In our model, the simulation using the solution algorithm developed in **Figure 3.16**, was terminated when the instantaneous time equals the calculated time for hydrate plug at the n^{th} timestep. For each run, the transient pressure-drop is calculated for a time t_n as explained earlier.

7.1.2 Hydrate Plugging Flowtime and Transient Pressure Drop

Equations 3.52 and 3.53, are the two sets of equations needed to predict the plugging flowtime of hydrates and transient pressure drop. The results of the calculations from these two equations are validated with experimental results from Di Lorenzo et al. (2014b) and Aman et al. (2016), Hydrates generation and deposition is not uniform along the pipe as reported in the literature. Thus, the flowtime has been modelled to be less than the actual runtime in the experiments. In theory, the gas phase is both upstream and downstream of the hydrates plug, hence the need to balance the pressure at both ends of the hydrates plug to prevent accidents.

The experimental results used for validation indicates that the hydrates are more stable at lower velocity of 4.6 m/s as the gas temperatures are below

292K. The model results at 4.6 m/s where the hydrates are stable have minimal relative error compared with predictions at 8.7 m/s. Hence, this model is very useful in predicting the severity of hydrates under low gas productivity scenario. The two sets of validations carried out with experimental results are discussed below.

7.1.3 Validation of model predictions at gas velocity of 4.6m/s

Aman et al. 2016 conducted a series of flowloop experiments to compare the formation and deposition rates of hydrates at low flow gas velocity. Details of the experiments are discussed extensively in the literature (Aman et al. 2016). Only two data sets representing experiment 1 and 2 from the literature were considered for validation based on the following reasons: (i) experiment 3 is reported with similar hydrates deposition rate with experiment 1, yet has higher gas consumption rate and a lower transient pressure drop; it is expected that at the same deposition rate and flow velocity the pressure drop is relatively equal; (ii) experiment 4 has a lower hydrates deposition rate compared with experiments 1 and 2, yet was reported with a higher pressure drop; it is expected from theory that higher deposition rates should have higher pressure drop at similar plugging flowtime; (iii) experiment 5 is reported with the highest gas consumption rate, yet with lower hydrates deposition rates compared with the outcomes of experiments 1, 2, 3 and 4, which is inconsistent with theory. From the model results, experiments 1 and 2 compared favourably with expected theoretical outcome, hence were used for the validation results presented in **Table 7.2**.

From **Table 7.2**, the transient pressure drop model underpredicted the experimental results by 2% relative error. The mean relative error of the pressure drop predictions from experimental results is 1%. The plugging flowtime model underpredicted the experimental values as expected. The predictions are in order as expected for a proactive predictive model, and an improvement over the predictions of (Di Lorenzo et al. 2018). From experimental observations at lower flow velocity, the pressure drop is not expected to vary significantly across different subcooling temperatures, because the gas shear stress on the hydrates at the pipe wall is low (Aman

et al. 2016). This position is replicated from the model performance in **Table 7.2**. Again, the indication from the model results is that early plugging occurs at higher hydrates deposition rate, which is also consistent with experimental observations.

Table 7.2: Comparing model predictions with experimental results by Aman et al. (2016) at 4.6 m/s

Exp.	Gas Press. (MPa)	Gas Temp. (K)	Sub-cooling, (K)	Hyd. Dep. Rate, (L/min)	Plugging Flowtime, t_{plug} (min)		Pressure Drop, dp (MPa)		
					Exp.	Analy. Model	Exp.	Analy. Model	Relative Error (%)
1	10.79	286.0	6.0	0.078	76.37	74.66	0.41	0.40	-2
2	10.91	284.4	7.3	0.105	68.43	55.46	0.41	0.41	0

7.1.4 Validation of model predictions at gas velocity of 8.7m/s

Di Lorenzo et al. (2014b) conducted a flowloop experiment to compare hydrates formation and deposition rates at constant higher gas flow velocity of 8.7 m/s. The resulting series of experimental results formed the basis for further work in this research area, and the results have been used to validate analytical hydrates deposition models (Wang et al. 2017; Liu et al. 2019). The hydrates deposition rate is estimated as 30% of the formation rate based on the results in (Di Lorenzo et al. 2014b).

Another source also reported an average deposition rate between 24-26% of hydrates formation rate (Wang et al. 2017). The 30% approximation was used because the results in (Di Lorenzo et al. 2014b) did not specifically present the average deposition rates. The experimental results were obtained at a gas velocity of approximately 8.7 m/s and the outcomes are compared with the model predictions in **Table 7.3**.

Table 7.3: Comparing model predictions with experimental results by (Di Lorenzo et al. 2014a) at 8.7 m/s.

Exp.	Gas Press. (MPa)	Gas Temp. (K)	Sub-cooling, (K)	Hyd. Dep. Rate, (L/min)	Plugging Flowtime, t_{plug} (min)		Pressure Drop, dp (MPa)		Relative Error (%)
					Exp.	Analy. Model	Exp.	Analy. Model	
					1	9.07	292.5	5.83	
2	8.99	292.5	5.94	0.147	41.46	39.61	1.04	1.08	4
3	8.43	292.0	10.3	0.369	22.49	15.78	1.01	1.02	1
4	8.83	292.5	8.6	0.207	31.21	28.13	1.01	1.06	5

As seen in **Table 7.3**, the model overpredicted the transient pressure drop by a maximum relative error of 6%, with a mean relative error of 4%. Also, the plugging flowtime model underpredicted the experimental values as expected. Both predictions are also in order since by overpredicting the transient pressure drop and underpredicting the plugging flowtime, it is possible to predict early hydrates obstruction in the pipeline for proactive intervention. Thus, the present work is an improvement over the predictions of (Di Lorenzo et al. 2018) at higher velocity of 8.7 m/s with pressure drop predictions within 10% relative error from experimental results.

7.2 Hydrates Transportability

Since hydrates formation and deposition rate is directly related to the gas consumption rate, the RHS of equation 3.33 can be modified with the density of hydrates to account for the rate of change in pipe volume (m^3/s) due to the presence of hydrates as shown below:

$$\frac{d}{dt}V_H = \dot{Q}_H = \frac{1}{\rho_H} \cdot \frac{dm_g}{dt} \quad (7.2)$$

where V_H is the volume change in the computational pipe domain due to the presence of hydrates; Q_H is the hydrates formation, agglomeration, and

deposition rate; and ρ_H is the density of hydrate. Since the density of gas increases towards the pipewall during hydrates formation and agglomeration, and remained stable during hydrates deposition, I have developed a new relation for estimating the hydrates density fitted to the experimental results in Li et al. (2013) at 10% water volume (α_w) fraction and gas volume fraction (α_g) equal to $1-\alpha_w$. This is because the existing relation for determining the density of hydrates in the literature (Sloan and Koh 2007; Carroll 2014) is not handy for gas pipeline since it requires the determination of the fractional occupancy of the cavities for the hydrate type, the volume of the unit cell of the hydrate and the number of hydrate forming components in a unit cell.

The density of hydrates is a necessary parameter in the estimation of the time for hydrates dissociation and the mass of hydrate projectile (McMullen 2011). Again, the knowledge of how the density of hydrates depends on the temperature and pressure of the gas is important in understanding the expected viscous resistance to gas flow and the resulting increase in transient pressure drop. Hence, the proposed model in this study can be used for reactive planning of hydrates field intervention work by first determining the gas density using equation (3.46), from the pressure and temperature recorded in the pipeline and using equation (7.3) to estimate the density of the deposited hydrates.

$$\rho_H = C_{\rho_H} \left[(\alpha_g \rho_g + \alpha_w \rho_w) + \frac{2\alpha_g \rho_g \cdot \alpha_w \rho_w}{\alpha_g \rho_g + \alpha_w \rho_w} \right] \quad (7.3)$$

$$C_{\rho_H} = 0.0325T - 1.985 \times 10^{-8}P - 3.0 \quad (7.4)$$

where C_{ρ_H} is an empirical constant; ρ_g is the temperature and pressure dependent natural gas density calculated from equation (3.46); ρ_w is the density of water (998kg/m³); T and P are the gas temperature (K) and Pressure (Pa.), respectively. The plot of hydrate density predicted by equation (7.3) compared with the experimental results indicates a good match in **Figure 7.2**.

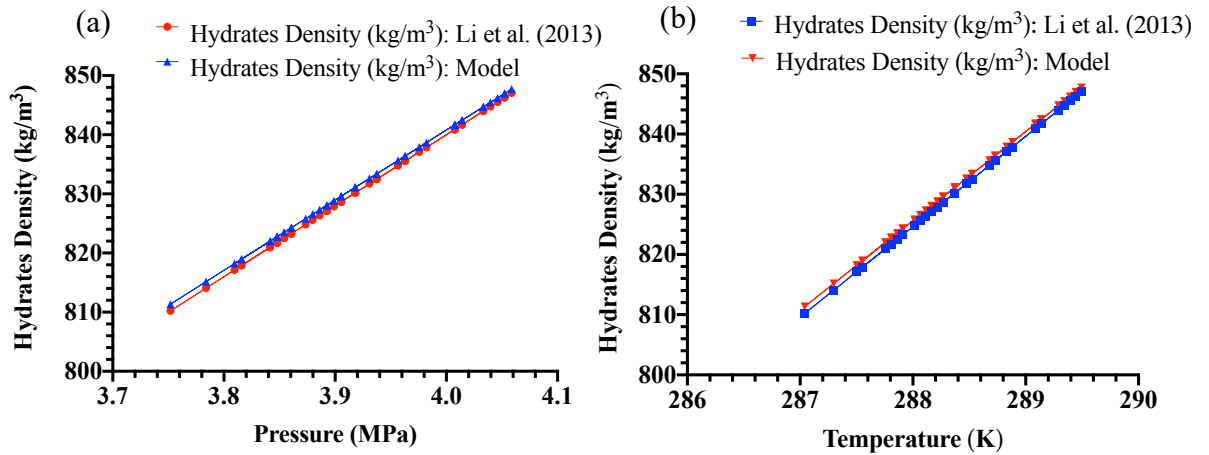


Figure 7.2. Comparing predictions of hydrates density estimation model with experimental results: (a) pressure and density of hydrates; (b) temperature and density of hydrates.

From **Figure 7.2**, the hydrate density estimation using equation 7.3 compares favourably with the results in (Li et al. 2013). In theory, there is a positive correlation between gas pressure and the density of hydrates (Carroll 2014). Also, in **Figure 7.2**, a positive linear relationship is observed between hydrates density and the temperature and pressure in the pipeline. For annular flow scenario, which is applicable to gas-dominated pipelines, the average density of hydrates measured from the experiment by (Ding et al. 2017) at 10% water volume fraction, temperature of 273K and pressure of 5.0 MPa is 825 kg/m³, and the prediction from equation 7.3 is 857 kg/m³, which represent 4% overprediction relative error from the experimental measurement.

Again, the hydrates growth rate equations in the literature (Aman et al. 2016; Di Lorenzo et al. 2018; Liu et al. 2019) assumed 950 kg/m³ as the density of hydrates, whereas the value obtained from equation 7.3 using the pressure (8.9MPa), temperature (289K) and water volume fraction (0.06) experimental conditions of (Di Lorenzo et al. 2014a) is 935 kg/m³. Implying that the result of the new hydrate density estimation equation for gas-dominated annular flow hydrates formation pipeline is consistent with experimental results.

Hence, instead of assuming the density of hydrates in future hydrates related experiments and models, the equation developed in this study for the density

of hydrates (Equation 7.3) can be used. This will ensure that the density of hydrates used is representative of the variation in gas pressure and temperature changes during the simulations. Again, since gas transportation in pipeline is related to gas temperature and pressure, this model is a handy tool for estimating the density of hydrate formed in the pipeline in the field. Also, accurate estimation of the density of hydrates enables the estimation of the right thrust to push the hydrate plug out of the pipeline using the relation for fluid force (Equation 7.3).

$$F = \rho_H v^2 A \quad (7.5)$$

where F is Thrust behind the hydrate plug (N); ρ_H is the density of the hydrate plug (kg/m^3); v is the velocity of the hydrate plug (m/s); and A is the cross-sectional area of the pipeline behind the plug (m^2). For a line plugged with hydrates, this study proposed that equation 7.3 can be used as guide during temperature and pressure intervention operations to enhance hydrates transportability. The density of hydrates in natural gas-dominated pipelines is usually less than that of water (Carroll 2014), ranging from 920-950 kg/m^3 (McMullen 2011; Aman et al. 2016; Di Lorenzo et al. 2018; Liu et al. 2019).

Thus, the pressure and temperature in the pipeline can be varied until the density of hydrates is greater than the density of water using equation 7.3. This effect, at a gas pressure of 6.0 MPa, is demonstrated in **Figure 7.3** below, where the graph of the calculated density of hydrates is compared with the density of water. The transportability of hydrates slurry is possible when the density of the hydrates slurry is greater than that of water (Berrouk et al. 2020).

Hence, the point beyond where the density of hydrates is greater than the density of water in **Figure 7.3**, can be used to define the temperature and pressure condition for transportability of hydrates. This guide can assist in the pigging of hydrates-forming gas pipelines.

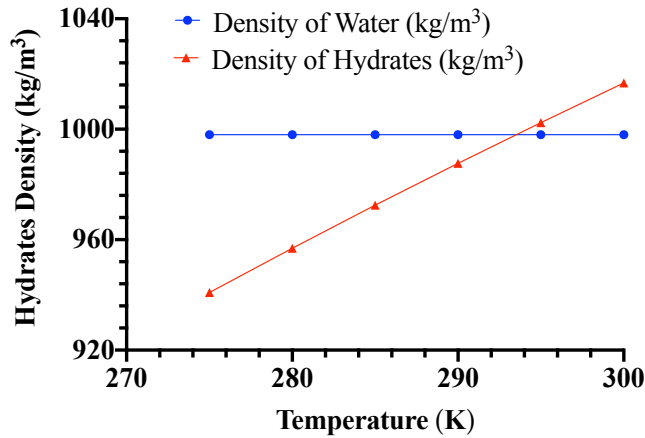


Figure 7.3: Determining the temperature for hydrates transportability at gas pressure of 6.0 MPa

From **Figure 7.3**, at a gas pressure of 6.0 MPa the calculated density of hydrates using equation 7.3 shows that the transportability of hydrates slurry can be achieved if the temperature is increased beyond 292K. This also corresponds to the point where the hydrates are unstable from the methane hydrate loci (**Figure 7.4**).

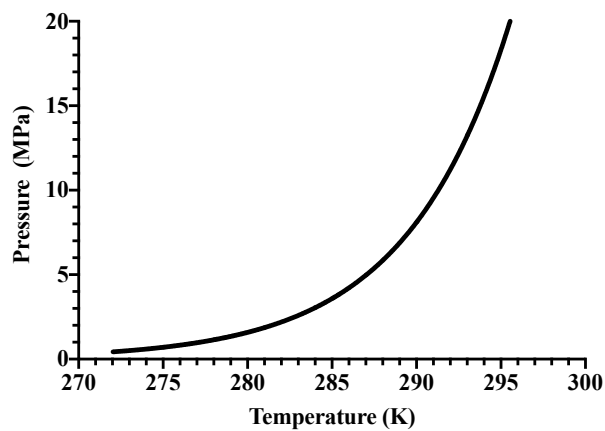


Figure 7.4: Methane hydrates loci (Di Lorenzo et al. 2014a)

7.3 Location of Hydrates Plugging Event

The purpose of the sensitivity simulations in this section is to use the hydraulic effect of hydrates deposition rates on transient pressure drop and hydrates plugging flowtime to locate hydrates plugging event along the pipeline. Hydrate plugs increases the line-pack upstream of the plug, leading to transient pressure waves moving upstream. This can trip the discharge compressor if the transient pressure equals the discharge shutdown setting

of the compressor (Menon 2005). When the compressor fails to trip, the pipeline can rupture because of overpressurisation. If the compressor trips, the pressure surge in the pipeline because of the locked-in gas will gradually disappear, and the gas velocity will reduce because of friction and drop in inertia (Menon 2005). However, the locked-in gas pressure behind the hydrate plug can still lead to failure, especially for older pipes with reduced pipeline wall thickness because of internal corrosion. Throughout the calculations and simulations in this section, it is assumed that a single plug is formed at any time along the pipeline.

In the simulations that follows, the transient pressure drop and plugging flowtime prediction models developed earlier, will be used to predict hydrates plugging event along a gas pipeline. Before determining the location of plugging events using the models developed earlier in this study, it is important to perform some parameter sensitivity simulation to investigate the performance of the models against related theoretical suggestions in the literature.

7.3.1 Effect of Hydrates Deposition on Transient Pressure Drop and Plugging Flowtime

The pressure in the pipeline determines the shear stress of the hydrate deposit on the wall. The shear stress determines how much differential pressure is needed to release the hydrate plug (McMullen 2011). Hence, it is important to determine the resulting transient pressure drop in the pipeline because of hydrate plugging event. Theoretically, increase in hydrates deposition rates at constant gas flow velocity due to increase in subcooling temperature leads to increase in transient pressure drop (Di Lorenzo et al. 2014a; Aman et al. 2016). This is because of the reduction in pipe annulus as hydrates are deposited on the pipe wall.

For practical application, it is expected that pipeline plugging, and early transient pressure rise should occur more in cold locations when the temperature is relatively stable below the hydrate equilibrium temperature and higher-pressure conditions that encourages hydrates formation. The results in **Figure 7.5** using equations 3.52 and 3.53 agrees with the expected theoretical outcome, that hydrates plugging risk increases with

increasing deposition rate under the same flow condition (Di Lorenzo et al. 2014b, 2014a; Aman et al. 2016).

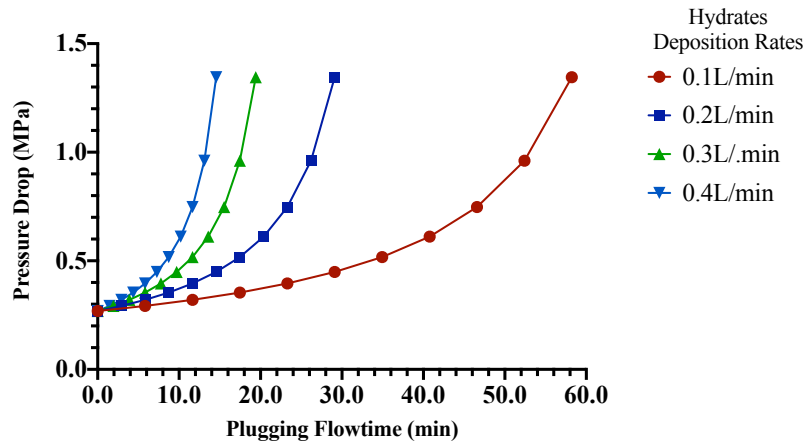


Figure 7.5: Comparing pressure drop curves at different rates of hydrates deposition at a gas velocity of 8.7 m/s, and pipeline temperature of 287.5K and pressure of 10.9 MPa.

Figure 7.5 demonstrates that the transient pressure drop exhibits relatively uniform behaviour across different hydrate deposition rates. However, the time to plug the pipeline varies, with lower deposition rates corresponding to longer plugging time. The observation that transient pressure drop exhibits relatively uniform behaviour across different hydrate deposition rates, while plugging time varies with lower rates leading to longer plugging times, has significant implications for gas transportation in subsea pipelines prone to hydrate formation.

First, a uniform pressure drop across different deposition rates can be misleading. It suggests that initial pressure changes might not be a reliable indicator of the severity of hydrate formation. Even with a seemingly small pressure drop, a pipeline with a lower deposition rate could be at greater risk of eventual plugging. This is because the slower accumulation allows the blockage to progress unnoticed for a longer period.

Second, since the pressure drop doesn't directly reflect the plugging risk from slower deposition, relying solely on this metric could lead to delayed detection of hydrate formation. This delay can be critical as it allows the hydrate plug to grow progressively, potentially leading to a complete

shutdown and requiring more complex and time-consuming remediation procedures.

Therefore, with a clear understanding of both pressure drop and deposition rate, operators can prioritise mitigation strategies. For rapid deposition, immediate action to stop hydrate formation might be necessary. For slower deposition, strategies like hydrate inhibitor injection or pipeline heating could be implemented to manage the issue before a complete blockage occurs.

7.3.2 Effect of increase in pipeline diameter

The purpose of this sensitivity using equations (3.52) and (3.53) is to investigate the effect of increasing diameter on pressure drop and plugging flowtime for diameters of 0.0204 m, 0.0408 m, 0.0612 m and corresponding deposition rates of 0.14 L/min, 0.28 L/min and 0.42 L/min. The hydrate plug is assumed to be located 50 m from the point of hydrates equilibrium condition, at the gas velocity of 8.7 m/s, pipeline temperature of 287.5 K and pressure of 10.9 MPa.

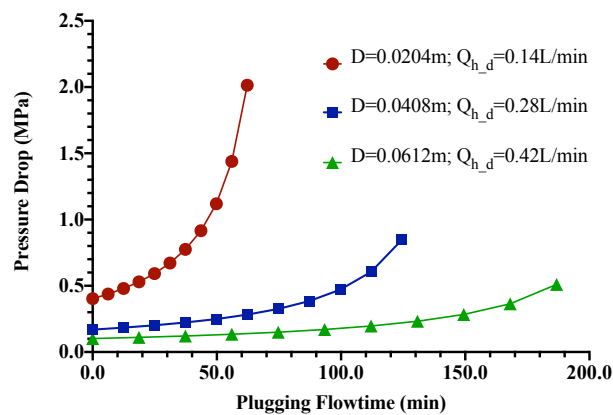


Figure 7.6: Comparing pressure drop curves at different pipeline diameter and corresponding hydrates deposition rates at gas velocity of 8.7 m/s, pipeline temperature of 287.5 K and pressure of 10.9 MPa.

The results in **Figure 7.6** suggests that though the hydrates deposition rate increases as the pipe diameter increases, the transient pressure drop is lower with extended plugging flowtime provided the upstream compressor discharge pressure is the same in larger pipes. The implication is if a pipeline is expected to have hydrates, increasing the pipe diameter can reduce the susceptibility of the pipeline to hydrates plugging. However, this decision

must be arrived at by considering the possible gas flowrate from the field throughout the useful life of the pipeline, to avoid issues of internal corrosion with under-capacity utilization because of the low liquid loading capacity of the flow (Chaudhari, Zerpa and Sum 2018). In essence, increasing pipe diameter can buy more time in hydrate plugging scenarios, but it should be balanced against the potential for corrosion due to reduced flow capacity.

7.3.3 Effect of hydrates deposition rates on pipe inner diameter

From equation (3.50), hydrates deposition on the pipe wall reduces the pipeline inner diameter in a nonuniform pattern as suggested from plots in **Figure 7.7**, below. This position is also corroborated in the literature (Wang et al. 2017).

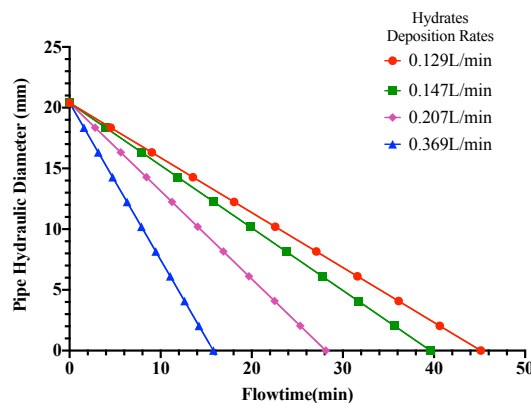


Figure 7.7: Comparing pipeline hydraulic diameter reduction at different hydrates deposition rates at gas velocity of 8.7 m/s, pipeline temperature of 287.5K and pressure of 10.9 MPa

From the plot in **Figure 7.7**, the pipeline is plugged earlier at higher deposition rates under the same fluid velocity of 8.7 m/s. Hydrates deposition rate under the same flow condition is a function of the subcooling temperature. Lower pipe surrounding temperature enhances gas solubility in water (Lekvam and Bishnoi 1997), leading to increasing hydrates formation and deposition. Hence, in deeper offshore sea floor conditions where the temperature is much lower, hydrates plugging will be earlier. The pipeline hydraulic diameter reduction rate (mm/min) increases from lower deposition rate to higher deposition rate (**Figure 7.8**).

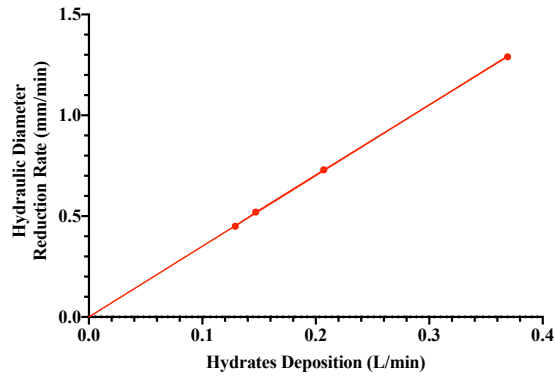


Figure 7.8: Pipeline hydraulic diameter reduction rate as hydrates deposition rates increases at gas velocity of 8.7 m/s, and pipeline temperature of 287.5K and pressure of 10.9 MPa.

7.3.4 Hydraulic Effect of Hydrates Plug at Different Sections of the Pipeline

The hydrates forming section in the pipe determines the pressure drop and plugging flowtime. By varying the length of the section at a deposition rate of 1.0 L/min plots of pressure drop for every sectional length are obtained in **Figure 7.9**.

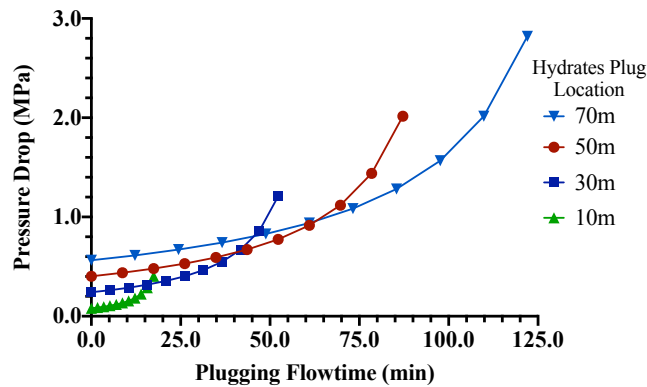


Figure 7.9: Pressure drop curves at different hydrates plug location along the pipeline at gas velocity of 8.7 m/s, and pipeline temperature of 287.5 K and pressure of 10.9 MPa

The sensitivity simulation in **Figure 7.9** is important because it indicates that the transient pressure drop model can be used to determine the location of hydrates plug in the pipeline. This observation agrees with the effect observed if valves at different locations along a horizontal pipeline are closed

one at a time. Hence, the hydrates plug nearer the discharge compressor will experience a lesser transient pressure drop because of the lower volume of the line pack. When the plug location is farther from the discharge compressor, the line pack increases behind the plug until it reaches the compressor station. Hence, the volume of gas behind the plug increases as the plug is farther from the compressor discharge point.

The transient pressure wave travelling upstream towards the discharge compressor station is from the hydrate plug location and at the speed of sound in the gas (Menon 2005; Munson et al. 2013). In sections 7.3.5 through 7.3.7, some parameters relating to the study of hydrate plug location and transportability have been studied. This is because in the beginning of every experiment, the relationship among the variables is not usually known until the end of the experiment (Munson et al. 2013). A matrix of the correlation between these parameters is presented in **Table 7.4**.

Table 7.4: Correlation between the location of hydrate plug and the parameters that defines the transportability of hydrates

Correlation Pearson, r	Hydrate Plug Location (m)	Transient Pipeline Pressure Drop (Pa)	Hydrate Plug Velocity (m/s)	Hydrate Plug Shear Stress (Pa)	Hydrates Plug Bulk Modulus (Pa)	Hydrate Plug Shear Rate (s ⁻¹)
Hydrate Plug Location (m)	1.00					
Transient Pipeline Pressure Drop (Pa)	0.80	1.00				
Hydrate Plug Velocity (m/s)	-0.86	-0.97	1.00			
Hydrate Plug Shear Stress (Pa)	-0.86	-0.96	1.00	1.00		
Hydrates Plug Bulk Modulus (Pa)	0.67	0.98	-0.93	-0.91	1.00	
Hydrate Plug Shear Rate (s ⁻¹)	-0.92	-0.91	0.98	0.99	-0.84	1.00

Parameters with $p > 0.05$ have been highlighted, implying non-significant relationship at two-tailed 95% confidence interval

From **Table 7.4**, the following relationships are significant at 95% confidence interval ($P < 0.05$): (i) There is a positive relationship between the location of hydrate plug and pressure drop, and a negative relationship between the

shear stress and shear rate of the hydrate plug. There is an increase in transient pressure drop the farther the location of the hydrate plug is from the hydrates equilibrium condition point along the pipeline, whereas the shear rate and shear stress of the hydrate plug reduces.

Hence, the transient pressure drop is inversely related to the shear stress and shear rate of the hydrate plug; (ii) The transient pressure drop is positively related to the bulk modulus and negatively related to the velocity of the hydrate plug. Implying that the pressure drop increases because of a reduction in the transportability of hydrates as a result of increasing resistance to shear; (iii) The velocity of hydrates determines their transportability in the pipeline. It is inferred also from the correlation in **Table 7.4**, that the velocity of the hydrate plug is positively related to the shear rate and negatively related to the bulk modulus, which agreed with the observation in (ii) above.

The non-significant correlation between hydrate plug location and bulk modulus ($p=0.07$); and hydrate plug velocity ($p=0.06$); and shear stress ($p=0.06$), indicates: (i) a positive relationship with the bulk modulus. Implying that the bulk modulus of the hydrate plug increases the farther the plug location; (ii) a negative relationship with the hydrate velocity. Suggesting that the hydrate plug velocity reduces the farther the plug location: and (iii) the hydrate shear stress reduces the father the plug location. Indicating that hydrate plugs farther from the equilibrium point will be more difficult to flow as hydrate slurries, and the reason why hydrate plugs on the base of the riser are more difficult to retrieve.

Consequently, the parameters measured above are the physical fluid properties relating to the transportability of hydrates in the pipeline. These properties are related to both hydrate plug location and the induced transient pressure drop; suggesting that hydrate plug location can be inferred directly from the transient pressure drop. Details of the parametric sensitivity simulations using the transient pressure drop model developed in this study are discussed further. In the simulations using equation (3.52), the operating pressure was increased from 4 MPa to 5, 6 and 7 MPa at constant temperature of 285 K with gas velocity of 8 m/s, hydrates plug location at

250 m, 500 m, 750 m and 1000 m, water volume fraction of 0.1, pipeline diameter of 0.102 m (4inches) and hydrates deposition rate of 10 L/min. This is to demonstrate the effect of hydrates location on transient pressure drop and the hydraulic behaviour of the physical flow parameters of hydrates.

7.3.5 Effect of Pressure Drop on the Bulk Modulus of Gas and Hydrate

Bulk modulus (E_v) defines the relationship between change in unit pressure of a fluid or solid to the corresponding change per unit volume (Munson et al. 2013). Hence, further explanation of the effect of increasing pressure drop as the hydrate plug location increases in **Figure 7.9** can be done from the Cauchy number (C_a) in equation 7.6 to determine the relative effects of inertia force and compressibility on hydrates plugging. Earlier in chapter 5, it was suggested that the inertia is the driving force during hydrates sloughing and pipewall shedding by hydrates. Compressibility in the gas can enhance thrust behind hydrate plug, while compressibility in the hydrates can increase compaction and increase projectile risk.

$$C_a = \frac{\rho_g v_g^2}{E_v} = \frac{\text{inertia force}}{\text{compressibility force}} \quad (7.6)$$

$$E_v = \frac{dp}{d\rho/\rho} \quad (7.7)$$

where E_v is the bulk modulus (Pa); ρ_g is the gas density (kg/m^3); v_g is the gas velocity (m/s); dp is change in pipeline pressure (Pa); and $d\rho$ change in density (kg/m^3). From equation 7.6, as the gas bulk modulus increases, the gas compressibility force increases because of increasing line pack. Although the gas density also increases, the inertia force diminishes as the velocity of the gas molecules reduces. The compressibility force will also increase the gas density by reducing the volume occupied by 1 kg mass of the gas. Since the temperature of the pipeline is assumed to be isothermal during hydrates formation, it is assumed that equation 7.8 holds.

$$\frac{p}{\rho} = K \quad (7.8)$$

where p is the gas pressure (Pa); ρ is the density (kg/m^3) and K is a constant. Implying from equation 7.8 that as the gas density increases because of increasing line pack during hydrates plugging the pipeline, the gas bulk modulus will also increase (Munson et al. 2013), leading to a rise in the transient pressure drop. To observe the compressibility of the gas upstream of the hydrate plug, the relationship between the ratio of change in transient pressure and density as the transient pressure drop increases is presented in **Figure 7.10**. The gas and hydrates densities have been computed from equations 3.46 and 7.3 respectively.

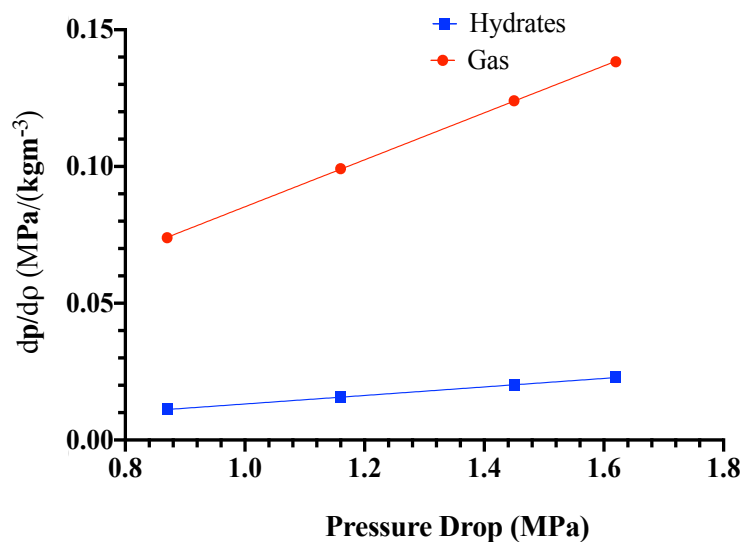


Figure 7.10: The hydraulic effect of transient pressure drop on the ratio of pressure drop to change in density at constant temperature of 285 K when the hydrate plug is located 500 m downstream of the hydrate equilibrium point along the pipeline.

From **Figure 7.10**, the transient pressure drop behind the hydrate plug is positively related to compressibility of the gas and hydrates. However, the gas experiences higher compressibility than the hydrates, which is expected from theory because of the low density of gas. This effect is responsible for the projectile thrust experienced in gas pipelines plugged by hydrates when the pressure upstream of the hydrates plug is higher than the downstream pressure. **Figure 7.11** indicates that the bulk modulus of the deposited hydrates on the pipe wall increases linearly as the transient pressure increases due to increasing operating pressure. The implication of this graph

is to explain how hydrate transportability and hydrate plugs can be achieved through the control of compressor discharge pressure.

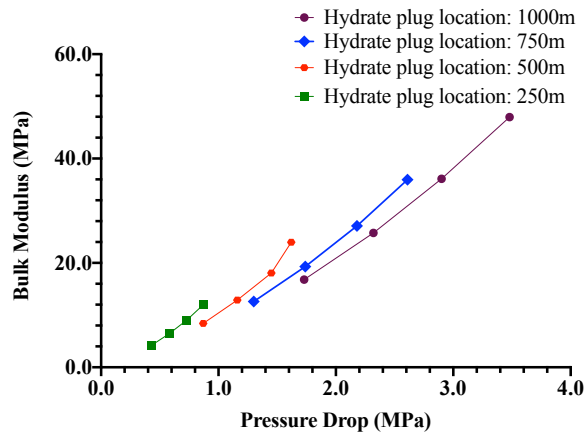


Figure 7.11: The hydraulic effect of transient pressure drop on bulk modulus of hydrates as the gas pressure was increased from 4-7 MPa at constant temperature 285 K and various hydrate plug location downstream of the hydrate equilibrium condition along the pipeline.

The indication in **Figure 7.11** implies that reducing the bulk modulus can enhance hydrates dissociation, detachment from the wall and transportability. Also, inferred from **Figure 7.11** is the fact that if continuous increase in pressure drop is experienced, the plug location is farther away from the equilibrium position with higher resistance to flow, and increased hydrate plug projectile risk.

7.3.6 Hydraulic Effect of Hydrate Plug Location on Shear Rate and Shear Stress

The shear stress determines how much differential pressure is needed to release the hydrate plug or enable transportability of hydrates in the pipeline (McMullen 2011). The relationship between shear stress and bulk modulus is important in understanding the transportability of hydrates. The shear stress of the deposited hydrates defines the possibility of hydrates sloughing and pipeline wall shedding by hydrate deposits. Shear stress σ (Pa) is defined as follows.

$$\sigma = \eta \dot{s} = \eta \frac{1}{\rho} \frac{d\rho}{dt} \quad (7.9)$$

To relate the shear stress to the bulk modulus, equation 7.7 was defined in terms of ρ . Then, equation 7.9 can be written as below.

$$\sigma = \eta \frac{1}{E_v} \frac{dp}{dt} \quad (7.10)$$

where η is the viscosity of hydrates (Pa.s); and \dot{s} is the shear rate ($\dot{s} = \frac{1}{E_v} \frac{\Delta p}{\Delta t}$) of the deposited hydrates (1/s). In **Figure 7.12** below, a negative relationship is observed between the shear rate and the bulk modulus of the deposited hydrate plug at the same transient pressure drop. The relationship was more of a curve at lower pressure drop and when the hydrate plug location was 250m, which became linear as the distance of the hydrate plug was farther at 1000m. Implying that hydrates transportability reduces as the bulk modulus increases. Thus, the reduction in shear rate is responsible for the growth of hydrate plugs as their location is further away from the hydrate equilibrium point along the gas pipeline.

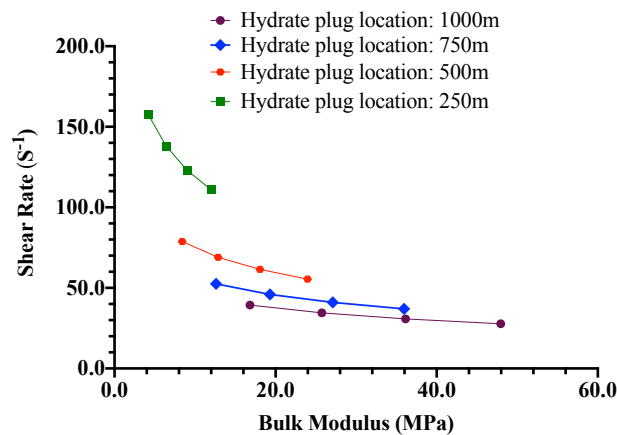


Figure 7.12: The hydraulic effect of bulk modulus on shear rate at constant temperature 285 K at various hydrate plug locations.

Hence, longer hydrates plug are expected as their location increases along the gas pipeline. The higher shear rate for hydrate plugs closer to the equilibrium point is due to hydrates sloughing and wall shedding phenomenon. This is because of the presence of higher kinetic activity of the gas molecules leading to higher liquid and hydrate loading. However, as the plugging event is further from the equilibrium point, more dispersed water is consumed in the formation of hydrates deposits and reducing the hydraulic

gradient, until the plugging event leads to increasing transient pressures. Hence, since bulk modulus is positively related to transient pressure drop, the shear rate is also negatively related to transient pressure drop as seen in **Figure 7.13**.

Lower shear rate can also be experienced by the hydrate deposit/plug due to lower deformation because the hydrates glides over a thin layer of water on the wall of the pipe (McMullen 2011). However, this scenario cannot lead to very high transient pressure drop because of the relative motion of the plug, in response to the gas compression behind the plug. The bulk modulus measures the pressure drop with respect to the strain in the hydrate layer/plug (**Figure 7.13**).

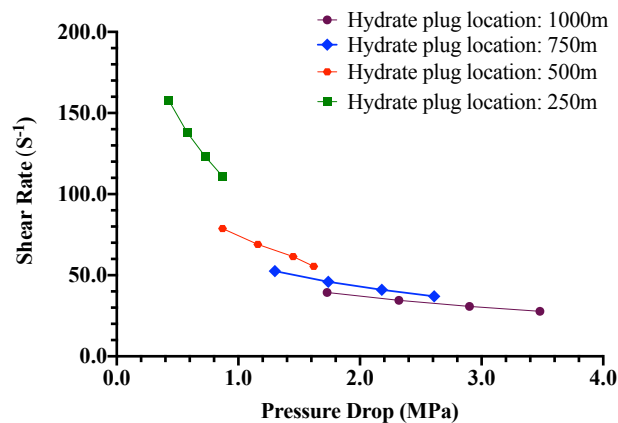


Figure 7.13: Comparing the hydraulic effect of pressure drop on shear rate at constant temperature of 285K and varying hydrate plug location along the gas pipeline.

As observed in **Figure 7.13**, the increase in pressure drop is because the shear rate reduces, implying higher resistance to flow and deformation. Thus, for the range of operating pressures of 4-7 MPa considered, shear rate decreases as the distance of the hydrate plug increases from the equilibrium position, implying increased plugging risk. The indication in **Figure 7.13**, suggests that for shorter pipelines hydrates deposits can be removed by increasing flow to increase the loading of hydrate particles. For longer pipelines, there is the need to estimate the pressure and temperature of dissociation and the force upstream of the flow to enable transportability of hydrate deposits and plugs.

To explain the phenomenon of hydrates shear stress and the thrust behind the hydrate plug (Equation 7.5), the viscosity of hydrates is first obtained. In this study, the viscosity of hydrates is regressed using the relation developed in equation 7.11 from the experimental measurements of the viscosity of hydrates in the literature (Pandey, Linga and Sangwai 2017).

$$\eta_H = C_{\eta_H} (0.6954T - 7.977 \times 10^{-6}P - 0.09314\dot{S} + 191\alpha_w) \begin{cases} \dot{S}: 1 - 200, & C_{\eta_H} = 0.447 - 2.0 \times 10^{-3}\dot{S} \\ \dot{S}: 200 - 600, & C_{\eta_H} = 0.066 - 1.1 \times 10^{-4}\dot{S} \\ \dot{S}: 600 - 1000, & C_{\eta_H} = 2.89 \times 10^{-3} \end{cases} \quad (7.11)$$

where, η_H is the viscosity of hydrates and C_{η_H} is an empirical constant, and other parameters have retained their earlier definitions. **Figure 7.14** was obtained by simulating the transient pressure drop (Equation 3.52) for the temperature, pressure, and water volume fraction. The shear rate is defined from equation 7.10 which is also related to the transient pressure drop obtained using equation 3.52, and the results are entered as inputs into equation 7.11.

The curves in **Figure 7.14** indicates that the viscosity increases at lower pressure drop and when the hydrate location was closer to the source of hydrates generation and increases as the hydrate plug distance and transient pressure drop increases.

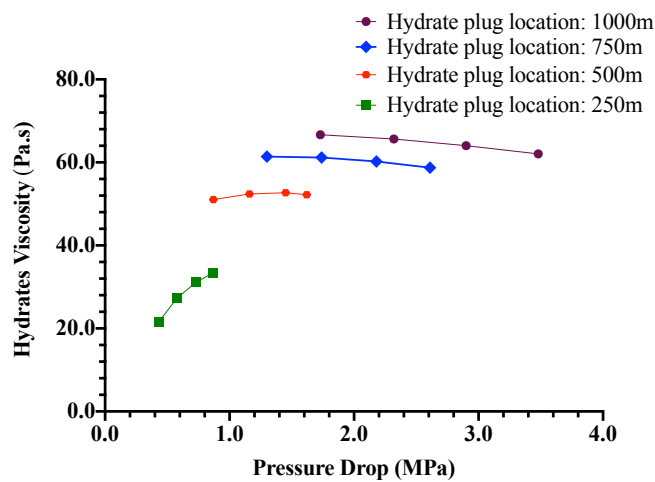


Figure 7.14: Comparing the hydraulic effect of transient pressure drop on the viscosity of hydrate at constant temperature of 285K and varying hydrate plug distance downstream of the hydrates generation point.

From **Figure 7.14**, it is observed that at lower pressure drop (0-1.5MPa) the viscosity increases with increase in transient pressure until the point (beyond 1.5MPa) when the viscosity decreases with increase in pressure. This phenomenon is corroborated from the experimental measurement of the viscosity of water (Schmelzer, Zanotto and Fokin 2005), and since the high density of hydrate is as a result of water molecules, it is expected that the viscosity of hydrates will behave in similar manner. Hence, the shear stress of the deposited hydrates is obtained using equation 7.9 in **Figure 7.15**.

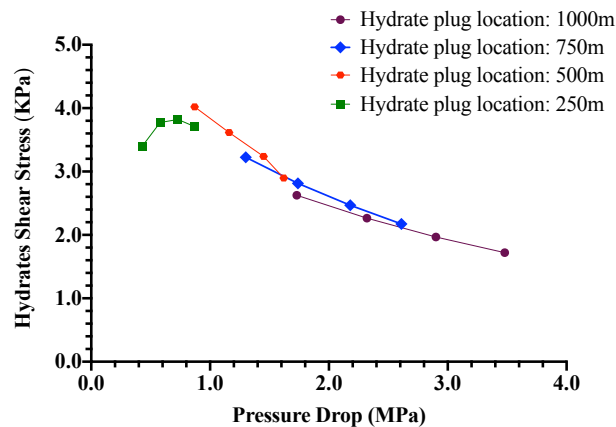


Figure 7.15. Comparing the hydraulic effect of transient pressure drop on the hydrates shear stress at constant temperature of 285K and varying hydrate plug location beyond the hydrate’s generation point.

The same effect of viscosity at lower pressure and when the hydrate plug location is closer to the point of hydrates generation along the pipeline (**Figure 7.14**), is observed for the hydrate shear stress curves in **Figure 7.15** because of the positive relationship between shear stress and viscosity (Equation 7.9). Theoretically, higher pressure drop is the result of lower shear stress in the flow domain as the pipeline length increases (Munson et al. 2013). This observation is also asserted in **Figure 7.15**.

Lower shear stress indicates poor transportability, and increased plugging severity, while higher shear stress indicates reduced plugging severity. Once the hydrate plug is stuck in the pipeline, the pressure drop increases and the shear stress reduces. Thus, hydrates sloughing, and wall shedding is possible when the hydrates deposit and plug location is closer to the source of hydrate generation. In section 7.3.7 the estimated hydrate shear stress was used to

determine the thrust needed to move the hydrate plug along the pipeline. This will help to estimate the pressure needed upstream of the hydrate plug.

7.3.7 Effect of Hydrate Plug Location on Hydraulic Thrust Upstream of the Hydrate Plug

By assuming that the hydrates plug experiences normal stress on the upstream cross-sectional surface, equation 7.3 can be applied to determine the density of the hydrate. Thereafter, equation 7.3 will be used to determine the hydrate velocity (**Figure 7.16**). The relationship between the hydrate plug velocity is related to the hydrate shear stress in equation 7.3.

$$\frac{F}{A} = \sigma = \rho_H v^2 \quad (7.12)$$

Defining equation 7.12 in terms of v , yields:

$$v = \sqrt{\frac{\sigma}{\rho_H}} \quad (7.13)$$

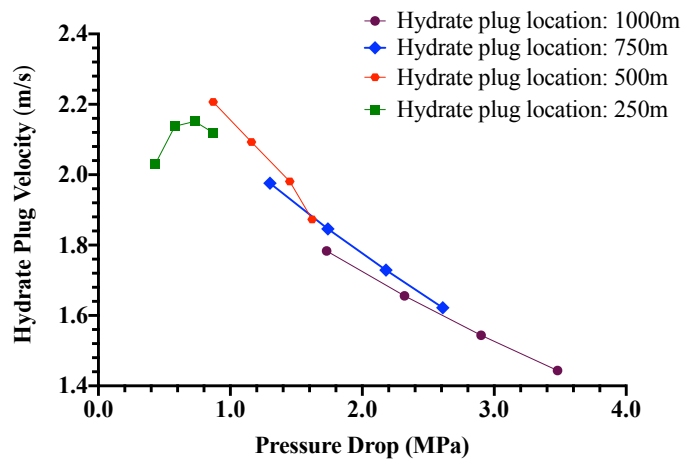


Figure 7.16: Comparing the hydraulic effect of pressure drop on the hydrates plug velocity at constant temperature of 285K and varying hydrate plug location downstream of the hydrates equilibrium condition point along the pipeline.

The observation in **Figure 7.16** is like the effect of shear stress on pressure drop discussed earlier. The increase in velocity of the hydrate plug located 250 m from the hydrate equilibrium position was positive until the transient

pressure drop of 0.8 MPa, after which the velocity reduced as the viscosity increases and shear stress reduced. According to Newton’s second law of motion, the change in momentum of the hydrate plug is driven by the gas upstream of the plug, hence a reduction in the velocity of the gas which happens when the hydrate plug location is farther from the compressor discharge point equally leads to a reduction in the velocity of the hydrate plug. Also, in accordance with Newton’s third law, there is equal and opposite reaction between the compressing gas and the hydrate plug, hence the compressive effect of the gas phase on the hydrate plug is in response to how much resistance the hydrate plug offers to the flow. This is also seen in the velocity of the plugs at each section investigated in **Figure 7.16**.

The thrust from the gas on the hydrate plug increases as the transient pressure drop increases, leading to more line-packed gas and a reduction of kinetic movement within the gas molecules upstream of the hydrate plug. In **Figure 7.17**, the thrust on the hydrate plug increased in like manner as the velocity and shear stress discussed earlier, when the hydrate plug location was at 250 m until the pressure drop value of 0.8 MPa. This is because the thrust is reduced due to increase in the bulk modulus of the hydrate plug.

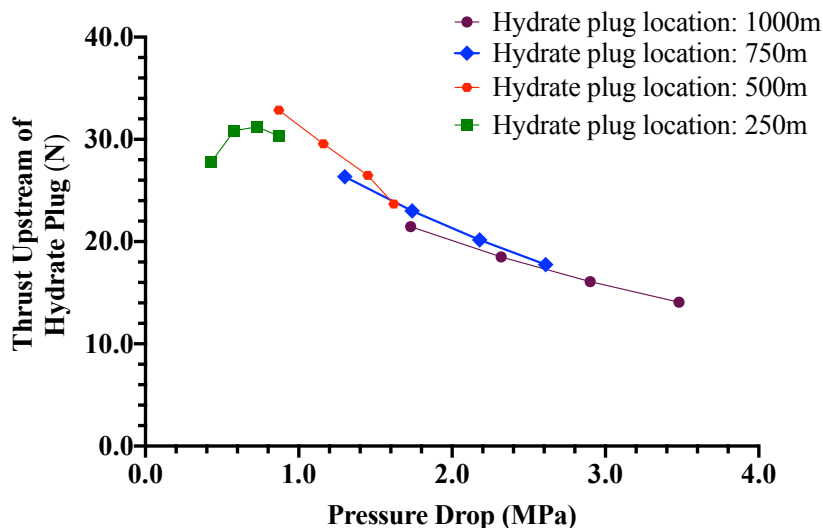


Figure 7.17: Comparing the hydraulic effect of pressure drop on the hydraulic thrust upstream of the hydrate plugs located at temperature of 285K and varying hydrate plug location downstream of the hydrates generation point along the pipeline.

The implication from **Figure 7.17** is the fact that since thrust decreases as the hydrate plug location is farther from the hydrate generation point, it is important to prevent hydrates settling on the base of the riser through early monitoring of hydrates formation. This way, the pipeline can be shut down once there are indications of increasing intermittent transient pressure drop which is the evidence of hydrates sloughing and wall shedding.

As stated in the assumptions for the development of our transient pressure drop model (Equation 3.52), hydrates sloughing, and wall shedding was neglected to enhance proactive prediction of hydrates plugging risk. Since higher pressure drop increases the risk of hydrate plugging event, the pressure drop must be continuously monitored to observe transient events. This approach can be modified to what work best for the specific field application. The pressure for the transportability analysis can be obtained as proposed in **Figure 7.3** earlier.

7.4 Hydraulic Flow Parameters for Locating Hydrate Plug

From **Table 7.4** presented earlier, the following parameters are directly related to the location of hydrate plugs. Temperature is not included because the system is isothermal once hydrates are deposited on the pipeline wall.

Hence,

$$L_{H_plug} = f(P, v_H, E_v, \sigma_H, \dot{s}) \quad (7.14)$$

Therefore, the rate of change of the location of the plug can be defined in relation to the rate of change of the parameters on the RHS of equation 7.14:

$$\frac{dL_{H_plug}}{dt} = \frac{dP}{dt} + \frac{dv_H}{dt} + \frac{dE_v}{dt} + \frac{d\sigma_H}{dt} + \frac{d\dot{s}}{dt} \quad (7.15)$$

Once the pipeline is blocked by hydrate plug at the location L_{H_plug} , other time-dependent parameters tend to "zero" except the transient pressure drop $\left(\frac{dP}{dt}\right)$. The consequence is that the location of the hydrate can now be predicted from $\frac{dP}{dt}$ only. Theoretically, depending on the gas flow velocity, hydrates are generated at the horizontal section of the pipeline and will

normally plug the base of the riser. Assuming the riser base is located about 70 m away from the point of hydrates generation, once the deposition rate is determined, it is possible to use the hydrate deposition rate to simulate various sectional length upstream of the plug as basis for locating hydrate plug.

Alternatively, readings from pressure and temperature sensors described in detail in section 7.6 can be used in the prediction of hydrates location by following the approach discussed. By assuming that single hydrate plug forms at these sections, monitoring the transient pressure drop upstream of the plug through a plot of transient pressure drop versus pipeline length, as indicated in **Figure 7.18**, can assist in locating the hydrate plug.

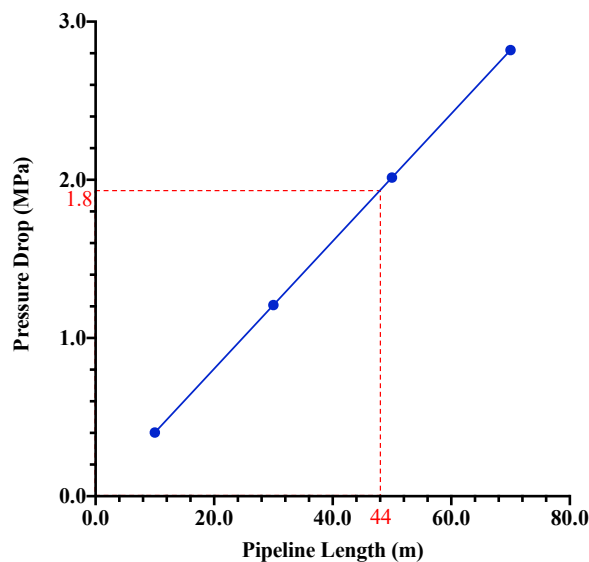


Figure 7.18: Locating hydrates plug at gas velocity of 8.7 m/s, and pipeline temperature of 287.5K and pressure of 10.9 MPa.

As shown in **Figure 7.18**, if the pressure drop is about 1.8 MPa the hydrate plug can be located about 44 m downstream of the hydrate generation point. The hydrates generation point (0.0) is the location along the pipeline where the temperature is equal to the hydrates equilibrium temperature, provided the pressure is equal to or above the hydrates equilibrium pressure. This location can also be determined using subsea temperature probes and transmitters installed on the pipeline. Therefore, this study proposes equation 7.3 for locating the position of hydrate plugs based on the resulting

transient pressure drop along the gas pipeline. How this model can be implemented for this purpose is discussed further in section 7.5.

7.5 Hydrates Plug Location Prediction Table

From the understanding in **Figure 7.18**, a table of hydrates plug locations can be developed as presented below. For field application, this table can be developed for any candidate pipeline experiencing hydrates to predict plug locations from the point of hydrates equilibrium temperature, if the pipeline pressure is greater than or equal to the equilibrium pressure. Hydrates equilibrium temperature T_{eq} (K) can be estimated using the relation developed by Sloan and Koh (Sloan and Koh 2007) for a range of methane hydrates temperature from 0 to 25°C (Equation 7.16).

$$P_{eq} = \exp\left(38.98 - \frac{8534}{T_{eq}}\right) \quad (7.16)$$

where P_{eq} is the equilibrium pressure (KPa). **Table 7.5** is populated for a pipeline with diameters of 4 inch (0.102m) and 6inch (0.152m), and 1 km in length, with the hydrates plug locations set at 0.2, 0.4, 0.6, 0.8 and 1 km. The riser is located 1 km downstream of the hydrate equilibrium point along the pipeline. The system pressure is greater than the equilibrium pressure condition for methane hydrates. The temperature of the hydrate plug is within the stable hydrate zone of the methane hydrate loci in **Figure 7.4**. Pipeline is gas-dominated with temperature of 292K at the equilibrium location; hence flow velocity and pressure are that of the gas behind the hydrates plug. **Figure 7.19** is derived from **Table 7.5** and **7.6** below. The transient pressure drop at each plug location is compared at velocity of 4 m/s and 8 m/s and for diameters of 0.102 m and 0.152 m.

Table 7.5: Hydrates plug location prediction at hydrates deposition rate of 10L/min

Hydrates Dep. Rate – $\dot{Q}_{H,d}$: 10L/min		Pressure – P :8.9MPa			Gas Temperature – T : 292K	
Vel. - V_g (m/s)	Pipe Dia. - D (m)	Pressure Drop - dp , MPa (Plugging Flowtime - t_{plug} , hr)				
		0.2km	0.4km	0.6km	0.8km	1km
4	0.102	0.24 (1.45)	0.47 (2.91)	0.71 (4.36)	0.94 (5.81)	1.18 (7.26)
	0.152	0.15 (3.22)	0.30 (6.45)	0.45 (9.68)	0.60 (12.91)	0.75 (16.13)
8	0.102	0.87 (1.45)	1.74 (2.91)	2.61 (4.36)	3.48 (5.81)	4.36 (7.26)
	0.152	0.56 (3.23)	1.11 (6.45)	1.67 (9.68)	2.23 (12.91)	2.78 (16.13)

Table 7.6: Hydrates plug location prediction at hydrates deposition rate of 20L/min

Hydrates Dep. Rate – $\dot{Q}_{H,d}$: 20L/min		Pressure – P :8.9MPa			Gas Temperature – T : 292K	
Vel. - V_g (m/s)	Pipe Dia. - D (m)	Pressure Drop - dp , MPa (Plugging Flowtime - t_{plug} , hr)				
		0.2km	0.4km	0.6km	0.8km	1km
4	0.102	0.24 (0.73)	0.47 (1.45)	0.70 (2.18)	0.94 (2.91)	1.18 (3.63)
	0.152	0.15 (1.61)	0.30 (3.23)	0.45 (4.84)	0.60 (6.45)	0.75 (8.07)
8	0.102	0.87 (0.73)	1.74 (1.45)	2.61 (2.18)	3.48 (2.91)	4.36 (3.63)
	0.152	0.56 (1.61)	1.11 (3.23)	1.67 (4.84)	2.23 (6.45)	2.78 (8.07)

The results in **Table 7.5** and **7.6** illustrates that the pressure drop at the hydrates plug locations under the same pipeline diameter and flow conditions is similar despite increasing the hydrates deposition rate. However, the time to plug the pipeline at each location reduces as the hydrates deposition rate

increases. Under the same gas velocity, inlet pressure and temperature, and pipeline diameter, increase in hydrates deposition rate by a factor of 2 reduces the plugging time by the similar factor. The implication of this is the need to improve hydrates intervention frequency during lower pipeline surrounding temperatures, because hydrate deposition increases with increasing subcooling temperatures.

In the industry, this kind of table can be developed for a candidate pipeline to relate pressure drop and time of flow to hydrates plug location along the horizontal section of the pipeline. The above simulation results demonstrate how the transient pressure drop model developed in this study can be used to locate the position of hydrate plugs based on the transient pressure drop and the time to the commencement of the plugging event. **Figure 7.19** below is the representation of the effect of plugging location on transient pressure drop when the hydrate deposition rate is 10 L/min.

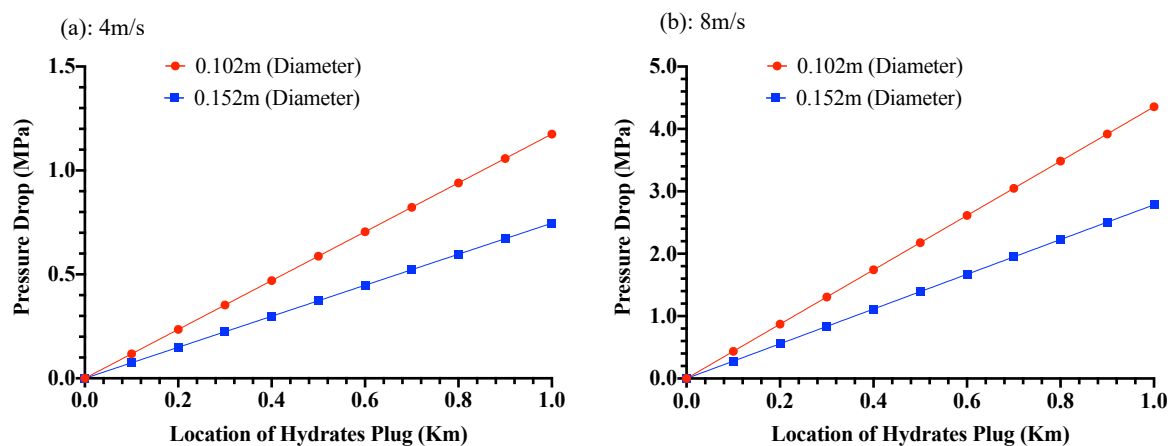


Figure 7.19: Comparing transient pressure drop at gas velocities of 4 m/s and 8 m/s with respect to the plugging distance when the hydrates deposition rate is 10 L/min.

As suggested from **Figure 7.19**, the transient pressure drop is positively related to the location of hydrate plugs. If this kind of graph is plotted for a candidate pipeline as also suggested earlier in **Figure 7.18**, the reading of the transient pressure drop can be used to predict the location of the hydrate plug. In section 7.6, this study propose a schematic of a real-time arrangement for predicting hydrate plug location in conjunction with the approach described in this section.

7.6 Hydrates Plug Location Prediction Steps

Figure 7.20 is a proposed hydrate forming and plugging pipeline section, installed with sensors for recording the temperatures and pressures in the pipeline, as these are the main real-time parameters needed by the models to predict the hydrates plug location. A real-time monitor registers the pressure fluctuations and temperature along with the time of flow. The time of flow starts when the pressure sensor indicates that the flow has achieved the operating pressure. The temperature plot is observed for a uniform temperature profile, which indicates hydrates formation, and the pressure plot is observed for a continuous rise in pressure. The pressure sensor is located at the hydrate equilibrium point predicted from hydraulic flow simulators and superimposing the temperature curve predicted by equation 7.16. The temperature sensor is located along the pipeline to obtain the average temperature along the hydrate forming section.

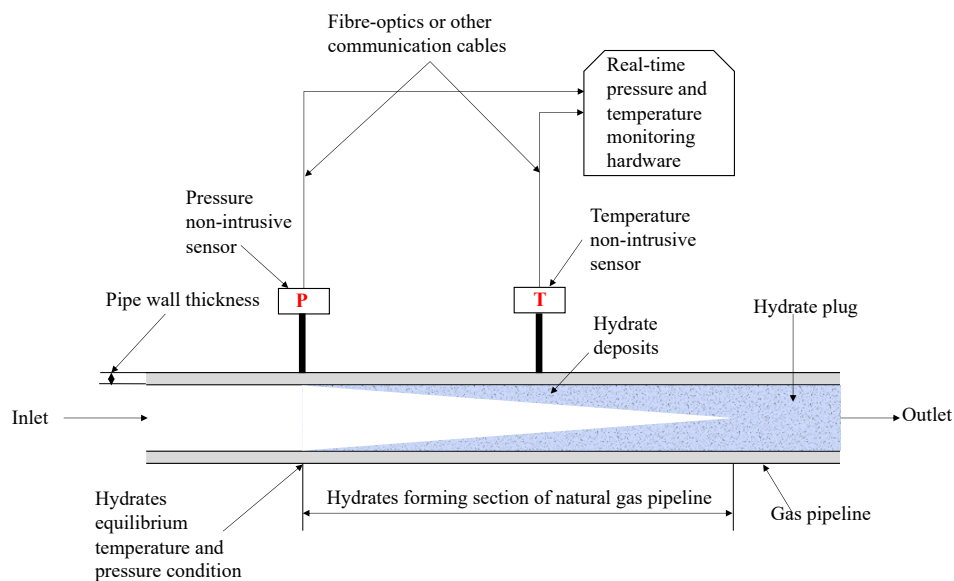


Figure 7.20: Proposed hardware installation on gas pipeline for real-time data transfer for hydrates plug location detection

The proposed steps for using the readings from the arrangement in **Figure 7.20** to predict the hydrates plug location are presented as follows:

- (i) Determine the pipeline hydrate equilibrium location by superimposing the equilibrium temperature determined from equation 7.3 on the operating temperature gradient for the pipeline.
- (ii) Simulate the deposition rate using the validated hydrates deposition rate model in chapter 4. The regression model (Equation 7.3) in chapter 6 can also be used.
- (iii) With the predicted deposition rate, determine the time to plug the candidate pipeline at the riser base (Equation 7.3).
- (iv) Determine the transient pressure drop from equation 7.3 by using predetermined hydrate plug locations along the pipeline as discussed extensively in sections 7.4 and 7.5.
- (v) Plot the profile of the transient pressure drop at predetermined hydrate plug location as discussed in section 7.5 and develop a table similar to **Table 7.5** or **7.6**.
- (vi) Plot a graph of transient pressure drop against the predetermined hydrates plug location.
- (vii) Monitor real-time pressure and temperature data from the pipeline using the arrangement in **Figure 7.20**.
- (viii) Obtain the real-time transient pressure drop (Pa) at time (s) when the first significant pressure spike is above the maximum operating pressure or pipeline design pressure.
- (ix) Compare the result with the plot of transient pressure versus hydrate plug location in step v to locate the probable hydrates plug location.
- (x) If the plug location predicted by the models is earlier or later than the actual position in the pipeline, the transient pressure drop model (Equation 7.3) should be calibrated appropriately to enhance the accuracy and consistency of future predictions by the model.

Also, to dissociate the deposited hydrates and transport the hydrates plug out of the pipeline, the following steps have been proposed:

- (i) Estimate the hydrate density using equation 7.3.
- (ii) Determine safe pressure and temperature to enhance transportability as described in **Figure 7.3**, where the density estimated from equation 7.3 is above the density of water (998kg/m³).

- (iii) Follow approved procedure to retrieve plug after depressurisation to the pressure determined from the previous step.
- (iv) Determine thrust to free the hydrate plug and push the plug along the horizontal section of the pipeline as discussed in section 7.3.7 of this chapter. For hydrates moving up the riser, the effect of gravity must be included, as this was not within the scope of this study.

7.7 Chapter Summary

Accurate prediction of the hydraulic effect of hydrate deposition and plug location is critical to the safety and operability of natural gas transport pipelines, especially for subsea gas transport pipelines where maintenance and intervention activities are more difficult. Hydraulic pressure drop analytical models exist in the literature for predicting the effect of hydrates deposition on the pipeline pressure because of reduction in pipeline hydraulic diameter. However, the existing models did not directly include the hydrates deposition rate in the pressure drop equation, making it difficult to directly investigate the effect of hydrates deposition rates on transient pressure drop. Also, the need to estimate the plugging time at various hydrates deposition rates requires another analytical model, which was lacking in the literature.

To close the identified gaps, the approach proposed in this study directly incorporates the hydrates deposition rate for gas-dominated pipeline in one mathematical relation and developed another model for the time to plug the pipeline hydrates section. The basic assumption behind the transient pressure drop model is to stop gas flow once the first spike in pressure drop is recorded as a precautionary measure. By using only one multiplier factor which is a function of the gas velocity, this model is an improvement over the analytical model of (Di Lorenzo et al. 2018) because it proves to be more adaptable for industry application without having to change the multiplier factor under various flow velocity.

The transient pressure drop predictions for all six cases at both high and low velocity are within 4% relative error (mean relative error of 2.3%). Similar predictions by (Di Lorenzo et al. 2018) were within 40% relative error. Also, the mean relative error of the transient pressure drop predictions by (Zhang

et al. 2019) was 7.43%. As a proactive hydrate plugging preventive analytical tool, it is essential that the model can “underpredict” the experimental plugging flowtime at the experimental transient pressure drop in the literature, which was also achieved with the models for all the six cases simulated for model validation.

Hence, the model is an improvement over existing analytical hydrates plugging pressure drop prediction models. New models for estimating the density and viscosity of hydrates were also developed in this work. Approach to determining the location of hydrate plug was also proposed, as hydrates plug location can be predicted from a tabular chart developed from both models for various hydrates deposition rates. This can be achieved by comparing the upstream pressures from pressure transmitters with the predictions from the models at specific flowtime from the onset of hydrates formation.

More importantly, because the pressure drop model incorporates the hydrates deposition rate directly, it is invaluable in real-time tracking of hydrates deposition volume when the pipeline is fitted with temperature and pressure transmitters. Hence, for practical application, the arrangement provided in section 7.6 for monitoring real-time pipeline pressure and temperature is advised for implementation to aid the detection of hydrate plug location.

In addition to the verification and improved performance of the models, their capability was extended to predict hydrates plug locations along the pipeline by assuming that a single hydrate plug exists in the pipeline at any given flowtime. The results suggest that pipeline plugging flowtime reduces as the hydrates deposition rate increases, and that the pressure drop and plugging flowtime increases along the length of the pipeline.

The main implications from the results of this study reveals the following:

- a. This work is an improvement over existing pressure drop predicting models for gas hydrates pipelines at 4% maximum relative error compared with 40% by the model of (Di Lorenzo et al. 2018) and 7.43% by the model of (Zhang et al. 2019).

- b. A new model to predict hydrates plugging flowtime for proactive intervention in gas-dominant pipelines has been developed, which underpredicts the experimental plugging time by a mean relative error of 9%. Thus, in alignment with the philosophy of proactive predictive intervention.
- c. By incorporating the hydrates deposition rate into the models, the predictions can capture real-time plugging events.
- d. This study also developed two other models: (i) hydrate density estimation model; and (ii) hydrate viscosity estimation model. These models were used in the parametric analysis that provided further insights into the hydraulic effect of transient pressure drop on the physical parameters of hydrates.
- e. Hydrates plug location has been predicted from a tabular chart for various hydrates deposition rates. By comparing the upstream pressure reports with the predictions from the model at specific flowtime from the onset of hydrates formation, the location of the hydrates plug can be predicted in field application.
- f. Therefore, for practical application, it is proposed that the arrangement for real-time monitoring of pipeline pressure and temperature can be implemented. To predict hydrates plugging risks and plug location.

CHAPTER 8: PREDICTING HYDRATES PLUGGING RISK: CASE STUDY

8.0 Introduction

Estimating the risk of hydrates plugging and mitigating the risk is not a straightforward science. Whereas other researchers have estimated this risk in aiding the planning of intervention programs, none had addressed this risk based on plugging flowtime. This was achieved through the combination of two earlier validated CFD and analytical model in this doctoral work that can predict the hydrates deposition rate, the plugging flowtime and the transient pressure drop. Through a detailed proactive predictive plugging risk mitigation algorithm, the plugging risks are classified into low, medium, and high risk. A monthly pigging frequency was set as the medium threshold, whereas the estimated plugging time less or higher than this threshold was considered low or high risk respectively. The approach suggested in this study can enhance the planning of hydrates intervention programs.

Global consumption of natural gas in 2020 was 4.4 trillion cubic meters (BP 2020), and it is not likely that the figure is going to reduce drastically in favour of renewables. The use of gas as a low-carbon energy source has been favoured because of increasing concern for the environment and climate change campaigns. Until there are enough renewables and biofuels that can meet the increasing energy demand of the world, natural gas will continue to be the energy source of choice compared to crude oil and coal. Ensuring the delivery of natural gas through pipelines to the point of utilisation is a flow assurance concern, as this effort can be compromised by the presence of ice-like crystals known as gas-hydrates.

Generally, hydrates in gas-dominated pipelines form at high gas pressure and low temperature. Other conditions include the right turbulence, presence of water either as film on the pipe wall or dispersed in the continuous gas phase (Aman et al. 2016; Wang et al. 2017). Extensive discussion on hydrates forming conditions and controls are presented in the literature (Koh et al. 2011; Carroll 2014). However, estimating the risk of hydrates plugging and mitigation in gas-dominated pipelines is not a straightforward science.

Hydrates plugging risk drives hydrates intervention and management activities in the oil and gas industry (Zerpa et al. 2012; Kinnari et al. 2015).

In gas pipelines, hydrates plugging risks increases under two main scenario: (i) increasing velocity at constant subcooling temperature, and (ii) increasing subcooling temperatures and constant gas flow velocity (Di Lorenzo et al. 2014a; Aman et al. 2016). Research emphasis in gas hydrates formation, agglomeration, wall deposition, and pipeline blockage has increased in the last decade with significant contributions from experimental (e.g., Aman et al., 2016; Di Lorenzo et al., 2014b, 2014a; Liu et al., 2020; Odutola et al., 2017), analytical (e.g., Di Lorenzo et al., 2018; Liu et al., 2019; Wang et al., 2018, 2017; Umuteme et al., 2021), and computational fluid dynamics (CFD) modelling (e.g., Berrouk et al., 2020; Neto et al., 2016; Sule et al., 2015; Umuteme et al., 2021).

Major findings from these studies include: (i) deposition rates prediction, (ii) hydrates-induced trainset pressure drop prediction, (iii) delayed reduction in pipe plugging due to hydrates sloughing and wall shedding, (iv) increasing hydrates formation and deposition at constant velocity and increasing subcooling temperatures, (v) increasing hydrates formation and deposition at constant subcooling temperature and increasing velocity, (vi) increase in hydrates deposition by a similar ratio of increase in pipe diameter under the same boundary condition, and (vii) impact of chemical injection on hydrate stability. What is left is to demonstrate in principle how the above findings can be applied to enhance the design, safe operations and maintenance intervention of hydrate plugging pipelines in an industrial scale. This is to mitigate the risk of hydrates plugs in the field, which includes pipeline isolation, very high intervention cost, loss of revenue, reputation, litigations and accidents (Sloan 2011; Carroll 2014).

So far, managing hydrates in the industry include the application of thermal, chemical and mechanical approaches. Further classification of hydrates control include prediction, prevention and problem-solving (Kinnari et al. 2015). Previous studies shows that insufficient amount of injection can lead to hydrates adhering to the wall of the pipe (Kinnari et al. 2015). Also, from a flow hydraulics perspective, methanol can lead to high gas losses due to

the ease of evaporation. Again, monoethylene glycol (MEG) can inhibit flow due to high viscosity (Palermo and Sloan 2011). Accurate predictive models are more cost effective than experiments (Sloan, Koh and Sum 2011a). Thus, with accurate prediction of plugging risks the performance of both thermal and chemical controls can be enhanced and applied where needed.

Studies have also emphasised the need for natural transportability of hydrates in pipelines without external control measures as a way of optimizing the operational strategies of existing production facilities (Sloan, Koh and Sum 2011b; Di Lorenzo et al. 2014a; Kinnari et al. 2015). This can amount to savings in operating costs if the outcome of the studies so far is implementable in the industry. However, the main gap in the literature is still on enhancing the capability of predictive models for field application in pipeline safety design (Duan et al. 2022). Hydrates intervention relies on transient pressure drop for limit state design based on reliability (probabilistic) theory and the need to plan mechanical intervention programs based on predicted pipeline plugging flowtime.

An attempt to classify the plugging risk level for a candidate pipeline was suggested in the literature (Zerpa et al. 2012). Since, hydrates transportability depends on water content in the gas and the subcooling temperature, a wetting index has been developed by Statoil ASA as a way of classifying hydrates risks quantitatively (Kinnari et al. 2015). Also, in a recent risk classification (Duan et al. 2022), emphasis was still on how flowrate, water droplet diameter, heat transfer, inlet temperature, and outlet pressure influence pipe blockage by hydrates. However, the risk classification needs to be extended to the plugging flowtime and transient pressure drop criteria. The plugging flowtime is needed for proactive intervention and preventive mechanistic measures such as pigging, while the transient pressure drop criterion is important as advisory input into pipeline strength design to ensure the selection of the right wall thickness.

Therefore, the purpose of this chapter is to demonstrate the capability of the CFD model (chapter 4) and analytical models (chapter 7) in predicting hydrates plugging risk in offshore gas-dominated pipelines. I have also extended the study to provide advisory information for a proposed 30 Km

offshore-onshore gas delivery pipelines. As a result, the four-fold objectives include to predict hydrates deposition rates, plugging flowtime, the transient pressure drop and the risk level classification. On the first objective, accurate prediction of hydrates deposition rate allows for the estimation of the operational do-nothing period before the pipeline is plugged.

The second objective is important in the planning of intervention and cleaning activities. On the third objective, accurate prediction of the expected transient pressure drop in combination with the plugging flowtime predicted in the second objective enables the operator to watch out for signs of pressure spikes. The final objective is an attempt to use the criterion of plugging flowtime and transient pressure drop in classifying the risk level.

Again, this activity can be carried out during the design of new lines by using the maximum transient pressure drop estimated in the estimation of the pipe wall thickness. The remainder of this chapter is presented as follows. Section 8.1 discusses the adopted stages hydrates severity investigation. Section 8.2 provides the details of the case study and any studies done so far; section 8.3 presents the results and the discussion of the findings; and section 8.4 presents the conclusion of the findings. A chapter summary is provided also.

8.1 Stages of Proposed Hydrates Severity Investigation

The stages inquiry leading to evidence-based decision making is proposed as indicated in **Figure 8.1**. Each of the stages above will be discussed further in the sub-sections that follows.

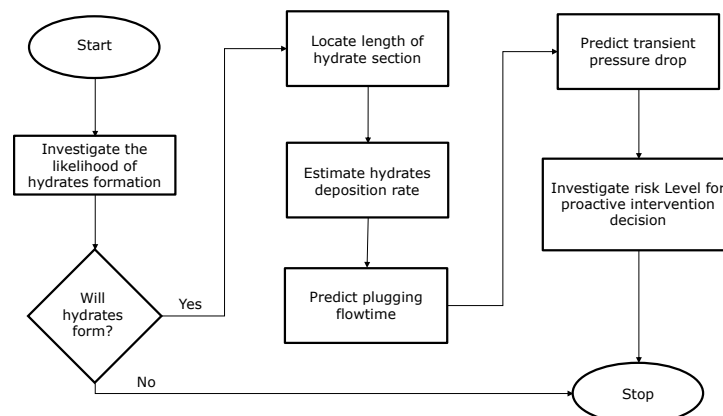


Figure 8.1: Proactive hydrates plugging risk investigative framework

This investigative framework can be done once in a quarter or once there is change in operating condition, such as increase or decrease in gas demand, or maloperation in gas dehydration process allowing for excess water into the pipeline outside the contractually agreed specification.

8.1.1 Investigating Hydrates Formation

Hydrates formation in gas pipelines can be investigated through the boundary conditions necessary for its formation and stability discussed extensively in the literature (Sloan and Koh 2007; Carroll 2014). These conditions include low temperature at or below the equilibrium hydrates formation temperature and high pressure at or above the equilibrium pressure, the right turbulence and presence of water in the gas and nucleation zones.

Parametric variations of gas velocity (turbulence) and subcooling temperatures impacts the rates of formation, agglomeration, and deposition (Aman 2021; Duan et al. 2022). Since natural gas hydrates can form with water mole fraction as low as 0.05 (Sloan and Koh 2007), the possibility of hydrates formation in the pipeline can be ascertained from a phase envelop, which is a thermodynamic analysis of the composition of the gas to display the phase behaviour of the gas under different flow condition (Sloan and Koh 2007; Carroll 2014).

Based on the temperature and pressure profile predicted from a pipeline flow hydraulic simulator, the calculated equilibrium pressure is compared with the pressure gradient along the pipeline. For hydrates to form in the pipeline, the difference between the pressure gradient and the hydrates equilibrium pressure at the corresponding temperature must be equal or above "zero." The equilibrium pressure for methane hydrates is estimated from the relation developed in Sloan and Koh (2007, p. 193) at 0 to 25°C.

$$P_{eq} = \exp\left(38.98 - \frac{8534}{T_{eq}}\right) \quad (8.1)$$

where, P_{eq} is the equilibrium pressure for methane hydrate formation (KPa). Once hydrates are predicted, the next step is to locate the hydrates section along the pipeline.

8.1.2 Locate Pipeline Hydrates Section

The length of the hydrates section is located by superimposing the calculated equilibrium pressure from equation 8.1 for the corresponding pipeline temperature on the pressure gradient curve. The interception point of both pressures is traced down to the distance along the pipeline. The position of the hydrate plug is downstream of this point (Carroll 2014). From that point to the riser base is the hydrates section, as indicated in **Figure 8.2**.

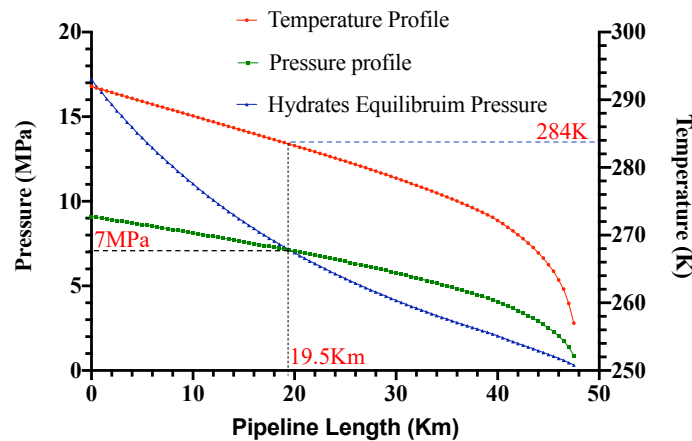


Figure 8.2: Locating pipeline hydrates section

8.1.3 Estimating Hydrates Deposition Rates

Hydrates deposition rate is predicted using the validated CFD model developed in chapter 4 or the regression model in chapter 6. The CFD model computational domain 10 m length by 0.0204 m diameter pipe section. The solution was achieved using the eulerian-eulerian multiphase framework, with Reynolds-Average-Navier-Stokes (RANS) momentum equation and kinetic-epsilon turbulence models. The predicted results were within 10% uncertainty bound and compared more favourable with experimental results at lower velocity of 4.7 m/s than the analytical model of (Di Lorenzo et al. 2018). From the sensitivity simulation of the effect of increase in diameter on hydrates deposition rates under the same flow boundary condition,

developed equation 8.2 to predict the hydrates deposition rate in an industrial scale pipeline.

$$Q_{h_d2} = K_{ex_factor} \cdot \frac{D_2}{D_1} \cdot Q_{h_d1} \quad (8.2)$$

where Q_{h_d1} (L/min) is the CFD model predicted hydrates deposition rate; Q_{h_d2} (L/min) is the estimated deposition rate for pipeline size; D_1 (m) is the CFD model pipe diameter, 0.0204 m; D_2 (m) is the pipeline diameter; and K_{ex_factor} is a dimensionless extrapolation factor, which can be adjusted from field studies for more accurate predictions. In this work, 1.1 is adopted as K_{ex_factor} . Details of the model development and parametric analysis been discussed in chapter 4. However, the regression model developed in chapter 6 do not require the size scaling and will be adopted going forward.

8.1.4 Predicting Hydrates Plugging Flowtime

The hydrates plugging flowtime, is the time from when the hydrates forming gas gets to the nucleation point to when the first hydrates-induced significant spike in pressure is expected. This corresponds to the time lag between hydrates nucleation to hydrates plugging. It is calculated from the analytical model (Equation (8.3)), developed in chapter 7 and presented below.

$$t_{plug} = K_{ft} \frac{\Pi \cdot D^2 \cdot L}{6 \dot{Q}_{H,d}} \quad (8.3)$$

where: t_{plug} (s), is the plugging flowtime; K_{ft} is a dimensionless factor with a value of 0.8; L (m); D (m) pipeline diameter; $\dot{Q}_{H,d}$ (m³/s). The plugging flowtime influences the transient pressure drop as discussed next.

8.1.5 Predicting Transient Pressure Drop

The purpose of predicting the transient pressure drop is to investigate the risk of equipment damage from excessive incidental pressure. Whereas pipeline safety recognises incidental transient pressure because of sudden valve closures or surge in gas flow due to equipment malfunctioning, the gradual reduction in the pipe hydraulic diameter can lead to build up of

transient pressure, which can be above the incidental pressure. In accordance with industry practice (DNVGL-ST-F101 2017), the maximum allowable incidental pressure (MAIP) is set at 10% above the maximum allowable operating pressure (MAOP) is set below (5%) the pipeline design pressure (DP). In estimating the hydrates-induced transient pressure drop, I have employed the mathematical relation developed in chapter 3, section 3.3, as restated in equation 8.4.

$$dp_n = \frac{K_H}{2D} \cdot f \cdot \rho_g \cdot \frac{6v_g^2 L \dot{Q}_{H,d}}{(\pi D^2 L - 6\dot{Q}_{H,d} t_n)} \cdot t_{plug} \quad (8.4)$$

8.1.6 Investigating Risk Level for Proactive Intervention Decision

The consequences of hydrates plugging in pipelines are always high, hence the plugging risk mitigation is only addressed by assessing the likelihood of occurrence. Three risk levels have been suggested in the literature (Zerpa et al. 2012), based on the ease of transportability to the riser as follows: (i) low-risk (easy flowing slurry), when the pressure drop is less than 2 MPa (300 psi), hydrate volume fraction is less than 0.10 and when the hydrates slurry viscosity is less than 10; (ii) intermediate-risk (slurry flow can be hindered by restrictions or change in pipe geometry leading to line plugging), when the pressure drop is less than 3.45 MPa (500 psi); hydrate volume fraction is greater than 0.1 but less than 0.40 and the hydrates slurry viscosity is greater than 10 but less than 100; and (iii) high-risk (highly viscous flow and easily plugs line) - when the pressure drop is greater than 3.45 MPa (500 psi); hydrate volume fraction is greater than 0.40 and the hydrates slurry viscosity is greater less than 100. This is the most extensive risk classification so far in the literature. However, the above risk definition was developed for oil and condensate pipelines.

From the risk definition above, there are still concerns on how to measure hydrates viscosity and volume fraction in a subsea gas pipeline. Thus, classifying plugging risk based on the above three conditions can be addressed from the estimation of plugging flowtime and the first significant transient pressure drop for the specific gas pipeline using the models developed so far in this study. Flowtime and pressure drop estimation forms

the basis for the risk regime adopted in this work. Among the approaches in hydrates prevention and problem solving is pipeline pigging, which is a mechanical approach. Therefore, this study have developed a conservative plugging risk criteria for mechanical intervention. Beyond the above classification, this research improved the plugging risk from the angle of the cost of operation based on the frequency of pipeline pigging intervention. A six-monthly baseline pigging operation frequency is adopted for intermediate risk (medium risk).

Plugging flowtime below the six-monthly threshold is considered high risk and beyond one year is considered low risk. Pressure drop above the pipeline MAOP, but less than 5% the MAOP is set as medium risk hydrates induced pressure drop; at or less than the MAOP is low risk, and greater than 5% above the MAOP is considered high risk operation. The above designation of hydrates plugging risks is to ensure the proactive intervention philosophy of this research for the safety of the pipeline.

The MAOP criterion informs the need to estimate the mechanical wall thickness of the pipe or the selection of a pipe with a specified minimum yield strength (SMYS) to overcome the transient pressure rise based on the anticipation of hydrates deposition. For existing pipelines, MAOP sets the criterion for shutting off gas supply to allow for mechanical pigging. Also considered is risk based on operating cost, where low risk is normal planned operating cost, up to 5% increase in operating cost is considered medium risk, and above 5% increase in operating cost is considered high risk.

The plugging flowtime is dependent on the length of the horizontal section from the point of hydrates nucleation to the point of plugging, such as riser base or rising undulating profile along the seabed. For longer pipelines, the plugging flowtime may not be a reasonable criterion, hence the need to compare with the pressure rise. The safe pressure band is between the MAOP and the maximum allowable incidental pressure (MAIP) or below the MAOP. Below the MAOP is the maximum operating pressure (MOP), which is usually set at 5% below the MAOP. However, there is need for the industry to improve on the cost-related risk designation. The proposed risk classification in this study presented in **Table 8.1**.

Table 8.1: Criteria for classifying hydrates plugging risk

Hydrates Plugging Risk Classification	Pipeline Hydraulics-Based Hydrates Plugging Risk Criteria	Cost Regime Risk Criteria	Mechanical Intervention
Low-Risk	Predicted plugging flowtime is equal to or greater than one year; Predicted transient pressure rise is equal to or less than MAOP	Normal planned operating cost	Yearly mechanical pigging intervention
Medium-Risk	Predicted plugging flowtime is greater than six months but less than one year; Predicted transient pressure rise is greater than MAOP but less than 5% above MAOP	Up to 5% increase in operating cost	Six-monthly mechanical pigging intervention
High-Risk	Predicted plugging flowtime is less than or equal to six months; Predicted transient pressure is greater than 5% above MAOP	Up to 10% increase in operating cost. There is need for further control measures based on cost assessment. These can include re-design of wall thickness for fresh lines and increasing the pigging frequency for already installed lines	Monthly or quarterly mechanical pigging intervention. For new lines, redesign wall thickness or select a higher SMYS pipe based on realistic hydrates influenced operating pressure

The MAOP is usually the design pressure (DP). 10% above this pressure is the maximum allowable incidental pressure (MAIP) to accommodate for short transient pressure rise due to compressor ramp up, for instance. However, from literature reports, hydrates plugging sequence involves sloughing and there is the tendency that the transient behaviour induced by hydrate plugs can be above the MAIP. The proposed risk classification in **Table 8.1** can ensure the proactive monitoring of the pipeline within the safe operating designed pressure band. Based on the bounded classification above, a breakdown of each risk classification and categories of classification is presented in **Table 8.2**.

Table 8.2: Breakdown of hydrates plugging risk by categories of measurement

	Low-Risk	Medium-Risk	High-Risk
Transient Pressure Rise	Predicted transient pressure rise is equal to or less than MAOP	Predicted transient pressure rise is greater than MAOP but less than 5% above MAOP	Predicted transient pressure is greater than 5% above MAOP
Pigging Flowtime	Predicted plugging flowtime is equal to or greater than one year	Predicted plugging flowtime is greater than six months but less than one year	Predicted plugging flowtime is less than or equal to six months
Intervention Cost	Normal planned operating cost	Up to 5% increase in operating cost	Up to 10% increase in operating cost.

8.2 Case Study

As part of the African road map to energy sufficiency by 2030, a 30km pipeline is proposed to transport natural gas from the Gazelle field in Côte d'Ivoire to a receiving station for processing (Marfo, Opoku Appau and Kpami 2018). The thermodynamic analysis of the gas composition (**Table 8.3**) indicates the possibility of hydrates formation. In a previous study by Marfo et al. (2018), the authors established the hydrates formation temperature as 292K and the gas landing pressure at the processing facility as 800 Psia(5.5MPa). Also, to optimise pipeline heat isolation from the environment and improve hydrates-free gas delivery, the authors recommended a 0.75 inch insulation material with a conductivity of 0.15 Btu/hr/ft/°F on a designed pipe size of 10 inch to satisfy the delivery pressure requirement, and 0.5 inch pipewall thickness for pressure containment.

However, the authors reported that the insulation thickness will not prevent hydrates in the pipeline, even as the thickness of the thermal insulation was increased to 1 inch. To mitigate against the risk of hydrates formation and its attendant effects, an additional direct electric heating (DEH) system was recommended to raise the external pipewall temperature to 300K. The gas flowrate at maximum production is projected as 50 MMSCFD and 20 MMSCFD maximum turndown.

The design questions are: (i) what happens if the DEH system becomes faulty? should the line be shut down immediately, or the pipeline can be operated for a period before the DEH system becomes operational? (ii) is it possible to avoid the DEH system and concentrate on routine mechanical cleaning while installing a re-gasification system as end-of-pipe solution at the receiving end? The purpose of the quantitative and analytical investigation in this section is to demonstrate the capability of the models discussed earlier in providing advisory input to enhance the management of hydrates in the proposed 30 km offshore gas pipeline.

Table 8.3: Gas Composition

Component	Methane	Nitrogen	Carbon (IV) oxide	Ethane	Propane	i-Butane	n-Butane	i-Pentane	n-Pentane	n-Hexane
Moles	92.23	2.1411	0.5483	2.832	1.1232	0.2855	0.2984	0.1319	0.0938	0.3159

With 92.23% methane gas, the hydrate is formed mainly by methane. The molar mass of the gas stream is approximately 18 kg/kmol and specific gravity of 0.6. The gas composition includes 10% (bbl/bbl) water content. **Figure 8.2** presents the calculated equilibrium pressure for methane hydrates, superimposed on the pressure and temperature gradients obtained from the literature for the 30 km pipeline with 0.75 inch insulation and without the DEH system.

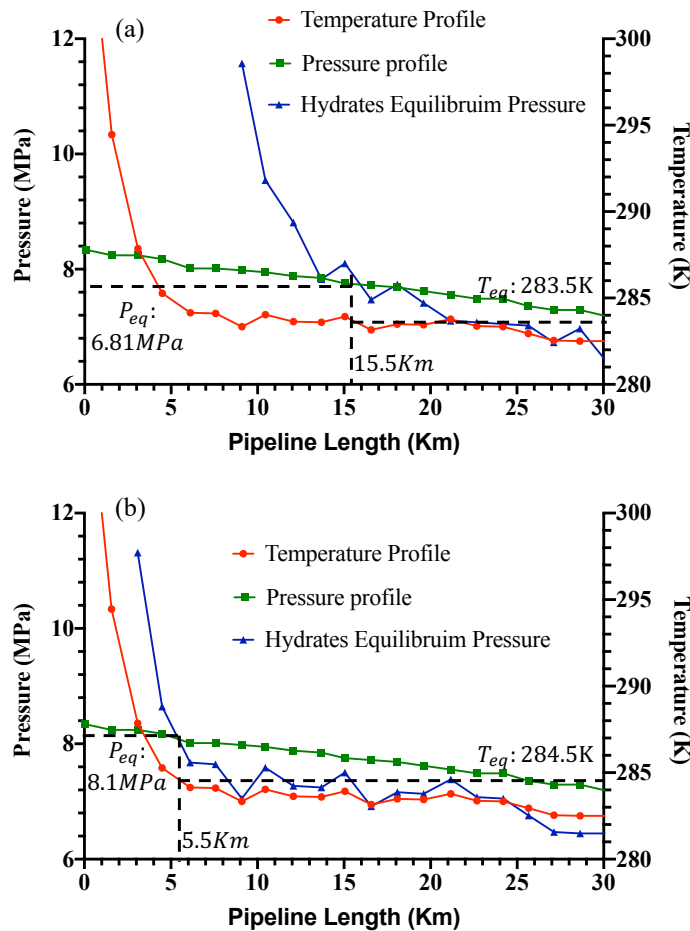


Figure 8.3: Locating the hydrates section: (a) at 50MMSCFD; (b) at 20MMSCFD

The results from **Figure 8.3** above are corroborated in the literature (Aman et al. 2016), that at lower volumetric flow rate (low gas velocity) and the same pipe diameter and boundary conditions, hydrates plugs the main line earlier than at higher volumetric flow rate (high gas velocity). At both gas flow regime, hydrates nucleation distance from the riser base are 14.5Km and 24.5Km at both high and low gas volumetric flow rate respectively. The

input data for the analysis based on steps discussed earlier are derived from the case study. The needed input data are presented in **Table 8.4** below. Gas velocity is calculated using the formular (Equation (8.5)) in the literature (Mohitpour, Golshan and Murray 2007).

$$v_{g(m/s)} = \frac{Q_g \cdot P_{ref} \cdot T_g}{\frac{\pi D^2}{4} \cdot T_{ref} \cdot P_g} \quad (8.5)$$

Where: P_{ref} and T_{ref} are reference pressure (0.1MPa) and temperature (288K) standard conditions for the natural gas industry; Q_g , is for gas flowrate (m³/s); T_g is gas temperature (K); P_g is gas average pressure (MPa); and D pipe diameter (m). 0.33 m³/s has been converted to 1 MMSCFD, with a reference temperature of 288K. The input data into the models are stated below.

Table 8.4: Input variables for CFD and analytical model simulation

Parameter	Q_g :50MMSCFD (16.5m ³ /s)	Q_g :20MMSCFD (6.6m ³ /s)
Hydrates Formation Temperature (K)	283.50	284.50
Hydrates Formation Pressure (MPa)	7.61	8.20
Gas Velocity (m/s)	4.33	1.60
Pipeline Diameter (m)	0.254	0.254
Hydrates Section (m)	14.5	24.5
Max. Allowable Operating Pressure (MAOP)/Design Pressure (MPa)	8.3	8.3

All other inputs into the CFD model are from **Table 3.1**-4.4 in chapter 4. The CFD and analytical models' analysis presented for this case study are for both high and low velocities scenario.

8.3 Results and Discussion

8.3.1 Likelihood of Hydrates in Pipeline

Without the DEH system, hydrates formation is predicted at 283.5K and 7.61 MPa at a distance 14.5 km from the base of the riser in the direction of flow at 50MMSCFD. Similarly, at 20 MMSCFD hydrates will commence at 284.5K and 8.2 MPa at a distance 24.5 km from the base of the riser in the direction

of flow. There is a 1K temperature increase at the hydrates start point when the flow reduced from 50 MMSCFD to 20 MMSCFD, this is because of a reduction in turbulence leading to a reduction in heat dissipation. The calculated temperature-pressure dependent density of gas (Equation (3.46)) at the point of hydrates initiation along the line for both high and low flow are 72.7 kg/m³ and 79.3 kg/m³, respectively.

8.3.2 Hydrates Section Length

From **Figure 8.3**, the hydrates section lengths are: 14.5Km at 50MMSCFD and 24.5Km at 20MMSCFD, representing 48.3% and 81.7% of the pipeline length respectively. Thus, at maximum gas production the likely point of hydrate plug is the riser base while at low flow it is expected that hydrates plugs will be along the pipeline. Implying there is need for increased intervention frequency at low flow. However, this will be confirmed after the plugging flowtime is calculated for both flow rates.

8.3.3 Deposition Rate

The hydrates deposition rates predicted by the regression model (Equation 8.6) developed earlier as Equation 6.4 in chapter 6, the deposition rate can be calculated as 1.72 L/min at 50 MMSCFD and 1.65 L/min at 20 MMSCFD. The regression results are more realistic for a proactive prediction of hydrates plugging risk because the regression model has been derived from 81 data sets. With these values and the data in **Table 8.4**, the plugging flowtime will now be estimated in the next section.

$$\dot{Q}_{hd} = 0.0163V + 0.0252\Delta T - 3.4127\alpha_w + 7.3412D - 0.0845 \quad (8.6)$$

8.3.4 Plugging Flowtime and Transient Pressure Drop

The plugging flowtime is predicted using the data in **Table 8.4** and the regression model predictions of hydrates deposition rates at both high and low flow scenario. The plugging flowtime and transient pressure drop depends on the time-varying hydraulic diameter of the pipe due to hydrates deposition.

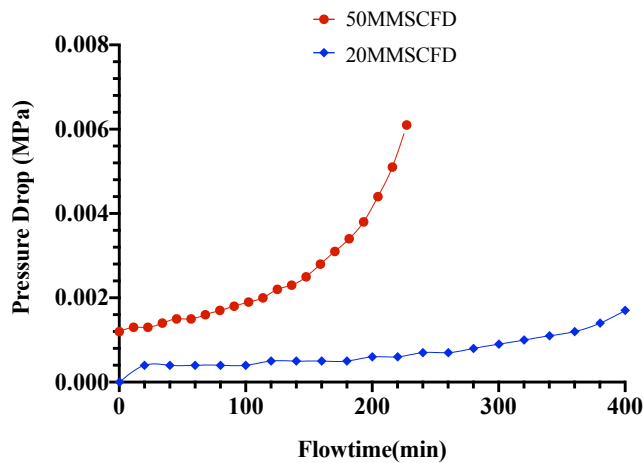


Figure 8.4: Transient Pressure Drop and Plugging Flowtime Predictions at 50 MMSCFD and 20 MMSCFD for the data in **Table 8.4**.

The plot above indicates how long it will take to plug the riser if the pipeline is operated without DEH system. The plugging risk investigation suggests that the pipeline cannot be operated without the DEH system as the pipeline is susceptible to hydrates plugging risk in within 227 min (approximately 4 hours) of operation at maximum flow of 50 MMSCFD and 400 min (approximately 7 hours) of operation at low flow of 20 MMSCFD. The estimated values for the density of hydrates in both flow scenario using equation 7.3 are 1132.6 kg/m³ and 1091.2 kg/m³, respectively. Implying high transportability of hydrates because the density of the hydrates formed are greater than that of water, as disused in section 7.2.

However, the frequency of mechanical cleaning is less than six-monthly which will not be cost effective. Details of this investigation are presented in appendix B as simulated in the MATLAB code (appendix A) that was developed in this study in the next chapter. Further analysis of the associated risk level and possible intervention options are discussed below based on the criteria set in **Table 8.1** and **8.2**.

8.3.5 Risk Level Estimation

As stated earlier, it is important to investigate the rise in pressure compared with the MAOP. From the given design pressure, 5% MAOP is 8.7MPa and 10% MAOP is 9.1 MPa. Implying that the allowable incidental transient pressure drop is 1.1 MPa to ensure continuous pipeline safety. The indication

from **Figure 8.4** is that at the transient pressure drop are within safe values, however since the pipeline is plugging in few hours, there will be rise in pressure outside safe operational limits. However, since the hydrates are transportable provided the water volume fraction is not decreasing, the hydrates could be transported to regasification facilities onshore. The higher density of hydrates and low transient pressure drop indicates less adhesion of hydrates to the wall of the pipeline. If the flow continues to be driven by inertia force, then it is possible that the hydrates can be transported for regasification.

Table 8.5: Overall hydrates plugging risk classification for the case study

	Low-Risk	Medium-Risk	High-Risk
Transient Pressure Rise	Predicted transient pressure rise is equal to or less than MAOP	Predicted transient pressure rise is greater than MAOP but less than 5% above MAOP	Predicted transient pressure is greater than 5% above MAOP
Plugging Flowtime	Predicted plugging flowtime is equal to or greater than one year	Predicted plugging flowtime is greater than six months but less than one year	Predicted plugging flowtime is less than or equal to six months
Intervention Cost	Normal planned operating cost	Up to 5% increase in operating cost	Up to 10% increase in operating cost
Overall Risk Classification	High-Risk		

The volume of hydrates generated is 3 times the deposition rate, as discussed in chapter 6 and 7 earlier. During the proposed pigging activity, the expected monthly volume of hydrates will be 75000 L (75kg) and 71000 L (71kg) of hydrates at both high and low flow scenario, respectively. Therefore, the decision to pig the pipeline must be compared with the cost of the DEH system and the re-gasification plant that must be installed at the receiving end-of-pipe facility during the economic feasibility study of the options.

8.4 Chapter Summary

This chapter have demonstrated the capability of the models developed in in this study in providing professional and quality advisory information that can enhance pipeline wall thickness design based on expected transit pressures

and pigging schedule. For the case study, the design and operational recommendations are as follows:

- a. If the continuous reliability of the DEH system cannot be 100%, it is important to consider a burst limit state design to increase the pipeline wall thickness to handle the transient pressure drop arising from pipeline plugging by hydrate deposits.
- b. A minimum pigging volume of 75kg at high flow and 71kg at low flow should be expected monthly. Therefore, it is important to consider the cost of monthly pigging activity and the cost of installing a receiving re-gasification facility at the end-of-pipe solution to handle the volume of hydrates.

The questions asked earlier can now be answered as follows: (i) if the DEH system becomes faulty, the pipeline cannot be operated because of high risk of hydrates plugging events. (ii) the pipeline can be operated without the DEH system provided a re-gasification unit is installed at the receiving facility to handle the volume of hydrates generated during the monthly pigging activities.

CHAPTER 9: MATLAB CODE FOR HYDRATES PLUGGING RISK PREDICTIVE (HPRP) MODEL FOR SUBSEA GAS PIPELINES

9.0 Introduction

The need to develop a computer code that can estimate plugging risk based on hydrates deposition rates and pressure drop is imminent. This can be inferred from the previous studies that have attempted to use computer codes in predicting hydrates forming temperatures. For instance, Merey and Sinayuc (2016) developed a MATLAB code for easily predicting the properties of hydrates using the formulas of Mann et al. (1989). The code was developed for each of the properties investigated (e.g., molecular weight, density, enthalpy of hydrate dissociation) using reservoir condition. The results revealed the ease of using computer programming codes such as MATLAB in modelling hydrate prediction equations with reliable accuracy.

The study have also adopted this line of reasoning in providing a MATLAB program for predicting hydrates plugging risk from the equations developed in this study. He (2022) developed extremely randomized stochastic hydrate formation temperature prediction model using 1000 experimental data points. However, this model is unable to predict the expected hydrates plugging time, pressure drop and transportability. Other recent studies where computer programming was adopted in the prediction of hydrates formation conditions include neural network modelling in the literature (El-hoshoudy et al. 2021; Nasir et al. 2022).

The new MATLAB code developed in this chapter provides a one-page handy report for intervention planning and schedules, and a means for ranking hydrates forming pipelines based on plugging severity. The rest of this chapter is structured as follows. Section 9.1 discusses the methodology, which includes the development of the plugging risk prediction algorithm, the equations, and risk definition. Section 9.2 validates the predictions of the HPRP model. Section 9.3 provides the outcome of the parametric studies and section 9.4 provide a concluding session on the chapter.

This chapter developed a hydrates plugging risk predictive (HPRP) model using MATLAB code built on the regression and analytical models developed in earlier chapter 6 and 7. The purpose is to have a computer code that can provide a one-pager report on the risk of hydrates in subsea pipelines. A sample of the output is provided in appendix B, which include the description of the pipeline, input data, calculated flowtime and transient pressure drop, a table of output values for the density of gas and hydrates, hydrates deposition rates and maximum pressure drop. The report also includes the risk classification and if the hydrates can be transported easily to surface processing facilities. Also, validation and critical parametric sensitivity studies were carried out to compare the results with observation in chapter 4, 6 and 7.

9.1 HPRP Model Algorithm

The HPRP algorithm is a flowchart that outlines the computational and logical steps coded in MATLAB.

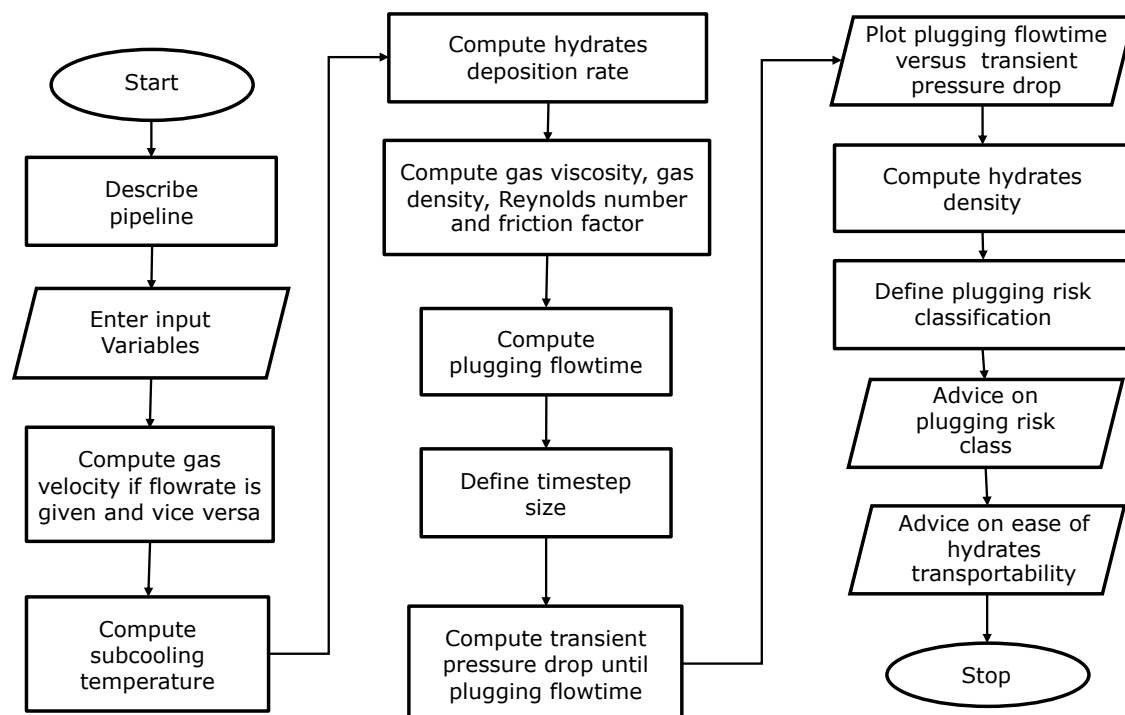


Figure 9.1: Algorithm for HPRP MATLAB code

The next section will be used to define the equations.

9.2 Equations

The main equations developed in this study are defined as follows. Credits for equations not unique to this study have also been cited accordingly in chapter 3, 6 and 7.

Hydrates deposition rate equation

The hydrates deposition rate regression equation was developed from 81 simulated data sets from the CFD model developed in chapter 4, and unique to this study. The equation is stated as follows:

$$\dot{Q}_{hd} = 0.0163V + 0.0252\Delta T - 3.4127\alpha_w + 7.3412D - 0.0845 \quad (9.1)$$

Plugging flowtime equation

The time to plug the pipeline based on the estimated hydrates deposition rate was developed in chapter 3, and unique to this study. This equation is stated as follows:

$$t_{plug} = K_{ft} \frac{\Pi \cdot D^2 \cdot L}{6\dot{Q}_{H,d}} \quad (9.2)$$

Transient pressure drop equation

The transient pressure drop equation is based on the estimated hydrates deposition rate and plugging flowtime and was also developed in chapter 3, and unique to this study. This equation is stated as follows:

$$dp_n = \frac{K_H}{2D} \cdot f \cdot \rho_g \cdot \frac{6v_g^2 L \dot{Q}_{H,d}}{(\Pi \cdot D^2 L - 6\dot{Q}_{H,d} t_n)} \cdot t_{plug} \quad (9.3)$$

Hydrates density estimation equation

The equation for estimating the density of hydrates was based on the simulated results of the CFD model in chapter 4, and was also developed in chapter 7, and unique to this study. This equation is stated as follows:

$$\rho_H = C_{\rho_H} \left[(\alpha_g \rho_g + \alpha_w \rho_w) + \frac{2\alpha_g \rho_g \cdot \alpha_w \rho_w}{\alpha_g \rho_g + \alpha_w \rho_w} \right] \quad (9.4)$$

$$C_{\rho_H} = 0.0325T - 1.985 \times 10^{-8}P - 3.0 \quad (9.5)$$

Gas velocity equation

The equation for estimating the velocity of the gas when the flowrate is given was retrieved from Mohitpour, Golshan and Murray (2007). The equation is provided below.

$$v_{g(m/s)} = \frac{Q_g \cdot P_{ref} \cdot T_g}{\frac{\pi D^2}{4} \cdot T_{ref} \cdot P_g} \quad (9.6)$$

Pipeline friction factor equation

The friction factor equation for smooth pipes was retrieved from Drew, Koo and McAdams (1932). This equation is given below.

$$f = 0.0056 + 0.5Re^{-0.32}; 3000 < Re < 3 \times 10^6 \quad (9.7)$$

Gas viscosity and density equation

The equations for estimating the pressure and temperature dependent gas density and viscosity were retrieved from (Di Lorenzo et al. 2018). Both equations have been provided below.

$$\eta_g = 6.45 \times 10^{-9}T + 7.36 \times 10^{-13}P + 5.555 \times 10^{-6} \quad (9.8)$$

$$\rho_g = -1.27 \times 10^{-7}PT + 0.49T + 4.79 \times 10^{-5}P - 156 \quad (9.9)$$

Reynolds number

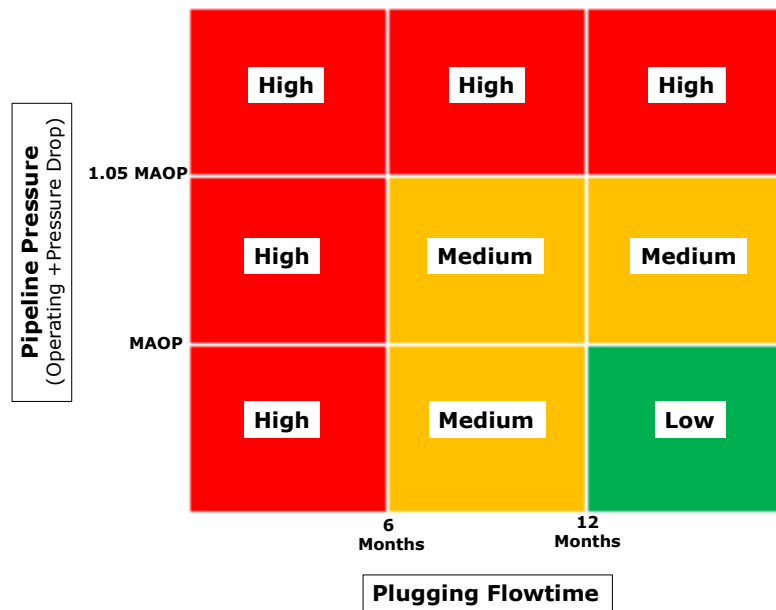
The Reynolds number was computed using the equation available in the fluid mechanics textbook by (Munson et al. 2013). However, this equation is also available in the public domain.

$$Re = \frac{\rho_g v_g D}{\eta_g} \quad (9.10)$$

9.3 Hydrates Plugging Risk Definition

The plugging risk definition provided in **Table 9.1** was developed based on the earlier risk classifications and definitions in **Table 8.1** and **Table 8.2**, which are also unique to this study.

Table 9.1: Hydrate plugging risk matrix



9.4 HPRP Model Validation

The MATLAB code is provided in appendix A. The validation of the code was achieved with the same experimental data used to validate the CFD, analytical and regression models in chapters 4, 6 and 8, respectively. The essence of this validation is to carry out a quality check on the code and ensure the program successfully predict hydrate plugging risk. Conditions for proactive predictions have been defined as follows. (i) The plugging time predicted by the HPRP MATLAB code must be less than the experimental plugging time, and (ii) the pressure drop predicted by the HPRP MATLAB code must be greater than the experimental pressure drop.

Table 9.2: Comparing model predictions with experimental results by Aman et al. (2016) at 4.6m/s

Exp.	Gas Press. (MPa)	Gas Temp. (K)	Sub-cooling, (K)	Hyd. Dep. Rate, (L/min)	Plugging Flowtime, t_{plug} (min)		Pressure Drop, dp (MPa)		
					Exp.	MATLAB Model	Exp.	MATLAB Model	Relative Error (%)
1	10.79	286.0	6.0	0.078 (0.087)	76.37	67.17	0.41	0.43	5
2	10.91	284.4	7.3	0.105 (0.119)	68.43	48.75	0.41	0.44	7

Table 9.3: Comparing model predictions with experimental results by (Di Lorenzo et al. 2014a) at 8.7m/s

Exp.	Gas Press. (MPa)	Gas Temp. (K)	Sub-cooling, (K)	Hyd. Dep. Rate, (L/min)*	Plugging Flowtime, t_{plug} (min)		Pressure Drop, dp (MPa)		
					Exp.	MATLAB Model	Exp.	MATLAB Model	Relative Error (%)
1	9.07	292.5	5.83	0.129 (0.137)	41.52	42.62	1.03	1.12	9
2	8.99	292.5	5.94	0.147 (0.139)	41.46	41.77	1.04	1.11	7
3	8.43	292.0	10.3	0.369 (0.262)	22.49	22.23	1.01	1.05	4
4	8.83	292.5	8.6	0.207 (0.207)	31.21	28.21	1.01	1.10	9

*Values in parenthesis are hydrates deposition rates computed by the HPRP MATLAB code

The estimated flowtime should be less than the experimental time for a proactive prediction. In the same way, the pressure should be higher than the experimental pressure drop. Both conditions have been met by the HPRP MATLAB code.

9.5 Parametric Analysis

The parametric analysis in this section using the HPRP code in MATLAB was conducted on a hydrate forming pipe section of a 40 m with the experimental diameter of 0.0204 m in the literature discussed earlier in chapter 4. For practical field application, the hydrate forming pipeline section is obtained as discussed extensively in chapter 8 (section 8.1.2). The gas inlet temperature is at 292K, operating pressure of 8.9 MPa, water volume fraction of 0.06, and pipe MAOP of 9.0 MPa. During the parametric sensitivity studies, these parameters will be varied as required.

9.5.1 Effect of Change in Subcooling Temperature on Hydrates Plugging Risk

From experiments and theory (Di Lorenzo et al. 2014b, 2014a; Aman et al. 2016), hydrates plugging risk increases with increase in subcooling temperature at constant gas velocity. Therefore, under this operating scenario the plugging flowtime should reduce, and the transient pressure

drop should increase. These observations are corroborated in **Figure 9.2**. **Table 9.4** provide the specific results at constant velocity of 8.0 m/s.

Table 9.4: Effect of subcooling temperature at constant velocity of 8.0 m/s

Pipe Wall Temp. (K)	Hydrates Dep. Rate (L/min)	Plugging Flowtime, t_n (min)	Pressure Drop, ΔP (MPa)	Gas Flowrate (m ³ /s)	Gas Density (kg/m ³)	Density of Hydrates (kg/m ³)	Plugging Risk		
							ΔP	t_n	Overall Risk
290	0.0143	168.85	1.109	0.2155	83.39	936.29	H	H	H
285	0.1673	44.68	1.126	0.2174	84.98	934.93	H	H	H
280	0.2933	23.77	1.144	0.2193	86.58	933.33	H	H	H
275	0.4193	16.63	1.161	0.2212	88.00	931.47	H	H	H

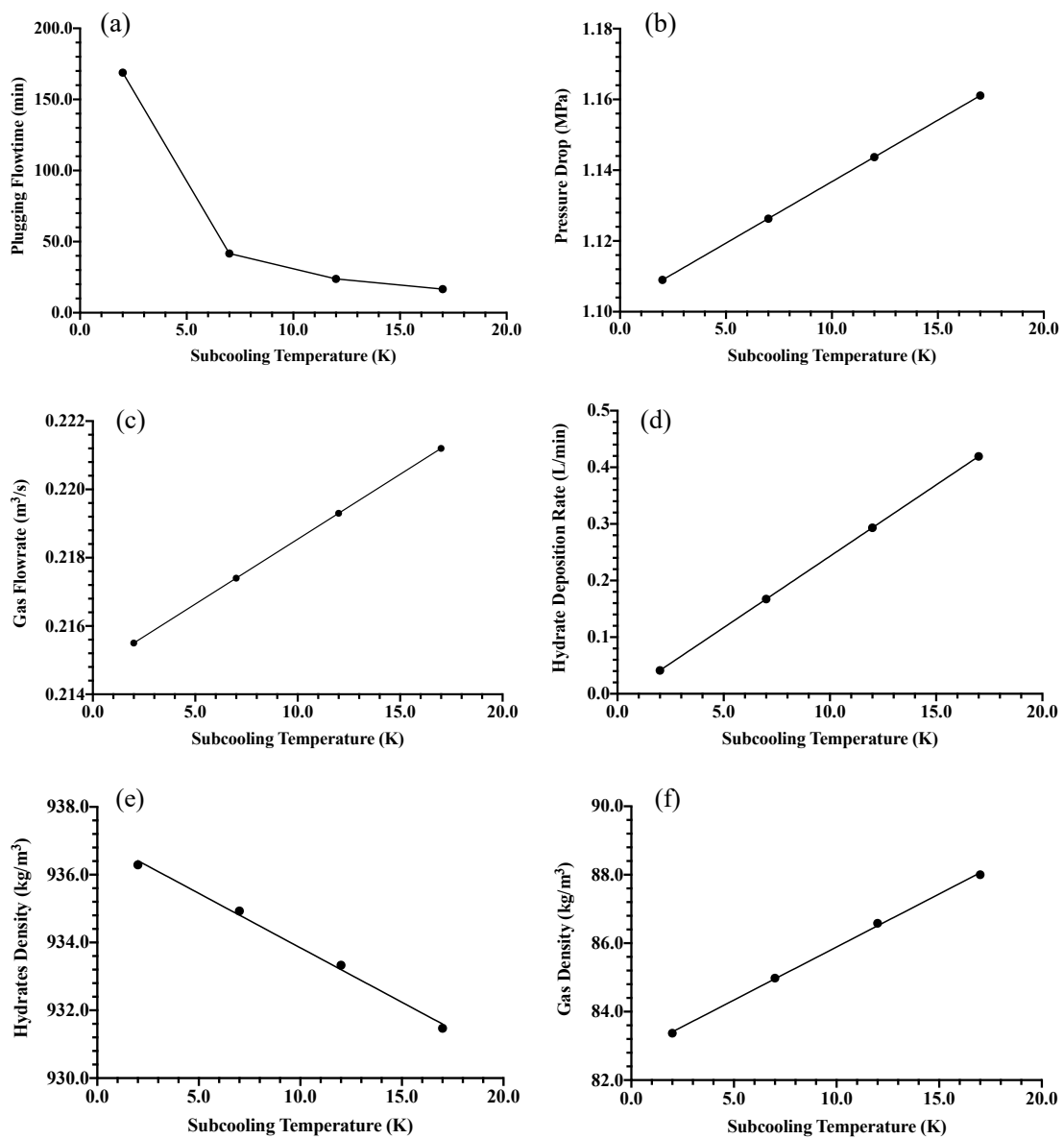


Figure 9.2. Effect of increase in subcooling temperature on hydrates plugging risk at constant gas velocity of 8.0 m/s. (a) reduction in plugging

flowtime. (b) increase in transient pressure drop. (c) slight increase in gas flowrate because of a reduction in gas temperature from equation (9.6). (d) increase in hydrates deposition rate. (e) increase in the density of hydrates. (f) increase in the density of the gas.

9.5.2 Effect of Velocity Change on Hydrates Plugging Risk at Constant Subcooling Temperature

It is equally reported in the literature (Aman et al. 2016), that gas velocity plays a dominate role in hydrates plugging risk. At lower velocity, the deposition rate is lower than at higher gas velocities. However, plugging risk along the horizontal section of the pipeline is higher at lower gas velocities, and the plugging risk at the riser base is higher at higher gas velocities. In the regression model developed earlier in chapter 6 and presented in equation 9.1, velocity has a positive effect on the prediction of hydrates deposition rate. This effect is also corroborated in **Figure 9.3** and **Figure 9.4**.

Table 9.5: Effect of velocity change at constant subcooling temperature of 7.0K

Gas Velocity (m/s)	Hydrates Dep. Rate (L/min)	Plugging Flowtime, t_n (min)	Pressure Drop, ΔP (MPa)	Gas Flowrate (m ³ /s)	Gas Density (kg/m ³)	Density of Hydrates (kg/m ³)	Plugging Risk		
							ΔP	t_n	Overall Risk
2	0.0700	100.33	0.089	0.0543	84.98	934.93	L	H	H
4	0.1021	68.30	0.313	0.1087	84.98	934.93	M	H	H
6	0.1347	51.77	0.660	0.1630	84.98	934.93	H	H	H
8	0.1673	41.68	1.126	0.2174	84.98	934.93	H	H	H

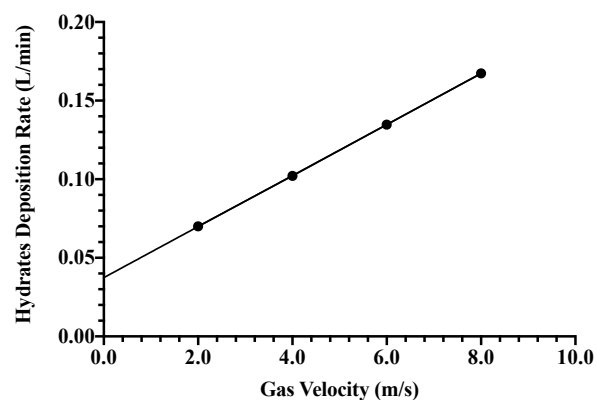


Figure 9.3: Effect of change in gas velocity on hydrates deposition rate

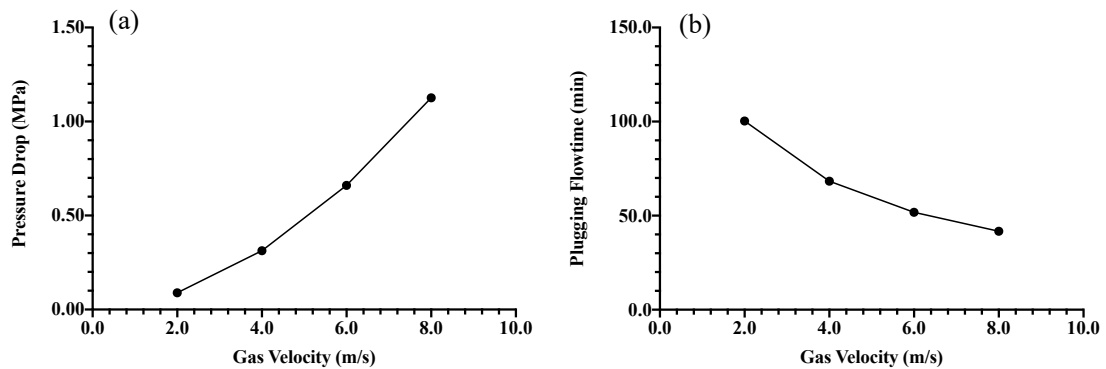


Figure 9.4: Effect of change in gas velocity on hydrates plugging risk. (a) pressure drop increases with increasing gas velocity. (b) plugging flowtime reduces with increasing gas velocity.

The increasing pressure drop as gas velocity increases is related to increasing hydrates deposition rate. Again, with increase in the volume of hydrates in the pipeline, there will be extension of time for hydrates blockage. This analysis was conducted with a pipewall temperature of 285K (subcooling of 7K).

9.5.3 Effect of Change in Pipeline Diameter on Hydrates Plugging Risk

Two scenarios can happen while changing pipeline diameter, especially during design phase. First scenario is the need to keep gas velocity constant to prevent pipewall erosion by designing for a larger pipe size, or the need to increase flowrate from producing wells. Second scenario is the effect of increasing pipe diameter on hydrates deposition rate at constant gas flowrate. Both scenarios have not been studied experimentally. The inference of the likely effect of changing pipe diameter at same operating condition on hydrates deposition rate and plugging risk was proposed in chapter 4 in this study, as one of the parametric outcomes. It was observed that increasing the diameter of the pipe also increases the deposition rate by similar factor provided the gas velocity was constant. This was the first scenario mentioned above.

The HPRP code provided a means to perform this sensitivity using the gas flowrate with ease. **Table 9.6** present the outcome of the simulation for

constant gas velocity, while **Table 9.7** presents the outcome for constant gas flowrate. **Figure 9.5** and **Figure 9.6** provides the plots for results at constant gas velocity, while **Figure 9.7** and **Figure 9.8** provides the plots for pipeline diameter.

The results suggest a similar behaviour under both scenarios, that increasing the diameter of the pipeline increases hydrates deposition rate, reduces pressure drop and extends the plugging flowtime. Hence, by increasing the pipeline size, it is possible to increase the intervention time. The density of the hydrate deposits across pipeline sizes is the same because the pressure, temperature and water volume fraction have been fixed. This parametric sensitivity approach provides an opportunity to decide which pipeline size is most appropriate to extend the plugging time based on the economics for mechanical pigging intervention.

Table 9.6: Effect of change in pipe diameter at constant velocity of 5.0m/s and subcooling temperature of 12K – pipe wall temperature of 280K

Diameter (m)	Hydrates Dep. Rate (L/min)	Plugging Flowtime, t_n (min)	Pressure Drop, ΔP (MPa)	Gas Flowrate (m^3/s)	Gas Density (kg/m^3)	Density of Hydrates (kg/m^3)	Plugging Risk		
							ΔP	t_n	Overall Risk
0.0204	0.2444	28.53	0.4782	0.137	86.58	933.33	M	H	H
0.0408	0.3942	70.76	0.2131	0.543	86.58	933.33	M	H	H
0.0612	0.5441	115.38	0.1332	1.233	86.58	933.33	M	H	H
0.0816	0.6941	160.83	0.0961	2.192	86.58	933.33	M	H	H

Table 9.7: Effect of change in pipe diameter at constant flowrate of 0.2 m^3/s and subcooling temperature of 12 K – pipe wall temperature of 280K

Diameter (m)	Hydrates Dep. Rate (L/min)	Plugging Flowtime, t_n (min)	Pressure Drop, ΔP (MPa)	Gas Velocity (m/s)	Gas Density (kg/m^3)	Density of Hydrates (kg/m^3)	Plugging Risk		
							ΔP	t_n	Overall Risk
0.0204	0.2818	24.74	0.9641	7.31	86.58	933.33	L	H	H
0.0408	0.3424	81.46	0.0333	1.82	86.58	933.33	L	H	H
0.0612	0.4756	131.94	0.0047	0.81	86.58	933.33	L	H	H
0.0816	0.6196	180.06	0.0012	0.46	86.58	933.33	L	H	H

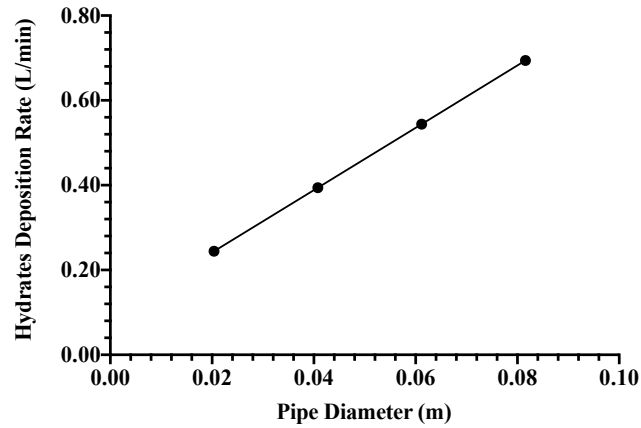


Figure 9.5: Effect of change in pipe diameter on hydrates deposition rate at gas velocity of 5.0m/s and subcooling temperature of 12K.

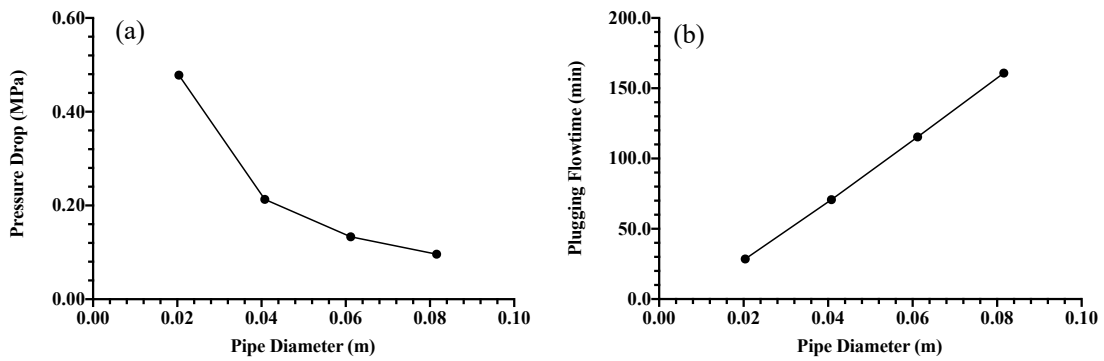


Figure 9.6: Effect of change in pipe diameter on hydrates plugging risk at constant velocity of 5 m/s and subcooling temperature of 12K. (a) pressure drop decreases with increasing gas velocity. (b) plugging flowtime increases with increasing pipe diameter.

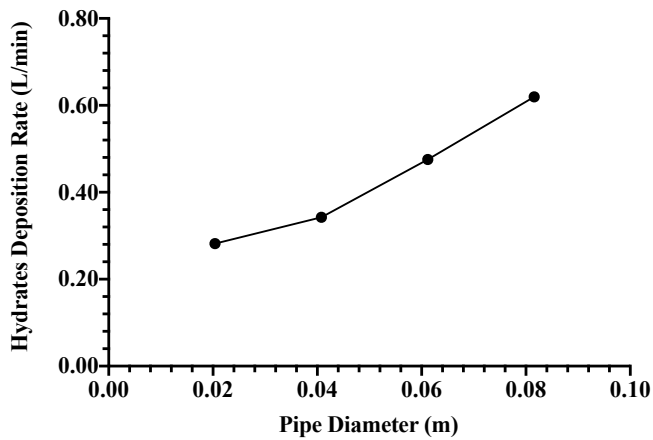


Figure 9.7: Effect of change in pipe diameter on hydrates deposition rate at gas constant gas flowrate 0.2 m³/s and subcooling temperature of 12K.

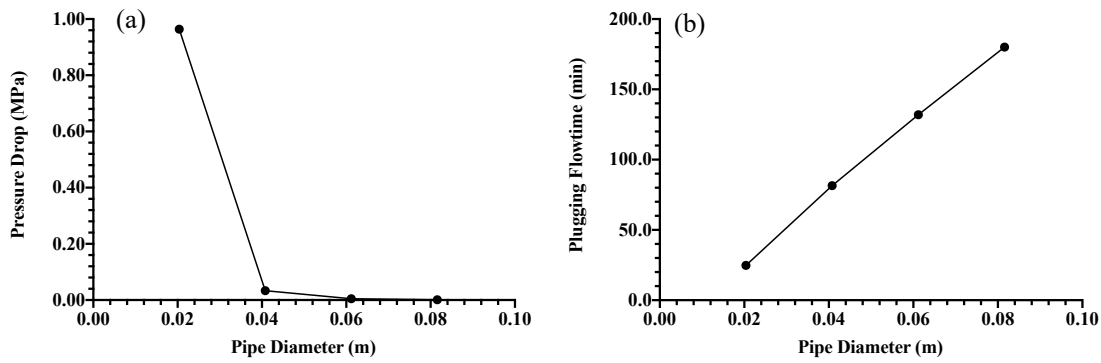


Figure 9.8: Effect of change in pipe diameter on hydrates plugging risk at constant gas flowrate 0.2 m³/s and subcooling temperature of 12K. (a) pressure drop decreases with increasing pipe diameter. (b) plugging flowtime increases with increasing pipe diameter.

9.5.4 Effect of Change in Hydrates Plug Distance

This sensitivity was achieved by changing the length of the hydrates section of the pipeline. The hydrate plug location is at the end of the hydrates forming pipeline section. For this parametric study, the hydrates forming section length ranges from 40 m to 100 m. The pipe diameter is 0.0408m and operating under a subcooling temperature of 12K at a constant gas flowrate of 0.88 m³/s. **Table 9.8** presents the result from the simulation of the HPRP code, while **Figure 9.9** provides a graphical resection of this effect on pressure drop and plugging flowtime. The results shows that increasing the hydrates forming section increases the pressure drop while extending the plugging in agreement with industry report (Kinnari et al. 2015).

Table 9.8: Effect of change in length of hydrates section at constant gas flowrate of 0.88 m³/s and subcooling temperature of 12K – pipe wall temperature of 280K)

Hydrates Plug Distance (m)	Hydrates Dep. Rate (L/min)	Plugging Flowtime, t _n (min)	Pressure Drop, ΔP (MPa)	Gas Velocity (m/s)	Gas Density (kg/m ³)	Density of Hydrates (kg/m ³)	Plugging Risk		
							ΔP	t _n	Overall Risk
40	0.4431	62.95	0.513	8.0	86.58	933.33	M	H	H
60	0.4431	94.43	0.771	8.0	86.58	933.33	H	H	H
80	0.4431	125.91	1.026	8.0	86.58	933.33	H	H	H
100	0.4431	157.38	1.283	8.0	86.58	933.33	H	H	H

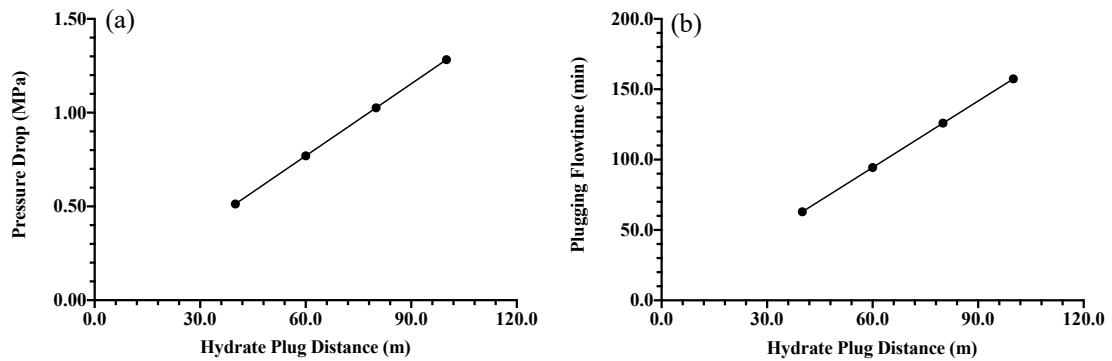


Figure 9.9: Effect of change in hydrates plug distance. (a) pressure drop increases. (b) extension of plugging time

9.5.5 Effect of Change in Water Volume Fraction on Hydrates Plugging Risk

Increasing the water volume fraction increases the transportability of hydrates since the deposition rate of hydrates is reduced under this operating scenario. This sensitivity was performed with a 0.0408 m diameter pipeline with hydrates forming section of 40 m and operating at a pressure of 8.9 MPa. The pipewall temperature of 280K enhances the 12K subcooling temperature of the gas at constant flowrate of 8 m/s.

Table 9.9: Effect of change in water volume fraction at constant velocity 8.0m/s, pipe diameter of 0.0408 m and subcooling temperature of 12K – pipe wall temperature of 280K

Water Volume Fraction	Hydrates Dep. Rate (L/min)	Plugging Flowtime, t_n (min)	Pressure Drop, ΔP (MPa)	Gas Flowrate (m^3/s)	Gas Density (kg/m^3)	Density of Hydrates (kg/m^3)	Plugging Risk		
							ΔP	t_n	Overall Risk
0.04	0.5113	54.55	0.513	0.877	86.58	806.74	M	H	H
0.06	0.4431	62.95	0.513	0.877	86.58	933.33	M	H	H
0.08	0.3748	74.42	0.513	0.877	86.58	1055.01	M	H	H
0.10	0.3066	90.98	0.513	0.877	86.58	1175.03	M	H	H

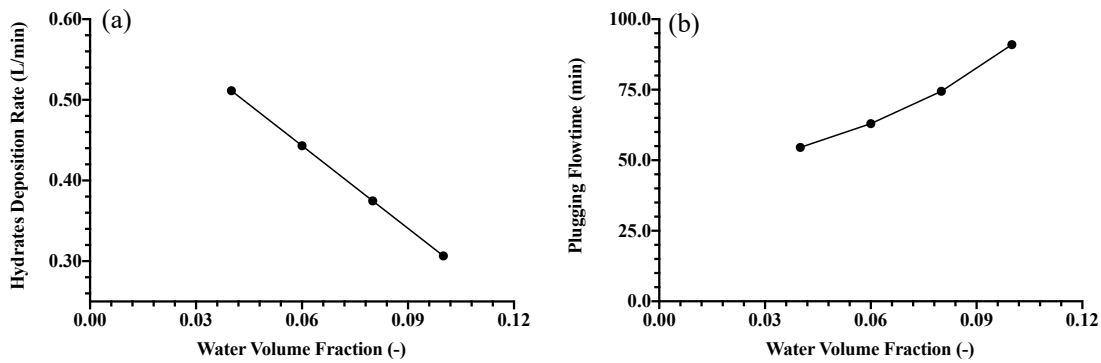


Figure 9.10: Effect of change in water volume fraction at constant velocity 8.0m/s, pipe diameter of 0.0408 m and subcooling temperature of 12K. (a) hydrates deposition rate reduces as water volume fraction increases. (b) plugging flowtime extends as water volume fraction increases.

As seen in **Figure 9.10**, the deposition rate decreases, and the plugging time increases, hence the risk of hydrate plugging reduces as the water volume fraction increases because of the formation of hydrate slurry. This explains why the pressure drop was constant at 0.5131 MPa as hydrates glide over the water film on the pipewall and reducing viscous resistance to inertia force. This effect was discussed earlier as an outcome of the CFD simulations in chapter 4. Previous studies have also indicated that hydrate slurries are formed in the presence of water (Berrouk et al. 2020). Earlier in chapter 7, it was demonstrated that the transportability of hydrates can be enhanced by ensuring the density is greater than that of water.

9.6 Prioritisation of Hydrates Intervention Planning

Hydrates intervention planning must be proactive to safeguard the pipeline from rupture and other safety issues. In some cases, hydrates intervention activities would have to be carried out on a network of flowlines or pipelines and there is the need for prioritisation. The programming of each flowline or pipeline for intervention based on hydrates forming conditions alone would not be a robust approach.

The HPRP code developed in this study can be implemented to provide insight into the order of intervention and provide a maintenance reference plan for the network. To demonstrate the capacity of the code in this scenario, three pipelines are compared with the description provided in **Table 9.10**. The

result of the investigation is presented in **Table 9.11**. in **Figure 9.11** the comparison based on hydrates deposition rate, hydrates density, pressure drop and plugging flowtime for the three pipelines was achieved using a bar chart.

Table 9.10: Input data for the three pipelines

Facility	Gas Hydrate Forming Temp. (K)	Pipewall Temp. (K)	Operating Pressure (MPa)	Hydrates section (m)	MAOP (MPa)	Pipe Diameter (m)	Gas Flowrate (m ³ /s)	Water Volume Fraction
Pipeline 1	292	280	8.0	30.0	9.0	0.204	13.00	0.10
Pipeline 2	292	280	8.0	50.0	9.0	0.204	11.18	0.15
Pipeline 3	292	280	8.0	43.0	9.0	0.204	14.03	0.08

Table 9.11: HPRP Code predicted results for hydrates intervention planning for the three pipelines

Facility	Hydrates Dep. Rate (L/min)	Plugging Flowtime, t _n (min)	Pressure Drop, ΔP (MPa)	Gas Velocity (m/s)	Density of Hydrates (kg/m ³)	Plugging Risk		
						ΔP	t _n	Overall Risk
Pipeline 1	1.46	359.25	0.0227	5.0	1114.3	L	H	H
Pipeline 2	1.28	684.32	0.0284	4.3	1406.2	L	H	H
Pipeline 3	1.53	489.76	0.0376	5.4	994.52	L	H	H

As suggested in **Table 9.11** below, the three pipelines have high-risk hydrates forming sections from a plugging flowtime perspective since the pressure drop is not up to 5% above the MAOP of 9.0 MPa. Hydrates density is highest in pipeline 2 of 1406.2 kg/m³ (**Figure 9.11b**), and above the density of water (998kg/m³), indicating presence of hydrates slurry. Hence, the hydrates in pipeline 2 can be easily transported to a regasifying facility. Pipeline 2 also has the highest plugging flowtime of 684.32 min (**Figure 9.11c**), hence last on the intervention plan.

The second pipeline on the intervention list is pipeline 1. The density of the hydrates in pipeline 1 is slightly above the density of water but having the lowest plugging time of 359.25 min (**Figure 9.11c**). The delay in intervention for pipeline 1 can be substantiated by the fact that the presence

of hydrates slurry can aid transportability to surface regasifying facility. Finally, pipeline 3 has the highest hydrates deposition rate (**Figure 9.11a**), and the density is lower than that of water implying highest plugging risk.

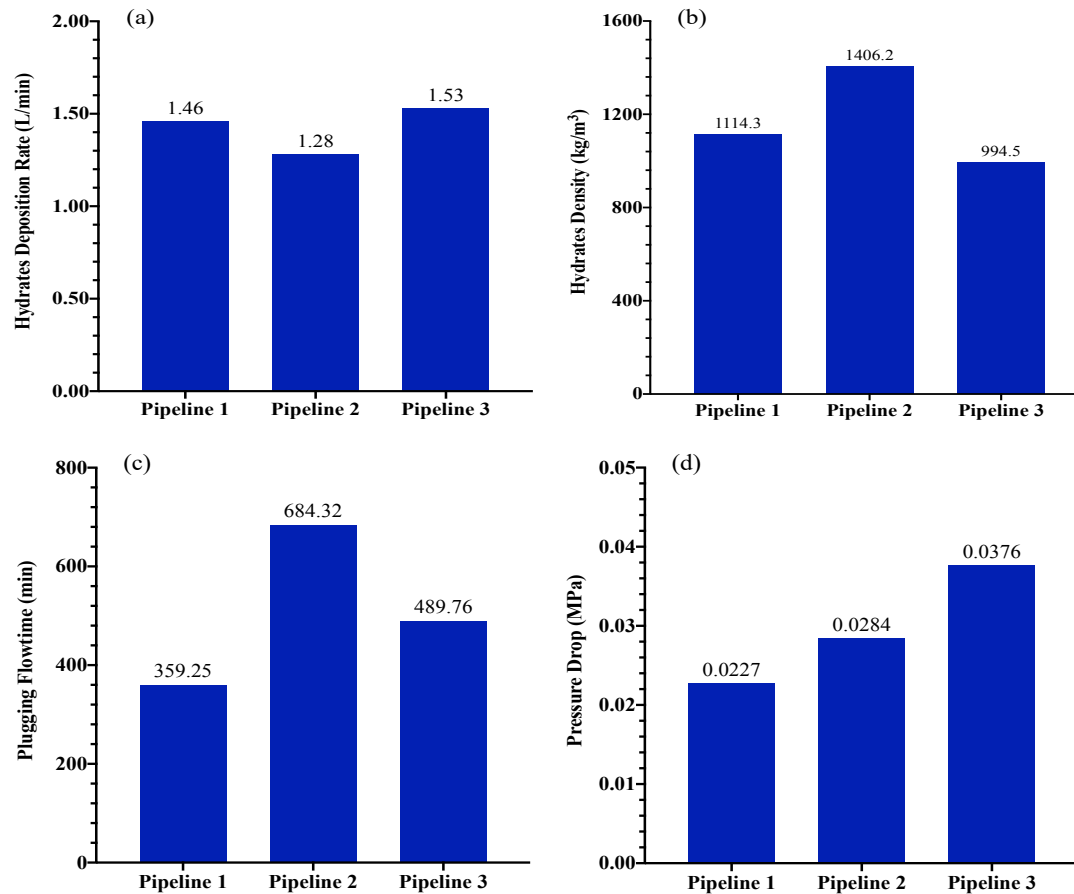


Figure 9.11: HPRP Code predicted results for hydrates intervention planning for the three pipelines. (a) hydrates deposition rate. (b) Hydrates density. (c) plugging flowtime. (d) transient pressure drop.

Although the plugging time is higher than that of pipeline 1, the fact that the hydrates are not easily transported out of the pipeline makes pipeline 3 highest on hydrates plugging threat. If the “plugging flowtime alone” was adopted, the order would have been *Pipeline 1* → *Pipeline 3* → *Pipeline 2*. Adopting the “pressure drop alone” approach would have yielded the order, *Pipeline 3* → *Pipeline 2* → *Pipeline 1*.

However, the right order based on the argument set forth above should be ***Pipeline 3*** → ***Pipeline 1*** → ***Pipeline 2***. A simple ranking approach scale of 1 to 3 is adopted with equal weighting for pressure drop risk, plugging flowtime

risk and transportability as provided in **Table 9.12**. For each ranking parameter, the pipeline with the highest risk is scored 3 and the one with least risk is scored 1. Transportability is based on the density of hydrates, where a value above 998 kg/m³ is termed low risk of plugging. Hence, the highest hydrates density receives a score of 1 and the lowest receives a score 3. The order of intervention is then planned on the graph of plugging flowtime versus the pressure drop as in **Figure 9.12**.

Table 9.12: Hydrates intervention prioritisation ranking table

Facility	Pressure Drop Risk	Plugging Flowtime Risk	Transportability	Total	Intervention Prioritisation
Pipeline 1	1	3	2	6	Second
Pipeline 2	2	1	1	4	Third
Pipeline 3	3	2	3	8	First

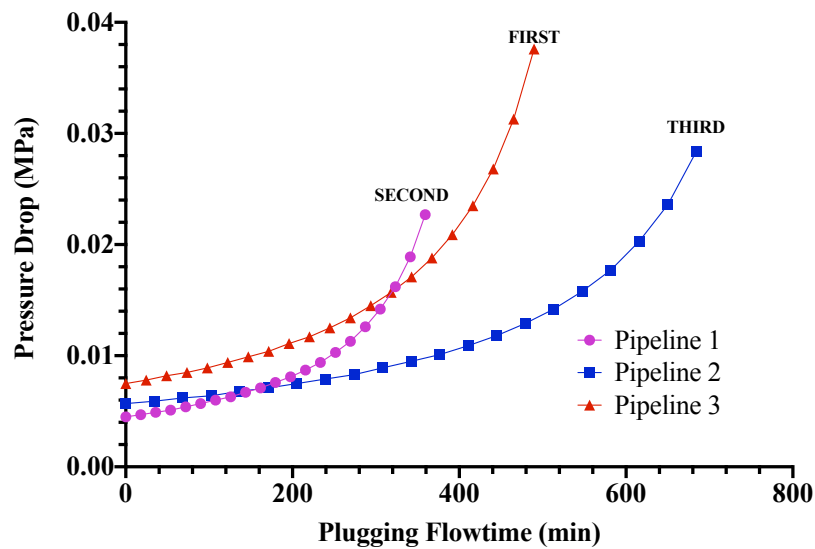


Figure 9.12: HPRP Code predicted plugging flowtime versus pressure drop for hydrates intervention planning of the three pipelines

9.7 Chapter Summary

The purpose of this chapter was to develop a computer code for estimating hydrates plugging risk in subsea gas pipelines. A unique multi-approach hydrates plugging risk prediction have been adopted to enhance the

confidence of the estimated risk level. The results of the parametric studies corroborate previous investigations in the literature, as discussed extensively in preceding chapters of this thesis report. Therefore, the new HPRP MATLAB code developed in this study completes the quest for estimating hydrates plugging risk in subsea gas pipeline.

CHAPTER 10: CONCLUSIONS AND RECOMMENDATIONS FOR FUTURE WORK

10.1 Major Conclusions from the Work

The purpose of this research was to estimate hydrate lugging risk in subsea gas pipelines. This was to close two main knowledge gaps of interest that necessitated in the extant literature: (i) The need to improve the prediction of hydrates deposition rates in gas-dominated pipelines, and (ii) the need to improve on the hydrates plugging flowtime and the resulting transient pressure drop predictions. The main emphasis of the study was to enhance to the practical application of the outcome of this study in the design, operations, and maintenance of hydrates-prone subsea gas pipeline. The major conclusion are as follows:

Objective i: Optimize hydrate prediction through CFD modeling

The four main conclusions of tyhis study based on the first objective include:

1. The new CFD model offers more accurate predictions of hydrate deposition rates, especially at lower gas velocities (4.7 m/s) compared to existing analytical models.
2. Unlike previous CFD models, this current improved model can predict deposition rates based on real-time system parameters like flow velocity, pressure, and temperature. This allows for proactive monitoring of hydrate plugging risk in gas pipelines.
3. The model successfully predicts the different phases (gas, water, and hydrates) during hydrate formation and deposition, aligning with existing analytical models.
4. This study proposes a new finding: hydrate deposition rate increases with larger pipe diameters under similar conditions. This information can be used to scale the CFD model for practical applications in industry.

Objective ii: Develop comprehensive hydrate hydrate-plugging risk management models

1. The study reveals a crucial link between gas velocity and hydrate shedding behavior. At lower velocities (2.0 m/s and 4.0 m/s), pipewall shedding dominates, leading to higher shear stress compared to sloughing locations. This information can be used to identify areas prone to severe internal corrosion due to hydrate formation.
2. As gas velocity increases (6.0 m/s and 8.0 m/s), both pipewall shedding and sloughing occur simultaneously. This finding highlights the complex dynamics of hydrate behavior at higher flow rates.
3. By analyzing the shear stress profile along the pipeline, the model can pinpoint locations with a higher risk of corrosion due to hydrate formation. This information is valuable for pipeline maintenance and risk mitigation strategies.
4. This research offers a suite of tools for managing hydrates in gas pipelines:
 - A regression model quantifies and estimates the risk of hydrates forming during pipeline shutdown periods.
 - A new mathematical model, with dimensional homogeneity, accurately predicts hydrate deposition rates.
 - A novel model predicts hydrate plugging flowtime, allowing for proactive intervention before pipeline blockage occurs.
5. The study proposes a method to predict hydrate plug location based on a table relating deposition rates and flow time. This can be used in real-world applications by comparing upstream pressure readings with model predictions to identify potential plug locations.

Objective iii: Create a gas-specific hydrate plugging risk assessment tool:

1. This research prioritizes flowtime and pressure drop estimations as the foundation for its risk assessment framework. These factors are essential for predicting pipeline behaviour during hydrate formation.
2. While this study incorporates operational costs (affected by pigging frequency) into its risk assessment, it acknowledges the need for

further industry-wide improvements in cost-related risk calculations.

3. The Maximum Allowable Operating Pressure (MAOP) criterion is used to determine the pipe wall thickness or minimum yield strength required to withstand the transient pressure rise caused by anticipated hydrate deposition. This helps ensure pipeline integrity.
4. For longer pipelines, focusing solely on hydrate plugging flowtime might not be sufficient. The model incorporates pressure rise as a complementary factor to ensure a more comprehensive risk assessment.
5. The proposed risk classification system allows for proactive pipeline monitoring by keeping the operation within the safe design pressure limits. This helps to prevent potential hydrate-related accidents.

Objective iv: Improve overall hydrate management strategy

1. The study introduces a novel MATLAB code named "Hydrates Plugging Risk Predictive (HPRP) code." This code aims to comprehensively estimate the risk of hydrate plugging in subsea gas pipelines.
2. The HPRP code goes beyond simply identifying pipelines susceptible to hydrates. It can be used to prioritize intervention scheduling based on predicted plugging risk. This allows for the creation of a more efficient maintenance reference plan for managing a network of pipelines.
3. By incorporating the HPRP code into pipeline management strategies, the reliance solely on hydrate formation conditions for intervention planning can be replaced with a more robust approach. This can lead to more efficient and targeted maintenance activities.

10.2 Contribution to Knowledge

The 7 main contributions of this study to knowledge include:

1. Improvement over the analytical model of Di Lorenzo et al 2018 in the prediction of hydrates deposition rate, especially at low flow gas velocity.
2. A new proposed analytical model for predicting the location of hydrates based on pressure drop.
3. A new approach to predicting hydrate plugging risk classification based on pressure drop compared with pipeline maximum allowable pressure and the time to plug the pipeline.
4. A new insight into the relationship between sloughing angle, which is a new term developed in this study and the length of hydrate plugs and plugging distance along the hydrates forming section of the pipeline.
5. A new insight into understanding the relationship between pipeline wall shedding by hydrates and pipewall shear stress.
6. A new regression modelling approach for predicting hydrate plugging risk during operating and shutdown scenario.
7. A new MATLAB code for predicting hydrate plugging risk in subsea gas pipelines.

10.3 Limitation of the Work

Field validation of the predicted hydrate volumes is essential for ensuring the accuracy and reliability of the hydrates deposition rates estimation, pressure drop and plugging time models in real-world applications. By comparing the models' predictions with actual hydrate formation data collected in the field under various operating conditions, we can identify any discrepancies between the models' assumptions and real-world behavior. This comparison allows us to determine the appropriate models tuning factor for each scenario. With accurate tuning factors for different operating scenarios, the model becomes more adaptable and trustworthy. This translates to several key benefits:

1. Improved decision-making: By having a more accurate model, engineers can make informed decisions about hydrate formation and mitigation strategies. This can involve optimizing production processes, selecting appropriate inhibitors, and minimizing the risk of hydrate blockages.

2. Reduced operational costs: Accurate hydrate prediction helps prevent unnecessary shutdowns or production slowdowns caused by hydrate formation. Additionally, it allows for more efficient use of hydrate inhibitors, reducing their consumption and associated costs.
3. Enhanced safety: Reliable hydrate prediction contributes to safer operation by minimizing the risk of unexpected hydrate blockages that could lead to equipment failures or pipeline ruptures

10.4 Future Work Recommendation

An extended work on hydrates plugging risk in gas pipelines have been achieved in this research effort. However, the propositions would have to be validated with field results. The outcome of this study recommends the following for future work:

- (i) A practical authentication of the CFD results on the parametric study suggesting that hydrates deposition rate increase with increase in pipeline diameter at constant gas velocity and gas flowrate. This verification is important to enhance pipeline sizing in the design stage of a new gas pipeline project.
- (ii) Another recommendation for future work is the need for field verification of the approach proposed in this work for determining the location of hydrate plugging events. This can enhance the injection of hydrates dissociating inhibitors and enhance hydrates transportability.

REFERENCES

- ABBASI, A. and HASHIM, F.M., 2014. Thermodynamic effects on hydrate formation in deepwater pipeline. In: *Applied Mechanics and Materials*. pp. 607–611.
- ABDULLAHI, M., 2020. Simulation and detection of blockage in a pipe under mean fluid flow using acoustic wave propagation technique. *Struct Control Health Monit.* 2020;E2449., e2449, pp. 1–22.
- ABOOALI, D. and KHAMEHCHI, E., 2019. New predictive method for estimation of natural gas hydrate formation temperature using genetic programming. *Neural Computing and Applications*, 31(7), pp. 2485–2494.
- ADELEKE, N., ITYOKUMBUL, M.T. and ADEWUMI, M., 2013. Blockage detection and characterization in natural gas pipelines by transient pressure-wave reflection analysis. *SPE Journal*, 18(2), pp. 355–365.
- AMAN, Z.M. et al., 2016. Hydrate formation and deposition in a gas-dominant flowloop: Initial studies of the effect of velocity and subcooling. *Journal of Natural Gas Science and Engineering*, pp. 1–9.
- AMAN, Z.M. et al., 2018. Deposition and shear stress initial investigations for hydrate blockage. In: *Proceedings of the Annual Offshore Technology Conference*.
- AMAN, Z.M., 2021. Hydrate Risk Management in Gas Transmission Lines. *Energy and Fuels*, 35(18), pp. 14265–14282.
- ANDREUSSI, P., ASALI, J.C. and HANRATTY, T.J., 1985. Initiation of roll waves in gas-liquid flows. *AIChE Journal*, 31(1).
- ASHRAFIZADEH, A., ALINIA, B. and MAYELI, P., 2015. A new co-located pressure-based discretization method for the numerical solution of incompressible navier-stokes equations. *Numerical Heat Transfer, Part B: Fundamentals*, 67(6), pp. 563–589.
- BAGHBAN, A. et al., 2016. Phase equilibrium modelling of natural gas hydrate formation conditions using LSSVM approach. *Petroleum Science and Technology*, 34(16), pp. 1431–1438.
- BAI, Y. and BAI, Q., 2005. Hydrates. In: Y. BAI and Q. BAI, eds. *Subsea Pipelines and Risers*. Gulf Professional Publishing. pp. 357–382.
- BAKER, O., 1954. Simultaneous Flow of Oil and Gas. *Oil Gas J*, 53.
- BALAKIN, B. V et al., 2010. Turbulent flow of hydrates in a pipeline of complex configuration. *Chemical Engineering Science*, 65(17), pp. 5007–5017.
- BALAKIN, B. V et al., 2016. Modelling agglomeration and deposition of gas

hydrates technique. *Chemical Engineering Science*. [online]. Available from: <http://dx.doi.org/10.1016/j.ces.2016.07.010>.

BALLARD, A., SHOUP, G. and SLOAN, D., 2011. Industrial Operating Procedures for Hydrate Control. In: E.D. SLOAN, C.A. KOH and A.K. SUM, eds. *Natural Gas Hydrates in Flow Assurance*. Gulf Professional Publishing. pp. 145–162.

BARRON, R.M. and NEYSHABOURI, A.A.S., 2003. Effects of under-relaxation factors on turbulent flow simulations. *International Journal for Numerical Methods in Fluids*, 42(8), pp. 923–928.

BEGGS, H.D. and BRILL, J.R., 1973. Study of Two-Phase Flow in Inclined Pipes. *JPT, Journal of Petroleum Technology*.

BENDLKSEN, K.H. et al., 2004. The dynamic two-fluid model OLGA: Theory and application. *SPE Reprint Series*, (58), pp. 52–61.

BERROUK, A.S. et al., 2020. CFD modelling of hydrate slurry flow in a pipeline based on Euler-Euler approach. *Progress in Computational Fluid Dynamics*, 20(3), pp. 156–168.

BESANCON, G. et al., 2013. Pipeline partial blockage modeling and identification. *IFAC Proceedings Volumes (IFAC-PapersOnline)*, 11, pp. 730–735.

BISGAARD, C., SORENSEN, H.H. and SPANGENBERG, S., 1987. A FINITE ELEMENT METHOD FOR TRANSIENT COMPRESSIBLE FLOW IN PIPELINES. *International Journal for Numerical Methods in Fluids*, 7(August 1986), pp. 291–303.

BP, 2020. *Statistical review of world energy 2020*. 69th ed. London: BP p.i.C. Available from: <https://www.bp.com/content/dam/bp/business-sites/en/global/corporate/pdfs/energy-economics/statistical-review/bp-stats-review-2020-full-report.pdf>.

BRENNEN, C.E., 2013. *Fundamentals of multiphase flow. Fundamentals of Multiphase Flow*, vol. 9780521848.

CAO, J. et al., 2020. Integrating support vector regression with genetic algorithm for hydrate formation condition prediction. *Processes*, 8(5), pp. 1–11.

CARROLL, J., 2014. *Natural Gas Hydrates: A Guide for Engineers*. 3rd ed. Waltham, MA 02451: Gulf Professional Publishing.

CHACZYKOWSKI, M., 2009. Sensitivity of pipeline gas flow model to the selection of the equation of state. *Chemical Engineering Research and Design*, 87(12), pp. 1596–1603.

CHARLTON, T.B. et al., 2018a. Simulating Hydrate Growth and Transport Behavior in Gas-Dominant Flow. *Energy and Fuels*, 32(2), pp. 1012–1023.

- CHARLTON, T.B. et al., 2018b. Predicting hydrate blockage formation in gas-dominant systems. In: *Offshore Technology Conference Asia 2018, OTCA 2018. Offshore Technology Conference*.
- CHAUDHARI, P., ZERPA, L.E. and SUM, A.K., 2018. A correlation to quantify hydrate plugging risk in oil and gas production pipelines based on hydrate transportability parameters. *Journal of Natural Gas Science and Engineering*.
- CHAUDHRY, M.H., 1979. *Applied hydraulic transients*. 3rd ed. New York, NY: Van Nostrand Reinhold.
- CHEN, X. et al., 2007. Pressure-wave propagation technique for blockage detection in subsea flowlines. *SPE Annual Technical Conference and Exhibition Held in Anaheim, California, U.S.A., 11–14 November 2007*.
- COELHO, P.M. and PINHO, C., 2007. Considerations about equations for steady state flow in natural gas pipelines. *Journal of the Brazilian Society of Mechanical Sciences and Engineering*, 29(3), pp. 262–273.
- COHEN, J., 1988. *Statistical power analysis for the behavioral sciences*. 2nd ed. Lawrence Erlbaum Associates.
- COHEN, J. et al., 2003. *Applied multiple regression/correlation analysis for the behavioral sciences*. 3rd ed. New Jersey: Lawrence Erlbaum Associates, Inc.
- DATTA, S., GAUTAM, N.K. and SARKAR, S., 2018. Pipe network blockage detection by frequency response and genetic algorithm technique. *Journal of Water Supply: Research and Technology - AQUA*, 67(6), pp. 543–555.
- DAVARNEJAD, R., 2014. Prediction of Gas Hydrate Formation using HYSYS Software. *International Journal of Engineering*, 27(9 (C)).
- DEMIRDZIC, I. et al., 1987. A calculation procedure for turbulent flow in complex geometries. *Computers and Fluids*, 15(3), pp. 251–273.
- DING, L. et al., 2017. Hydrate Formation and Plugging Mechanisms in Different Gas-Liquid Flow Patterns. *Industrial and Engineering Chemistry Research*, 56(14), pp. 4173–4184.
- DNVGL-ST-F101, 2017. *Submarine pipeline systems*. October Ed. Det Norske Veritas.
- DREW, T.B., KOO, E.C. and MCADAMS, W.H., 1932. The friction factor for clean round pipes. *Trans. AIChE*, 28(1932), pp. 56–72.
- DUAN, X. et al., 2022. Quantitative assessment of hydrate blockage risk in pipelines based on reliability theory. *Journal of Natural Gas Science and Engineering*, 98, p. 104345. Available from: <https://doi.org/10.1016/j.jngse.2021.104345>.
- EL-HOSHOUDY, A.N. et al., 2021. An Artificial Neural Network model for

predicting the hydrate formation temperature. *Arabian Journal for Science and Engineering*. [online]. Available from: <https://doi.org/10.1007/s13369-021-06340-w>.

ENGLEZOS, P. et al., 1987. Kinetics of gas hydrate formation from mixtures of methane and ethane. *Chemical Engineering Science*, 42(11), pp. 2659–2666.

FAUL, F. et al., 2007. G*Power 3: A flexible statistical power analysis program for the social, behavioral, and biomedical sciences. *Behavior Research Methods*, 39(2), pp. 175–191.

FERREIRA, G.G.S.S. et al., 2019. Implementation of an implicit pressure–velocity coupling for the Eulerian multi-fluid model. *Computers and Fluids*, 181, pp. 188–207.

FOX, R.O., 2014. On multiphase turbulence models for collisional fluid-particle flows. *Journal of Fluid Mechanics*, 742, pp. 368–424.

HAMMERSCHMIDT, E.G., 1934. Formation of Gas Hydrates in Natural Gas Transmission Lines. *Industrial and Engineering Chemistry*, 26(8), pp. 851–855.

HE, W., 2022. Study on model of natural gas hydrate formation based on extremely randomized trees. *Journal of Physics: Conference Series*, 2263(1), p. 12022. Available from: <https://doi.org/10.1088/1742-6596/2263/1/012022>.

HEGDE, G.A., SUM, A.K. and DANIELSON, T.J., 2015. Multiphase flow modeling for gas hydrates in flow assurance. *Proceedings of the Annual Offshore Technology Conference*, 2(May), pp. 946–959.

HOU, P. et al., 2019. Numerical Simulation of Hydrate Slurry Flow Characteristics in Vertical Tubes by CFD-PBM. *Shiyou Huagong Gaodeng Xuexiao Xuebao/Journal of Petrochemical Universities*.

HUBBARD, M.G. and DUKLER, A.E., 1966. The Characterisation of flow regimes for horizontal two phase flow. *Proc Heat Transfer Fluid Mechanics*.

IBRAGIMOVNA, K.G., NIKOLAEVNA, E.N. and BORISOVICH, P.V., 2018. Effective calculation methods of the gas flow characteristics and offshore gas pipeline glaciation. In: *AIP Conference Proceedings*.

IBRAHIM, A.A.A. et al., 2016. Prediction of Gas Hydrate Formation Using Radial Basis Function Network and Support Vector Machines. *Applied Mechanics and Materials*, 819, pp. 569–574.

JAFARIZADEH, B. and BRATVOLD, R.B., 2019. Exploration economics : taking opportunities and the risk of double-counting risk. *Mineral Economics*.

JAMALUDDIN, A.K.M., KALOGERAKIS, N. and BISHNOI, P.R., 1991. Hydrate plugging problems in undersea natural gas pipelines under shutdown

conditions. *Journal of Petroleum Science and Engineering*, 5(1991), pp. 323–335.

JASSIM, E., ABDI, M.A. and MUZYCHKA, Y., 2010. A new approach to investigate hydrate deposition in gas-dominated flowlines. *Journal of Natural Gas Science and Engineering*, 2(4), pp. 163–177.

JUJULY, M.M. et al., 2017. Hydrate induced vibration in an offshore pipeline. In: *Proceedings - SPE Annual Technical Conference and Exhibition*.

JUJULY, M.M. et al., 2020. Hydrate-Induced Vibration in an Offshore Pipeline. *SPE Journal*, 25(02).

KADER, B.A., 1981. Temperature and concentration profiles in fully turbulent boundary layers. *International Journal of Heat and Mass Transfer*, 24(9), pp. 1541–1544.

KHAN, M.N., WARRIER, P. and KOH, C.A., 2023. An Overview of Thermodynamics and Growth Kinetics of Gas Hydrate Systems. *Transactions of the Indian Institute of Metals*.

KINNARI, K. et al., 2015. Hydrate management in practice. *Journal of Chemical and Engineering Data*, 60(2), pp. 437–446.

KLETTING, P. and GLATTING, G., 2009. Model selection for time-activity curves: The corrected Akaike information criterion and the F-test. *Zeitschrift Fur Medizinische Physik*, 19(3), pp. 200–206.

KOH, C.A. et al., 2011. Fundamentals and applications of gas hydrates. *Annual Review of Chemical and Biomolecular Engineering*.

KOH, C. and CREEK, J., 2011. Safety in Hydrate Plug Removal. In: D. SLOAN, C.A. KOH and A.K. SUM, eds. *Natural Gas Hydrates in Flow Assurance*. Gulf Professional Publishing: An Imprint of Elsevier. pp. 37–48.

KUNDU, P.K., COHEN, I.M. and DOWLING, D.R., 2016. *Fluid mechanics*. 6th ed. Academic Press.

LANDGREBE, M.K.B. and NKAZI, D., 2019. Toward a Robust, Universal Predictor of Gas Hydrate Equilibria by Means of a Deep Learning Regression. *ACS Omega*, 4(27), pp. 22399–22417.

LEDERHOS, J.P. et al., 1996. Effective kinetic inhibitors for natural gas hydrates. *Chemical Engineering Science*, 51(8), pp. 1221–1229.

LEKVAM, K. and BISHNOI, P.R., 1997. Dissolution of methane in water at low temperatures and intermediate pressures. *Fluid Phase Equilibria*, 131(1–2), pp. 297–309.

LI, D., 2019. Turbulent Prandtl number in the atmospheric boundary layer - where are we now? *Atmospheric Research*, 216, pp. 86–105.

LI, N., 2015. Comparison between three different CFD software and

numerical simulation of an ambulance hall.

LI, P., ZHANG, X. and LU, X., 2019. Three-dimensional Eulerian modeling of gas–liquid–solid flow with gas hydrate dissociation in a vertical pipe. *Chemical Engineering Science*, 196, pp. 145–165. Available from: <https://www.sciencedirect.com/science/article/pii/S0009250918307747>.

LI, W. et al., 2013. A study of hydrate plug formation in a subsea natural gas pipeline using a novel high-pressure flow loop. *Petroleum Science*, 10(1), pp. 97–105.

LI, Y. et al., 2021. Characterization and development of natural gas hydrate in marine clayey-silt reservoirs: A review and discussion. *Advances in Geo-Energy Research*, 5(1), pp. 75–86.

LIM, V.W.S.S. et al., 2020. Gas hydrate formation probability and growth rate as a function of kinetic hydrate inhibitor (KHI) concentration. *Chemical Engineering Journal*, 388(January).

LINGELEM, M.N., MAJEED, A.I. and STANGE, E., 1994. Industrial Experience in Evaluation of Hydrate Formation, Inhibition, and Dissociation in Pipeline Design and Operation. *Annals of the New York Academy of Sciences*, 715(1).

LIU, W. et al., 2019. A new hydrate deposition prediction model considering hydrate shedding and decomposition in horizontal gas-dominated pipelines. *Petroleum Science and Technology*, 37(12), pp. 1370–1386.

LIU, W. et al., 2018. Assessment of hydrate blockage risk in long-distance natural gas transmission pipelines. *Journal of Natural Gas Science and Engineering*, 60.

LIU, Z. et al., 2020. Hydrate slurry flow characteristics influenced by formation, agglomeration and deposition in a fully visual flow loop. *Fuel*, 277(May), p. 118066. Available from: <https://doi.org/10.1016/j.fuel.2020.118066>.

LO, S., 2011. CFD modelling of hydrate formation in oil-dominated flows. In: *Offshore Technology Conference*. Houston, Texas, USA.

DI LORENZO, M. et al., 2014a. Hydrate formation in gas-dominant systems using a single-pass flowloop. *Energy and Fuels*, 28(5).

DI LORENZO, M. et al., 2014b. Underinhibited hydrate formation and transport investigated using a single-pass gas-dominant flowloop. *Energy and Fuels*, 28(11).

DI LORENZO, M. et al., 2018. Modelling hydrate deposition and sloughing in gas-dominant pipelines. *Journal of Chemical Thermodynamics*, 117, pp. 81–90.

LV, X.-F. et al., 2023. Numerical simulation study on multiphase flow pattern of hydrate slurry. *Petroleum Science*, 20(6), pp. 3897–3917.

- MA, N. et al., 2024. Hydrate deposition characteristics analysis and structural optimization design of reduced-diameter pipe based on an improved model. *Ocean Engineering*, 291, p. 116437.
- MACKENZIE, A. et al., 2015. A comparison of CFD software packages' ability to model a submerged jet. In: *Eleventh International Conference on CFD in the Minerals and Process Industries CSIRO*.
- MANN, S.L. et al., 1989. Vapor-Solid Equilibrium Ratios for Structure I and II Natural Gas Hydrates. In: *The 68th Gas Processors Association (GPA) Convention*.
- MARFO, S.A. et al., 2019. Flow Assurance in Subsea Pipeline Design - A Case Study of Ghana's Jubilee and TEN Fields. *Ghana Mining Journal*, 19(1), pp. 72–85.
- MARFO, S.A.A., OPOKU APPAU, P. and KPAMI, L.A.A.A.A., 2018. Subsea Pipeline Design for Natural Gas Transportation: A Case Study of Côte D'ivoire's Gazelle Field. *International Journal of Petroleum and Petrochemical Engineering (IJPPE)*, 4(3), pp. 21–34.
- MARQUES, D.C. et al., 2022. Mapping wall deposition trends of gas hydrates: I. gas-water-hydrate systems. *Industrial & Engineering Chemistry Research*.
- MAY, E.F. et al., 2018. Gas Hydrate Formation Probability Distributions: The Effect of Shear and Comparisons with Nucleation Theory. *Langmuir*, 34(10), pp. 3186–3196.
- MCMULLEN, N., 2011. How hydrate plugs are remediated. In: D. SLOAN, C.A. KOH and A.K. SUM, eds. *Natural Gas Hydrates in Flow Assurance*. Gulf Professional Publishing Is an Imprint of Elsevier.
- MEINDINYO, R.-E.E.T., SVARTAS, T.M. and SVARTÅS, T.M., 2015. Intermolecular forces in clathrate hydrate related processes. In: *Proceedings of the International Conference on Offshore Mechanics and Arctic Engineering - OMAE*.
- MEINDINYO, R.E.T. et al., 2015. Gas hydrate growth estimation based on heat transfer. *Energy and Fuels*, 29(2), pp. 587–594.
- MELAINA, M., ANTONIA, O. and PENEV, M., 2013. Blending Hydrogen into Natural Gas Pipeline Networks: A Review of Key Issues. *Contract*, 303(March), pp. 275–3000.
- MENG, B. et al., 2017. Hydrogen effects on X80 pipeline steel in high-pressure natural gas/hydrogen mixtures. *International Journal of Hydrogen Energy*, 42(11), pp. 7404–7412.
- MENON, E.S., 2005. *Gas pipeline hydraulics. Gas Pipeline Hydraulics*. Boca Raton, FL: Taylor & Francis.
- MEREY, S. and SINAYUC, C., 2016. New Software That Predicts Hydrate

Properties and Its Use in Gas Hydrate Studies. *Journal of Chemical and Engineering Data*, 61(5), pp. 1930–1951.

MERTLER, C.A. and REINHART, R.V., 2016. *Advanced and multivariate statistical methods: Practical application and interpretation*. 6th ed. *Advanced and Multivariate Statistical Methods*. New York, NY: Routledge – Taylor and Francis.

MESBAH, M., SOROUSH, E. and REZAKAZEMI, M., 2017. Development of a least squares support vector machine model for prediction of natural gas hydrate formation temperature. *Chinese Journal of Chemical Engineering*, 25(9), pp. 1238–1248.

MIN, C.H. and TAO, W.Q., 2007. An under-relaxation factor control method for accelerating the iteration convergence of flow field simulation. *Engineering Computations (Swansea, Wales)*, 24(8), pp. 793–813.

MISHRIKY, F. and WALSH, P., 2017. Towards understanding the influence of gradient reconstruction methods on unstructured flowsimulations. *Transactions of the Canadian Society for Mechanical Engineering*, 41(2), pp. 169–179.

MOHAPATRA, P.K. et al., 2006. Detection of partial blockages in a branched piping system by the frequency response method. *Journal of Fluids Engineering, Transactions of the ASME*, 128(5), pp. 1106–1114.

MOHITPOUR, M., GOLSHAN, H. and MURRAY, A., 2007. *Pipeline Design & Construction: A Practical Approach, Third Edition*. 3rd ed. New York: ASME Press.

MONTGOMERY, D.C. and RUNGER, G.C., 2014. *Applied statistics and probability for engineers*. 6th ed. Danvers, MA: John Wiley & Sons, Inc.

MOTTAGHIAN, P., YUAN, J. and PIOMELLI, U., 2018. Boundary layer separation under strong adverse pressure gradient over smooth and rough walls. *ERCRAFT Series*, 24, pp. 173–179.

MUNSON, B.R. et al., 2013. *Fundamentals of Fluid Mechanics*. 7th ed. Hoboken, NJ: John Wiley & Sons, Inc.

MUNSON, B.R., YOUNG, D.F. and OKIISHI, T.H., 1994. Fundamentals of fluid mechanics. *Fundamentals of Fluid Mechanics*.

NASEER, M. and BRANDSTÄTTER, W., 2011. Hydrate formation in natural gas pipelines. In: *WIT Transactions on Engineering Sciences*.

NASIR, Q. et al., 2022. A multi-layer perceptron neural network model for predicting the hydrate equilibrium conditions in multi-component hydrocarbon systems. *Neural Computing and Applications*. [online]. Available from: <https://doi.org/10.1007/s00521-022-07284-4>.

NETO, E.T. et al., 2015. Coupled Heat and Mass Transfer CFD Model for Methane Hydrate, pp. 2–7.

- NETO, E.T. et al., 2016. Numerical flow analysis of hydrate formation in offshore pipelines using computational fluid dynamics (CFD). In: *Proceedings of the International Conference on Offshore Mechanics and Arctic Engineering - OMAE*. Busan, South Korea: ASME.
- OBANIJESU, E.O., 2009. Modeling the H₂S contribution to internal corrosion rate of natural gas pipeline. *Energy Sources, Part A*, 31, pp. 348–363.
- OBANIJESU, E.O. et al., 2011. *Modelling the Natural Gas Pipeline Internal Corrosion Rate Resulting from Hydrate Formation*. *Computer Aided Chemical Engineering*, vol. 29. Elsevier B.V. Available from: <http://dx.doi.org/10.1016/B978-0-444-54298-4.50011-8>.
- OBANIJESU, E.O., 2012. Corrosion and Hydrate Formation in Natural Gas Pipelines, (May), p. 239.
- ODUTOLA, T.O. et al., 2017. Fabrication and Validation of a Laboratory Flow Loop for Hydrate Studies. *American Journal of Chemical Engineering. Special Issue: Oil Field Chemicals and Petrochemicals*, 5(1), pp. 28–41. Available from: <http://www.sciencepublishinggroup.com/j/ajche>.
- ODUTOLA, T.O. and UGWU, C.E., 2019. Simulation of Laboratory Hydrate Loop Using Aspen Hysys. *Engineering and Applied Sciences*, 4(3).
- OSIADACZ, A.J. and CHACZYKOWSKI, M., 2001. Comparison of isothermal and non-isothermal pipeline gas flow models. *Chemical Engineering Journal*, 81(1–3).
- PALERMO, T. and SLOAN, D., 2011. Artificial and natural Inhibition of hydrates. In: E.D. SLOAN, C.A. KOH and A.K. SUM, eds. *Natural Gas Hydrates in Flow Assurance*. Gulf Professional Publishing: An Imprint of Elsevier. pp. 87–103.
- PAN, L. and HANRATTY, T.J., 2002. Correlation of entrainment for annular flow in horizontal pipes. *International Journal of Multiphase Flow*, 28(3).
- PANDEY, G., LINGA, P. and SANGWAI, J.S., 2017. High pressure rheology of gas hydrate formed from multiphase systems using modified Couette rheometer. *Review of Scientific Instruments*, 88(2).
- PENG, D.Y. and ROBINSON, D.B., 1976. A New Two-Constant Equation of State. *Industrial and Engineering Chemistry Fundamentals*, 15(1), pp. 59–64.
- PICKARTS, M.A. et al., 2020. Gas hydrate formation & transportability during transient shut-in/restart conditions. In: *Proceedings of the Annual Offshore Technology Conference*.
- PRUTEANU, C.G. et al., 2017. When immiscible becomes miscible-Methane in water at high pressures. *Science Advances*, 3(8), pp. 1–6.
- QIN, H. et al., 2019. Machine learning models to predict gas hydrate

plugging risks using flowloop and field data. In: *Proceedings of the Annual Offshore Technology Conference*.

RAO, Y. et al., 2022. Experimental study on hydrate safe flow in pipelines under a swirl flow system. *ACS Omega*, 7(19), pp. 16629–16643. Available from: <https://doi.org/10.1021/acsomega.2c00892>.

RAZVARZ, S., JAFARI, R. and GEGOV, A., 2020. Leakage detection in pipeline based on second order extended kalman filter observer. *Studies in Systems, Decision and Control*, 321, pp. 161–174.

RUDINGER, G., 1965. Some effects of finite particle volume on the dynamics of gas-particle mixtures. *AIAA Journal*, 3(7).

SCHMELZER, J.W.P., ZANOTTO, E.D. and FOKIN, V.M., 2005. Pressure dependence of viscosity. *Journal of Chemical Physics*, 122(7).

SHIH, T.-H. et al., 1995. A new $k-\epsilon$ eddy viscosity model for high reynolds number turbulent flows. *Computers and Fluids*, 24(3), pp. 227–238.

SHYY, W., THAKUR, S. and WRIGHTT, J., 1992. Second-order upwind and central difference schemes for recirculating flow computation. *AIAA Journal*, 30(4), pp. 923–932.

SIMONIN, O. and VIOLLET, P.L., 1990. Predictions of an Oxygen Droplet Pulverization in a Compressible Subsonic Coflowing Hydrogen Flow. *Numer. Methods Multiph. Flows FED91*, FED91, pp. 65–82.

SKOVBORG, P. and RASMUSSEN, P., 1994. A mass transport limited model for the growth of methane and ethane gas hydrates. *Chemical Engineering Science*, 49(8), pp. 923–932.

SLOAN, D. et al., 2011. Conclusion. *Natural Gas Hydrates in Flow Assurance*, pp. 163–170.

SLOAN, D.E. and KOH, C.A., 2007. *Clathrate hydrates of natural gases*. 3rd ed. *Clathrate Hydrates of Natural Gases, Third Edition*. Boca Raton, FL: CRC Press.

SLOAN, E., 2011. *Introduction: What are hydrates?* Edited by D Sloan, C A Koh and A K Sum. *Natural Gas Hydrates in Flow Assurance*. Gulf Professional Publishing Is an Imprint of Elsevier.

SLOAN, E.D., KOH, C.A. and SUM, A.K., 2011a. *Natural gas hydrates in flow assurance*. Edited by E Dendy Sloan, Carolyn A Koh and Amadeu K Sum. Gulf Professional Publishing: An Imprint of Elsevier.

SLOAN, E.D., KOH, C.A. and SUM, A.K., 2011b. Six Industrial Hydrate Blockage Examples and Lessons Learned. In: *Natural Gas Hydrates in Flow Assurance*. pp. 171–191.

SONG, G. et al., 2018a. Numerical simulation of hydrate slurry flow behavior in oil-water systems based on hydrate agglomeration modelling.

Journal of Petroleum Science and Engineering, 169, pp. 393–404. Available from:

<https://www.sciencedirect.com/science/article/pii/S092041051830473X>.

SONG, G. et al., 2018b. Numerical simulation of pipeline hydrate particle agglomeration based on population balance theory. *Journal of Natural Gas Science and Engineering*, 51, pp. 251–261. Available from:

<https://www.sciencedirect.com/science/article/pii/S1875510018300143>.

SROUR, O., SABER, E. and ELGAMAL, H.A., 2016. Pipeline blockage detection. *International Journal of Engineering Research & Technology (IJERT)*, 5(6), pp. 592–598.

STEWART, N. and JACK, G., 2017. Pipeline blockage location by pressure wave analysis. *Society of Petroleum Engineers - SPE Abu Dhabi International Petroleum Exhibition and Conference 2017, 2017-Janua(November)*, pp. 13–16.

SULE, I.O. et al., 2015. CFD analysis of hydrate formation in pipelines. *Petroleum Science and Technology*, 33(5), pp. 571–578.

SUM, A.K., KOH, C.A. and SLOAN, E.D., 2012. Developing a comprehensive understanding and model of hydrate in multiphase flow: From laboratory measurements to field applications. In: *Energy and Fuels*.

SUYKENS, J.A.K. and VANDEWALLE, J., 1999. Least squares support vector machine classifiers. *Neural Processing Letters*, 9(3).

TEIXEIRA, R.G.D., SECCHI, A.R. and BISCAIA, E.C., 2015. Écoulements diphasiques dans les conduites : Améliorations numériques et analyse qualitative pour un procédé de raffinage. *Oil and Gas Science and Technology*, 70(3), pp. 497–510.

THEORY, F., 2017. *ANSYS fluent theory guide version 18.1*. ANSYS, Inc., 275 Technology Drive Canonsburg,.

THORLEY, A.R.D. and TILEY, C.H., 1987. Unsteady and transient flow of compressible fluids in pipelines-a review of theoretical and some experimental studies. *International Journal of Heat and Fluid Flow*, 8(1).

TU, J., YEOH, G.H. and LIU, C., 2018. *Computational fluid dynamics: A practical approach*. 3rd ed. *Computational Fluid Dynamics*. Butterworth-Heinemann.

TURNER, D. et al., 2005. Development of a Hydrate Kinetic Model and Its Incorporation Into the OLGA2000® Transient Multi-Phase Flow Simulator. *Proceedings of the 5th International Conference on Gas Hydrates*, (July 2015).

TURNER, D. and TALLEY, L., 2008. Hydrate Inhibition Via Cold Flow - No Chemicals or Insulation. In: *Proceedings of the 6th International Conference on Gas Hydrates (ICGH 2008)*. Vancouver, British Columbia, Canada, July 6-10, 2008. Available from:

<https://open.library.ubc.ca/cIRcle/collections/59278/items/1.0041089>.

UMUTEME, O.M., 2020. Computational fluid dynamics (CFD) transient pressure and temperature simulation of a natural gas – hydrogen gas transportation pipeline. *International Journal of Innovative Research and Development*, 9(6), pp. 112–116.

UMUTEME, O.M. et al., 2021. Computational fluid dynamics prediction of hydrates deposition rates in subsea gas pipelines. In: *34th Scottish Fluid Mechanics Meeting (SFMM) - Poster Presentation*. School of Engineering, Robert Gordon University, Aberdeen, Scotland, UK.

UMUTEME, O.M. et al., 2022. An improved computational fluid dynamics (CFD) model for predicting hydrate deposition rate and wall shear stress in offshore gas-dominated pipeline. *Journal of Natural Gas Science and Engineering*, 107. [online]. Available from: doi.org/10.1016/j.jngse.2022.104800.

UMUTEME, O.M. et al., 2023a. Computational fluid dynamics simulation of natural gas hydrate sloughing and pipewall shedding temperature profile: Implications for CO₂ transportation in subsea pipeline. *Gas Science and Engineering*, 116, p. 205048.

UMUTEME, O.M. et al., 2023b. Analytical modelling of the hydraulic effect of hydrate deposition on transportability and plugging location in subsea gas pipelines. *Proceedings of the Institution of Mechanical Engineers, Part C: Journal of Mechanical Engineering Science*.

UMUTEME, O.M. et al., 2023c. Modelling Hydrate Deposition in Gas-Dominant Subsea Pipelines in Operating and Shutdown Scenarios. *Sustainability (Switzerland)*, 15(13824).

UMUTEME, O. and UMEH, E., 2019. A mechanistic approach to subsea gas pipeline capacity utilization – Case study. In: *Society of Petroleum Engineers - SPE Nigeria Annual International Conference and Exhibition 2019, NAIC 2019*.

VAKILIPOUR, S. et al., 2019. Developing a physical influence upwind scheme for pressure-based cell-centered finite volume methods. *International Journal for Numerical Methods in Fluids*, 89(1–2), pp. 43–70.

VYSNIAUSKAS, A. and BISHNOI, P.R., 1983. A kinetic study of methane hydrate formation. *Chemical Engineering Science*, 38(7).

WANG, Z. et al., 2017. A new hydrate deposition prediction model for gas-dominated systems with free water. *Chemical Engineering Science*, 163, pp. 145–154.

WANG, Z. et al., 2018. Modeling of hydrate layer growth in horizontal gas-dominated pipelines with free water. *Journal of Natural Gas Science and Engineering*, 50, pp. 364–373.

WEISMAN, J., 1983. Two-phase flow patterns. Edited by N P Cheremisinoff

and R Gupta. *Handbook of Fluids in Motion*, pp. 409–425.

YANG, L. et al., 2019. Detection of pipeline blockage using lab experiment and computational fluid dynamic simulation. *Journal of Petroleum Science and Engineering*, 183(August), p. 106421. Available from: <https://doi.org/10.1016/j.petrol.2019.106421>.

YIN, Z. et al., 2018. A review of gas hydrate growth kinetic models. *Chemical Engineering Journal*.

YONGCHAO, R. et al., 2019. Numerical simulation study on the law of attenuation of hydrate particles in a gas transmission pipeline. *Energies*, 12(1).

YU, Z. and TIAN, H., 2022. Application of Machine Learning in Predicting Formation Condition of Multi-Gas Hydrate. *Energies*.

ZERPA, L.E. et al., 2012. Extension of a simple hydrodynamic slug flow model for transient hydrate kinetics. *8th BHR Group Multiphase Technology North American Conference (Banff, Canada, 6/20-22/2012) Proceedings*.

ZERPA, L.E. et al., 2013. Multiphase flow modeling of gas hydrates with a simple hydrodynamic slug flow model. *Chemical Engineering Science*, 99, pp. 298–304.

ZHANG, J. et al., 2019. Prediction of hydrate deposition in pipelines to improve gas transportation efficiency and safety. *Applied Energy*, 253(2019), p. 113521. Available from: <https://doi.org/10.1016/j.apenergy.2019.113521>.

ZHANG, J. et al., 2023. An improved model for predicting hydrate formation and deposition in horizontal annular flow. *Ocean Engineering*, 286, p. 115603.

ZHANG, P., WU, Q. and MU, C., 2017. Influence of temperature on methane hydrate formation. *Scientific Reports*, 7(1).

ZHANG, S. et al., 2022a. Hydrate deposition model and flow assurance technology in gas-dominant pipeline transportation Systems: A review. *Energy & Fuels*, 36(4), pp. 1747–1775. Available from: <https://doi.org/10.1021/acs.energyfuels.1c03812>.

ZHANG, S. et al., 2022b. Mechanism and control factors of hydrate plugging in multiphase liquid-rich pipeline flow systems: a review. *Frontiers in Energy*. [online]. Available from: <https://doi.org/10.1007/s11708-022-0830-z>.

APPENDIX A: MATLAB CODE FOR HYDRATES PLUGGING RISK PREDICTION

```

clc %clear all
clf % clear figure

% This Matlab program estimates the deposition rate of hydrates in a subsea
% gas pipeline and the resulting pressure drop, time to plug the hydrate
% forming section of the line and
% plugging risk

fprintf ('                               <strong> Hydrates Plugging Risk
Investigation Report');

prompt = 'pipeline description: ';
pipe_description=input(prompt, 's')

% Input for main variables
Pg = input('Average gas pressure in the pipeline section (MPa): ');
while Pg>11.0
    Pg = input('Error! Average gas pressure in the pipeline section must be
<=8.8MPa: ');
end
Pg=Pg*1000000;% Pg in Pa
Tg = input('Average gas temperature in the pipeline section (K): ');

while Tg>292
    Tg = input('Error! Average gas temperature in the pipeline section must be
<=292K: ');
end
Tw = input('Average pipewall temperature in the pipeline section (K): ');
while Tw>292
    Tw = input('Error! Average pipewall temperature in the pipeline section must
be <292K: ');
end
D = input('Pipe diameter (m): ');
Vg = input('Gas velocity (m/s. Input zero(0)if only flowrate is given): ');
while Vg<=0
    Qg = input('Gas flowrate (m^3/s): ');
    Vg = (Qg*101325*0.5*(Tw+Tg)*4)/(3.142*D^2*288*Pg); % Computes the gas
velocity from the gas flowrate based on the relation provided in the
Mohitpour et al. (2007)
end
Qg = (Vg*3.142*D^2*288*Pg)/(101325*0.5*(Tw+Tg)*4);% Computed based on the
relation provided in the Mohitpour et al. (2007)
L = input('Hydrates section length (m): ');

```

```

MAOP = input('Maximum allowable pipeline pressure (MPa): ');
MAOP=MAOP*1000000; % MAOP in Pa
Wvof = input('Water volume fraction: ');

%Compute the subcooling temperature, deposition rate of hydrate (Qhd), Gas
Viscosity (Vg), Gas density (Gd), Reynolds number (Re), Friction factor (f),
Equation tuning
%empirical factor (KH)

DeltaT = Tg-Tw;% Computes the subcooling temperature
Qhd = (0.0163*Vg)+(0.0252*DeltaT)-(3.4127*Wvof)+(7.3412*D)-0.0845; % Computes
the deposition rate of hydrates, L/min based on the regression model
developed in this study
Gv = (0.00000000645*0.5*(Tw+Tg))+(0.0000000000736*Pg)+0.000005555; %
Computes the gas viscosity, Pa.s
Gd = (-0.000000127*Pg*0.5*(Tw+Tg))+(0.49*0.5*(Tw+Tg))+(0.0000479*Pg)-156.6; %
Computes the gas density, Kg/m^3
Re = (Gd*Vg*D)/Gv; % Computes the Reynolds number
f = 0.0056+0.5*Re^(-0.32); % Friction factor_Re>3000 (Drew et al. (1932))
KH = (0.0188*Vg)+4.392; % Empirical model tuning factor
Kft = 0.8; % Hydrate forming section hydraulic diameter reduction factor

%This section prints the input variables to ensure the inputs are
%accurate
fprintf ('<strong> INPUT VARIABLES');
Input_Variables =
table([Tg;Pg/1000000;Wvof;D;L;DeltaT;Vg;Qg], 'VariableNames', {'Values'}, 'RowNa
mes', {'Gas Temp. (K)' 'Gas Pressure (MPa)' 'Water Volume Fraction' 'Pipe
Diameter (m)' 'Pipeline Hydrate Section (m)' 'Subcooling Temp. (K)' 'Gas
Velocity (m/s)' 'Gas Flowrate (m^3/s)'})

% This section computes the hydrates-induced pressure drop and time to plug
the line based
% on the relationship developed in this study

%Calculate the total plug time
tplug = Kft*(pi*D^2*L*1000*60/(6*Qhd)); % Computes the pipe plug time (s)
%Calculate time step
tstep = tplug/20; %time step equal 20 steps
% Calculate the instantaneous pressure drop
fprintf ('<strong> RESULTS');
fprintf ('_____');
fprintf ('<strong> Flowtime Pressure Drop');
fprintf ('<strong> (min) (MPa)');

for i = 0:tstep:tplug

    delta_P_Pa =
((KH/(2*D))*f*Gd*(Vg^2)*(6*(Qhd/(60*1000)))*L/((L*pi*(D^2))-

```

```

(6*(Qhd/(60*1000))*i))*tplug); % Transient pressure (Pa) as developed in
this study
    tn_min = i/60; %Transient time (min)
    delta_P_MPa = delta_P_Pa/1000000; % Reports the transient pressure drop
in Mp

    Results = [tn_min, delta_P_MPa];
    disp(Results);

    plot(tn_min, delta_P_MPa, 'b .', 'MarkerSize', 15); hold on
    grid on;
    xlabel('Flowtime (min)')
    ylabel('Pressure Drop (MPa)')
    title('Hydrate Plugging Risk: Pressure Drop Versus Flowtime')
end
New_Pg_Pa = delta_P_Pa+Pg; % Simulated new pipeline pressure (Pa)
MAOP_Rise_Limit = MAOP+0.05*MAOP; % Preventive risk limit for MAOP (Pa)

%This section displays both input and computed variables for parametric
analysis
% This section computes the density of hydrates based on the relationship
% developed in this study.

C_rho_h=(0.0325*0.5*(Tw+Tg))-(0.00000001985*Pg)-3; % Hydrate density
estimation empirical tuning factor
Hd = C_rho_h*(((1-Wvof)*Gd)+(Wvof*998))+((2*(1-Wvof)*Gd*Wvof*998)/(((1-
Wvof)*Gd)+(Wvof*998)));
fprintf ('OUTPUT VARIABLES');

Output_Variables = table([Gd;Hd;Qhd;tn_min;delta_P_MPa;New_Pg_Pa/1000000],
'VariableNames',{'Values'},'RowNames', {'Gas Density (kg/m^3)' 'Hydrates
Density (kg/m^3)' 'Hydrates Deposition Rate (L/min)' 'Plugging Flowtime
(min)' 'Pressure Drop (Mpa)' 'New Pipeline Pressure (MPa)'});

%This section defines the hydrates plugging risk
fprintf('<strong>Hydrates Plugging Risk Classification');

if New_Pg_Pa<MAOP
    fprintf("Pressure Related Hydrate plugging Risk Classification: low-
risk. Pressure is below MAOP");
end
if tn_min>=525600
    fprintf("Flowtime Related Hydrate plugging Risk Classification: low-
risk. Pipeline will plug after 12 months of operation");
end
if New_Pg_Pa>MAOP && New_Pg_Pa<=MAOP_Rise_Limit
    fprintf("Pressure Related Hydrate plugging Risk Classification:
medium-risk. Pressure is within 5% below MAOP");
end
if tn_min>262800
    fprintf("Flowtime Related Hydrate plugging Risk Classification:
medium-risk. Pipeline will plug after 6 months of operation");

```

```

end
    if New_Pg_Pa>MAOP_Rise_Limit
        fprintf("Pressure Related Hydrate plugging Risk
Classification: High-risk. Pressure is above 5% of MAOP and pipeline can
burst");
    end
    if tn_min<=262800
        fprintf("Flowtime Related Hydrate plugging Risk
Classification: High-risk. Pipeline will plug within 6 months of operation");

        else fprintf("Hydrate plugging Risk Classification: None.
Please confirm your input data");
    end

    if Hd<998 % Compare the estimated density of hydrates with the density of
water, being a condition for the formation of
    % hydrates slurry and transportability

        fprintf(['Low transportability: High adhesion of hydrates to pipe
wall']);
        else fprintf(['High transportability: Low adhesion of hydrates to pipe
wall\n']);
    end

    fprintf ('                (c) 2022: Oghenethoja Monday Umuteme, Robert
Gordon University, Aberdeen')

```

APPENDIX B: SAMPLE OUTPUT OF MATLAB CODE

Hydrates Plugging Risk Investigation Report

pipe_description: 'Proposed 0.254m x 30km Gazelle Offshore Pipeline
Cote D'Ivoire' - 50MMSCFD

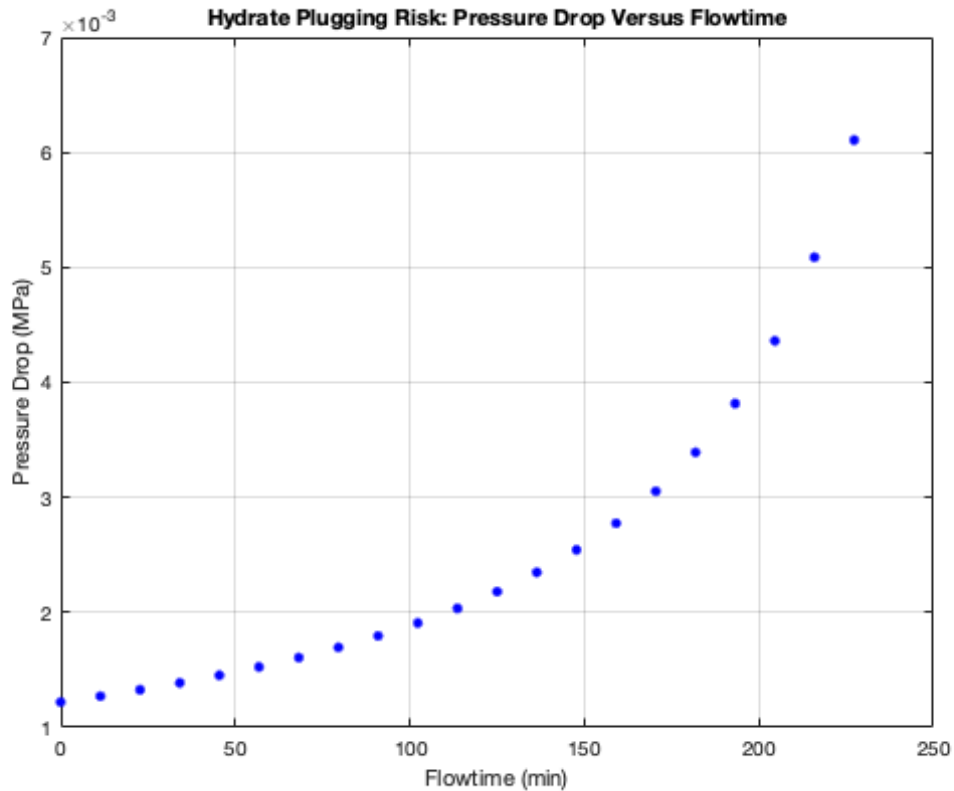
INPUT VARIABLES

Input_Variables = 8x1 table

	Values
1 Gas Temp. (K)	292.0000
2 Gas Pressure (MPa)	7.6000
3 Water Volume Fraction	0.1000
4 Pipe Diameter (m)	0.2540
5 Pipeline Hydrate Section (m)	14.5000
6 Subcooling Temp. (K)	8.5000
7 Gas Velocity (m/s)	4.3371
8 Gas Flowrate (m ³ /s)	16.5000

RESULTS

Flowtime (min)	Pressure Drop (MPa)
0	0.0012
11.3661	0.0013
22.7321	0.0013
34.0982	0.0014
45.4642	0.0015
56.8303	0.0015
68.1964	0.0016
79.5624	0.0017
90.9285	0.0018
102.2945	0.0019
113.6606	0.0020
125.0267	0.0022
136.3927	0.0023
147.7588	0.0025
159.1248	0.0028
170.4909	0.0031
181.8570	0.0034
193.2230	0.0038
204.5891	0.0044
215.9551	0.0051
227.3212	0.0061



OUTPUT VARIABLES

Output_Variables = 6×1 table

	Values
1 Gas Density (kg/m ³)	70.7012
2 Hydrates Density (kg/m ³)	1091.2
3 Hydrates Deposition Rate (L/min)	1.7238
4 Plugging Flowtime (min)	227.3212
5 Pressure Drop (Mpa)	0.0061
6 New Pipeline Pressure (MPa)	7.6061

Hydrates Plugging Risk Classification

Pressure Related Hydrate plugging Risk Classification: low-risk.
 Pressure is below MAOP
 Flowtime Related Hydrate plugging Risk Classification: High-risk.
 Pipeline will plug within 6 months of operation
 High transportability: Low adhesion of hydrates to pipe wall

(c) 2022: Oghenethoja Monday Umuteme, Robert Gordon University, Aberdeen

Hydrates Plugging Risk Investigation Report

pipe_description = ' Proposed 0.254m x 30km Gazelle Offshore Pipeline
Cote D'Ivoire - 20MMSCFD'

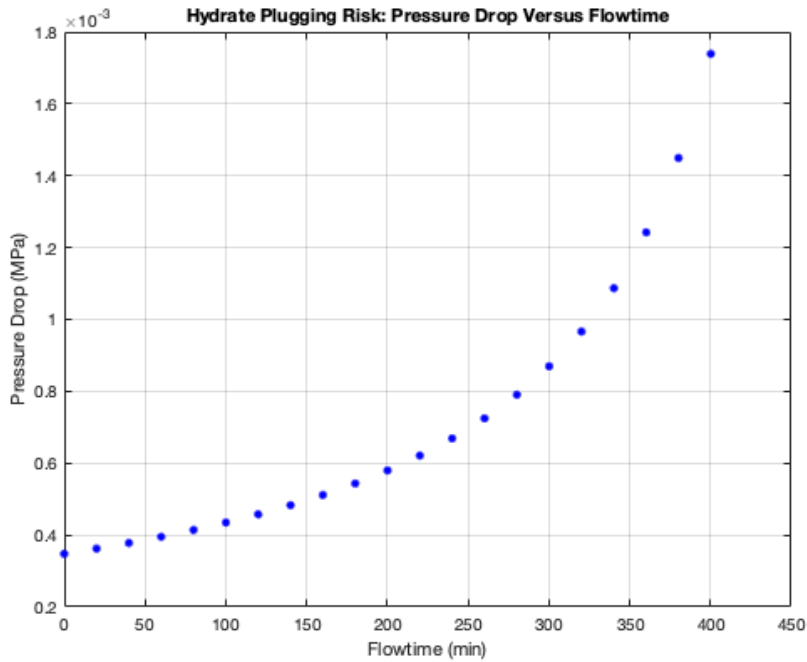
INPUT VARIABLES

Input_Variables = 8x1 table

	Values
1 Gas Temp. (K)	292.0000
2 Gas Pressure (MPa)	8.2000
3 Water Volume Fraction	0.1000
4 Pipe Diameter (m)	0.2540
5 Pipeline Hydrate Section (m)	24.5000
6 Subcooling Temp. (K)	7.5000
7 Gas Velocity (m/s)	1.6107
8 Gas Flowrate (m ³ /s)	6.6000

RESULTS

Flowtime (min)	Pressure Drop (MPa)
1.0e-03 *	
0	0.3478
20.0132	0.0004
40.0265	0.0004
60.0397	0.0004
80.0530	0.0004
100.0662	0.0004
120.0795	0.0005
140.0927	0.0005
160.1060	0.0005
180.1192	0.0005
200.1325	0.0006
220.1457	0.0006
240.1589	0.0007
260.1722	0.0007
280.1854	0.0008
300.1987	0.0009
320.2119	0.0010
340.2252	0.0011
360.2384	0.0012
380.2517	0.0014
400.2649	0.0017



OUTPUT VARIABLES

Output_Variables = 6×1 table

	Values
1 Gas Density (kg/m ³)	77.2390
2 Hydrates Density (kg/m ³)	1132.6
3 Hydrates Deposition Rate (L/min)	1.6541
4 Plugging Flowtime (min)	400.2649
5 Pressure Drop (Mpa)	0.0017
6 New Pipeline Pressure (MPa)	8.2017

Hydrates Plugging Risk Classification

Pressure Related Hydrate plugging Risk Classification: low-risk.

Pressure is below MAOP

Flowtime Related Hydrate plugging Risk Classification: High-risk.

Pipeline will plug within 6 months of operation

High transportability: Low adhesion of hydrates to pipe wall

(c) 2022: Oghenethoja Monday Umuteme, Robert Gordon University, Aberdeen.

APPENDIX C: UDF CODES

```
/*
*****
Calculating the Source Energy for Hydrates formation
*****
*****/

#include "udf.h"
/*Constants used in reaction kinetics calculations based on Turner et al, 2005 */
#define K1 7.3548e17 /*Hydrate formation rate Constant */
#define K2 -13600 /* Hydrate formation constant 2 , K */
#define HF_ENTHALPY 6.4e5 /* Hydrate Formation Enthalpy, J/kg */
#define pipe_diam 0.0204 /*diameter of pipe section, m*/
#define pipe_length 10 /* length of pipe section, m*/
#define sub_temp -7.0 /* sub cooling temperature, Di Lorenzo et al (2017), K*/
#define gas_vel 8.8 /*gas velocity m/s*/

DEFINE_SOURCE(energy_source, c, t, dS, eqn)
{
real z[ND_ND];
real source, interfacial_area, fluid_domain_volume, press_equiv, temp_equiv,
CURRENT_TEMPERATURE, CURRENT_PRESSURE;
CURRENT_TEMPERATURE = C_T(c, t); /*primary phase (gas) temperature*/
CURRENT_PRESSURE = C_P(c, t); /*primary phase (gas) pressure*/

C_CENTROID(z,c,t);
interfacial_area = (((0.06*gas_vel)-0.18)*pipe_length*(pipe_diam/0.0204));
//computes the interfacial area/
fluid_domain_volume = (3.142 * pow(pipe_diam, 2) * pipe_length)/4;
temp_equiv = sub_temp + CURRENT_TEMPERATURE;
press_equiv = (exp(38.98 - (8534 / temp_equiv)))*1e3;/*Pa*/
if (press_equiv <= CURRENT_PRESSURE)
{
source = K1 * exp(K2 / CURRENT_TEMPERATURE) * interfacial_area * sub_temp
* HF_ENTHALPY/fluid_domain_volume; /*J/s-m3*/
dS[eqn] = 0;
}
else
{
source = 0;
dS[eqn] = 0;
}
return source;
}
```

```

/*****
*****
Calculating the Gas Source Mass in Hydrates formation
*****
*****/

#include "udf.h"
/*Constants used in reaction kinetics calculations based on Turner et al, 2005 */
#define K1 7.3548e17 /*Hydrate formation rate Constant */
#define K2 -13600 /* Hydrate formation constant 2 , K */
#define pipe_diam 0.0204 /*diameter of pipe section, m*/
#define pipe_length 10 /* length of pipe section, m*/
#define sub_temp -7.0 /* sub cooling temperature, Di Lorenzo et al (2017), K*/
#define gas_vel 8.8 /*gas velocity m/s*/
DEFINE_SOURCE(Gas_Mass_source, c, t, dS, eqn)
{
real z[ND_ND];
real source, interfacial_area, fluid_domain_volume, press_equiv, temp_equiv,
CURRENT_TEMPERATURE, CURRENT_PRESSURE;
CURRENT_TEMPERATURE = C_T(c, t); /*primary phase (gas) temperature*/
CURRENT_PRESSURE = C_P(c, t); /*primary phase (gas) pressure*/

C_CENTROID(z,c,t);
interfacial_area = (((0.06*gas_vel)-0.18)*pipe_length*(pipe_diam/0.0204));
/*computes the interfacial area*/
fluid_domain_volume = (3.142 * pow(pipe_diam, 2) * pipe_length) / 4;
temp_equiv = sub_temp + CURRENT_TEMPERATURE;
press_equiv = (exp(38.98 - (8534 / temp_equiv)))*1e3;/*Pa*/
if (press_equiv <= CURRENT_PRESSURE)
{
source = (K1 * exp(K2 / CURRENT_TEMPERATURE) * interfacial_area *
sub_temp/ fluid_domain_volume); /*kg/s-m3*/
dS[eqn] = 0;
}
else
{
source = 0;
dS[eqn] = 0;
}
return source;
}

```